Particulate organic carbon and mineral export from the North and South Atlantic gyres: the $^{234}Th/^{238}U$ disequilibrium approach

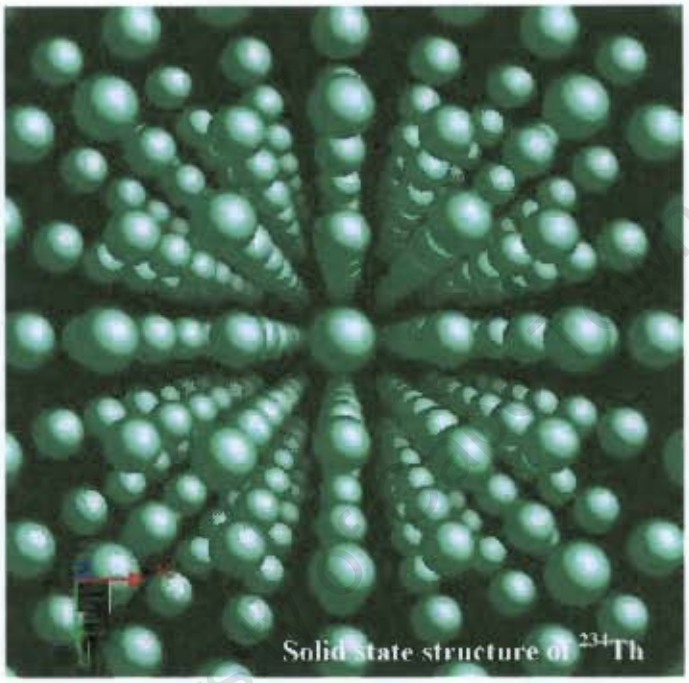

by

Sandy Jane Thomalla

Thesis for the Degree of Doctor of Philosophy

Department of Oceanography

University of Cape Town

June 2007

Particulate organic carbon and mineral export from the North and South Atlantic gyres: the $^{234}Th/^{238}U$ disequilibrium approach

Sandy Jane Thomalla

June 2007

Abstract

Subtropical ocean gyres are typically characterised by low carbon export into the deep ocean. However, due to their large area, even relatively small average carbon export may be globally significant. Strong correlations observed between deep-sea organic carbon, calcite and opal suggest that mineral phases may enhance the export and survival of organic matter as it sinks (the 'ballast effect'). However, the processes underlying these correlations are not well understood and remain key uncertainties in models that predict global carbon cycling. To better constrain carbon and mineral export from the surface ocean of subtropical gyres, radioactive disequilibria between ^{234}Th and ^{238}U were used to estimate fluxes of particulate organic carbon (POC), calcite and opal in the North and South Atlantic subtropical gyres. Samples were collected from three Atlantic Meridional Transect (AMT) cruises in May/June 2003 (AMT 12), September/October 2003 (AMT 13) and April/June 2004 (AMT 14) as well as from a time series at the Porcupine Abyssal Plain (PAP) observatory (49° N 16.5° W) in June/July 2003-2006.

Lowest POC export (~2 mmol C m^{-2} d^{-1}) was associated with the central subtropical gyres, where productivity was lowest (~18 mmol C m^{-2} d^{-2}), characterised by tightly coupled regeneration based microbial food webs. Enhanced POC export (~8 mmol C m^{-2} d^{-1}) typified the equatorial divergence and upwelling region north of the equator. Increased POC export (~15 mmol C m^{-2} d^{-1}) was also found at higher latitudes where higher productivity (~31 mmol C m^{-2} d^{-1}) is supported by increased nutrient supply from the deep ocean. Estimates of biomineral and POC production were compared with ^{234}Th derived export to investigate the efficiency of the biological pump (*ThE*). Similarities in

average *ThE* for calcite (0.26), opal (0.31) and POC (0.29), imply a potential association between biomineral and POC export, but there is substantial uncorrelated variability when *ThE* are compared on regional scales. Higher euphotic zone *ThE* for POC (~0.22) relative to that in deep-sea sediment traps (<0.05) supports considerable re-mineralisation below the euphotic zone. POC flux and *ThE* from the PAP were low (~5 mmol C m^{-2} d^{-1}; 0.06) in pre and post bloom years but high in years that sampled during peak (~24 mmol C m^{-2} d^{-1}; 0.31) and early decline (~15 mmol C m^{-2} d^{-1}; 0.19) bloom conditions.

Conclusions from this study suggest that: (i) carbon export in the central oligotrophic gyres may be low, but carbon sequestration at their temperate fringes, as well as in the equatorial and upwelling region can be substantial; (ii) regional variability in the mechanisms by which biominerals and POC become associated are more important determinants of carbon export than the efficient export of ballast materials themselves; (iii) due to preferential aphotic remineralisation of POC relative to calcite/opal dissolution, potential for effective ballasting increases with depth; (iv) inter-annual variability in POC flux and *ThE* at the PAP site was governed by the seasonal timing of sampling relative to the North Atlantic spring bloom. Environmental controls (physical stability, light, nutrients) on phytoplankton community succession (diatoms to non-diatoms) determine the characteristics of the sinking flux and ultimately the efficiency of carbon export to depth and (v) seasonal and inter-annual variability in surface POC flux at the PAP is translated into comparable variability at depth.

Acknowledgments

I would like to thank my supervisors; Dr Mike Lucas, whose invaluable help, guidance, time and patience have made the completion of this thesis possible. Thank you also to Dr Howard Waldron for his ever friendly counsel and encouragement over the years. I am especially indebted to my co-supervisor Dr Robert Turnewitsch for his indispensable knowledge, experience and expert advice on thorium analysis.

I am enormously grateful to numerous scientists and co-workers who have aided my research, understanding and interpretation throughout my PhD. In particular I would like to thank Dr Alex Poulton for his ever friendly advice and informative discussions. Thank you also to Dr. Richard Sanders, Dr. Richard Lampitt and Prof. Patrick Holligan for their insightful comments and encouragement. Particular mention must also go to Stuart Painter for his forthcoming assistance with miscellaneous requests that have on many occasions made my life easier.

I would like to extend my sincere appreciation to Tarron Lamont from the Marine Remote Sensing Unit at UCT for her friendly approach and willingness to provide the SeaWiFs surface chlorophyll-a composite images, as well as to Ingrid Vöge for teaching me the art of origami with forceps and filters and to Tammy Robinson for advice on statistical analysis.

I would like to thank the following of my colleagues for providing me with the results of their collaborative studies that were fundamental in the interpretation of my data. From the AMT cruises; Dr. Alex Poulton, Tim Adey and Mark Stinchcombe for primary production, calcification and silification rates. Dr Stuart Painter for new production, Malcolm Woodward and Katie Chamberlain for nutrients. From the PAP site; Dr Mike Lucas for primary and new production rates, Dr Richard Lampitt and Ian Salter for PELAGRA and sediment trap data.

A very big thank you to all the officers and crew on board the *RRS James Clark Ross*, *RRS Discovery*, *RRS Charles Darwin and HMS Poseidon*. Our jobs as scientists would be considerably more difficult were it not for the dedication, hard work and friendly assistance by dozens of these nameless souls.

I am most grateful to the British Commonwealth split-site bursary for providing the unique opportunity of being able to work with the National Oceanography Centre, Southampton (NOC) and have access to their wonderful facilities and resources, both with respect to equipment and academic support. Particular thanks are due to the George Deacon division at NOC for their financial aid that was fundamental in obtaining much of my data.

I feel truly privileged to have been a part of the Atlantic Meridional Transect Programme (AMT) and would like to thank all those involved, in particular to everyone that I have sailed with for making every cruise (and workshop) such an enjoyable and truly memorable experience.

Outside of science I would like to thank all my friends in Southampton and the UK who are too numerous to mention individually but have all played such a vital role in making my stay abroad so rewarding. A very big thank you to all my friends in Cape Town who have been a great comfort in tough times and who have done such a great job in keeping me sane (or at least mostly sane) during the often arduous write up. Thank you all for always listening and sympathising and for providing such a vibrant distraction to life when necessary. My sincerest thanks go especially to Alison Breen and Daniel Steyn for their precious source of comfort, love and support.

To all my family in the UK and South Africa thank you for being so wonderful. In particular I wish to thank my parents for providing me with all the best of life's opportunities together with an endless source of love and encouragement to make the most of them. An extraordinary thank you to my sister Lisé for being the best big sister in

the universe! Thank you for always being there, for knowing the right things to say and for providing such a loving home in the UK.

Finally a very special thank you to Winston Leukes, whose unwavering belief in me and my abilities were fundamental in installing the resolution necessary to complete this thesis. Though your company is so sorely missed, your love and support will always be cherished.

1 General Introduction

1.1 The global carbon cycle

Present atmospheric CO_2 concentration is rising at least 10 and possibly 100 times faster than at any other time in the past 420 000 years (Falkowski et al., 2000). The CO_2 concentration in the atmosphere is governed primarily by the rate of anthropogenic emissions and by the exchange of CO_2 between two dynamic global reservoirs, the oceans and the land biosphere (Figure 1.1). Since the beginning of the industrial era (circa 1750), about 200 billion tons of carbon have been released into the atmosphere as CO_2 from various industrial sources such as the burning of fossil fuels and cement production (Takahashi et al., 1993). Given present trends in energy demands, and a lack of globally concerted alternative energy strategies, atmospheric CO_2 concentrations appear likely to continue increasing throughout the coming century (Houghton et al., 1996a; Hoffert, 1998). We can be certain, therefore, that human activities are having a major effect on the climate of the planet. Evidence from the geologically recent past indicates that quite small changes in atmospheric CO_2 have big effects on planetary climate (Li et al., 1998; Shackleton, 2000). With current trends, atmospheric CO_2 concentrations are increasing by ~3 billion tonnes y^{-1}, about half the annual emission rate from fossil fuel combustion (Keeling et al., 1989).

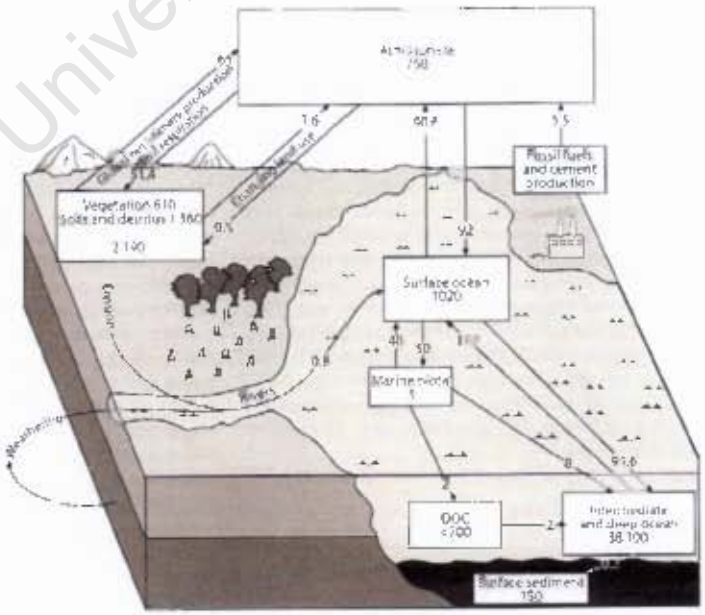

Figure 1.1. Schematic of global carbon cycle budget, including the natural background cycle as well as anthropogenic perturbations. Reservoir sizes given in Pg C (1 Pg = 10^{15} g) and fluxes in Pg C yr^{-1}. Figure reproduced from Doney et al. (2003).

The strength of the ocean and land reservoir sinks determines their capacity to absorb excess or anthropogenic CO_2. While measurements in the atmosphere have provided an accurate measure of the fraction of CO_2 staying in the atmosphere, the fate of the remaining anthropogenic carbon has remained ill-constrained by direct measurements of carbon. A new global data set of inorganic carbon in the ocean and new tools to interpret them have recently determined that the ocean has been the primary sink for anthropogenic carbon over the last 200 years, taking up 118+/-19 Pg C, or about 50% of the cumulative fossil fuel emissions (Mikaloff-Fletcher et al., 2006). For this reason it is important to understand the nature of the physical, chemical and biological processes which govern the oceanic carbon cycle. However, our understanding of how biogeochemical cycling in the oceans affects climate, and of how changes in climate influence the structure and activity of oceanic ecosystems is still incomplete, hindering accurate predictions of the future global environment.

1.1.1 Oceans and climate change: the biological carbon pump

There is an inverse gradient in Dissolved Inorganic Carbon (DIC) in the ocean, such that higher concentrations of DIC are found at greater depths. In contrast, the upper portion of the water column is in overall equilibrium with the atmosphere to first order. This gradient dictates the ocean's capacity to remove CO_2 from the atmosphere and is maintained by two carbon pumps; the physical solubility pump and the biological pump. The strength of the physical solubility pump is set primarily by temperature and the degree of warming and cooling that, together with salinity, regulates density and the rate of surface water sinking, taking with it atmospheric CO_2 (Watson and Orr, 2003). As the solubility of cold, deep water is about twice that of near-surface equatorial water, the net effect of sinking surface waters through thermohaline circulation is to enrich deeper waters in carbon (Falkowski et al., 2000). One of the best-known global CO_2 sinks driven by physical solubility and surface water sinking is associated with North Atlantic Deep Water (NADW) formation. This thesis however does not concern itself with the physical solubility pump, but only the biological carbon pump.

The biological carbon pump is regulated initially by the sequestration of CO_2 by primary producers, notably by phytoplankton. The rate at which inorganic carbon is

fixed into particulate and dissolved organic carbon that sinks, or is otherwise transported through the water column to below the seasonal thermocline, sets the strength of the biological carbon pump. Thus factors that regulate phytoplankton growth (light, nutrients), particle formation and rates of sinking (aggregation, ballasting, senescence, grazing) and re-mineralisation (bacterial activity, chemical dissolution) all modify particulate and dissolved carbon fluxes and the strength of the biological carbon pump.

The combined effects of the physical solubility pump and the biological carbon pump leads to an oceanic mosaic of "sinks" and "sources" of CO_2 (e.g. Takahashi et al., 1997) where "sinks" are regions of net CO_2 uptake by the oceans, while "sources" are regions of net CO_2 flux into the atmosphere. The two largest pools of dissolved carbon found in the ocean are dissolved inorganic carbon (DIC) and dissolved organic carbon (DOC). A chemical disequilibrium between DIC and organic matter is produced and maintained by biologically-mediated processes which collectively define the oceanic carbon cycle (Figure 1.2) (Karl et al., 1996). In open oceans, the main source of organic particle production (dissolved and particulate) is generally restricted to the euphotic zone and is derived from biogenic photosynthetic carbon fixation controlled by light and nutrient supply. Photosynthetic sequestration of inorganic carbon converts CO_2 to organic carbon thereby decreasing the partial pressure gradient at the air sea interface and driving the draw down of CO_2 from the atmosphere into the ocean. Conversely heterotrophic oxidation of organic solutes and particles can lead to the formation of CO_2 and the potential efflux of CO_2 from the ocean to the atmosphere (Figure 1.2) (Falkowski et al., 1998).

Although particulate organic carbon (POC) flux transports atmospheric CO_2 into the deep ocean, most POC is recycled in surface waters after decomposition to DOC or by remineralisation/respiration to DIC. Only a small fraction of POC (~10%) is exported from the euphotic layer and subsequently either recycled in deep waters or reaches the sediments (~1%) (Figure 1.2) (e.g. Suess, 1980). The percentage of primary production that is exported to the deep water is termed the export ratio (Baines et al., 1994) and ranges from < 10% in oligotrophic waters to >50% in productive coastal regions. The biological pump enriches the ocean interior with inorganic carbon in excess of that which would be supported solely by air-sea exchange (Broeker et al.,

1980) and is therefore crucial in maintaining the steady-state levels of atmospheric CO_2 (Sarmiento et al., 1992; Siegenthaler and Sarmiento, 1993). Once organic carbon produced in the photic zone sinks beneath the seasonal thermocline, it is effectively sequestered from the atmosphere for centuries to millennia (Falkowski et al., 1998) since the subsequent and eventual upward transport of nutrients and DIC stored in the ocean interior occurs only at a slow rate (Figure.1.2).

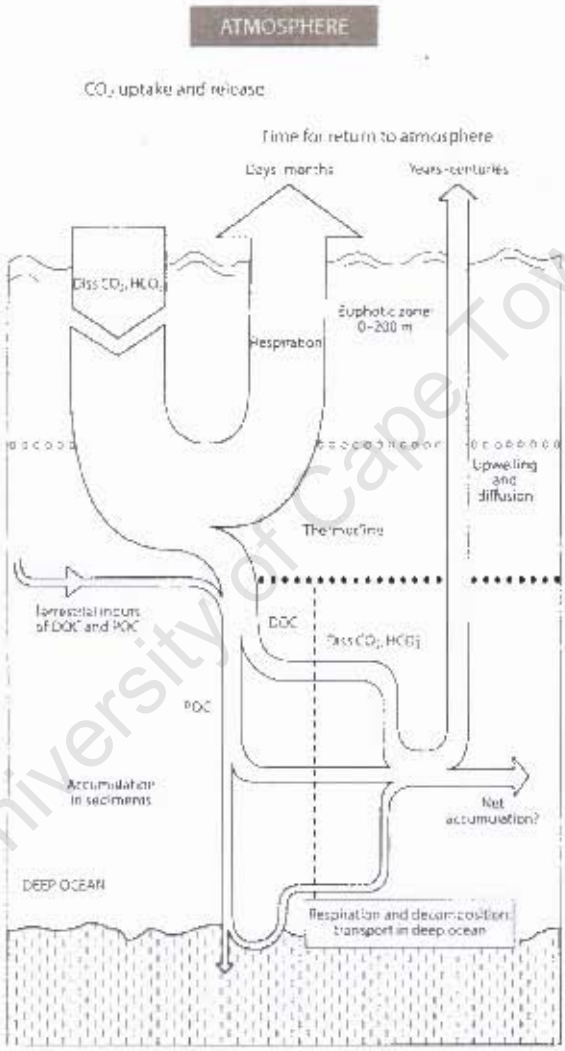

Figure 1.2. The classical JGOFS one dimensional vision of the oceanic carbon pump with time scaling in the different layers and the sediment. Figure reproduced from Treguer et al. (2003)

The role of the ocean as a net carbon sink depends on the balance between the export flux of planktonic primary production and the rate of DIC re-supply to surface waters (Figure 1.3) (Karl et al., 1996). The intensity of the biological pump is of particular

importance when the food web has been perturbed. Under such conditions, the mechanisms controlling production and consumption of organic matter are uncoupled, resulting in an accumulation of biomass and an increase in export flux. Perturbations include seasonal changes in irradiance, wind mixing events, and seasonal or pulsed inputs of nutrients (including iron) due to changes in nutricline depth, upwelling and atmospheric events (Falkowski et al., 2003).

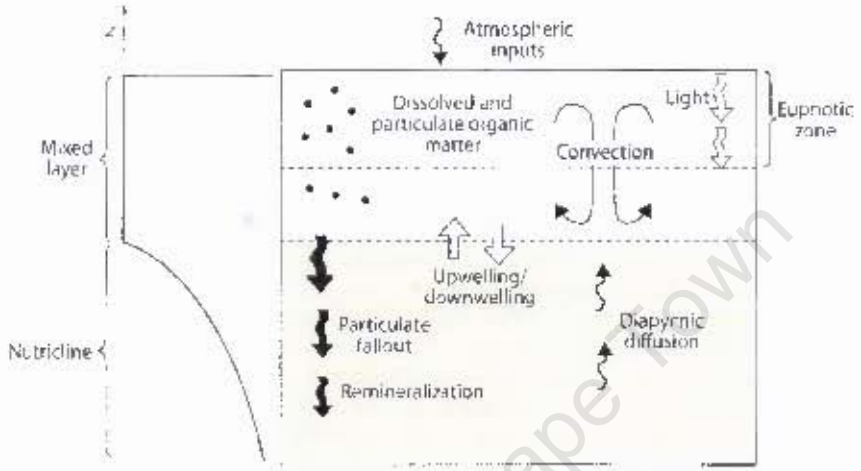

Figure 1.3. A one dimensional view of the physical processes that affect the biological carbon cycle. Phytoplankton growth within the euphotic zone provides export of organic matter which is remineralised at depth. Input of new nutrients to the euphotic zone is maintained through the physical transfer of nutrients involving vertical advection, diapycnic diffusion and convection. Figure reproduced from Williams and Follows (2003).

From earliest times, photoautotrophic organisms have continuously altered the chemical composition of the ocean and through air-sea exchange, have influenced the composition of the atmosphere. Variations in the concentration of radiatively sensitive gases in the atmosphere (e.g. CO_2, CH_4, DMS) in turn influence global climate and consequently ocean circulation, stratification and inorganic nutrient supply. Coupled climate-ocean simulations (Manabe and Stouffer, 1993; Mitchell et al., 1995) suggest that global warming will lead to increased stratification of the water column, reduced vertical nutrient flux and consequently reduced primary production. This may reduce carbon export from the upper ocean to the deep ocean, resulting in decreased sequestration of anthropogenic carbon into the ocean (Sarmiento et al., 1998; Joos et al., 1999). Furthermore, increased temperature will probably lead to higher microbial heterotrophic respiration, contributing to CO_2 sources. Predicted changes in atmospheric circulation will likely alter the transport of dust and Fe to remote ocean

regions. These physical forcings govern spatio-temporal variability in phytoplankton distributions through the direct effect of temperature on growth and through their secondary influence on factors such as mixed layer, light availability and the distribution of macro and micronutrients (Behrenfeld et al., 2002).

Several phytoplankton and zooplankton species form $CaCO_3$ shells that sink into the interior of the ocean, where some fraction dissolves. This "carbonate pump" reduces surface ocean DIC relative to the deep ocean and increases the partial pressure of CO_2. As CO_2 dissolves in seawater, it forms carbonic acid, which is now lowering the surface ocean pH (Kleypas et al., 1999, Bellerby et al., 2005), causing significant changes in carbonate chemistry, slowing calcification in surface oceans (Wolf-Gladrow et al., 1999; Riebesell et al., 2000). As calcification releases CO_2 to the atmosphere, a decrease in global ocean calcification would enhance CO_2 storage in the upper ocean (Houghton et al., 1996b; Purdie and Finch, 1994; Kheshgi et al., 1991), thus providing a potential negative feedback on atmospheric CO_2 (Riebesell et al., 2000).

Enhanced Dimethyl Sulphide (DMS) production associated with phytoplankton blooms may tend to act as a significant negative feedback on global warming. The ventilation of DMS to the atmosphere produces aerosol particles which act as cloud condensation nuclei, influencing cloud formation and albedo (Malin, 1997). DMS mediated increases in cloud albedo are estimated to potentially cool the planet globally by 1°K (Houghton et al., 1996b).

1.2 Controls on phytoplankton growth and community structure

To improve our understanding of the ocean carbon cycle, we must enhance our understanding of the biological pump. The rates at which individual components of the biological carbon pump operate are controlled by physical (light, temperature, turbulence), biological (species composition, growth rate, food web structure) and bio-geochemical (new and regenerated nutrient supply) processes that vary in space and time, leading to significant variability in phytoplankton distribution, diversity and growth rates. Phytoplankton are taxonomically diverse and there is an immense

literature dealing with the factors governing their distribution, physiology and ecology (Inter alia: Hart 1934; Holm-Hansen et al., 1977; Tranter, 1982; Witek et al., 1982; Jacques, 1983; Tett and Edwards, 1984; Tilzer et al., 1985; Bidigare et al., 1986; Martin et al., 1990; Cullen, 1991; Dugdale and Wilkerson, 1991; Nelson and Smith, 1991; de Baar et al., 1995; Falkowski and Raven, 1997, Bathmann,1998, Bracher et al., 1999; Marañón et al., 2000; Smith et al., 2000, Sharples et al., 2001).

In brief summary, phytoplankton distribution, diversity, biomass and production depend on the physiological responses of phytoplankton to the often extreme conditions under which they live. Part of what makes the study of phytoplankton ecology and productivity difficult is the diversity of phytoplankton assemblages and their differing responses to environmental and biological controls. Differences in species, size, the plasticity of their ultra-structure, bulk biochemical composition, pigment type and content, nutrient preferences, nutrient assimilation rates and rates of photosynthesis all contribute to the unpredictability of their collective response to physical, chemical and biological forcing from a bottom-up perspective. Added to that however, there is also a need to recognise that biomass, phytoplankton productivity and community structure can also be controlled from a top-down perspective.

1.2.1 Macronutrients

The operation of the biological carbon pump is inextricably linked to the biogeochemical cycling of other nutrient elements. Limitation by macronutrients, such as nitrogen diminishes phytoplankton growth and ultimately the export of organic carbon to the deep sea (Brzezinski et al., 2003). Nitrogen plays a critical role in determining the productivity, size structure and species succession of phytoplankton communities in much of the world's oceans (Dugdale and Goering, 1967; Carpenter and Capone, 1983; Probyn, 1992; Bronk et al., 1994; Harrison et al., 1996; Karl, 1999; Tremblay et al., 2000). Phytoplankton nitrogen nutrition is sustained mainly (but not exclusively) through the assimilation of nitrogen as either nitrate (NO_3), ammonium (NH_4) or urea, with an order of preference being established on the basis of the energetic requirements needed to assimilate each of the nitrogenous nutrients; typically NH_4 > urea > NO_3 (McCarthy et al., 1977; Probyn, 1988). Uptake and regeneration of nutrients causes their depletion in surface waters and enrichment at

depth, resulting in pronounced increases in concentrations within the upper 600-1000m (the nutricline) (Sunda and Huntsman, 1995). The consumption of primary production by heterotrophs in the euphotic zone leads to the excretion of ammonium and other reduced nitrogen such as urea and amino acids (Glibert et al, 1982a,b) that supports 'regenerated' production. In contrast, when waters from the ocean interior are mixed into the euphotic zone, nitrate is the primary form of 'new' nitrogen that becomes available for 'new' production.

Nitrogen uptake (ρN) and the partitioning of 'new' and 'regenerated' nitrogen uptake by phytoplankton depends, classically, on the relationship between ambient NO_3 and NH_4 concentrations as first proposed by Dugdale and Goering (1967). Recently, dissolved iron has also been shown to regulate the balance between ρNO_3 and ρNH_4 in an HNLC region of the Southern Ocean because of the Fe-dependence of nitrate metabolism, although separating the difference between Fe-limited ρNO_3 and the potential for NH_4 inhibition of ρNO_3 is difficult (Lucas et al., in press). The preference of phytoplankton for NH_4 over NO_3 extends over the full spectrum of nitrogen concentration (Harrison et al., 1996) and it has been shown that where NH_4 concentrations are greater than 1 $\mu mol.l^{-1}$, nitrate uptake (ρNO_3) can be inhibited (Wheeler and Kokkinakis, 1990). Some studies confirm that extremely low concentrations of NH_4 are capable of significant inhibition of ρNO_3, although complete inhibition is a rarity (Eppley and Renger, 1988; Wheeler and Kokkinakis, 1990; Harrison et al., 1996). These results highlight the important role NH_4 plays in regulating new production even at nanomolar concentrations. In particular, a preference for NH_4 can strongly influence phytoplankton community structure and productivity at the end of the season when NO_3 concentrations are low. Under such conditions, large diatoms that usually characterise high rates of new production are typically out competed by smaller cells able to scavenge reduced nitrogen at low concentrations, thus negatively affecting export production that is mediated primarily by large diatoms.

Phytoplankton production is further supported by other major inorganic macronutrients such as phosphate (PO_4) and silicate ($Si(OH)_4$) (Koeve, 2001), which if present at growth-limiting concentrations, can set upper limits to production. Although significant limitation of primary production by P in coastal waters is

restricted by P loading (Howarth, 1996), P limitation does occur in the Mediteranean and parts of the western North Atlantic (Wu et al., 2000) as well as in the central (Sanudo-Wilhelmy et al., 2001) and north eastern Atlantic subtropical gyre (Mills et al., 2005).

Establishing factors that influence the nutrient stoichiometry of phytoplankton growth and export is crucial for increasing our understanding of global nutrient cycling, both in the modern and paleo-ocean (Brzezinski et al., 2002; Sarmiento et al., 2004a). The elemental stoichiometry of biogeochemical cycles is often assumed to be relatively conserved, conforming to a C:N:Si:P ratio of 106:16:16:1 (the Redfield ratio). Redfield et al. (1963) and Dugdale and Wilkerson, (1998) demonstrated that the Redfield ratio is controlled by the requirements of phytoplankton that subsequently release these nutrients in constant atomic proportions as they are remineralised. In surface waters, the Redfield ratio is largely due to nutrient uptake by phytoplankton, while in deeper waters, it largely reflects re-mineralisation processes.

However, considerable plasticity in phytoplankton elemental composition is known to exist (Geider and La Roche, 2002), due to anomalies including changes in exogenous nutrient delivery (Fanning, 1989), microbial metabolism (Kuypers, 2003) (e.g. nitrogen fixation and denitrification) and N:Si recycling rates (Queguiner et al., 1997; de Baar et al., 1997). Phytoplankton elemental composition is also known to vary between taxa (i.e. genotypically) and with growth condition for a single taxa (i.e. phenotypically) (e.g. Geider and La Roche, 2002; Price, 2005; Quigg et al., 2003; Timmermans et al., 2004). Both of which have been hypothesised to influence biogeochemistry in the Southern Ocean. For example diatoms prefer high Si:N and low C:P and N:P (Quigg et al., 2003), blue-green algae prefer low N:P (Read et al., 2000), dinoflagellates prefer low N and low P (Margalef, 1978) but the colonial prymensiophyte *Phaeocystis antarctica* prefers high ratios of N:P (Arrigo et al., 1999, 2002; Smith and Asper, 2001).

Some of these preferences can be explained by different cellular components having differing cellular stoichiometry. For example, resource (light or nutrient) acquisition machinery (e.g. proteins and chlorophyll) is high in N but low in P, whereas growth machinery (e.g. ribisomal RNA) is high in both N and P (Falkowski, 2000, Geider and La Roche, 2002). Klausmeiers (2004)'s optimisation model predicts that during

exponential growth, bloom-forming phytoplankton will increase production in their growth machinery, reducing their N:P ratio, whereas when resources are limited, slow-growing phytoplankton will synthesize additional resource acquisition machinery, thus increasing their N:P ratio. The model also explains the unusually high cellular N:P ratio of N_2 fixers by their need for large amounts of P-poor light harvesting machinery required to drive the energy expensive fixation of N_2 (La Roche and Breitbarth, 2005).

In most marine environments, the rate of Si uptake is controlled primarily by the concentration and supply of inorganic Si in the surface ocean. Most surface waters in subtropical and tropical areas has Si concentrations <1 μM, which limits the rate of biogenic Si production in every natural diatom assemblage whose response to Si limitation has been studied (data summarised by Nelson and Tregeur, 1992). Limitation of diatom metabolism by Si results in a physiological cascade that affects diatom primary productivity, potentially altering regional carbon and silica cycling. This situation is evident in Antarctic diatoms which have high cellular ratios Si:C and Si:N and therefore require high silicate concentrations to achieve optimal growth (Jaques, 1989), although dissolved Fe plays a major role in altering both Si:N stoichiometry and growth (Moore et al., in press). Thus the NO_3:Si ratio combined with Fe availability significantly effects diatom/non-diatom community succession, with implications for food chains, export rates and CO_2 sequestration (Brzezinski et al., 2002; Sarmiento et al., 2004a).

Regions characterised by high residual nitrate concentrations, but low chlorophyll concentrations such the Southern Ocean and north-eastern equatorial Pacific are known as high nutrient low chlorophyll (HNLC) regions. Differential export of Si relative to N is known to occur in HNLC waters where zooplankton grazing on diatoms result in much greater regeneration of N than Si, so that Si:NO_3:ratios of <1 were found in the equatorial Pacific and as low as 0.25 in the Southern Ocean (Dugdale and Wilkerson, 1998). These systems are eventually driven into Si limitation when the rate of Si uptake exceeds the rate of Si supply (Geider and La Roche, 2002; Price, 2005; Quigg et al., 2003; Timmermans et al., 2004). However, silicate concentrations alone are not the sole determinant of algal biomass or productivity which instead is co-limited by nitrate, silicate, iron and light (Sunda and

Huntsman, 1997; Boyd et al., 1999, Franck et al., 2000, Read et al., 2000, Geider and La Roche, 2002; Timmermans et al., 2004; Arrigo, 2005; Kudo et al., 2005; Hoffmann et al., 2006; Moore et al., 2006). For example, low Fe concentrations in HNLC regions alter the elemental composition of phytoplankton. A number of studies have demonstrated that diatoms growing under Fe replete conditions have Si:N uptake ratios of ~1:1, while their ratios when Fe limited often exceed 2:1 (Franck et al., 2000; Hutchins and Bruland, 1998; Takeda, 1998; Moore et al, in press). These interactions complicate Si:C:N cycles as well as relative rates of mineral (opal, calcite) and carbon export in the Southern Ocean (e.g. Pondaven et al., 1999; Charette and Buesseler, 2000; Buesseler et al., 2001a).

1.2.2 Micronutrients

Mineral micronutrients such as Mo, Mn, Co, Zn, Cu, N, B, Cl, Mg and Fe are also important for algal growth, as are a number of organic substrates, especially vitamins, that are required for sustained plant growth (Knox, 1994). Iron has received more attention than other trace elements because 40% of the world ocean is thought to be Fe limited (Moore and Abbot, 2002). Radiotracer studies indicate that Fe is rapidly cycled within the planktonic community and is subject to the same uptake and regeneration processes that occur for other major nutrients (Hutchins et al., 1993). Iron is a particularly important micronutrient within photosystems I and II and is also instrumental in the biosynthesis of chlorophyll. It is a main component of ferrodoxin, which facilitates the intracellular transfer and storage of photosynthetically incorporated energy and Fe occurs in both nitrate and nitrite reductase (Verstraete et al., 1980). These Fe dependent enzymes reduce nitrate via nitrite into ammonium, which is required for the synthesis of amino acids and proteins (Raven, 1988, 1990; Sunda and Huntsman, 1997; Boyd et al., 1999; de Baar et al., 2005) Nitrate assimilation and reduction increases the iron requirement for growth by 60% and N_2 fixation by about 100 fold (Raven, 1988; de Baar, 1994; Geider and La Roche, 1994), while the assimilation of ammonium requires less iron. Hence in open ocean regions with extremely low iron concentrations (<0.2 nM), nitrate uptake becomes Fe limited (e.g. Lucas et al., in press) and instead, phytoplankton become reliant primarily on ammonium within a recycling ecosystem. Under these conditions, biomass accumulation and export into deeper waters is limited (de Baar et al., 1997), thus

indirectly contributing to the raised atmospheric CO_2 concentrations typical of previous and present interglacial periods (Martin et al., 1990). Martin's (1990) "Iron Hypothesis" was based on the theory that the lowered atmospheric CO_2 concentration observed during the Last Glacial Maximum was due to increased phytoplankton production and sequestration of atmospheric CO_2, which he proposed was a result of increased iron supply to the Southern Ocean at that time.

Iron enrichment experiments provide evidence that low iron concentrations limit productivity and control species diversity in many oceanic algal communities, particularly those in HNLC regions (Martin et al., 1989, 1991; Moore et al., 2006; Moore et al., in press). Fe has been found to sequentially stimulate net chlorophyll increase, carbon build up, nitrate ; uptake and PO_4 uptake in that order (de Baar et al., 1990; Scharek et al., 1997; Martin et al., 1990, Moore et al., in press, Lucas et al., in press). Other experimental studies by Price et al., (1991,1994) in the west equatorial Pacific showed that Fe additions stimulate NO_3 reduction and CO_2 fixation in cells >3μm but not in picophytoplankton, however, studies by Greene et al. (1994) in the equatorial Pacific concluded that all size-classes were Fe limited to some extent, including picophytoplankton.

Mesoscale Fe fertilisation experiments in HNLC environments of the equatorial Pacific: IronEx I (Martin et al., 1994) and IronEx II (Coale et al., 1996) and the Southern Ocean: SOIREE (Boyd et al., 2000, Boyd and Law, 2001), EISENEX (Gervais et al., 2002), SOFEX (Coale et al., 2004) EIFEX (Hoffmann et al., 2006), and KEOPS (Blain et al., 2007) provided convincing *in situ* evidence for the Fe dependence on phytoplankton growth, particularly by diatoms (de Baar and Boyd, 2000, 2007; de Baar et al., 2005). Without exception, these experiments resulted in increased chlorophyll-a biomass, increased NO_3 'draw-down' and improved photo-physiological competency as shown by elevated Fv/Fm values after Fe additions. However, evidence for higher rates of particulate carbon or nitrogen export associated with elevated productivity in Fe-fertilised patches is ambiguous, despite strong evidence for CO_2 draw-down based on fCO_2 values (e.g. Bakker et al., 2001; 2005; 2006).

Satellite observations of the Southern Ocean have revealed the presence of persistent blooms associated with most of the sub-Antarctic islands (Moore et al., 2002; Korb et al., 2004; Venables et al., in press), prompting the suggestion that these regions of shallow bathymetry may be naturally fertilising the seas surrounding them with iron (Owens et al., 1991; Blain et al., 2001; Bucciarelli et al., 2001; Moore and Abbott, 2002; Korb and Whitehouse, 2004; Holeton et al., 2005; Pollard et al., in press; Venables et al., in press). The extended time-scales and perennial nature of the blooms surrounding such islands offer potential advantages in understanding the complexities of Fe interactions in planktonic communities relative to those generated by artificial iron fertilisation experiments. The interdisciplinary CROZet natural iron bloom and EXport experiment (CROZEX) was designed to investigate one such naturally occurring bloom in the vicinity of the Crozet islands (Pollard et al., in press) to establish whether the bloom resulted in elevated particulate organic carbon and nitrogen export below the seasonal thermocline as a result of natural Fe fertilisation. (Planquette et al., in press; Seeyave et al., in press; Lucas et al., in press; Moore et al., in press and Salter et al., in press) have collectively established, respectively, that natural Fe fertilisation of the region to the north of the Crozet islands results in elevated phytoplankton biomass and production, improved nitrate uptake, improved physiological competency (Fv/Fm) and increased POC/N export.

In contrast to the HNLC regions, primary production in the permanently stratified oligotrophic regions is limited by macronutrients year round (e.g. N Atlantic: Graziano et al., 1996; Mills et al., 2004). Despite the low ratios of Fe:NO_3 in upwelled waters of the tropical and subtropical North Atlantic (Fung et al., 2000; Wu and Boyle, 2002), the spring bloom results in the complete removal of NO_3 from the mixed layer. The supply of Fe through mineral aerosols from the African continent (Gao et al., 2001) is thought to be sufficient to preclude Fe limitation of phytoplankton growth. However, studies in the North Atlantic indicate that in certain areas, phytoplankton production is indeed limited by Fe availability (Moore et al., 2006; Martin et al., 1993; Fung et al., 2000; Mills et al., 2004). These results demonstrate the significant role in aeolian Fe supply in controlling the initiation, duration and magnitude of the spring bloom (Moore et al., 2006).

Aeolian iron fluxes are the principal source of Fe to the open ocean and its supply is coupled both to land use and the hydrological cycle (Fung et al., 2000) as episodic aridity affects aeolian Fe supplies. In the future, Fe fluxes to the ocean could increase because of increased evaporation of soil moisture or decrease because of increased precipitation (Dai et al., 1997). Aeolian inputs are also highly spatially variable with about half the global aeolian input entering the North Pacific Ocean, from mainland Asia, and a third deposited into the North Atlantic from the Sahara (Duce and Tindale, 1991; Jickells and Spokes, 2001).

1.2.3 Light, mixed layer depth and Sverdrup's Critical Depth

The amount of photosynthetically available radiation (PAR) arriving at the sea surface is dependent upon latitudinal, seasonal and diurnal affects. These include meteorological conditions such as cloud cover and optical thickness, atmospheric aerosols and their composition. As light enters the oceans it is further modified by absorption and scattering of the water itself, and by dissolved organic materials and particles, including phytoplankton.

Light attenuation with depth approximately follows an exponential function, the attenuation co-efficient (k_d). Light penetration determined from k_d nominally defines the euphotic zone (the 1% or 0.1% light depth), where light is sufficient to support net primary production. The compensation depth (Dc) is defined as the depth at which the oxygen consumed by a cells' respiration over a 24 hour period, equals the amount produced by photosynthesis. The average Dc frequently corresponds to the 1% or 0.1% light depth (Falkowski and Raven, 1997). In aquatic environments, the surface mixed layer (SML) is usually identified by thermal or density profiles that reveal an upper isopycnal (i.e. equal density) layer separated from a lower, denser layer by the pycnocline. If, for example turbulent mixing creates a SML that is deeper than the euphotic zone, phytoplankton will likely spend more time in an unfavourable light environment. Under such conditions, integrated water column photosynthesis is likely to be less than integrated community respiration so that phytoplankton cannot sustain net positive growth. The depth at which gross primary production, integrated through the water column over a day, equals the daily water column integrated respiratory rate is called the critical depth (DCr) (Sverdrup, 1953). The DCr is almost always greater

than Dc (Parsons et al., 1984) and when the SML is shallower than DCr, phytoplankton are maintained within the euphotic zone, and as long as nutrients are in excess, net organic carbon fixation can increase, resulting in a bloom. However, as chlorophyll increases in the surface layer, DCr shoals because K_d increases, making blooms ultimately self light-limited (Figure 1.4).

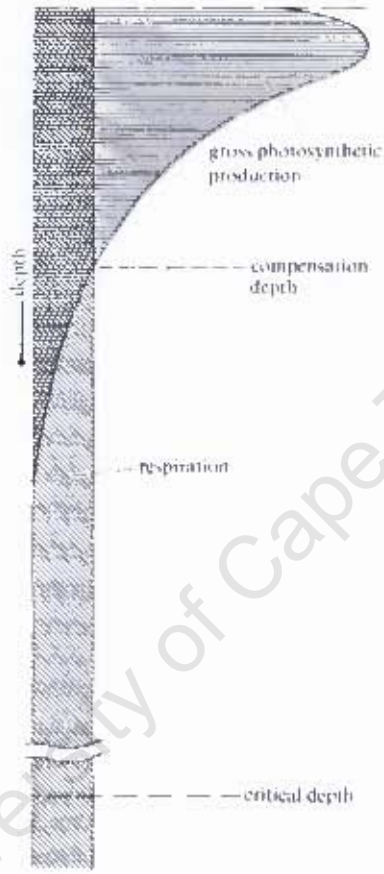

Figure 1.4. The relationship between gross primary production, respiration and depth. The compensation depth (Dc) is the depth at which the oxygen consumed by respiration equals that released by photosynthesis (over a 24 hour period). The critical depth (DCr) is the depth at which the area under the photosynthesis curve equals that under the respiration curve. Figure reproduced from Stewart and Evans (1978).

1.2.3.1 Adaptations to a changing light field

Of the factors that limit primary production (light, nutrients, CO_2, temperature), light is the most variable. Surface irradiances can be at levels so high as to be damaging, to low levels at depth that cannot support photosynthesis (Kirk, 1994). One way of examining the light-dependent responses of photosynthesis is to experimentally construct photosynthesis vs. irradiance (P vs E) curves (Sakshaug et al., 1997). The

physiological parameters of P. vs. E. curves can be divided into three distinct regions, namely a light limited initial slope (α), a light saturated region (P_{max}), and a photo-inhibited region at high irradiances (β). The index of photoadaptation, E_k, is defined by P_{max}/α which represents an irradiance optimum. An idealised P vs E curve is shown in Figure 1.5. The light intensity required to attain P_{max}, the slope (α) and the light value for E_k vary considerably between species and depend on CO_2 concentration, temperature and the previous light history that cells have experienced. The photoinhibition parameter β, describes the increasing destruction of photosynthesis at excessively high irradiances, although there is some doubt since this parameter may be an artefact of the experimental procedure (Falkowski and Raven, 1997).

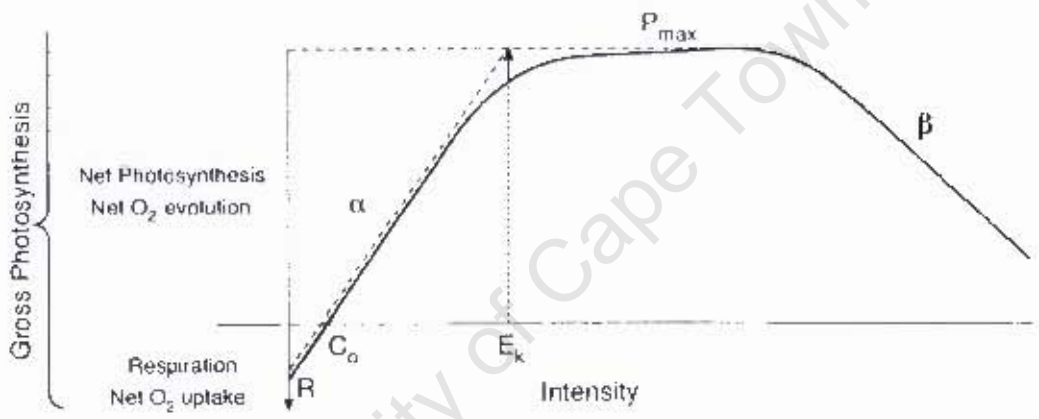

Figure 1.5. An idealised photosynthesis vs. irradiance curve (P vs E). The initial slope (α) is the light limited slope, the light saturated rate is (P_{max}), and the photo-inhibited region at high irradiances (β). The index of photoadaptation, E_k, is defined by P_{max}/α which represents an irradiance optimum. Co is the compensation light intensity where photosynthesis balances respiration. Figure adapted from Falkowski and Raven (1997).

The value of P vs E curves is that they describe the adaptive responses of phytoplankton to variable light regimes. For example, diatoms from surface waters characteristically exhibit high values for P_{max} and E_k, meaning that they grow fast at high irradiances to which they are typically adapted. Conversely, phytoflagellates, that frequently characterise the deep chlorophyll maximum (DCM), are adapted to low irradiances; as reflected in typically low P_{max} and E_k values. Taking this further, should diatoms be advected to a depth characterised by low irradiances, they may be unable to photosynthesise within their light saturated range and may also be out-competed for light by phytoflagellates which are able to attain P_{max} at depth.

Similarly, if phytoflagellates, that normally inhabit the DCM, are subjected to excessive surface irradiances, their delicate photosynthetic machinery may be damaged. This is reflected in their strong photoinhibition (Yoder and Bishop, 1985; Kirk, 1994; Sakshaug et al., 1997).

Variations in photosynthetic responses to changing light environments occur on both short and long time scales. Long time scales refer to ecological and evolutionary adaptation by assemblages through selection of phenotypic traits. Short time scales represent physical, biochemical and physiological responses within the life span of individuals or assemblages of organisms. These responses are collectively called acclimations (Falkowski and Raven, 1997). When a photosynthetic organism is placed for a long period of time in a given light regime, it acclimates to that regime within the limits of its genetic potential and environmental constraints by changing its pigmentation. Thus, phytoplankton communities synthesize appropriate chlorophylls and carotenoids to optimize their light harvesting capabilities (Kirk, 1994).

One adaptive response by phytoplankton to high light intensity is to reduce the quantities of photosynthetic light harvesting pigments. Another is to increase the concentration of photoprotective carotenoids. Carotenoids such as β-carotene and zeaxanthin do not transfer excitation energy to the reaction centre and consequently screen the cell from excess light (Siefermann-Harms, 1985).

Conversely, adaptation to low irradiance can take the form of lowering respiration rates or increasing their investment in light harvesting pigments. For example, as much as a five- to tenfold increase in chlorophyll-a per cell has been observed with decreasing irradiance (Falkowski, 1980; Prezelin and Matlick, 1980; Ramus, 1990; Richardson et al., 1983). There are two basic ways to increase the photosynthetic pigment content. Firstly, acclimation is accomplished by increasing the number of photosynthetic reaction centres while the absorptive cross-section of the reaction centres remains relatively constant. The second is characterised by large increases in the functional size of the antennae serving the reaction centres, while the number of reaction centres remains relatively constant (Falkowski et al., 1980). Accessory photosynthetic pigments may also increase to a greater extent than chl-a as light intensity decreases (Dring, 1990).

1.2.4 Temperature

The temperature dependence of light-saturated photosynthesis has been well established (e.g. Knox, 1994) and is expected because carbon fixation is controlled by enzymatic processes. When the photosynthetic rate of a phytoplankton population is measured under saturating light, at a range of temperatures, the photosynthetic rate per unit biomass will increase with temperature, then level off and finally begins to decrease again. Thus there is a temperature optimum that varies in accordance with the temperature of the normal habitat of the organism. The reasons for decreased photosynthetic rates at temperatures above the optimum are not well understood, but de-naturation of enzymes, a runaway increase in respiration and other forms of thermal damage are probable causes (Kirk, 1994).

The effect of short-term changes in temperature on the P vs. E parameter, α, is relatively minor (Malone and Neale, 1981; Tilzer et al., 1986). However, as P_{max} is strongly affected by temperature, there is a reduction in E_k at low temperatures (Cote and Platt, 1984; Cota et al., 1994). The effects of reduced temperatures are comparable to those due to increased irradiance (photoacclimation), since low temperatures tend to reduce cellular chlorophyll (Davison, 1991). These alterations reduce light adsorption capacity while increasing photosynthetic capacity. The effect is that P_{max} rates per unit carbon biomass can often be maintained at reduced temperatures, while simultaneously reducing the susceptibility of the cell to photoinhibition (Falkowski and Raven, 1997).

Nevertheless, in natural ecosystems there is little temperature adaptation in most oceanic phytoplankton species and the lack of temperature-dependent photosynthetic rates is more likely due to the dominance of different and presumably genetically adapted species in different temperature environments (Yentsch, 1974). A notable exception, however, is seen in the nutrient-saturated Antarctic ocean. Studies have show that when light energy is low, due to short days and/or deep mixing, the carbon mass balance of phytoplankton is mainly controlled by respiration rates, which are more temperature sensitive than photosynthesis (Tilzer and Dubinsky, 1987). Low temperatures enable the algae to efficiently conserve carbon and stored energy.

However, if temperatures were to rise even slightly, the maintenance of biomass might no longer be possible due to increased respiratory losses.

Despite the adaptations of Antarctic phytoplankton to variable light conditions and low light intensities, the photosynthetic capacity (photosynthesis per chl-a at optimum light) and maximum quantum yield of photosynthesis (moles CO_2 assimilated per mole light quantum absorbed) are on average smaller by a factor of 7 and 4 respectively, than in phytoplankton at lower latitudes. This suggests that in Antarctic waters constraints on the efficiency of photosynthetic energy conversion imposed by low temperature become rate limiting in otherwise light saturated situations, and ultimately restrict phytoplankton productivity (Tilzer et al., 1985).

1.2.5 Resource co-limitation

Resource co-limitation has replaced the old notion of a single limiting resource with a more complex view that allows for limitation by multiple resources, both at the individual and community level Arrigo (2005). Resource co-limitation is observed most commonly in oligotrophic oceans, where high irradiance at low latitudes effectively ensures a permanently stratified water column and limitation.

Arrigo (2005) defines three distinct categories of nutrient co-limitation that apply most often in the marine environment. In the first, *multi-nutrient co-limitation* exists when two or more nutrients are limiting. For example the simultaneous addition of both P and Fe is required to simulate growth of N_2 fixing bacteria in the tropical North Atlantic (Mills et al., 2004). In the latter two cases, although both resources may be limiting, the addition of only one is required to elicit a growth response. In *biochemical co-limitation* a single species responds to the addition of one limiting resource which facilitates the uptake of the other limiting resource. The uptake of one of the nutrients depends on its concentration and on the cellular machinery available for its assimilation, whereas the other nutrient (often a trace metal) is integral to the functioning of the machinery required for its assimilation. For example where inorganic P is limiting, some phytoplankton can access the dissolved organic P (DOP) pool (Dyhrman and Palenik, 2003), but this requires a trace of zinc (Zn), such that at reduced Zn concentrations, the ability to access the DOP pool is compromised

(Arrigo, 2005). In *community co-limitation*, members of the community are each limited by a different nutrient so that an increase in one nutrient resource will create a growth response from one segment of the community. For example in well stratified Fe-replete oligotrophic subtropical waters where N_2 fixing cyanobacteria are abundant and N and P are scarce, addition of NO_3 stimulates non-N_2 fixers that are capable of fixing DOP. Addition of P on the other hand stimulates *Trichodesmium* growth by supporting their high N requirement through N_2 fixation (Karl et al., 1997; Wu et al., 2000).

Another example of co-limitation is that between light and nutrients as phytoplankton production requires both resources to grow. In subtropical regions, light limitation is confined to the thermocline region, where shade adapted communities take advantage of nutrients diffusing across the nutricline, but in high latitude HNLC regions, for example the Southern Ocean, there is frequently both light and Fe co-limitation throughout the euphotic layer (de Baar et al., 2005). In addition to the potential for reduced growth rates as a direct result of low mean irradiances in deep mixed layers, the physiological effects of light and Fe co-limitation impair the photochemical efficiency of photosystem II (PSII) and photosystem I (PSI) electron transport systems further reducing phytoplankton growth (Raven, 1990; Sunda and Huntsman, 1997; de Baar et al., 2005; Moore et al., 2006 and Moore et al., in press).

In well-stratified tropical and subtropical oceans, surface irradiance is always sufficient for growth, but nutrients are limiting. However, at the base of the surface mixed layer ambient NO_3 concentrations increase dramatically, providing a nutrient source to phytoplankton able to make use of it, but the disadvantage is that irradiance is greatly reduced. As nutrients are limiting at the surface, low light adapted phytoplankton communities accumulate within a deep chlorophyll maximum (DCM) which is dominated by pico and nanophytoplankton (Zubkov et al., 1998; 2000). Small size confers a competitive advantage relative to large cells when taking up nutrients at low concentrations as occurs within the thermocline. Larger cells do however occur in the DCM and certain large diatom species have developed an effective mechanism for overcoming nutrient limitation in oligotrophic gyres by regulating their buoyancy to commute between the deep nutricline and the sunlit surface layer (Villareal et al., 1999). The primary advantage of large phytoplankton

occurring at low densities in a nano- and picoplankton dominated environments is that they experience comparatively low grazing pressure (Riebesell and Wolf-Gladrow, 2002).

1.2.6 Consequences of phytoplankton size structure on grazing and export

A "bottom-up" control of pelagic ecosystems from plants to predators is mediated by fluxes of essential nutrients (e.g. nitrate) into the euphotic zone (Falkowski et al., 1998). In addition to growth rate limitation, "top-down" controls, including zooplankton grazing, exert a strong influence on ecosystem structure and the accumulation of biomass (Smetacek et al., 2004). Both processes are important regulators of organic carbon export into the deep ocean (Azam et al., 1983; Tremblay and Legendre, 1994), which is mainly governed by the rate at which particles sink, or are consumed and is largely size-dependent (Probyn, 1992; Hansen et al., 1994; Smetacek et al., 2004; Thingstad et al., 2005). However, the magnitude of organic matter flux also depends on the rates of mineralisation within the water column which, apart from size structure and sinking velocity, also depend on the elemental composition of the exported material (Treguer et al., 2003) and the way in which particles are modified by zooplankton and their different feeding strategies, of which the latter is not well understood (Lochte et al., 2003). Among fast-sinking particles are diatom aggregates and large faecal pellets such as those of salps, pteropods, euphausiids, large copepods and pteropods. These large organisms are able to ingest microbial-sized particles and repackage them into large and rapidly sinking faeces (Treguer et al., 2003) which may sink at speeds of 100's to 1000's of meters per day (e.g. Madin, 1982; Noji et al., 1997), thereby avoiding degradation in the mesopelagic zone and becoming important vehicles for the transport of organic matter into the deep ocean.

Phytoplankton may be classified into three main size categories based on their cell diameters (e.g. Sieburth, 1979) which include small picoplankton (0.2 – 2 μm) such as prochlorophytes, *Synechococcus* spp. and small eukaryotes. Medium sized nanoplankton (2 - 20 μm) include prymnesiophytes, pelagophytes, small diatoms and dinoflagellates. Larger microphytoplankton (>20 – 200 μm) are dominated by larger diatoms and dinoflagellates. Since each size class of phytoplankton exerts a unique

impact on its biotic and abiotic environments, spatial transitions and seasonal variability in the abundance and taxonomic composition of phytoplankton biomass are of great importance to biogeochemical cycling and ultimately to climate change (Sarmiento and Bender, 1994; Gibb et al., 2000).

Two pathways dominate energy flow in all ecological situations (Jaques, 1989). Firstly, mesozooplankton (~3-5mm in length), feeding on microphytoplankton, typify a short food chain where carbon is efficiently passed to higher trophic levels with minimal respiratory CO_2 losses. For example in coastal upwelling regions, seasonally mixed temperate and boreal seas and divergent sub-polar gyres or mesoscale features, where nutrients can support transient chlorophyll concentrations >5 mg m^{-3} (Walsh et al., 1978; Falkowski et al., 1991). In such conditions, a competitive advantage is conferred to larger cells by their ability to rapidly take up nutrients. Blooms occur when the fast-growing larger phytoplankton (e.g. diatoms) temporally escape their slower growing grazers (who regenerate via larval stages and have a reproductive delay of a few days) (Falkowski et al., 1998). Hence, the production of large phytoplankton and grazing losses become temporarily uncoupled (Smetacek et al., 1978), and the vertical flux of organic matter into the ocean interior is greatly enhanced through the rapid sinking of large diatoms and faecal pellets (Falkowski et al., 1998; Tremblay et al., 2000). With subsequent nutrient limitation, individual cells often form large and rapidly sinking aggregates that also scavenge other particles from the water column (Alldredge and Silver, 1988), further enhancing the export of carbon and bio-minerals into the oceans interior.

Secondly and alternatively, small nano-/picophytoplankton and microzooplankton characterise the microbial food web (Azam et al., 1983) which has many steps in the food chain and is inefficient at energy transfer or carbon export. This food web predominates in nutrient poor central ocean gyres and in HNLC regions where small cells numerically dominate the phytoplankton community as they are better able to scavenge nutrients at low ambient concentrations (Koike et al., 1981, 1986; Holm-Hansen, 1985; Probyn and Painting, 1985, Hudson and Morel, 1993; Sunda and Huntsman, 1995, Timmermans et al., 2001; 2004). At some point however, the benefits of a smaller cell-size in terms of nutrient acquisition are likely to be offset by increased mortality due to grazing by microzooplankton with comparable fast growth

rates (Banse, 1982). Hence, any increase in biomass on alleviation of nutrient limitation, may be minor, with the population size of small phytoplankton ultimately being controlled by severe microzooplankton grazing pressure (Cullen, 1991; Price et al., 1994; Smetacek et al., 2004). In such ecosystems, very little organic matter escapes remineralisation (Azam, 1998) and only weak biological CO_2 draw-down is observed or there is a net CO_2 source to the atmosphere (Karl, 1999). Nevertheless, in a recent study, Richardson and Jackson, (2007) concluded that despite their small size, picoplankton may contribute more to oceanic carbon export than is currently recognised.

1.3 The ballast effect

Processes that regulate the synthesis and sinking rates of organic matter have the potential to affect the magnitude of the biological carbon pump, and in turn, the flux of CO_2 from atmosphere to ocean. Although the density of particulate organic matter (~1.05 g m^{-3}) is roughly equivalent to that of seawater (~1.03 g m^{-3}), time series sediment traps have established that this material nevertheless sinks rapidly into the deep sea (Francois et al., 2002; Lam and Bishop in press), facilitated by particle aggregation (Honjo et al., 1982a; 1982b; Honjo and Manganini, 1993) and ballasting by minerals (Ittekkott, 1993; Armstrong et al., 2002). Multiple correlation analysis of deep (>1000 m) sea sediment trap data (Armstrong et al., 2002, Klaas and Archer, 2002) have identified a strong correlation and near constant ratio between POC and ballast mineral fluxes, implying that the association promotes efficient POC transfer to depth (the "ballast effect"). Lithogenic (clay particles, dust) and biogenic (silicate and carbonate) ballast materials are denser than either seawater or typical organic matter and are thus thought to provide the density differential needed to promote sinking (Armstrong et al., 2002). Two major phytoplankton groups produce ballast minerals; the coccolithophores which form calcareous coccoliths (particulate inorganic carbon, PIC) through calcification, and diatoms which form opaline frustules (biogenic silica, BSi) through silicification (Poulton et al., 2006a) (Figure 1.6a,b).

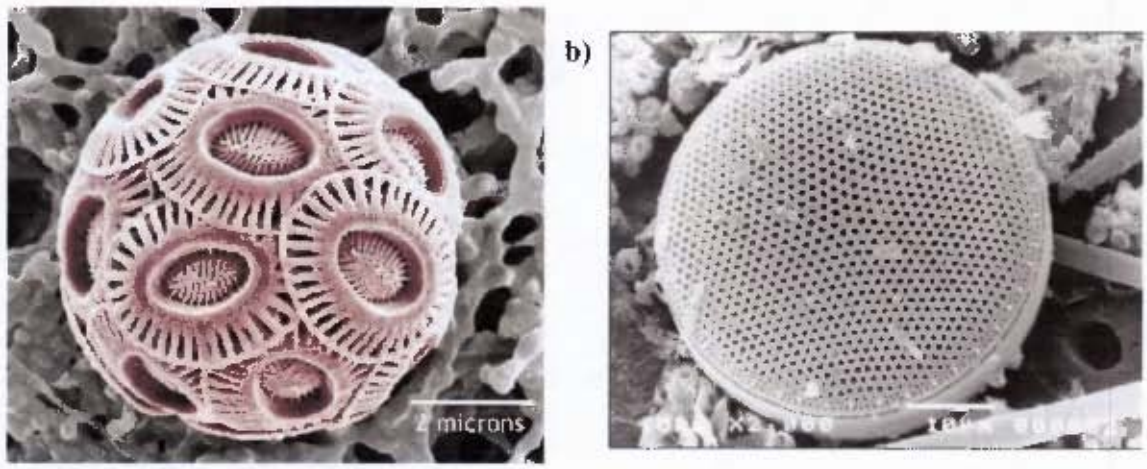

Figure 1.6. Scanning electron microscope (SEM) images of a) a coccolithophore with calcareous coccoliths (particulate inorganic carbon, PIC plates) formed through calcification and b) a diatom encased in an opaline frustule (biogenic silica, BSi) formed through silicification. Figure a) sourced from http://staffwww.fullcoll.edu and b) from http://www.uib.no.

The fate of particulate matter produced within the euphotic zone is governed by competition between dissolution/remineralisation and export, with a return to the solution phase being enhanced by long residence times in the upper ocean. Intrinsic physical properties governing dissolution (e.g. temperature, residence times, ambient concentrations) combine with biological processes (e.g. aggregation, grazing, bacterial action) to control the balance between dissolution and export (Ragueneau et al., 2000). Calcite has a density of 2.71 g m^{-3} and is considered the more effective ballast material as it is denser than opal (2.0 g m^{-3}) and more abundant than terrigenous material (Hurd and Theyer, 1977; Klaas and Archer, 2002) and it has a lower susceptibility to dissolution compared to opal in the upper ocean (Nelson et al., 1995; Nelson and Brzezinski, 1997). The ballast composition also significantly affects the sinking rates of particles, and when significant, decreases particle transit time between the surface and deep-ocean. As a result, for a given remineralisation rate, regions with faster settling particles are expected to have more POC penetration to depth than regions with slower settling particles (Francois et al., 2002; Klaas and Archer, 2002; Lam and Bishop (in press). Additionally, mineral ballast can provide physical or chemical protection to the associated organic carbon from degradation through adsorption or other interactions between organic matter and minerals (Armstrong et al., 2002; Passow et al., 2003).

However, processes underlying correlations between POC and biomineral fluxes are not well understood. For example, it has been suggested that organic aggregates can

scavenge non-sinking mineral material, in which case the POC flux may determine biomineral flux to the deep-sea and not the reverse (Passow, 2004; Passow and De La Rocha, 2006). Francois et al. (2002) confirmed the importance of carbonate ballast for transferring POC to the deep sea, however, their results showed that POC flux to the deep sea was unaffected by the accompanying flux of biogenic opal. and suggested that although diatoms play an important role in surface water carbon export (Buesseler, 1998; Sarmiento, 2006), their role in POC export to the ocean interior may be limited (Ragueneau et al., 2006). These findings suggest that excess density cannot be the only mechanism explaining the correlation between POC and ballast minerals. Instead, Francois et al. (2002) proposed that calcium carbonate plays an indirect role in POC flux, either by altering the labile nature of POC, or by affecting the porosity or packaging of aggregates. Thus in less seasonal, warm, oligotrophic carbonate-dominated systems, organic material is processed by more complex food webs before being exported from the euphotic zone in tightly packaged, refractory and hydrodynamic faecal pellets that facilitate export to the deep sea. By contrast, in colder more seasonal and highly productive regions where diatoms dominate, high opal flux may export more labile organic matter in looser, less hydrodynamic aggregates that can disaggregate easily and so be more effectively remineralised during transit to the deep sea (Francois et al., 2002). These results were substantiated by Lam and Bishop (in press) who found that regions characterised by a high surface biomass of large particles are associated with low rates of POC export, suggesting that the simplest models of export which predict increased POC flux with increasing surface productivity and cell size should be viewed with caution.

Contrasting results were however found by Bueseller et al. (2007) in a mesopelagic study (150-500m) that compared the transfer efficiency of POC between the north Pacific subtropical gyre (warm, low productivity, small cells, PIC predominant ballast) and the Northwest Pacific subarctic gyre (cold, high productivity, diatom dominated, BSi predominant ballast). Their results showed more efficient transport of POC through the twighlight zone in the diatom dominated Northwest Pacific suggesting preferential deep ocean POC flux in association with BSi than PIC (Buesseler et al., 2007).

Overall it appears that the mechanisms whereby mineral material and POC become associated (grazing, aggregation) or uncoupled (fragmentation and remineralisation) are more important for particle export than the amount of ballast material provided. These latitudinal differences probably result from regional differences in pelagic ecosystem structure, including differences in the size structure of the phytoplankton and grazer community. Of importance also is the time scale over which grazers are able to respond to rapid changes in phytoplankton biomass and / or composition (Lam and Bishop, in press).

1.3.1 Understanding the oceanic silica cycle

Silica uptake by diatoms and the subsequent dissolution of their frustules exert a major control on the oceanic silica cycle. Direct comparisons between measured production and dissolution rates in several marine habitats reveal that 10% to 100% (mean ~60%) of Si production in the euphotic zone dissolves in the upper 50-100m (Nelson et al., 1995). A simple link between surface processes and the sediment record has often been assumed (DeMaster et al., 1991; Mortlock et al., 2001), as fluxes below the euphotic zone are thought to remain unaltered during further sinking. This is consistent with the idea that rapid export of biogenic opal (e.g. aggregates, faecal pellets) to the sea floor minimises dissolution. However, slower remineralisation of Si compared to carbon (Officer and Ryther, 1980) leads to a relative better preservation of biogenic silica compared to organic carbon during sedimentation and a subsequent increase in Si:C ratios with depth (Ragueneau et al., 2002).

1.3.1.1 Factors affecting the dissolution of biogenic silica

A process that effects the draw down of Si and its associated C or N is the formation of more highly silicified cells (thicker frustules) when limited by temperature (Durbin, 1977), light (Taylor, 1985) or by micronutrients, especially Fe (Takeda, 1998, Timmermans et al., 2004; Moore et al., in press). Silicate metabolism is regarded as a relatively energy-cheap metabolic process (Raven, 1983) so that Si uptake may continue in specific phases of the cell cycle that are prolonged under iron limitation (Claquin et al., 2002), leading to higher silicate uptake per cell. The ecological

consequences of highly silicified cells remain unclear, but a thicker Si wall may make division possible even under low ambient Si concentrations (Claquin et al. 2002) or greater silicification may offer better protection against grazing (Hamm et al. 2003). The growth of heavy, more silicified diatoms under Fe-limiting conditions results in a more efficient draw down of silicate and carbon (silicate pump; Dugdale et al. 1995), leading to low silicate, high nitrate, but low chlorophyll waters (De La Rocha et al. 2000).

Factors influencing the dissolution of biogenic silica (BSi) and so regulating Si and C interactions are summarised by Ragueneau et al. (2006). The slower remineralisation of Si compared to carbon (Officer and Ryther, 1980) is the basis for the silicate pump (Dugdale et al., 1995) and for the increase in Si:C with depth (Ragueneau et al., 2002). Historically, the rates of Si and C remineralisation were studied independently as BSi dissolution was thought to be a physico-chemical process whereas organic carbon remineralisation was considered to be a biological process. Physico-chemical controls on BSi dissolution include temperature, aluminium content, departure from equilibrium and specific area (Nelson et al., 1995; Ragueneau et al., 2000; Van Cappellen et al., 2002), but only temperature is included in recent biogeochemical models (Fuji and Chai, 2005) with an almost 50 fold increase in the specific dissolution rate of opal between 0°C and 25°C (Hurd and Birdwhistell, 1983). However, living diatoms protect their frustules from dissolution with an organic matrix (Lewin, 1961) consisting of glycoproteins and polysaccharides, thus making BSi dissolution from intact diatom detritus remarkably resistant to dissolution even at temperatures as high as 33°C (Bidle et al., 2002). Hence BSi dissolution requires frustules to be stripped of this protective organic matrix (Kamatani, 1982; Bidle et al., 2002), revealing a critical role for bacteria in both BSi and POC regeneration processes (Ragueneau et al., 2006). Conversely, grazing of diatoms by larger zooplankton increases opal preservation. Since diatom silica is not readily assimilated by zooplankton, the majority of the opal consumed is packed into fast sinking faecal pellets which are often covered by an organic membrane that further retards silica dissolution (Nelson et al., 1995). In contrast, oligotrophic oceans are dominated by the microbial food web where faecal pellets produced by microhetrotrophic grazers are too small to sink rapidly (e.g. Gowing and Silver, 1985). Microzooplankton grazing is therefore expected to retain siliceous particles in the surface layer, and may at times

accelerate dissolution by stripping organic matter from the frustule and exposing the silica surface to sea water (Jacobson and Anderson, 1986). This together with the relatively high temperatures of oligotrophic gyres can result in intense near-surface recycling of siliceous material and minimal export. Grazing activity can also increase the number of broken diatom frustules in the water column (e.g. Roman and Rublee, 1980), preparing them for subsequent colonization by bacteria (Ragueneau et al., 2006). The important role that bacteria play in single cells and Si:C decoupling is however attenuated in aggregates as bacteria mostly act on detrital diatoms whereas diatoms in aggregates stay alive longer (Moriceau et al., 2007). Furthermore, the net impact of aggregation is a lowering of Si remineralisation and exchange to bulk water phase because silicic acid is retained inside aggregates (Ragueneau et al., 2006).

1.3.1.2 The opal paradox

Comparisons of global rates of BSi production in surface waters and opal sediment accumulation reveal two different systems. The first are areas where diatomaceous sediments are actively accumulating (coastal upwelling areas, subarctic Pacific and Southern Ocean). These areas have high specific silica uptake rates with a maximum range of 40-60mmol Si m^{-2} d^{-1} in the Southern Ocean and adjoining marginal seas (e.g. Smith et al., 1999; Nelson et al., 2001; Queguiner and Brzezinski, 2002), rising to >200mmol Si m^{-2} d^{-1} in coastal upwelling blooms (Nelson and Goering, 1978; Brzezinski et al., 1997). However, they only account for 10-25% of global biogenic silica production (Nelson et al., 1995). The second system comprises the oligotrophic gyres which have low rates of specific silica production ranging from <0.5-3mmol Si m^{-2} d^{-1} (Brzezinski and Kosman, 1996; Nelson and Brzezinski, 1997; Brown et al., 2003), but owing to their large spatial extent, account for the remaining 75-90% of global silica production (Nelson et al., 1995). In these regions however, virtually no siliceous sediment is accumulating (e.g. DeMaster, 1981), implying almost complete BSi dissolution within the water column and at the sediment surface. This bi-model character of the world's oceans, or the so-called "opal-paradox", suggests that regional differences in silica preservation dominate over regional differences in BSi productivity to produce the observed geographic distribution of opal sediments (Nelson et al., 1995). A more recent study by Pondaven et al. (2000) in the Indian Ocean sector of the Southern Ocean however demonstrates that the overall

preservation efficiency of this region is substantially lower than previously thought (Nelson et al., 1995) and that spatial differences in preservation efficiencies are not the primary reason for the differences observed in sedimentary opal accumulation. They concluded that by reconciling surface production rates with sedimentary accumulation rates, BSi signatures could be used to reconstruct palaeoproductivity when the factors that affect the Si:C ratio are better understood.

An analysis of the Si:C ratio with depth in nine biogeochemical provinces by Ragueneau et al., (2002) showed that some consistency exists in terms of regional or downward variations in Si:C ratios, in that i) regional differences in Si:C during production are conveyed to the sediment water interface and ii) similar increases in Si:C with depth occur in all nine provinces which Ragueneau et al. (2006) attributed to the role of the mesopelagic food web. They concluded that in regions of low export, recycling takes place predominantly in surface waters and that Si : C decoupling is achieved above the depth of export. Conversely, in regions of high export where diatoms bloom, more carbon is exported and Si : C decoupling is achieved in the mesopelagic. Nevertheless, diatom blooms appear to be the main source of opal preserved in sediments (Nelson et al., 1995).

For a given rate of BSi dissolution, the extent of recycling will depend on the residence time of particles in the water column, especially in warm surface waters (Ragueneau et al., 2000). One biological process which reduces the residence time of particles in undersaturated and warm surface waters is the aggregation and mass settlement of diatoms at the termination of a bloom, which reduces the exposed surface area of opal and increases the settling speed of material (Smetacek, 1985; von Bodungen et al., 1986; Alldredge and Gotschalk, 1989; Jackson, 1990; Hill, 1992; Alldredge and Jackson, 1995). Furthermore, sporadic export events may be important contributors to the biological pump as they may lead to a rapid settling flux through a mesopelagic ecosystem not geared to fully exploit it and in so doing bypass substantial remineralisation (Ragueneau et al., 2006). Nelson et al. (1995) suggested that the formation of siliceous sediments is related more directly to the tendency of a region to support occasional diatom blooms than to the total annual primary productivity or annual rate of silica production.

1.3.2 Understanding the oceanic calcite cycle

Unlike silicate, calcium carbonate has historically been considered to have a conservative nature in shallow oceanic waters (e.g., Murray and Renard, 1981, Sverdrup et al., 1941), with significant dissolution only occurring below the chemical lysocline, at approximately 4000-4500 m in the Atlantic Ocean (Milliman et al., 1999), 3000m in the Pacific, and 3500-4500m in the Indian Ocean (Biscaye et al., 1976; Kolla et al., 1976). However an increasing number of observations suggest considerable dissolution of $CaCO_3$ in the upper 500-1000 m of the ocean, well above the chemical lysocline. Milliman et al. (1999) concluded that the same biological processes that promote rapid particulate carbonate sedimentation (i.e. faecal pellet and aggregate production) may result in micro-environments that directly or indirectly facilitate dissolution.

Carbonate sediments blanket much of the Atlantic Basin, and are formed from the shells of both coccolithophores and foraminifera. In the Pacific however, the carbonate compensation depth is generally shallower than the bottom, and hence in that basin, tends to dissolve rather than become buried. Unlike diatoms, coccolithophores do not store nutrients very effectively, but bloom when nutrients are supplied at slow rates. Coccolithophores are therefore primarily found at low abundance in tropical and subtropical seas, and at higher concentrations at high latitudes in midsummer, following diatom blooms. Hence, carbon export by diatoms in spring at high latitudes can be offset by CO_2 out-gassing to the atmosphere with the formation of coccolithophore blooms later in the year (Falkowski et al., 2003). Due to their characteristically small size (5-20 μm in diameter; Baumann et al., 2004) and slow sinking speeds (0.1-0.2 m d^{-1}; Honjo et al., 1976; Balch et al., 1996a; Lecourt et al., 1996), efficient calcite export by slow sinking cells is thought to be insignificant. Rather, active repackaging, either in zooplankton faecel pellets or in "marine snow" is expected to facilitate efficient calcite export as the sinking speeds of such aggregates are relatively fast (~100 m d^{-1}) (Poulton et al., 2006a). The sinking speed and porosity of faecal pellet and marine snow aggregates is also important in determining the degree of calcite remineralisation in the upper ocean (Jansen et al., 2002). Several studies have observed active (and often selective) feeding of micro and macrozooplankton on coccolithophores (Holligan et al., 1993; Harris, 1994;

Nejstgaard et al., 1994; Hansen et al., 1996). In low nutrient environments such as the subtopical gyres, the turnover rate of calcite is more likely to be mediated by microzooplankton (Poulton et al., 2006a). Active feeding on coccoliths also enhances the dissolution of calcite in surface waters which is only possible under acidic conditions, such as may be found in zooplankton guts or within aggregates where decomposition of reduced organic matter lowers the pH.

Apart from the important role that calcifiers play in export, calcification has a further effect on ocean-atmosphere CO_2 exchange by releasing dimethyl sulphide (DMS) to the atmosphere, leading to cloud formation and increased albedo (Charlson et al., 1987), an effect 20x greater for coccolithophores relative to diatoms (Keller et al., 1989).

1.4 Biogeochemical cycles and export in a global context

The paucity of robust long term observations in the remote regions of the open ocean have led to an incomplete mechanistic understanding of the global carbon cycle, especially for key issues related to carbon sequestration in the oceans interior. It was realized that a comprehensive understanding of the oceanic habitat and its biota would require a multidisciplinary experimental approach and extensive field observations. In response to the need for such information, the Joint Global Ocean Flux Study (JGOFS) was established in 1987. During the past two decades, several time series programs have emerged that have collectively contributed to our understanding of biogeochemical processes in the sea. These include the Hawaii Ocean Time-Series (HOTS) (Karl and Lukas, 1996; Karl et al., 2001), the Bermuda Atlantic Time-Series Study (BATS) (Michaels and Knap, 1996; Siegel et al., 2001), the Kerguelen Point Fixe (KERFIX) 60 miles southwest of Kerguelen Islands (Jeandel et al., 1998), DYFAMED in the Northwestern Mediterranean (Marty et al., 2001), European Station for Time-Series in the Ocean Canary Islands (ESTOC) in the North Atlantic ~100 km north of Gran Canaria (Davenport et al., 1999), Kyodo Northwest Pacific Ocean Time-Series (KNOT) in the southwest margin of the North Pacific subarctic gyre (Tsurushima et al., 2002), the South-East Asia Time-Series Station (SEATS) in the south China Sea, the Central Irminger Sea (CIS), the Cape Verde time series site

(CV) and the Porcupine Abyssal Plain (PAP) observatory in the northeast Atlantic (Billett et al., 1983; Lampitt et al., 2001; Vanucci et al., 2001).

Repeated oceanographic measurements provide an understanding of natural processes or phenomena that exhibit slow or irregular change, as well as rapid event-driven variations that are impossible to document reliably from a single field expedition. Time-series studies are also ideally suited to document complex natural phenomena under the combined influences of physical, chemical and biological controls.

1.4.1 Modelling primary production and export

Modelling JGOFS and other time series data sets have allowed a greater appreciation of the interactions between physical and biological processes on a global scale. In the JGOFS program, measurements of radiocarbon assimilation were coupled with high quality phytoplankton pigment analyses to provide a basis for calibrating satellite-based models of net primary production (NPP) (Falkowski et al., 2003). There are several models for estimating global NPP, but fundamentally all models are conceptually similar. The models basically couple data on primary production with satellite-based estimates of phytoplankton chlorophyll concentration and incident solar radiation (400-700 nm) to derive vertically integrated estimates of NPP for the world oceans for each pixel set (generally 20 km by 20 km) (Figure 1.7a,b) (Antoine et al., 1996; Behrenfeld and Falkowski, 1997; Longhurst et al., 1995). The estimates are then averaged for a set of monthly global observations and summed over a year (Falkowski et al., 2003).

The striking feature that emerged from these models is the similar contribution of marine and terrestrial NPP to global NPP (Falkowski et al., 2003). In the context of the global carbon cycle, carbon fixed in terrestrial ecosystems can be "stored" in living organic matter (e.g. forests), whereas carbon fixed by marine phytoplankton is rapidly consumed by grazers and transferred from the surface ocean to the ocean interior as predominantly inorganic carbon (Falkowski et al., 2003). Based on the f-ratio principles of Eppley and Peterson (1979)(a more detailed explanation of the f-ratio follows in section 1.8.8), Laws et al., (2000) developed a model of export production that assumed primary production is partitioned through both large and

small phytoplankton and that the food web adjusts to changes in the rate of "new" nutrient inputs in a way that maximises stability, i.e. how rapidly the system returns to steady state following a perturbation (Figure 1.7c).

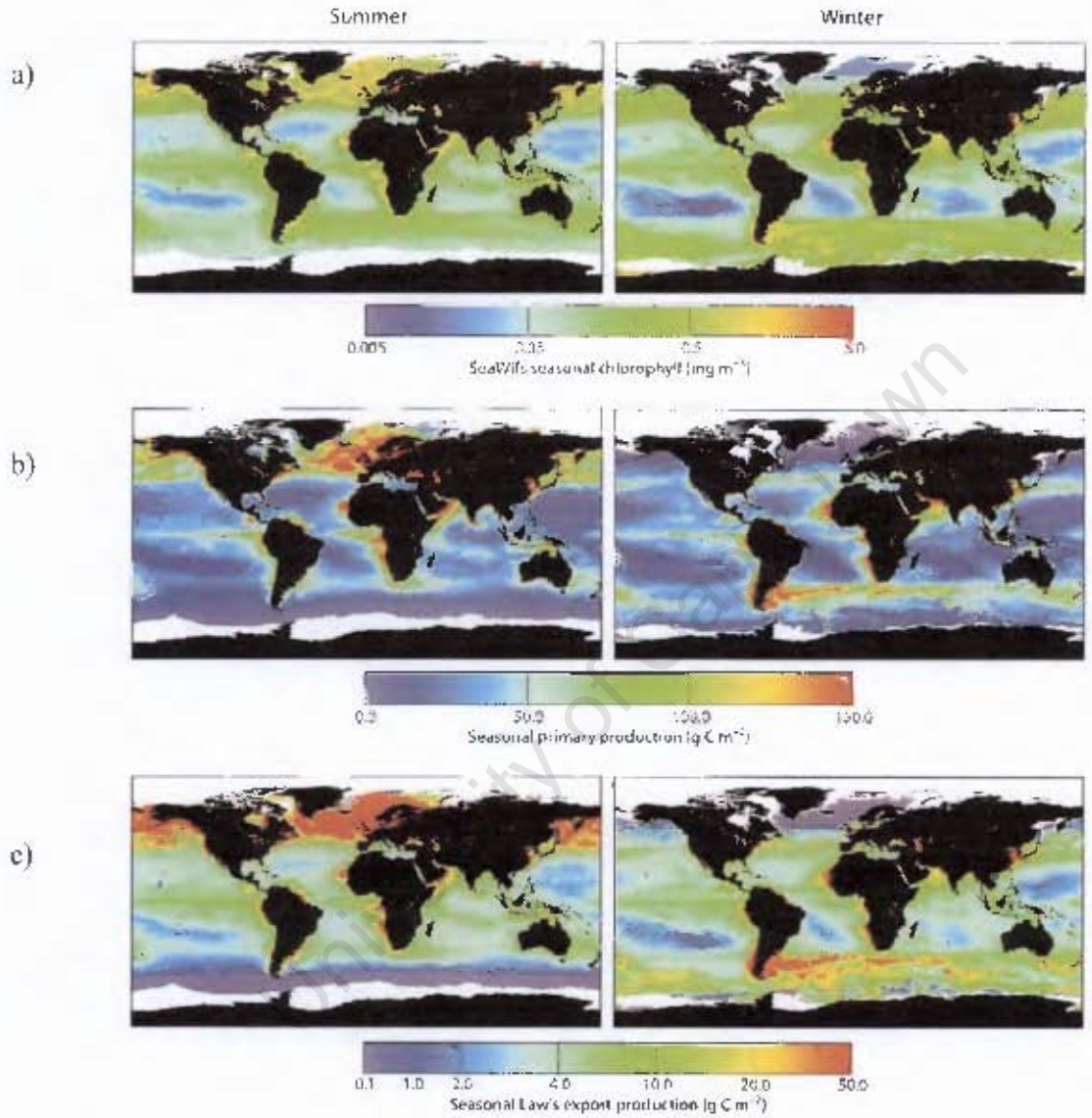

Figure 1.7 Summer (left column) and winter (right column) distributions of a) oceanic chlorophyll, b) primary production, and c) export production. Oceanic chlorophyll fields are derived from standard SeaWiFS ocean colour algorithms applied to 20x20km pixels for the monthly averaged data collected in January-March and June-August 1998-2001. The seasonal chlorophyll maps were used to generate monthly averaged net primary production fields using the algorithm described in Behrenfeld and Falkowski (1997a). Global estimates of carbon export are generated by inputting the primary production fields into an export model described by Laws et al. (2000). Figure reproduced from Falkowski et al. (2003)

The Laws model assumes a balance between new production (NP) and export production (EP) over a time frame of several weeks or more, but this assumption may be violated on a short time frame. Indeed, EP based on ^{234}Th measurements and

primary production illustrate the difficulty of extrapolating export from total primary production in energetic ecosystems (e.g. Buesseler et al., 1992a; 1998; Cochran et al., 2000). Furthermore, nitrification is now known to account for around half of the nitrate consumed by growing phytoplankton (Yool et al., in press), particularly in low latitudes. Model estimates of EP based solely on bulk nitrate uptake will therefore substantially overestimate carbon export on a global scale (Yool et al., in press). While still in its infancy, models have revealed that changes in ocean circulation and stratification can lead to significant changes in EP. In increasingly stratified oceans of the future one might expect diatom blooms to occur less frequently or with lower amplitude, and that coccolithophores might become relatively more abundant (Falkowski et al., 2003), having a significant effect on the ability of the oceans to take up excess anthroprogenic CO_2.

1.5 The AMT programme (1995-2000)

During JGOFS and other time series programs, most studies were carried out in coastal, meso- and eutrophic waters, neglecting the north and south Atlantic oligotrophic gyres. Much of what is known about oligotrophic gyres comes from the US JGOFS Hawaii Ocean Time Series (HOTS) (Karl and Winn, 1991; Karl and Lukas 1996; Karl, 1999), the Bermuda Atlantic Time Series (BATS) (Michaels and Knap 1996; Steinberg et al., 2001) and the North Atlantic Bloom Experiment (NABE) which visited several sites along 20°W and north of 40°N (Ducklow and Harris, 1993; Eglinton et al., 1995). Despite these efforts, conspicuously little was known about the centres of oligotrophic gyres and the north and south Atlantic gyres in particular.

The Atlantic Meridional Transect (AMT) programme sought to approach this lack in available information by undertaking biological, chemical and physical oceanographic research during the annual return passage of the *Royal Research Ship, James Clark Ross* (JCR) through the Atlantic Ocean between the UK (50°N) and the Falkland Islands (52°S), a distance of over 13,500 km. The initial programme completed a series of 12 bi-annual transect cruises which took place between 1995 and 2000 to provide a unique decadal time series of spatially extensive observations on the structure and biogeochemical properties of planktonic ecosystems in the Atlantic

Ocean. In September the JCR sailed southward, sampling the North Atlantic during the boreal fall and the South Atlantic during the austral spring and returned to the UK the following April, sampling the South Atlantic during fall and the North Atlantic in spring conditions. The ship's track crosses a range of ecosystems and physico-chemical regimes within which conditions range from subpolar to tropical and from eutrophic shelf seas and upwelling systems to oligotrophic mid-ocean gyres. The AMT programme thus provided an ideal platform for measuring physical, biological and bio-optical properties and processes through the diverse ecosystems of the North and South Atlantic.

The scientific aims of the initial AMT programme included the acquisition of data for the development of remote sensing algorithms and the functional interpretation of remotely sensed bio-optical signatures, the assessment of mesoscale and basin scale variability in phytoplankton processes and mesozooplankton dynamics. Additional to these were the development of climatologies of key parameters for regional and basin-scale productivity and ecosystem dynamics models.

1.6 An overview of AMT data

Measurements of hydrographic and bio-optical properties, plankton community structure and primary production have led to several important discoveries concerning the characterisation of oceanic provinces (Hooker et al., 2000), the distributions of picoplankton (Zubkov et al., 2000) and the spatio-temporal variability in rates of primary production (Marañón et al., 2000).

1.6.1 General hydrographic features

The predominant large-scale hydrographical and current feature on the AMT transects is the equatorial current system which has a banded structure (Figure 1.8). The North Equatorial Current (NEC) is a region of broad westward flow, north of 10°N, while the South Equatorial Current (SEC) is a broad westward flow extending from about 3°N to 15°S. The easterly flowing North Equatorial Counter Current (NECC) is highly seasonal and is at its strongest during the boreal fall when it is clearly seen between

9°N and 3°N. The strongest equatorial current is the westward flowing Equatorial Undercurrent centred on the equator at a depth of ~100 m (Aiken et al., 2000).

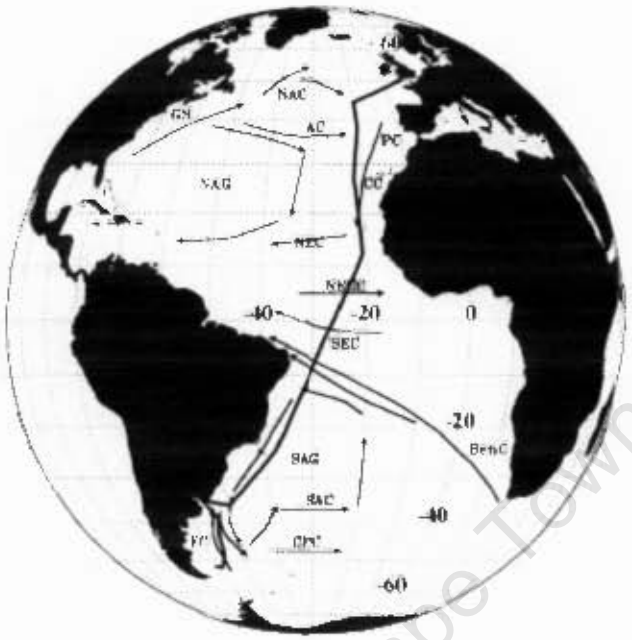

Figure 1.8. The predominant large-scale surface circulation patterns adapted from Tomczak and Godfrey (1994) and showing the AMT-2 cruise track. Figure taken from Aiken et al. (2000).

The subtropical gyres are characterised by a deep pycnocline at their centres and strong horizontal gradients of temperature and salinity at their fringes due to pycnocline outcropping. The pycnocline shoals in mid-latitudes, where isopycnals outcrop at the Subtropical Front (STF) and at the equator, characterised by Ekman divergence that promotes upwelling. The lowest density values are found just north of the equator where the surface water forming the North Equatorial Current/Counter Current is both relatively fresh (minimum salinity 34-35), due to local rainfall and the seasonal influence of the Amazon outflow, and warm (~28°C) (Robinson et al., 2006). The interior zones of the subtropical gyres above the pycnocline are regions of extremely low nutrient concentrations (nano-molar NO_3) and low vertical nutrient re-supply rates across strong temperature and nutrient gradients (Figure 2d). Consequently, phytoplankton biomass is low (~0.2-0.5 µg chlorophyll l^{-1}) throughout the year and takes the form of a deep chlorophyll maximum (McClain et al., 2004). The pycnocline and nitracline shallow at the temperate fringes, around the equator and close to North West Africa and are associated with increased chlorophyll

concentrations. All these features show some degree of seasonality (McClain et al., 2004; Perez et al., 2005a) driven by surface heating/cooling cycles and variations in wind strength. For example, the subtropical convergence (which marks the transition between temperate and subtropical waters) moves poleward in summer and back towards the equator in winter. Deep winter overturning in the temperate North Atlantic injects nitrate into surface waters causing transient high nutrient conditions that can result in a marked spring bloom, with accumulation of phytoplankton biomass. Upwelling occurs throughout most of the year off the NW African region but is strongest in May-June, particularly at 20-25°N (Wooster et al., 1976). Consequently high chlorophyll concentrations are found in this region and have been known to extend for a distance of 350km offshore (Barlow et al., 2004).

1.6.2 Phytoplankton community structure and production

Highest chlorophyll concentrations are found in temperate waters at the northern and southern extremities of the cruise track and are associated with the highest concentrations of microplankton (Gibb et al., 2000). As with concentrations of total chlorophyll, the greatest seasonality in accessory pigment abundance is observed in the temperate regions. The use of accessory pigments as a means to characterise a phytoplankton community is expanded on in section 2.2.3. The (occasional/ temporal) abundance of microplankton in the temperate regions reflects the importance of large eukaryotes such as diatoms during local spring blooms before their succession by smaller organisms such as prymnesiophytes and other nanoflagellates when key nutrients decline (Gibb et al., 2000; Barlow et al., 2002). Higher concentrations of nanoplankton have also been recorded in the temperate regions, but their abundance exhibits a weaker seasonal signal than that of large eukaryotes, suggesting that while nanoflagellates are less well adapted to exploit spring bloom conditions than diatoms, they are a more ubiquitous and stable component of the phytoplankton community for a greater part of the year (Gibb et al., 2000). The spring bloom in the North Atlantic represents the most marked seasonal signal in global maps of oceanic autotrophic biomass (Esaias et al., 1986; Longhurst, 1998) and it is responsible for a considerable flux of organic carbon to the deep ocean (Honjo and Manganini, 1993). The initiation of the spring bloom results principally from a seasonal increase in surface irradiance during spring which triggers the development of water column stratification and a

shoaling of the mixed layer to depths less than the critical depth (Sverdrup, 1953). This transient period of increased light and nutrients (from winter overturning) provides a window of opportunity for blooms to occur. The southern temperate region (>35°S) exhibits additional meso-scale variability in total chlorophyll concentrations that appear to be associated with a region of recirculation cells and eddy structures (see Wilson and Rees, 2000) off the South American Shelf. In temperate waters, the biomass of picoeukaryotes increases and *Synechococcus* in particular are more numerous in spring compared to autumn (Zubkov et al., 2000).

In the equatorial Atlantic, elevated phytoplankton biomass and primary productivity are observed throughout most of the year (Perez et al., 2005a,b). Although increases in nanoplankton (Tarran et al., 2006) and microplankton (Gibb et al., 2000; Barlow et al., 2002, 2004) are observed and tend to contribute more to primary production than to total chlorophyll-a (Marañón et al., 2000, 2001; Perez et al., 2005b), the typical size structure of the community remains dominated by picoplankton (Herbland et al., 1987; Marañón et al., 2001; Zubkov et al., 1998; 2000 Perez et al., 2005b). In coastal upwelling areas (e.g. Mauritania upwelling off NW Africa) elevated chlorophyll and primary productivity are also found, but in these regions nano and microplankton dominate both production and biomass (Marañón et al., 2000, 2001; Tarran et al., 2006).

In the oligotrophic gyres chlorophyll concentrations are generally low with non siliceous picoplankton being numerically dominant (mainly *Prochlorococcus* spp. and picoeucaryotic algae) and comprising a significant fraction of the autotrophic biomass and primary productivity (e.g. Chrisholm, 1992; Marañón et al., 2000; Zubkov et al., 1998; 2000). Consistently low phytoplankton biomass and productivity in oligotrophic gyres reflects efficient top-down control exerted by micro-herbivores on micro-algal assemblages (Banse, 1995). A significant proportion of the primary productivity in oligotrophic gyres is nevertheless also attributed to nano- and microphytoplankton which contribute disproportionately to their share of the biomass (Marañón et al., 2000, 2001; Fernandez et al., 2003). Although diatoms are found in oligotrophic oceans year-round, they are seldom a major component of the phytoplankton assemblage except during spring blooms and at other brief episodes of high productivity (e.g. Hulburt, 1990). Higher concentrations of larger picoeukaryotic

algae are associated with the equatorial region and their biomass can equal that of the *Prochlorococcus* (Zubkov et al., 2000).

Chlorophyll biomass in the southern oligotrophic gyre tends to be higher than in the northern gyre and dominated by picoplankton, whereas nanoplankton and fewer picoplankton tend to dominate in the northern oligotrophic gyre (Barlow et al., 2004). Barlow et al., (2002) have shown that the euphotic zone, nitracline and subsurface chlorophyll maxima tend to be shallower in the southern region (~40 m) than in the northern region (~150 m). This implies that prokaryote cells in the shallower nitracline waters of the southern region exploit a more readily available supply of micronutrients, elevating phytoplankton biomass relative to the north (Barlow et al., 2004). *Prochlorococcus* dominate plant biomass in both the northern and southern gyres. Higher standing stocks of both P*rochlorococcus* and picoeukaryotes are present in spring rather than in autumn in both gyres. Picoeukaryotes are more tolerant of low temperatures and lower light levels and are often more abundant in samples from greater depths, where they contribute to the deep chlorophyll maximum (Zubkov et al., 2000).

1.6.2.1 The Deep Chlorophyll Maximum (DCM)

The low chlorophyll concentrations characteristic of the subtropical gyres are maintained by low nutrient concentrations above the pycnocline and low vertical nutrient re-supply across strong temperature and nutrient gradients. Consequently, phytoplankton biomass positions itself as a DCM, taking advantage of slow diffusive nutrient fluxes across the thermocline or nitracline, but needing to adapt to low light. One adaptation to low light is increased cellular chlorophyll, which makes the DCM a pigment rather than productivity maxima, where the latter is above the DCM (Marañón et al., 2000). Within the subtropical gyres, rates of primary production are considerably more variable than chlorophyll concentration or phytoplankton C biomass. This type of variability has been linked to fluctuations in nutrient flux to the euphotic layer, as estimated from variations in the depth of the nitracline. The precise nature of the relationship between the depth of the DCM and the nitracline is however uncertain. The depths of the DCM and nitracline appear to be consistent with seasonal variations when comparing autumn and summer conditions. However, low rates of C

fixation within the DCM due to light limitation and the dominance of *Prochlorococcus* (most of which are thought not to possess nitrate reductase [Veldhuis et al., 2005; Rocap et al., 2003]) suggest that eukaryotic growth (assuming normal Redfield C:N ratio) can only account for a relatively small fraction of nitrate assimilation within the DCM of the subtropical Atlantic (Robinson et al., 2006), despite apparently high rates of nitrate uptake measured by Painter et al. (in press).

The presence of ecologically distinct phytoplankton residing in the DCM compared to the rest of the euphotic zone advocates division of the euphotic zone into an upper and lower region supported to different degrees by new and regenerated nutrients and therefore providing different contributions to export production. A layered structure is also evident in the pigment distributions, where cyanobacteria (zeazanthin) and prymnesiophytes (Hex) are dominant in the upper 80-100 m, while mixed flagellates are abundant in the DCM and below. Surface waters are additionally characterised by high photo-protective carotenoids (PPC) (attributable mainly to zeaxanthin in cyanobacteria), while in the lower euphotic zone PPC adsorption declines and photosynthetic carotinoids (PSC) and chlorophyll-c adsorption increases. Chlorophyll-b is also most prominent in the DCM due to the increased synthesis of divinyl chlorophyll-b in prochlorophyte cells at depth to maximise their adsorption of low intensity blue light (Barlow et al., 2002).

*1.6.2.2 Trichodesmium distribution along the AMT tran*sect

Filamentous cyanobacteria belonging to the genus *Trichodesmium* represent the major group of N_2-fixing planktonic organisms in the ocean (Capone et al., 1997) and are most common in highly stratified, low nutrient waters of tropical and subtropical latitudes, often forming small- to large-scale blooms which can be seen from space (e.g. Subramanian and Carpenter et al., 1994). Abundances (from AMT) were highest between the equator and ~15°N, and absent or extremely low between 5 and 30°S, while elsewhere abundances were intermediate or more variable in concentration (Tyrrell et al., 2003). Possible correlations between *Trichodesmium* abundance and several physical and chemical variables were examined to elucidate factors that determined their distribution, particularly the relationship between N_2 fixation and iron requirement (Raven, 1988; Rueter, 1998).

The subtropical North Atlantic underlies the path of trade winds blowing westwards from the Sahara Desert, contributing some of the highest particle deposition on the surface of the ocean with associated high iron inputs. This region of high dust flux corresponds well to the areas of highest *Trichodesmium* abundance along the AMT transect (Tyrrell et al., 2003). As dust concentrations over the South Atlantic are much lower than over the (sub)-tropical North Atlantic (Volkening and Heumann, 1990; Losno et al., 1992; Radlein and Heumann, 1992; Bates et al., 2001), owing to much weaker dust sources, the abundance of *Trichodesmium* there diminishes sharply.

Trichodesmium abundance is also well correlated with mixed layer depth and it has been suggested that they are able to migrate vertically via active buoyancy regulation to below the nutricline where they can retrieve phosphate (Tyrell et al., 2003). Such a strategy would clearly be favoured in shallow mixed layers with sufficient irradiance to fuel photosynthesis and migration.

If the distribution of N_2 fixers is controlled by iron input, then it is likely that increased N_2 fixation would occur during the dryer, more arid and dustier ice ages, inferring extra draw-down of atmospheric CO_2 by phytoplankton whose N limitation is reduced. If however, the distribution of N_2 fixers is controlled by the need for a shallow mixed layer to recover P, then climate change could stimulate increased N_2 fixation as the oceans become more strongly stratified (Karl et al., 1995).

1.7 Continuation of the AMT programme (2003-2005)

In 2002, the AMT programme was funded as the first NERC Consortium Grant to address a suite of cross-disciplinary questions concerning ocean plankton ecology and biogeochemistry and their links to atmospheric processes. A primary aim was to provide data for use in the development of models to describe the interactions between the global climate system, plankton functional biodiversity and ocean/atmosphere biogeochemistry (Robinson et al., 2006).

Between 2003 and 2005, six research cruises formed part of the current AMT programme. The first two cruises of the second phase of the AMT Programme

occurred in May/June (AMT12 northbound) and September/October 2003 (AMT13 southbound), focussing respectively on the northern subtropical gyre of the Atlantic and on the upwelling region off NW Africa. Both cruises included transects across the southern subtropical gyre. For AMT 14 (northbound), a comparable track across the southern gyre and the equator was maintained, but a more westerly route north of the equator facilitated sampling of the central northern gyre. The main purpose of work in this region was to determine the trophic state of the plankton ecosystem with respect to large-scale patterns in ambient nutrient concentrations and supply rates.

The specific objectives of the 2003 to 2005 AMT project were to test nine interrelated hypotheses within the following three scientific objectives (Figure 1.9).

1) To determine how the structure, functional properties and trophic status of the major planktonic ecosystems vary in space and time.
2) To determine the role of physical processes in controlling the rates of nutrient supply, including dissolved organic matter to the planktonic ecosystem.
3) To determine the role of atmosphere-ocean exchange and photo-degradation in the formation and fate of organic matter.

Within objective 1, the first four hypotheses are as follows:

Hypothesis 1 -The size spectra, and mineralisation capacity of planktonic organisms are major determinants of CO_2 and organic matter export to the atmosphere and deep water.
Hypothesis 2 - Growth rates of phytoplankton in tropical and subtropical waters are correlated with the f ratio and, for the surface layer, with the relative contribution of nanophytoplankton.
Hypothesis 3 - The biodiversity of the microbial planktonic community significantly influences C, N and P recycling and ecosystem trophic state.
Hypothesis 4 - Basin scale variability in photosynthetic growth rates and pCO_2 flux can be derived from remotely sensed data.

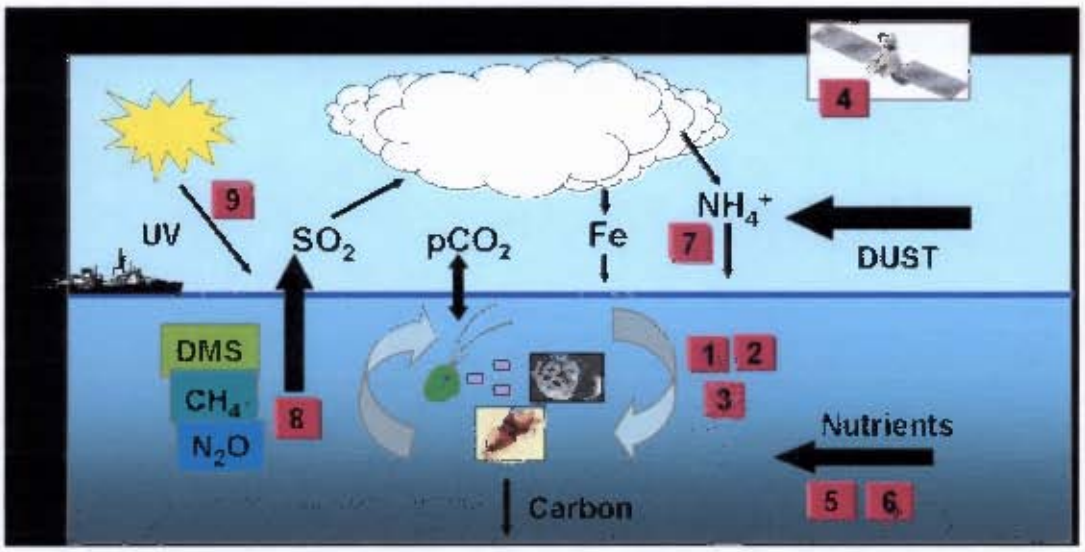

Figure 1.9. Schematic representing the nine interlinked hypotheses that were tested within three specific objectives of the 2003-2005 Atlantic Meridional Transect (AMT) programme. Image source http://web.pml.ac.uk/amt/research/amt_research.htm

One of the main aims of the continued AMT programme that was not covered in the original programme was to quantify and better constrain the role of the North and South Atlantic in the global carbon budget and to specifically measure how much photosynthetically fixed CO_2 is exported below the seasonal thermocline. This aim falls within Objective 1 and provides the main focus of this PhD study which is to provide measurements of carbon export over the North and South Atlantic gyres and to determine the efficiency of the biological pump in transporting carbon fixed at the surface into the deep ocean.

1.8 Review of methods for measuring export

Knowledge of the mechanisms that drive the flux of carbon and other elements into the deep sea is an important prerequisite for understanding the marine carbon cycle and thus the potential impacts of rising atmospheric CO_2 concentrations (Passow et al., 2006).

The downward flux of particulate material from the upper mixed layer of the ocean is one that has a major effect on biogeochemical processes in the oceans and on the earth system as a whole. Loss of this material affects the chemical inventory of the upper ocean and is the principal means by which deep ocean biological communities are

sustained. This flux necessarily decreases with increased depth as the material is remineralised or dissolves and it is widely accepted that the rate of decrease in flux diminishes with depth such that in the deep water column (eg >2000 m), the rate of decrease with depth is slight. Several models have been developed to describe this change in flux with depth (see review by Antia et al., 2001) and although these have a seductive mathematical simplicity, the uncertainties in their predictive abilities in the upper ocean are very large. This is particularly unfortunate as the depth at which the material is remineralised or dissolves determines the time before it is once again able to contribute to the biogeochemistry of the surface ocean and hence be relevant to air sea interactions. For instance carbon dioxide released as a result of remineralised organic matter affects air sea fluxes within a year if remineralisation occurs above the depth of winter mixing (200-800 m depending on location), but if below that depth, carbon is sequestered for hundreds of years. A clear understanding of the rates of change in flux with depth and the factors that control this is obviously of very great importance in ocean biogeochemistry and biology.

There are a variety of both direct and indirect methods that exist that enable us to estimate the flux of organic carbon from surface waters into the deep ocean. Each method has individual pros and cons depending on the environment being studied or the logistical constraints inherent in the study. Below is a review of the more widely used methods for estimating export flux.

1.8.1 New production: f-ratio

The pioneering work of Dugdale and Goering (1967) allowed primary production to be partitioned into "new" and "regenerated" production according to the source and oxidation state of the nitrogen resource. This partition is based on whether the nitrogen is supplied from within the euphotic zone (regenerated production), or from outside the euphotic zone (new production). Regenerated production is based on the uptake of reduced nitrogenous compounds; ammonium (NH_4), urea, or dissolved organic nitrogen (DON). Their uptake is related to the rates of remineralisation of organic matter by biological and chemical processes within the euphotic zone. New production on the other hand, is based on nutrients introduced into the euphotic zone (NO_3, N_2 fixation) and can be derived from the deep sea, the land and the atmosphere

(Dugdale and Goering, 1967). In high latitude or upwelling regions, the upward NO_3 flux is high and N_2 fixation is negligible so that the distinction between new and regenerated production is relatively straight-forward. However, recent evidence for euphotic layer nitrification and N_2 fixation in the oligotrophic gyres in particular complicates this distinction (Bianchi et al., 1997; Lipschultz, 2001; Falkowski et al., 2003; Capone et al., 2005; Fernandez and Raimbault, in press; Yool et al., in press).

Partitioning between new and regenerated nitrogen uptake can be summarised in the form of f-ratios, a quantitative measure of the proportion of phytoplankton growth dependant upon NO_3 relative to total N (Eppley and Peterson, 1979). Using ^{15}N stable isotope techniques, it is possible to directly measure the rate of uptake of a particular nitrogenous nutrient and the f-ratio is simply calculated according to the equation:

$$f = \frac{[\rho NO3]}{[\rho NO3] + [\rho NH4] + [\rho Urea]} .$$

Where ρ signifies the uptake rate (nmoles per litre per hour) of a particular nitrogen source. Implicit in this therefore, is a measure of that fraction of primary production, which is available for export to the deep ocean or to higher trophic levels (new production); which is surplus to phytoplanktonic community maintenance requirements (regenerated production) (Tremblay et al., 1997). The f-ratio therefore provides an index of coupling between the euphotic zone and the rest of the water column, being classically related to the rates of vertical NO_3 flux from below over suitable time (annual / seasonal) and space scales (Probyn et al., 1996). As nitrogen flux into surface waters must ultimately be balanced by equivalent losses, nitrate uptake yields an indirect estimate of downward carbon flux when Redfield ratio stoichiometry is inferred (Eppley and Peterson, 1979; Minas et al., 1986) or measured (Figure 1.10a). F-ratio calculations rely on the assumptions of steady state, no storage of N in surface waters (Eppley and Peterson, 1979; Eppley, 1989; Knauer et al., 1990) and minimal euphotic layer nitrification. Given that these assumptions are not always the case can render the f-ratio approach severely flawed (Fernandez and Raimbault, in press; Yool et al., in press). As f-ratios are calculated from 12-24 hr incubations, their indirect estimation of carbon flux gives a snapshot view of new production. If the system is not in steady state over suitable time scales, then new production, rather

than being a proxy of export production is considered to represent the potential for export, i.e. as 'exportable' production (e.g. Sambrotto and Mace, 2000).

Nitrification is the major route by which heterotrophically-regenerated N is remineralised by bacteria through the oxidation of ammonium to nitrite and nitrate. In the open oceans, nitrification was originally thought to be confined to the deeper, aphotic layers of the water column due to light inhibition (Olson, 1981). However, recent findings suggest that significant rates of nitrification may take place in the euphotic zone (Dore and Karl, 1996; Raimbault et al., 1999; Diaz and Raimbault, 2000; Rees et al., 2002; Fernandez and Raimbault, in press; Yool et al., in press). Unlike nitrate that originates below the nutricline, nitrate derived from nitrification in the euphotic zone should be considered as regenerated N. Consequently, primary productivity that is supported by regenerated nitrate is not relevant to the calculation of new production. Nitrification therefore substantially distorts estimates of "new" and export production when based on bulk nitrate uptake. While these distortions are greatest in the oligotrophic regions (where "regenerated" nitrate can form more than 70% of the total euphotic zone nitrate pool), the wider results suggest that estimates of "new" production based solely on the relative uptake rates of nitrate and ammonium may significantly overestimate this process at the global scale (Yool et al., in press). Although in many ecological systems the f-ratio may remain useful (e.g. over seasonal time scales in polar waters), blanket use of the f-ratio to diagnose export production no longer appears either justified or practical (Yool et al., in press).

Another nitrogen pool conspicuously absent from the traditional approach to f-ratio calculations and flux estimates is dissolved organic nitrogen (DON). Traditional ^{15}N stable isotope measurements of nutrient uptake refer to the net uptake rate. However, in oceanic, coastal, and estuarine environments an average of 25 to 41% of the dissolved inorganic nitrogen taken up by phytoplankton is released as DON. Failure to account for the production of DON during nitrogen-15 uptake experiments results in an underestimate of gross nitrogen uptake rates and thus an underestimate of new and regenerated production by up to 74 and 50 percent respectively (Bronk et al., 1994). A revised view of the traditional nitrogen flow (Figure 1.10a) provided in Bronk et al. (1994), clearly indicates the roles of nitrification, atmospheric deposition, DON

release and gross primary production in particulate nitrogen flux estimates (Figure 1.10b).

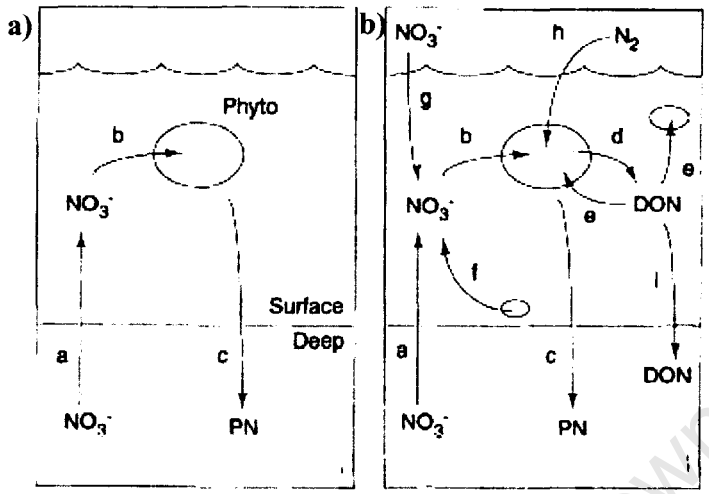

Figure 1.10. (A). The traditional view of new production where (a) upward vertical flux of NO_3 is equal to (b) the rate of net NO_3 uptake and (c) the downward flux of PN to the deep ocean. (B) The revised view of new production where (a) upward vertical flux of NO_3 plus (f) nitrification plus (g) atmospheric deposition is equal to (b) the net NO_3 uptake plus (d) the rate of DON release. The sum of (b) and (d) equals the gross NO_3 uptake. Over appropriate time and space scales, (b) the net uptake rate plus (h) the N_2 fixation rate plus (e) the incorporation of DON into bacterial or autotrophic biomass is equal to (c) the downewardflux of PN plus (i) the downward advection of DON. Figures reproduced from Bronk et al. (1994).

Further problems arise with using the f-ratio to express PON export in carbon terms as phytoplankton growth frequently follows non-Redfield ratios because of disturbance to cellular Redfield elemental stoichiometry by light and/or available Si and Fe (Geider and La Roche, 2002; Timmermans et al., 2004; Arrigo, 2005; Hoffmann et al., 2006; Moore et al., in press). For example, Brzezinski et al., (2003) and Franck et al. (2005) show considerable uncoupling of Si:C:N uptake ratios in the Southern Ocean, particularly at low dissolved Fe concentrations when f-ratios are low. This complicates the biogeochemical cycles of Si:C:N as well as the relative rates of mineral (opal, calcite) and carbon export in the Southern Ocean (e.g. Pondaven et al., 1999; Charette and Buesseler, 2000; Buesseler et al., 2001). Cautious f-ratio estimates of export over seasonal time scales in polar waters however still remain useful (Yool et al., in press; Lucas et al., in press).

1.8.2 New production from nutrient mass balance

The net transfer of organic carbon from the atmosphere to the ocean is limited by the consumption of new nutrients within the euphotic layer. Because biological processes in the ocean are largely seasonal, particularly in extra-tropical waters, a pronounced annual cycle is often observed. In particular, nutrients are removed from surface waters by biological activity in summer when light availability is high and replenished in winter when vertical physical exchange dominates (e.g. Takahashi et al., 1993, Koeve, 2001). Using a simple mass balance, the summertime nutrient drawdown provides an unambiguous lower bound estimate of export production (Louanchi and Najjar, 2000). Export in high latitudes is often dominated by diatoms which, if nutrient replete, are thought to take up silicate and nitrate in an approximately equimolar ratio (Brzezinski, 1985). Thus in addition to the supply of nitrate into surface waters, which potentially controls new production, the supply of silicate also has the potential to control export production (Sanders et al., 2005). The magnitude of new and export production can be estimated by observing the depth integrated seasonal decrease in nutrient concentrations over an annual cycle (e.g. Priddle et al., 1998; Garside and Garside, 1993; Sanders et al., 2005). As new production proceeds and removes nutrients from the upper water column, the size of the residual nutrient pool compared to the initial pool seasonally integrates the amount of new production.

This method of estimating new production forms the basis of some satellite-based methods which calculate seasonal changes in nitrate inventories based on sea surface temperature and chlorophyll concentrations (e.g. Goes et al., 2000). The obvious advantage of this method over other methods of estimating export production such as the f-ratio and thorium measurements is that it integrates production over a seasonal cycle. However the nutrient drawdown approach is affected by exchange of nutrients from other water masses through lateral advection or mesoscale eddies, effectively reducing the spatial scale of these estimates. Furthermore, inputs or removals of nutrients through processes such as nitrogen fixation and denitrification are not incorporated. A further complication is that a fraction of the nitrate utilised during new production is converted to dissolved and particulate organic nitrogen which accumulates in the surface waters before mineralisation in winter and thus represents new production that has not been exported (Anderson and Williams, 1999).

1.8.3 Sediment traps

An alternative to indirect measurements of particle flux using new production is to directly quantify the rate of accumulation of organic matter in sediment traps which began in the late 1970s. For reasons of technical convenience, traps have hitherto been either attached to moorings or tethered from surface floats (Figure 1.11). They are generally designed to collect, over a period of days to weeks, any particle that sinks into the mouth of the trap, with the unique advantage of also capturing and preserving material for biological and chemical analysis. Deployments of sediment traps have revolutionised our understanding of the connections between the surface and deep ocean by affording spatial, temporal and depth-varying studies of the changing flux and composition of settling material. Averaged over appropriate time and space scales, trap fluxes provide one means to estimate new production, since the input of new nutrients into the euphotic zone must be balanced by losses (e.g. Eppley 1989, Michaels et al., 1994). Trap-derived relationships of flux versus depth have also been used to estimate remineralisation rates for a wide range of compounds (e.g. Martin et al., 1987), which are critical to calculating the overall efficiency of removal of carbon and other associated elements from the surface ocean. These data have further been used to parameterise large-scale biogeochemical models (e.g. Gnanadesikan, 1999; Christian et al., 2002).

Although the overall patterns of particle fluxes derived from fixed traps seem reasonable, the extent to which they provide unbiased estimates of vertical fluxes remains contentious. Tethered sediment traps appear to give a good record of long term data in the deep ocean (>1000 m) when compared to fluxes of conservative and constrained tracers such as ^{230}Thorium or Aluminium (Scholten et al 2001), however, trapping problems in the upper ocean confound attempts to obtain reliable data in near-surface waters. For example, the use of trap-derived POC fluxes at the JGOFS BATS station resulted in a large upper ocean carbon imbalance (Michaels et al., 1994). Differences between radionuclide fluxes calculated from measured water column ^{234}Th inventories and measured trap ^{234}Th fluxes have suggested that traps can both over-collect and under-collect by up to a factor of 10 in the upper ocean (Buesseler, 1991; Buesseler et al., 1994; Murray et al., 1996; Gustafsson et al., 2004). Furthermore, large between-trap variations in shallow particle fluxes have been

observed when traps of different designs are deployed as part of the same experiment. The main causes for discrepancies in trap-measured fluxes are primarily from hydrodynamic biases (e.g. Gardner 1980a,b; Butman et al., 1986; Gust et al., 1992, 1994; Gardner, 1997). Sediment falls through the water at ~10-200 m d^{-1}, while it is carried horizontally by currents at ~5-50 km d^{-1} (typical of upper ocean currents). Flow past the trap sets up vortices that can either enhance or reduce the collection of sediment, depending on sinking rates, current speeds and the tilt and geometry of the trap (Valdes et al., 1997). Further problems stem from the preservation of the collected sample (Knauer et al., 1984; Wakeham et al., 1993; Kortzinger et al., 1994), and to effects caused by material/organisms entering the traps by means other than passive settling (i.e. "swimmers/surfers"; e.g. Lee et al., 1988; Michaels et al., 1990; Steinberg et al., 1998; Buesseler et al., 1994, 2000). Swimmers/surfers are planktonic organisms which are attracted to the traps and swim into them causing massive contamination of the collected material by their carcasses and probably severe modification of the material before they die (eating, defecation, moulting etc) (Gardner, 1980b, 1997).

The Indented Rotating Sphere (IRS) Sediment Trap (Peterson et al 1993, 2005) was developed to address concerns pertaining to vertical particle flux collection, especially in productive, high energy environments. The trap consists of four cylindrical modules; a particle interceptor, an IRS valve, a skewed funnel and a twelve sample carousel (an IRSC trap). The sample accumulator section of the trap is designed to be isolated from the ambient environment thereby minimizing washout of solid and dissolved materials. Contact between live animals and biocides contained in the brine layers at the bottom of the trap are also greatly reduced thereby significantly minimising contamination of trapped particulate matter by free-swimming animals. Another advantage of the IRSC trap is that it can collect particle flux based on the time of arrival of the flux or on particle settling velocities, thereby providing both temporal and settling velocity resolution of the particle flux.

Another solution to the problems of hydrodynamic biases and swimmer contamination was the development of lagrangian / neutrally buoyant sediment traps that drift freely with the currents, so that flow past the trap is effectively zero (Figure 1.11). The principal design problem was to make the trap descend to and stay near a

prescribed depth and then follow the motion of the surrounding water very precisely. An example is the Neutrally Buoyant Sediment Trap (NBST), developed at Woods Hole Oceanographic Institution (WHOI), which is auto-ballasted and can hold a prescribed depth to within 10 m (Valdes et al., 1997; Valdes and Price, 1999; 2000). Results from two concurrent deployments of NBST's and conventional tethered sediment traps (STSTs) at the Bermuda Atlantic Times Series indicate that the total mass of collected material was generally similar in the two traps. However, other variables, including the composition of the material and the fraction contributed by swimmers, were markedly different (Buesseler et al., 2000). Another example is the novel drifting sediment trap PELAGRA (**P**article **E**xport measurement using a **Lagra**ngian trap) (developed at NOC). The traps were designed around commercially available APEX floats from the Webb Research Corporation, USA. These are neutrally buoyant platforms with active buoyancy control to maintain the instrument at a level of constant pressure or salinity using a hydraulic pump which adjusts the density of the vehicle by changing the volume of an external oil-filled bladder. Tests on this trap have been carried out at the Porcupine Abyssal Plain (PAP) site where direct flux measurements are compared with proxy based estimates. The vertical fluxes measured made by the trap are similar to, but not the same as, fluxes measured by independent proxy based techniques (^{234}Th and new production f-ratio) (see Chapter 4).

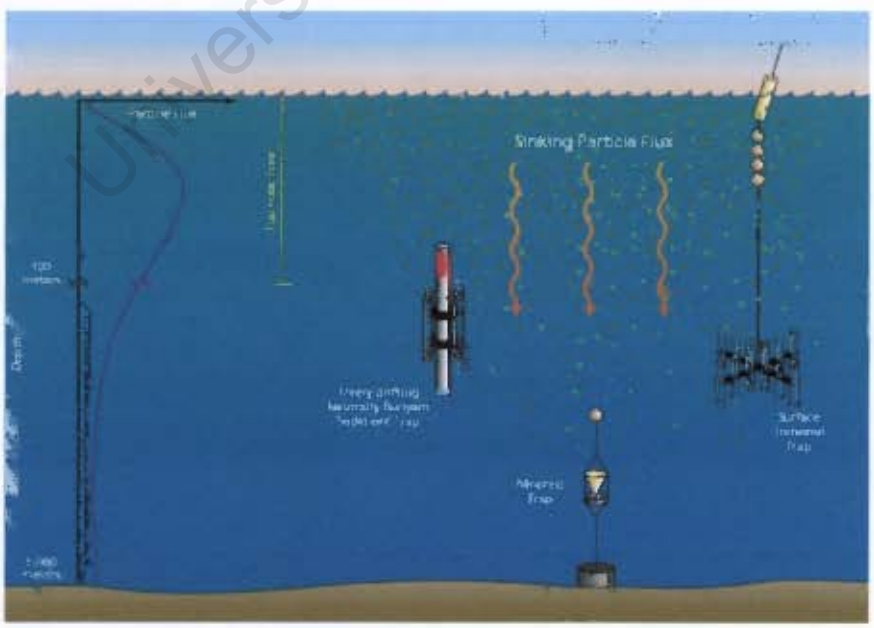

Figure 1.11. A schematic (not drawn to scale) representing three designs of sediment traps for directly measuring particle flux. Deep water traps are attached to moorings whereas surface tethered and free drifting neutrally buoyant traps serve in shallow waters. The graph on the left hand side of the figure represents the general pattern of particle flux which increases with depth from the surface to ~50m and decreases substantially below the euphotic zone. Figure reproduced from Valdes et al. (1997).

1.8.4 $^{234}Th/^{238}U$ disequilibrium approach

Particulate matter export from the surface waters can also be quantified using the radioactive disequilibrium between naturally occurring particle-reactive ^{234}Th ($t_{1/2}$ = 24.1 d) and its conservative (soluble) parent ^{238}U ($t_{1/2}$ = 4.47 x 10^9 yr). The link between ^{234}Th removal from the water column and biological processes was first demonstrated by Coale and Bruland (1985, 1987) and Bruland and Coale (1986). If the rate of ^{234}Th removal from the surface ocean on rapidly settling particles is high compared to its production rate, from ^{238}U decay and ^{234}Th adsorption onto particles, then the activity of total ^{234}Th becomes less than the ^{238}U activity, i.e., the $^{234}Th/^{238}U$ activity ratio is <1 and a ^{234}Th activity deficit occurs. If in a given parcel of water, the loss terms of ^{234}Th are smaller than the sum of ^{234}Th production and input through particle settling combined with particle breakdown and remineralisation, ^{234}Th activity excess can occur with $^{234}Th/^{238}U$ activity ratios >1. As ^{234}Th excess is considered an indicator of remineralisation processes in the mesopelagic zone, such activity ratios would imply that shallow remineralisation processes were relatively more significant than particle export at the time. The situation where ^{234}Th activity does not equal ^{238}U activity is called radioactive disequilibrium. Estimates of the rates of these processes may be obtained from simple box models of ^{234}Th uptake and removal (Coale and Bruland, 1985,Cochran et al., 1995,2000).

Since the half-life of ^{234}Th is only 24.1 d and this element is very particle reactive, the observed disequilibrium reflects the net rate of particle export from the upper ocean on time scales of days to weeks (e.g., Coale and Bruland 1985, 1987; Murray et al., 1989; Buesseler et al., 1992a; Benitez-Nelson et al., 2001). Elemental fluxes can be determined by multiplying the measured ^{234}Th flux (derived from the ^{234}Th:^{238}U disequilibria) by the ratio of an element to ^{234}Th on sinking particles. This empirical method was first formalised in a study by Buesseler et al. (1992a) to determine organic carbon export associated with the spring bloom in the North Atlantic. Since then, the thorium approach has been expanded to include other elemental fluxes such as particulate inorganic carbon (Bacon et al., 1996), polycyclic aromatic hydrocarbons and polychlorinated biphenyls (Gustafsson et al., 1997a,b), biogenic silica (Buesseler et al., 2001a; Rutgers van der Loeff et al., 2002) and trace metals (Gustafsson et al., 2000; Weinstein and Moran, 2005).

Any oceanographic study that aims to investigate particle fluxes by means of a selected proxy requires knowledge of the proxy's interactions with biological, geological and chemical compartments in order to attain a reliable application of the tracer methodology. The use of ^{234}Th as a flux tracer has strengths and weaknesses. As a radioactive tracer, ^{234}Th provides a more integrative view of particle export with respect to both time and space, while sample collection over a substantial depth range allows fine scale examination of particle fluxes and remineralisation with depth. However, this method depends on there being a statistically significant deficit of ^{234}Th in the surface waters, a condition which makes the application of this method problematic in oligotrophic sites such as BATS (Buesseler et al., 1994) and HOT (Benetiz-Nelson, et al., 2001). Other problem areas involve thorium measurement techniques, modelling strategies and thorium speciation and reactivity.

The interpretation of thorium distributions in aquatic systems requires a synthesis of laboratory and field data and the application of models that help set the data in the context of natural processes. The most difficult aspect in obtaining this synthesis is matching the complexity of the model and constraining model parameters with the ability to make appropriate measurements (Passow et al., 2006; Savoye et al., 2006). The simplest and by far the most commonly used ^{234}Th export models combine particulate and dissolved thorium into a single box assuming steady-state and that physical transport is negligible (Broeker et al., 1973, Matsumoto, 1975, Tanaka et al., 1983). While these models produce a straightforward measure of the ^{234}Th deficit to a given depth, the assumption of steady state and negligible advection and diffusion are oversimplifications that prevent the effects of blooms, eddies, etc, from being explicitly considered (Savoye et al., 2006).

The steady state assumption may be checked by repeated occupations of a single station to determine the extent to which the ^{234}Th deficit changes with time. This is especially important in situations such as blooms when fluxes are expected to be higher than ca. 800 dpm m^{-2} d^{-1} and when the flux of particulate material (and ^{234}Th) is changing on a time scale similar to the half-life of ^{234}Th. Studies based on the analysis of uncertainties associated with estimates of non-steady state recommend that reoccupation on a time scale of 1–4 weeks is the most appropriate for evaluation of non-steady state (Savoye et al., 2006). Physical processes also affect ^{234}Th profiles

and all physical models of thorium are greatly dependant on the accuracy of the fluid field in which the study occurs. Although physical processes may be relatively unimportant in regions such as the central gyres, knowledge of the physical oceanography of the study area is essential in areas of established upwelling such as the Equatorial Pacific and ocean margins. In these areas, advection and diffusion processes are likely to be important and measurements of the spatial gradients in $^{234}Th/^{238}U$ disequilibrium need to be incorporated into the model to evaluate the importance of lateral transport and more accurately determine measurements of particle flux. Although it is preferable to use non steady state models to determine particle flux, the logistics of most open ocean cruises do not permit stations to be reoccupied and steady state has to be assumed. See sections 2.4.1 and 4.4.5.1 for further discussions on steady versus non-steady state models.

Most applications of thorium models are possible with little knowledge of the dissolved chemical properties of thorium, other than its oxidation state (IV) and its tendency to strongly adsorb to particle surfaces. However the use of any tracer is hindered by any lack of knowledge of its chemical properties (Santschi et al., 2006). Arguably, one of the largest uncertainties in the application of the thorium approach is the ability to reliably characterise the ratio of POC:^{234}Th on particles that are representative of the sinking flux (Buesseler et al., 2006). To begin with, POC:^{234}Th ratios depend on the different particle collection devices used, such as sediment traps, filtration from Nisken bottles, or *in situ* filtration using pumps (Buesseler et al., 2006). Furthermore, regional differences and changes with depth and season also occur and there appears to be no single process or model that can explain how particulate POC:^{234}Th ratios vary with time, depth, particle type, size, or sinking velocity (for review see Buesseler et el., 2006).

As ^{234}Th is assumed to adhere to particle surfaces and POC to be determined by particle volume, POC/^{234}Th ratios are expected to increase with increasing particle size (see review by Buesseler et al., 2006), such as were found in the mid Atlantic (Charette and Moran, 1999), the Arabian Sea (Buesseler et al., 1998), the Ross Sea (Cochran et al., 2000) and the Labrador Sea (Moran et al., 2003). However, opposite trends have also been observed in the Equatorial Pacific (Buesseler et al., 1995; Bacon et al., 1996) and the Gulf of Mexico (Hung et al., 2004). This latter situation is

expected if preferential carbon losses occur relative to ^{234}Th activity because of, for example, particle decomposition or heterotrophic grazing resulting in large faecal pellets characterised by low POC/^{234}Th ratios (Buesseler et al., 2006). Equal ratios would be expected if organic carbon is biologically or chemically remineralised during the aggregation process. The most systematic studies to date indicate that POC/^{234}Th either increases or is relatively invariant with increasing particle size (size classes >1 to 100s μm) (Buesseler et al., 2006). For further discussions on POC/^{234}Th ratios see section 2.4.4.1.

General trends in decreasing POC:^{234}Th ratios with depth make choosing the depths corresponding to export prediction critical. For instance, application of a shallow POC:^{234}Th ratio to determine flux at depth would be inappropriate. One should ideally measure POC:^{234}Th (or other elemental ratios) below the layer where export is to be quantified (for example a standard depth of 100m is useful for more direct comparisons between studies). Another complication arises from the time difference inherent within the POC:^{234}Th ratio itself. POC is measured on sinking particles at single points in space and time relative to the measured thorium flux, which integrates over several days to weeks prior to sampling. The POC particles collected may therefore not truly represent the preceding ^{234}Th flux. It has been postulated that the POC:^{234}Th ratio should increase with particle size, but opposite trends have also been observed (Buesseler et al., 2006). Potential causes for this variability include: the lifetime of particles in the surface with respect to sinking, the surface to volume ratio of particles, biases during particle collection and differential binding to specific substance classes (Passow et al., 2006). Results from Passow et al. (2006) point toward a greater dependency of the POC:^{234}Th ratio with the type of particles present than on the size of particles, except in size classes smaller than 1μm.

As the use of ^{234}Th as a particle tracer becomes more widespread, it is essential that the mechanisms that control its particle reactivity are better understood. At the very least, improved knowledge of the chemical speciation of ^{234}Th would allow one to better resolve and assess the variability of POC:^{234}Th ratios. Numerous thorium isotope studies have suggested that the Th(IV)-binding ligand is surface active and can occur in all size fractions (dissolved, colloidal and suspended particle) (Guo et al., 1997; Passow et al., 2006, Alvarado-Quiroz et al., 2006).

Preferential binding of thorium to acid polysaccharides has been postulated (Niven et al., 1995) and established in the laboratory (Guo et al., 2002a,b; Quigley et al., 2002). Acid polysaccharides are released by phytoplankton and bacteria to form fibrillar exopolymeric particles (EPS) and transparent exopolymeric particles (TEP) (Passow et al., 2002, Santschi et al., 2006). Both EPS and TEP are highly surface active (sticky), promoting coagulation and often forming the matrix of marine snow (Passow et al., 1994, Santschi et al., 2006). Preferential binding of ^{234}Th to EPS/TEP could substantially impact the distribution of ^{234}Th as EPS/TEP may sink when incorporated into large aggregates, or remain suspended or even ascend when existing as individual particles or microaggregates (Passow et al., 2006). The fact that marine snow aggregation abundance closely tracks ^{234}Th/^{238}U disequilibrium is an indication of their importance in ^{234}Th removal (Santschi et al., 2006). Field observations also suggest a relationship between acid polysaccharide (APS) or uronic acid (URA) abundance and POC:^{234}Th ratios (Guo et al., 2002a; Santschi et al., 2003; Passow et al., 2006), and the abundance of prymnesiophytes and/or cyanobacteria and POC:^{234}Th ratios (Santschi et al., 2003). Despite the known affinity of ^{234}Th for inorganic particles, ^{234}Th has been known to exhibit a higher affinity for lithogenic particles (Passow et al., 2006) biogenic silica (Ducklow et al., 2001; Buesseler et al., 2006) and MnO_2 (e.g. Anderson et al., 1983). However, rather than being an indication of high intrinsic adsorption capacities for these minerals, it is suggested that these inorganic particle surfaces (such as diatoms) have an organic coating of acid polysaccharides (Decho, 1990; Leppard, 1995; 1997; Passow et al., 2006), with a sorption capacity potentially much higher than that of a pure silica surface. It has also been suggested that the correlation between ^{234}Th deficit and diatom blooms (Ducklow et al., 2001; Buesseler et al., 2006) despite the low affinity of ^{234}Th for opal (Osthols, 1995; Chase et al., 2002) reflects the efficient export of particulate matter to depth by the ballast action of diatom frustules (Santschi et al., 2006).

In contrast to the fairly extensive investigations on the geochemical behaviour of thorium in the marine environment, relatively few studies have explored its interactions with biota. The different applications of ^{234}Th with regards to particle fluxes and carbon export studies in particular merely consider the chemical and geological properties of the radionuclide and generally overlook biologically related ^{234}Th dynamics, most likely due to the lack of available information (Rodriguez et al.,

2006). Although Dunne et al., (2000) suggested that ^{234}Th contamination from zooplankton swimmers accidentally caught in sediment traps is negligible due to their low ^{234}Th activity: mass ratio, other studies have measured a significant ^{234}Th activity: mass ratio when compared to that reported for sinking particles (Krishnaswami et al., 1985; Coale, 1990). Furthermore, significant values of natural ^{234}Th have recently been reported in different marine benthic organisms (Ishikawa et al., 2004). This together with the fact that field measurements of ^{234}Th and ^{238}U activities on biota indicate a selective uptake of ^{234}Th relative to ^{238}U (Fisher et al., 1987; Krishnaswami et al., 1985; Ishikawa et al., 2004) means that any influence of zooplankton on the ^{234}Th distribution will impact the ^{234}Th /^{238}U disequilibrium and ultimately carbon export. If a significant amount of ^{234}Th is removed from or released to a system by living organisms, then particle dynamics (sedimentation/remineralisation) and hydrodynamic constraints alone will not always be sufficient to account for the observed ^{234}Th deficit in the water column.

A study by Rodriguez et al. (2006) was aimed at testing the implications of biologically related ^{234}Th dynamics and bioaccumulation on three small Antarctic crustaceans. Their results indicate that a substantial amount of accumulated ^{234}Th (16-49%) was associated with animal soft parts, when compared with reported values for other particle reactive transuranic elements. Crustacean zooplankton abundance however must reach at least 650mg.l^{-1} wet wt before significantly impacting the ^{234}Th water column distribution. Since the biomass of crustacean plankton is generally in the range ±µg.l^{-1} wet wt., any bias in ^{234}Th flux measurements from biological interactions is considered negligible in most oceanic environments. However in waters sustaining very a high biomass, such as the southern ocean (where krill concentrations can reach 25000-65000 individuals per cubic metre (Hamner et al., 1983; Higginbottom and Hosie, 1989; Hamner and Hamner, 2000; Watkins, 2000), ^{234}Th distribution would be largely determined by these organisms. Since krill are not representatively captured by conventional particle collection devices (sediment traps, in situ pumps, Niskin bottles) due to their avoidance behaviour (Hamner et al., 1983; Hamner and Hamner, 2000), the apparent ^{234}Th deficit could be wrongly interpreted as vertical ^{234}Th export (as opposed to biosorption on krill), the result of which would be an overestimate of the true export flux through sinking particles. Thus in waters with very high crustacean biomass, the biological compartment needs to be addressed

as they will negatively affect the reliability of vertical flux assessments using ^{234}Th (Rodriguez et al., 2006).

1.8.5 Differential time and space scales of export methods

The various methods used to estimate new production and export production are clearly not intended to measure rates of the same process. Although the rates are equal in a steady state system or when averaged over large enough time and space scales, there is otherwise no *a priori* reason why the rates should be identical. A major complication involved in reconciling these biogeochemical budgets lies in the fact that tracer observations reveal integral balances on time and space scales not revealed by discrete bottle sampling or by short-term incubation experiments. The potential incompatibility of explicitly resolved scales in these two types of measurement raises at least two possible explanations for some apparent discrepancies between different export measurements. First, biogeochemical budgets could be inherently three-dimensional. A second possibility is that traditional time series sampling under-resolves intermittent events that have a disproportionately large impact on the overall budgets (McGillicuddy et al., 1997). For example sporadic bursts of diapycnal mixing or mesoscale eddies could entrain large fluxes of nitrate into the euphotic zone to combine with atmospheric deposition of iron and nitrogen, leading to elevated but transient production. Under sampling such episodic events of higher associated production would have a profound effect on estimates of the metabolic balance of the sea (Karl et al., 2003). Not least, phytoplankton productivity measurements in the surface ocean at spot locations may not represent mesoscale averages over ~200 x 200 km which more likely represents the potential carbon available for association with ^{234}Th over the half-life of the tracer and the depth at which POC: ^{234}Th ratios are normally derived (~100 m). Additional discussions on comparing export measurements with differential time and space scales follows in chapter four.

Another factor to bear in mind when comparing export using different methods; is that sediment traps and $^{234}Th/^{238}U$ disequilibria measure the export of particulate material only, whereas new production estimates of export (both f-ratio and nutrient mass balance) deal with the export of both dissolved and particulate material.

2 Particulate organic carbon export from the North and South Atlantic gyres: the $^{234}Th/^{238}U$ disequilibrium approach

2.1 Introduction

The central subtropical gyres of the open oceans have long been regarded as homogenous and static "marine deserts" with low rates of primary production (Karl et al., 1996, Teira et al., 2005). However more recent studies have shown a large degree of physical, chemical and biological variability on a range of time and space scales (McClain et al., 2004). Variability in phytoplankton productivity, including pulsed high-productivity events, coupled with the immense size of the subtropical gyres (> 40% of the Earth's surface) makes current estimates of overall carbon fixation for these areas significant, accounting for ~25% of global primary production and up to 50% of global carbon export (Longhurst, 1995, Teira et al., 2005). Nevertheless, despite their large areas we know very little about the specific role of the north and south Atlantic gyres in the context of global carbon export. This is a serious short-coming when the role of the global oceans as a sink for atmospheric CO_2 is being considered.

Quantifying and better constraining the role of the North and South Atlantic in the global carbon budget and specifically measuring how much photosynthetically fixed CO_2 is exported below the seasonal thermocline is addressed as part of the AMT programme. In this chapter, measurements of $^{234}Th/^{238}U$ disequilibrium along three transects through the Atlantic Ocean between ~50°S and ~50°N (Figure 2.1, Table 2.1) are presented to provide an estimate of downward particulate carbon flux (e.g. Buesseler, 1998). The estimated downward flux of ^{234}Th is combined with measured ratios of $POC/^{234}Th$ on large (>50 μm) filtered particles to quantify POC export. These measurements were used in conjunction with primary production estimates to investigate the efficiency of the biological pump in transferring carbon fixed at the surface into deeper waters of the tropical, subtropical and temperate open ocean regions of the Atlantic Ocean.

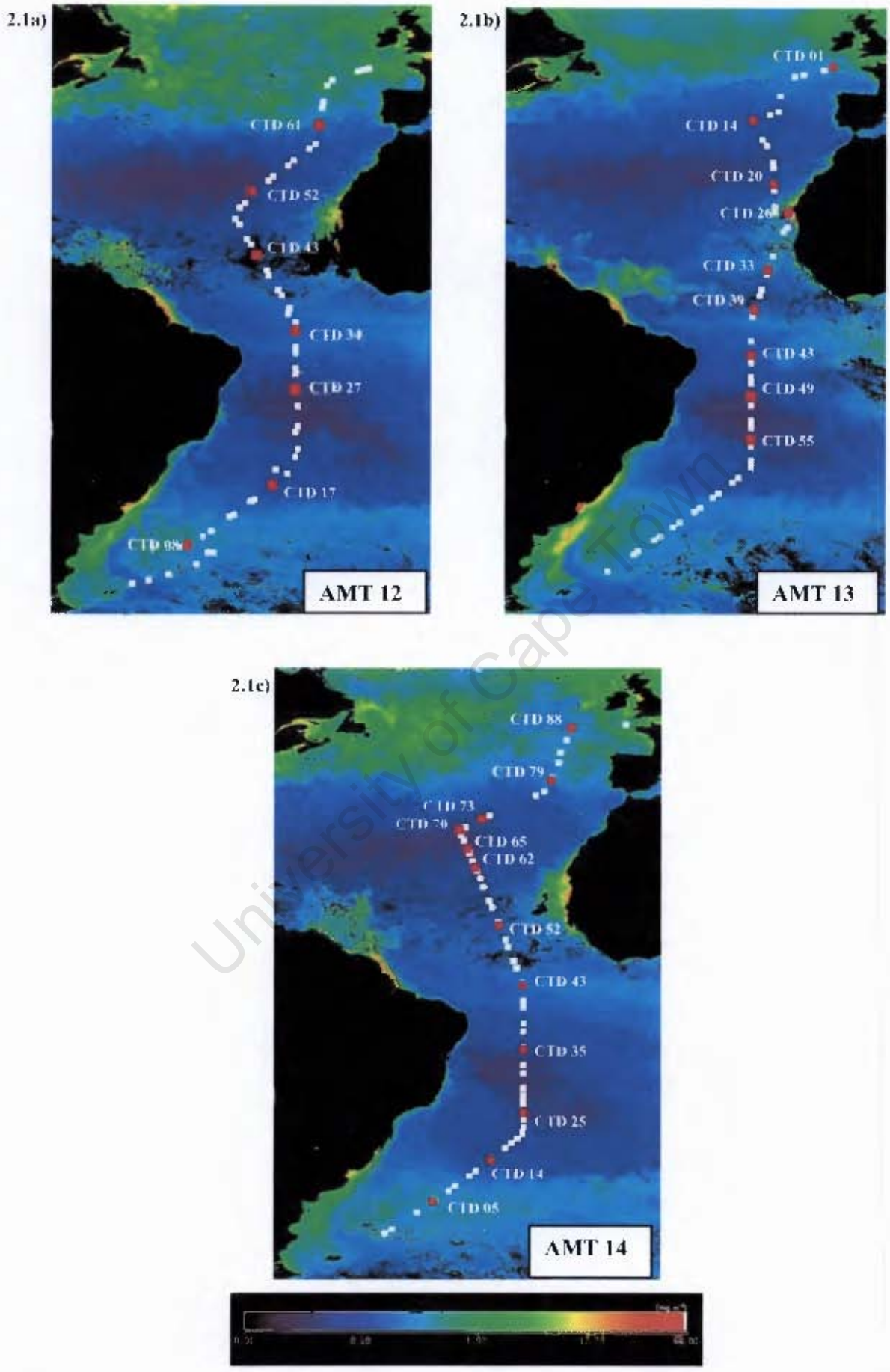

Figure 2.1. Monthly composite SeaWiFS images of surface chlorophyll for the Atlantic showing the cruise track for a) AMT 12, b) AMT 13 and c) AMT 14. Locations of thorium CTD's are marked in red and labelled. Other stations are indicated as small white squares.

Table 2.1. ^{234}Th station positions and sampling dates

Cruise ID	Station ID	Latitude (deg N)	Longitude (deg W)	Sampling Date
AMT 12	CTD 08	-43.21	-45.32	17/05/2003
	CTD 17	-31.79	-29.71	21/05/2003
	CTD 27	-13.93	-25.00	26/05/2003
	CTD 34	-2.24	-25.00	29/05/2003
	CTD 43	12.23	-32.29	02/06/2003
	CTD 52	24.33	-32.57	06/06/2003
	CTD 61	36.74	-20.81	10/06/2003
AMT 13	CTD 01	48.36	-9.86	14/09/2003
	CTD 14	34.69	-22.99	19/09/2003
	CTD 20	26.17	-20.79	21/09/2003
	CTD 26	20.60	-18.16	23/09/2003
	CTD 33	9.95	-21.84	26/09/2003
	CTD 39	2.16	-24.32	28/09/2003
	CTD 43	-6.58	-25.00	30/09/2003
	CTD 49	-14.83	-25.00	02/10/2003
	CTD 55	-22.68	-25.01	04/10/2003
AMT 14	CTD 05	-41.04	41.56	02/05/2004
	CTD 14	-32.97	31.01	05/05/2004
	CTD 25	-24.23	25.00	08/05/2004
	CTD 35	-12.28	25.00	11/05/2004
	CTD 43	-0.94	25.00	14/05/2004
	CTD 52	11.40	29.37	17/05/2004
	CTD 62	22.33	33.74	20/05/2004
	CTD 65	24.96	34.86	20/05/2004
	CTD 70	29.30	36.70	22/05/2004
	CTD 73	31.28	32.56	23/05/2004
	CTD 79	38.67	16.39	26/05/2004
	CTD 88	49.00	16.39	29/05/2004

2.2 Sampling and analytical methods

2.2.1 Temperature, salinity, nitrate, silicate, phosphate

Temperature and salinity data were obtained from calibrated conductivity. Temperature, depth (CTD) casts to 300 or 1000 m using a Sea-Bird 9/11 CTD system (AMT 12 – 69 CTD's, AMT 13 – 78 and AMT 14 – 89). Seawater density (sigma-theta) was computed by the British Oceanographic Data Centre (BODC) using the UNESCO SVEN function. Micromolar (μmol l^{-1}) concentrations of nitrate (NO_3), nitrite (NO_2), silicate (Si) and phosphate (PO_4) were measured colorimetrically using a 5-channel Bran and Luebbe AAIII segmented flow autoanalyser, following Kirkwood (1989) and Woodward and Rees (2001). Where ambient nitrate

concentrations were below the detection limit of the autoanlyser (<0.1 μmol l^{-1}) nutrient concentrations were measured using a colorimetric segmented flow analytical system with 2 m long Liquid Waveguide Capillary cells (World Guide Precision) and photo-diode detectors to provide nanomolar nutrient concentrations at a detection limit of <2 nmol l^{-1} (Woodward, 2002). Sampling was carried out using clean techniques. All nutrient samples were held in the dark in a refrigerator until analysed within two hours of sampling. No samples were frozen, preserved or stored.

2.2.2 Particulate organic carbon

Measurements of particulate organic carbon (POC) and nitrogen (PON) were prepared by filtering seawater samples (1–4.2 l) onto pre-combusted (~400°C, 12 hours) 25 mm Whatman GF/F glass-fibre filters and stored at -20°C prior to subsequent POC and PON analysis. Inorganic carbonates were removed from the filters by acidification with fuming concentrated hydrochloric acid. The filters were dried in a 60°C oven for 24 hours, packaged in pre-combusted aluminium foil (Hilton et al., 1986) and analysed on a Thermo Finnegan flash EA112 elemental analyser using acetanilide as calibration standard.

2.2.3 Chlorophyll and accessory pigments

Total chlorophyll was measured fluorometrically on board ship using a TD-700 Turner Designs fluorometer, calibrated with fresh chlorophyll standard (Sigma, UK) and set up to measure chlorophyll-a in the presence of chlorophyll-b following Welschmeyer (1994). The particulate matter in the samples was recovered by filtering 250 ml of seawater through glass fibre filters (Whatman GF/F) which were then stored in 90% acetone at -20°C overnight to extract pigments prior to reading on the Turner Designs fluorometer. The relative standard deviation for triplicate chlorophyll measurements >200 ml is generally <10% (Poulton, 2002). For High Performance Liquid Chromatography (HPLC) analyses, duplicate 1-4.2 l water samples were collected from 3-5 light depths and filtered under positive pressure through 25 mm Whatman GF/F and stored at -60°C. One replicate was analysed according to Barlow et al. (1997) on a 3 μm Hypersil MOS2 C8 column using a ThermoFinnigan Spectra HPLC system with a Thermo Separations AS3000 auto-sampler, a Thermo

Separations UV6000 diode array absorbance detector, and PC1000 and ChromoQuest chromatography software. Standards for accessory pigments were purchased from the DHI Institute for Water and Environment, Denmark. Detection limits were ≥0.002 mg m^{-3}. Analysis of replicates gave relative standard deviations of <20% (for chlorophyll-a) to <40% (for total pigments). Chlorophyllide-a was not resolved in this study, and thus HPLC chlorophyll-a (TChl-a) measurements include only mono-vinyl (Chl-a) and divinyl – (DvChl-a) chlorophyll-a.

Table 2.2. Symbols, names and formulae for chlorophylls, carotenoids, pigment sums and pigment indices. Following the method of Vidussi et al. (2001).

Symbol	Pigment	Abbreviation
Chla	Chlorophyll a	
DVChla	Divinyl chlorophyl a	
Chlidea	Chlorophyllide a	
Chlb	Chlorophyll b	
All	Alloxanthin	
But	19'-Butanoyloxyfucoxanthin	
Fuc	Fucoxanthin	
Hex	19'-Hexanoyloxyfucoxanthin	
Per	Peridinin	
Zea	Zeaxanthin	
Tchla	Total chlorophyll a	Chla + DVChla + Chlidea
DP	Diagnostic pigments	Chlb + All + But + Fuc + Hex + Per + Zea
Micro	Microplankton	Fuc + Per
Nano	Nanoplankton	All + But + Hex
Pico	Picoplankton	Chlb + Zea
Micro DP	Microplankton proportion of DP (%)	Micro / DP * 100
Nano DP	Nanoplankton proportion of DP (%)	Nano / DP * 100
Pico DP	Picoplankton proportion of DP (%)	Pico / DP *100

Diagnostic pigment indices were derived to asses the composition of phytoplankton communities following the method of Vidussi et al. (2001) and Barlow et al. (2004). Diagnostic pigments (DP) were defined as the sum of seven selected biomarker pigments (Table 2.2) based on their taxonomic and associated size affinity and are considered a valid estimate of phytoplankton biomass (Barlow et al., 2004). Three major phytoplankton groups were characterised, namely microplankton (Micro; >20–200 μm), nanoplankton (Nano; 2-20 μm) and picoplankton (Pico; 0.2–2 μm), following criteria of Vidussi et al. (2001). Diagnostic microplankton pigments characterised diatoms (Fuc) and dinoflagellates (Per), the nanoplankton of golden-brown flagellates; prymnesiophytes (Hex), pelagophytes (But) and cryophytes (All), while picoplankton comprised the cyanobacteria plus prochlorophytes (Zea) and green flagellates (Chlb). The proportion of each group contributing to the biomass was calculated by dividing Pico, Nano and Micro by DP. The use of such an index

must however be viewed with caution as eukaryotic picoplankton pigments e.g. pelagophytes (But) are included solely in the nanoplankton rather than the picoplankton, small (<20 μm) oceanic diatoms and dinoflagellates are solely included in the microplankton rather than the nanoplankton, and Chlb is regarded as being solely derived from low-light adapted prochlorophytes rather than from prasinophytes (Poulton et al., 2006b).

2.2.4 Primary production

Water sampling and incubations were started before dawn with the deployment of a CTD rosette sampler. Samples were collected from 4-6 light depths determined from previous light measurements and assuming the fluorescence maximum approximates 1% of surface irradiance (E_0). Water samples (3 light, 3 dark) were spiked with 20 μCi ^{14}C-labelled sodium bicarbonate ($NaH^{14}CO_3$) in polycarbonate bottles and incubated over a daylight period (dawn to dusk, typically 10-13 hrs). Simulated *in situ* incubators were cooled with either surface seawater or chilled freshwater to *in situ* temperatures (± 3°C) while *in situ* light levels were reconstructed using Lee Misty Blue and Grey neutral density filters. Following incubation, samples were filtered onto 0.2 μm (25 mm diameter) polycarbonate filters under gentle vacuum (<200 mbar), washed with filtered seawater and fumed for 30 minutes over concentrated hydrochloric acid in a desiccator to remove labelled inorganic carbon. After fuming, samples were placed in 6 ml pony vials with 5 ml of Optiphase HiSafe 3 scintillation cocktail and DPM activity was counted in a TriCarb 2100TR low activity Liquid Scintillation Counter (LSC) on board ship. The mean relative standard deviation of DPM's (RSD = standard deviation/mean * 100%) was 14% and ranged from 1-34% with the slightly higher RSD's for deep samples. Spike stock solutions were prepared daily with fresh filtered seawater and activity was checked by addition of 100 μl aliquots of stock solution to 9.9 ml Carbosorb followed by LS counting of five 100 μl replicates from this mixture in 5 ml PermaFluor E+ cocktail. The coefficient of variance for replicate standards was <2%.

2.2.5 New production

Nitrate uptake was measured with the stable isotope tracer technique of Dugdale and Goering (1967), where a ^{15}N labelled spike is added to a seawater samples at ~10% of the expected ambient NO_3 concentration. Water samples collected from 6 light depths were measured into 2 l Nalgene polycarbonate bottles, spiked with ^{15}N labelled KNO_3 (99.5% purity, obtained from Isotech or CIL laboratories) and placed into simulated *in situ* on-deck incubators within 1 hr of collection and incubated from dawn till dusk (~10-12 hrs) under appropriate light shading as for the ^{14}C incubations. Simulated *in situ* temperatures were maintained by flushing the surface samples (97-14% E_o) with surface seawater while deep samples (1 and 0.1% E_o) were chilled with freshwater. Once removed from the incubators, samples were filtered onto pre-ashed (450°C, >4 hrs) Whatman 25 mm GF/F filters. Filtration was performed under subdued lighting and gentle vacuum pressure. Filters were stored frozen (–20°C) until returned to the laboratory where they were dried and prepared for mass spectrometry analysis. Analysis for ^{15}N enrichment was conducted either at the Biomedical Mass Spectrometry Unit (BMSU) at the University of Newcastle (AMT 12) or at the Stable Isotope Ratio Mass Spectrometry (SIRMS) laboratory at the National Oceanography Centre, Southampton (AMT 14). The analysis at Newcastle used an Automated Nitrogen Carbon Analysis unit for Solids and Liquids (ANCA-SL) linked to a PDZ Europa 20/20 Mass Spectrometer (PDZ Europa Ltd, Crewe, UK). The analysis at Southampton used a Europa elemental analyser coupled to a GV Isoprime mass spectrometer (GV Instruments, Manchester, UK). Both analyses used standards traceable to IAEA (International Atomic Energy Authority) reference material. Measurements of particulate organic nitrogen (PON) concentration and ^{15}N atom% enrichment were obtained via the mass spectrometer analyses and uptake rates (nmol l^{-1} hr^{-1}) were obtained using calculations described by Dugdale and Wilkerson (1992).

Estimates of carbon-based new production were obtained by multiplying hourly nitrate uptake rates by a C:N ratio of 6.625:1 (Redfield et al., 1963; Eppley, 1989; Dugdale et al., 1992) and expressed in mmol C m^2 d^{-1}. A 12 hour daylight period of NO_3 uptake was assumed to be representative of the autotrophic period of carbon fixation and was therefore used to convert from hourly to daily rates. However, since dark uptake of NO_3 is known (e.g. Cochlan et al., 1991), these uptake rates must be

viewed as minimum 24 hr daily rates. Furthermore, recent evidence for extensive nitrification in surface waters (Fernandez and Raimbault, in press; Yool et al., in press) may significantly over-estimate "new" production because of high rates of regenerated nitrate production.

2.2.6 Total ^{234}Th (dissolved + particulate)

CTD profiles and productivity stations were conducted daily, however, only a subset of these stations were sampled for ^{234}Th. Seven stations were sampled during AMT 12, nine during AMT 13 and ten during AMT 14 (Figure 2.1; Table 2.1). Water samples of 20 litres (10 litres for AMT 14 CTD 88) were taken from the CTD bottle rosette from 7-10 depths to a maximum depth of ~1000 m. Vertical sampling resolution was highest within the upper 100 m where significant disequilibrium is expected to result from thorium removal on settling particles. During AMT 12 and AMT 13 particulate and dissolved thorium were measured independently whereas on AMT 14 total ^{234}Th (dissolved + particulate) was measured. Although more time consuming, measuring both dissolved and particulate ^{234}Th activities is preferable as it provides additional information on surface water export such as particle residence times. However due to contaminated particulate filters (0.4 μm) on AMT 12 and AMT 13, residence time calculations were not possible and only total ^{234}Th measurements were made on AMT 14 using 0.8 μm filters.

To separate the particulate from the dissolved phase, the water sample was vigorously mixed and filtered through a 0.4 μm (142 mm) polycarbonate membrane to collect the particulate ^{234}Th (AMT 12, AMT 13). The dissolved ^{234}Th (AMT 12, AMT 13) and total ^{234}Th (AMT 14) were extracted from the water using a medium-volume technique based on procedures described by Rutgers van der Loeff and Moore (1999), Buesseler et al. (2001b), Turnewitsch and Springer (2001), and Rutgers van der Loeff et al. (2006). Potassium permanganate, manganese chloride and ammonium reagents were added to the seawater sample to form a MnO_2 precipitate which preferentially scavenges ^{234}Th, leaving its parent ^{238}U in the dissolved phase. The precipitate was allowed to accumulate and grow for a minimum of 8 hrs before being filtered onto 142 mm diameter polycarbonate filters (0.8 μm pore size) together with the natural particles. Care was taken to maximise the collection of the precipitate from each

sample in the following ways; each sample was mixed fifteen times to remove any precipitate from the sides of the container, any sample remaining in the carbouy after filtration was collected and filtered through the filter in vacuum mode, all apparatus was acid washed (100ml 30% H_2O_2 in 10 l of 1M HCl) between each filtration. No ^{230}Th yield tracer was added to the samples as the sample volumes were considerably higher than the volumes used for the small-volume technique, where the use of a yield tracer has been recommended (Pike et al., 2005; Rutgers van der Loeff et al., 2006). The extraction efficiency for each cruise was tested by collecting the filtrate of eight to ten samples to which the potassium permanganate, manganese chloride and ammonium reagents were added and the filtration process repeated after 8 hrs. As the extraction efficiencies for medium and large volumes were very close to 100%, the use of a yield tracer is not required (Rutgers van der Loeff and Moore, 1999; Turnewitsch and Springer, 2001; Rutgers van der Loeff et al., 2006).

After filtration, all filters were air dried in covered plastic petri dishes and folded in a reproducible manner to form 18x18 mm packages that were wrapped in mylar foil (Rutgers van der Loeff and Moore, 1999). These filters were analysed for ^{234}Th activity onboard using non-destructive beta counting on a RISØ National Laboratory low-background gas flow counter, operated in anti-coincidence mode. ^{234}Th decays via beta decay to ^{234}Pa which has higher energy betas than ^{234}Th, a short half life of 1.2 minutes and is therefore always is radioactive equilibrium with ^{234}Th. Hence, what actually is measured by the beta counter is ^{234}Pa decaying via beta decay to ^{234}U. Samples were counted as soon as possible after sampling and at multiple times over the following months (at least six ^{234}Th half lives). This verified that the activity decrease followed the decay constant of ^{234}Th and also determined the background activity due to intrinsic detector background and long-lived radionuclides that contribute to the beta signal on the filter. All the ^{234}Th data were decay corrected to the point of sample collection and are reported in units of disintegrations per minute per litre of sea water (dpm l^{-1}). In most oceanic settings at depths greater than ~300 m and well away from the seafloor, the rates of processes other than radioactive production and decay of ^{234}Th are negligible (e.g., Clegg et al., 1991) and total ^{234}Th activity should equal ^{238}U activity (Bacon et al., 1996). The counting efficiency was thus determined by assuming that total ^{234}Th was in radioactive equilibrium with its parent ^{238}U at depth (500-1000m).

Uranium-238 activity (A_U, dpm kg^{-1}) was calculated from salinity where A_U = 0.0686* salinity, based on the average uranium concentration in seawater normalised to salinity 35 of 3.238 ng g^{-1} (Chen et al., 1986). The *in situ* activity per unit volume of water (dpm l^{-1}) was calculated based on *in situ* density.

2.2.6.1 Technical complications and their corrections

Typically, polycarbonate filters have very low and often undetectable background activities. However, the Nuclepore 0.4 μm pore size filters used for particulate filtrations on AMT 12 and AMT 13 and the second batch of 0.8 μm filters used for total thorium on AMT 14 had unusually high background counts probably due to variable standards of filter membrane manufacture.

Is there any evidence for unusual filter properties in the high-background filters that might originate from differences in filter manufacturing? As differences in manufacturing can have an effect on the self absorption of radiation by the filter, this in turn could have an effect on the counting efficiency. To investigate this for the AMT 14 filters, an average counting efficiency was determined for the uncontaminated set of samples as well as for the contaminated (high-background) set of samples. Interestingly, the average counting efficiencies and the average uncertainties of the two filter batches differed considerably. The mean counting efficiency for the 1st (low background) filter batch (CTD's 5, 14, 25 and 35), calculated using water samples from between 500 m and 1000 m depth, was 0.25 ± 0.01 cpm dpm^{-1} (mean ± 1SD). The average counting efficiency for the second (high background) filter batch (CTD's 43, 52, 62, 70, 79 and 88), calculated using water samples from 1000 m depth, was 0.34 ± 0.03 cpm dpm^{-1} (mean ± 1SD). As a further check on the reproducibility of the procedures for determining total ^{234}Th, 15 replicate deep-water samples (1000 m depth) from two stations (CTD's 65 and 73) were analysed using high-background filters. Again, the counting efficiency was higher for the high-background filters (0.33 ± 0.01 cpm dpm^{-1} [mean ± 1SD]). The difference in counting efficiency between the two filter batches indicates differences in filter density and/or thickness, probably resulting from differences in the manufacturing procedure.

Although the second batch of AMT 14 filter backgrounds were higher than usual it was still possible to calculate total ^{234}Th activities of reasonable quality. However, high background counts (mean = 2.72 cpm) on the second batch of filters used on AMT 14 meant that propagated errors for total ^{234}Th activities from CTD's 43, 52, 62, 70, 79 and 88 were higher than for CTD's 5, 14, 25 and 35 which had low background filter counts (mean = 0.79 cpm) and low errors (1st filter batch). When subtracting an unusually high background count from total beta activities for each consecutive measurement of a given sample, high count uncertainties arose that increased for older samples as the difference between background and total activity decreased. Consequently, for high-background samples, the uncertainty for each data point of the time series of decaying ^{234}Th activity became increasingly higher than for normal low-background samples. Uncertainty in the activity time series then translated into a high uncertainty of total ^{234}Th activity estimated for the time of sampling.

The mean total ^{234}Th activity of all deep water measurements on AMT 14 was 2.50 ± 0.09 dpm^{-1} (mean ± 1SD). This uncertainty of ± 3.6% is close to the estimates of overall analytical uncertainty on individual samples based on propagated errors including uncertainties in pressure, temperature, salinity, density, detector differences, counts per minute, estimates of activity at time of sampling, counting efficiency, filtered volume and ^{238}U activity. Based on the methodological results for AMT 14 samples it can be concluded that despite unusually high filter background activities and associated increased uncertainties on individual samples the reproducibility of total ^{234}Th measurements seems to be unaffected by filter contamination.

On AMT 12 and AMT 13 high background counts associated with the filters posed much more of a problem as the 0.4 μm filters used to measure the particulate ^{234}Th were contaminated with particularly high levels of radiation (mean = 3.17 cpm) from an unknown radionuclide (Figure 2.2a). This background contamination was not constant but itself decayed with an unknown half life over the time that the activity on the filters was being counted. It was therefore impossible to subtract a constant (high) background from all previous measurements, as the background count when the filter was initially counted would have been significantly higher than it was at the end of the six thorium half lives.

To still estimate the activity of particulate ^{234}Th, the background contamination of the particulate filters was required. The approach to this problem went as follows: given that in the ocean interior, the sum of particulate and dissolved ^{234}Th activity should equal the ^{238}U activity (Bacon et al., 1996), the particulate ^{234}Th activities at 500 and 1000 m were calculated (for the time of sampling) by subtracting the measured dissolved ^{234}Th activity (whose samples were unaffected by filter contamination) from the ^{238}U activity (as calculated from salinity). Based on the decay constant of ^{234}Th, the particulate activity could be calculated for each point in time that the 500 and 1000m samples were counted (Figure 2.2b). By subtracting this predicted activity (in counts per minute) from the total measured activity (also in counts per minute) for each time the sample was counted, an activity curve was derived which theoretically represented the evolution of the background contamination over the time span that the sample was counted (Figure 2.2c). The averaged contamination curve created from the 500 m and 1000 m samples (replicate 1000 m samples on AMT 12) was then subtracted from the remaining samples in the profile. The application of this correction produced seemingly accurate profiles. However due to the assumption of equilibrium at depth it is not possible to calculate error propagations for particulate and total thorium.

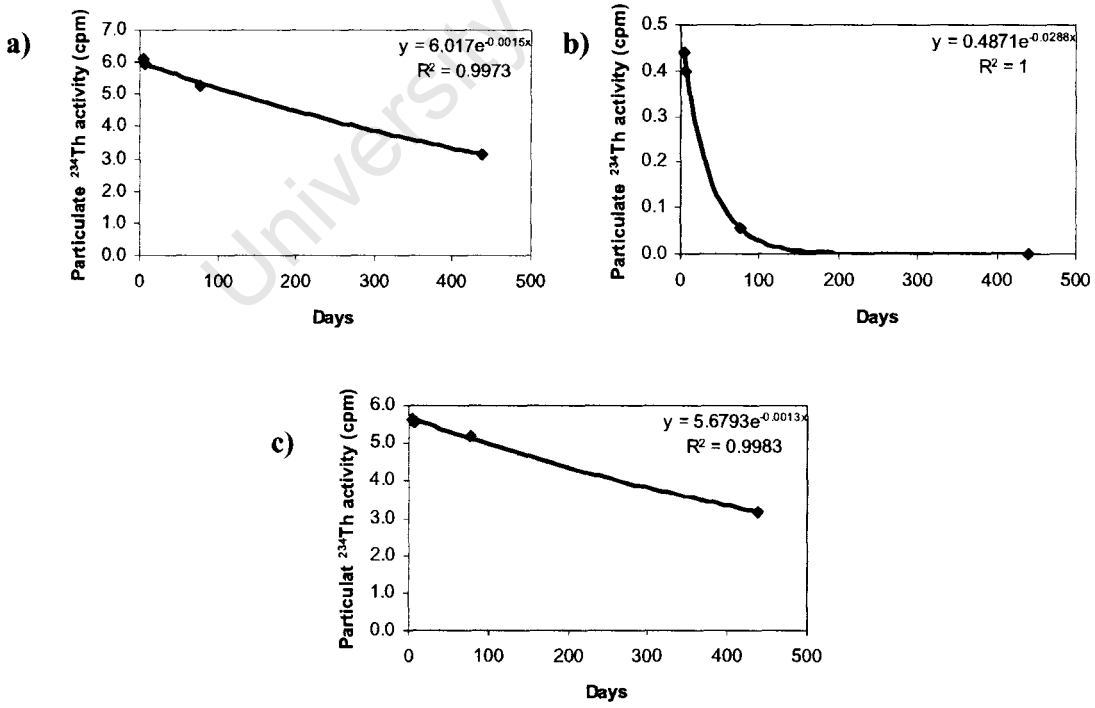

Figure 2.2. An example of the correction applied to the contaminated (high background) particulate filters. a) The ^{234}Th activity decay curve in counts per minute of a 1000m sample taken from AMT 12 CTD 52. b) The predicted decay curve for the same sample calculated from the ^{238}U activity minus the dissolved ^{234}Th activity at 1000m and the decay constant of ^{234}Th (see text for details). c) The contamination decay curve calculated by subtracting graph b) from graph a). The contamination curve was subtracted from the remaining samples in each profile to obtain a corrected ^{234}Th decay curve for each sample.

Using the aforementioned approach to estimate particulate ^{234}Th activities we arrived at reasonable values. However, the exact reason for the contamination is unkown and we are aware that the procedure used to estimate the contamination is based on unproven assumptions. Moreover, no error propagations could be run. These isues reduce the quality of the particulate ^{234}Th data from AMT 12/13. Without accurate measurements of particulate thorium, calculations of total thorium at 1000 m were not possible and counting efficiencies for these two cruises were not determined. Instead, a counting efficiency was used from a cruise carried out in June 2004 over the Porcupine Abyssal Plain (PAP) in the north Atlantic at ~ 48.99°N and 16.50°W, close to the northern end of the AMT transect. This cruise used the same uncontaminated batch of 0.8 µm pore width polycarbonate filters that were used for the dissolved ^{234}Th measurements on AMT 12 and AMT 13. Five 500 m samples from five CTD's and six replicate samples at 1000 m gave a mean counting efficiency of 0.26 $\pm$ 0.01 cpm dpm^{-1} and made it possible to calculate dissolved (and, hence, total) thorium activities for each sample during AMT 12/13.

2.2.7 Large particulate material

The ratio of POC to ^{234}Th on the sinking particulate pool was measured as large particles are considered to be the vehicle for POC export. The issues involved in measuring POC/^{234}Th ratios and their implications in converting ^{234}Th disequilibrium into POC flux is discussed in detail in sections 1.8.4 and 2.4.4.1. Large particles >50 µm are considered to represent the bulk (~90%) of particulates rapidly settling out of the water column into traps (Bishop et al., 1977, Clegg and Witfield, 1990). This size class was therefore collected by filtering large volumes of sea water (average 1500 l) through a 50 µm (293 mm diameter) nylon mesh using battery operated *in situ* pumps (Stand Alone Pumping Systems – SAPS). However, no SAPS were available for AMT 13. During AMT 12, the pumps were placed at 100 m (considered the base of the export layer and in accordance with the majority of ^{234}Th/^{238}U based export studies). However, as the deep chlorophyll maximum (DCM) was occasionally situated below 100 m, it was decided during AMT 14 that when this occurred, the SAPS would be placed just below the DCM. Once on board, the sample on the mesh was re-suspended using thorium-free filtered seawater and split into fractions using a 'Fulsom' splitter. One fraction was filtered onto pre-combusted 25 mm GF/F filters

and stored frozen for subsequent POC analysis as described above. Another fraction was filtered onto 142 mm diameter (0.8 μm pore size) polycarbonate filters for ^{234}Th analysis. The efficiency of the rinsing step was not incorporated into the calculation as it is not expected to affect the final POC /^{234}Th ratio (Buesseler et al., 1995; Amiel et al., 2002).

As SAPS pumps were not available on AMT 13, the >50 μm particle size fraction required to attain a POC/^{234}Th ratio representative of the large settling particulate pool was not sampled. Information on the POC/^{234}Th ratio of particles >0.7 μm collected from the CTD bottle data was however available. Since bottle filtration does not process sufficient volume for the analyses of ^{234}Th on rarer large particles, it is assumed that this ratio is only representative of the smaller size classes. This ratio could have been multiplied by the thorium deficit to attain a lower limit on the POC flux prediction (Buesseler et al., 1992a; Buesseler et al., 2006), however since small particles are not usually considered to dominate export flux and since the POC/^{234}Th ratio varies considerably with the size of particles, the dependence on bottle data was not ideal. As an alternative approach, a range of probable >50 μm POC/^{234}Th ratios was developed by scaling up the AMT 13 >0.7 μm POC/^{234}Th ratios at the depths that SAPS pumps would have sampled had they been available. The range in scaling up was based on the proportional increase between the >0.7 μm POC/^{234}Th and the >50 μm POC/^{234}Th ratios from AMT 12 (2.37 times higher; range = 1.24-6.97) and AMT 14 (6.06 times higher; range = 2.48-17.68). In so doing, a range of probable >50 μm POC/^{234}Th ratios was created for AMT 13. The minimum range was calculated by multiplying the measured >0.7 μm POC/^{234}Th ratio on AMT 13 by the proportional increase in POC/^{234}Th with particle size measured on AMT 12 (2.37), whereas the maximum range was calculated by multiplying the measured >0.7 μm POC/^{234}Th ratio on AMT 13 by 6.06 (the proportional increase in POC/^{234}Th with particle size measured on AMT 14).

2.3 Results

2.3.1 Hydrographic environment

From the sections of temperature, salinity, and density (Figures 2.2, 2.3, 2.4), the range of oceanic regimes sampled during the three AMT cruises and the temporal and seasonal differences between the cruises become evident. The boundaries of the subtropical gyres were marked by upward sloping isolines of temperature and salinity. The boundary to the north is the subtropical convergence (STC) that separates warm salty water of the subtropics from the cooler fresher water to the north. The southern boundary is the South Subtropical Convergence (SSC), which lies between the warmer Brazil Current and the colder Falklands Current. The boundaries vary seasonally, with a southward movement of the STC during boreal spring (AMT 12, AMT 14) and a northward movement of the SSC during austral spring (AMT 13). To facilitate the conceptualisation of predominant large scale surface circulation patterns of the North and South subtropical Gyre see section 1.6.1 and Figure 1.8.

Both the northern and southern subtropical gyres had a highly stratified water column with deep mixed layer depths (MLD) in the centre of the gyres. During AMT 12 and AMT 14, the MLD in the southern subtropical gyre was 50-75 m (Figures 2.3a, 2.5a) compared with >100 m during AMT 13 (Figure 2.4a). In the northern subtropical gyre, the MLD was only 20-40 m during AMT 13 and between 50-75 m during AMT 12 and AMT 14. The surface mixed layer isotherms of AMT 13 also extended further north than during AMT 12 and AMT 14. Higher surface temperatures and more intense stratification correspond with the autumn period (southern hemisphere AMT 12, AMT 14 and northern hemisphere AMT 13) and result from summer warming. The stability of the water column increased from spring to summer, when the seasonal mixed layer (SML) was shallowest (10-30 m). A deepening of the mixed layer was seen from autumn to winter, favouring the entrainment of cold nutrient rich waters into the photic zone. Seasonal variations were less apparent at the equator and in deeper waters. Maximum sea surface temperatures (SST ~28°C) were reached at the equator where the surface mixed layer also shallowed and a strong thermocline was evident. A further decrease in the SML was seen between 17°-20°N on AMT 13 (Figure 2.4a) which corresponded to the Mauritanian upwelling system off the NW coast of Africa. In temperate latitudes at the northern and southern ends of the transect, there was once again a reduction in SST and a shoaling of the surface mixed layer to 40-50 m.

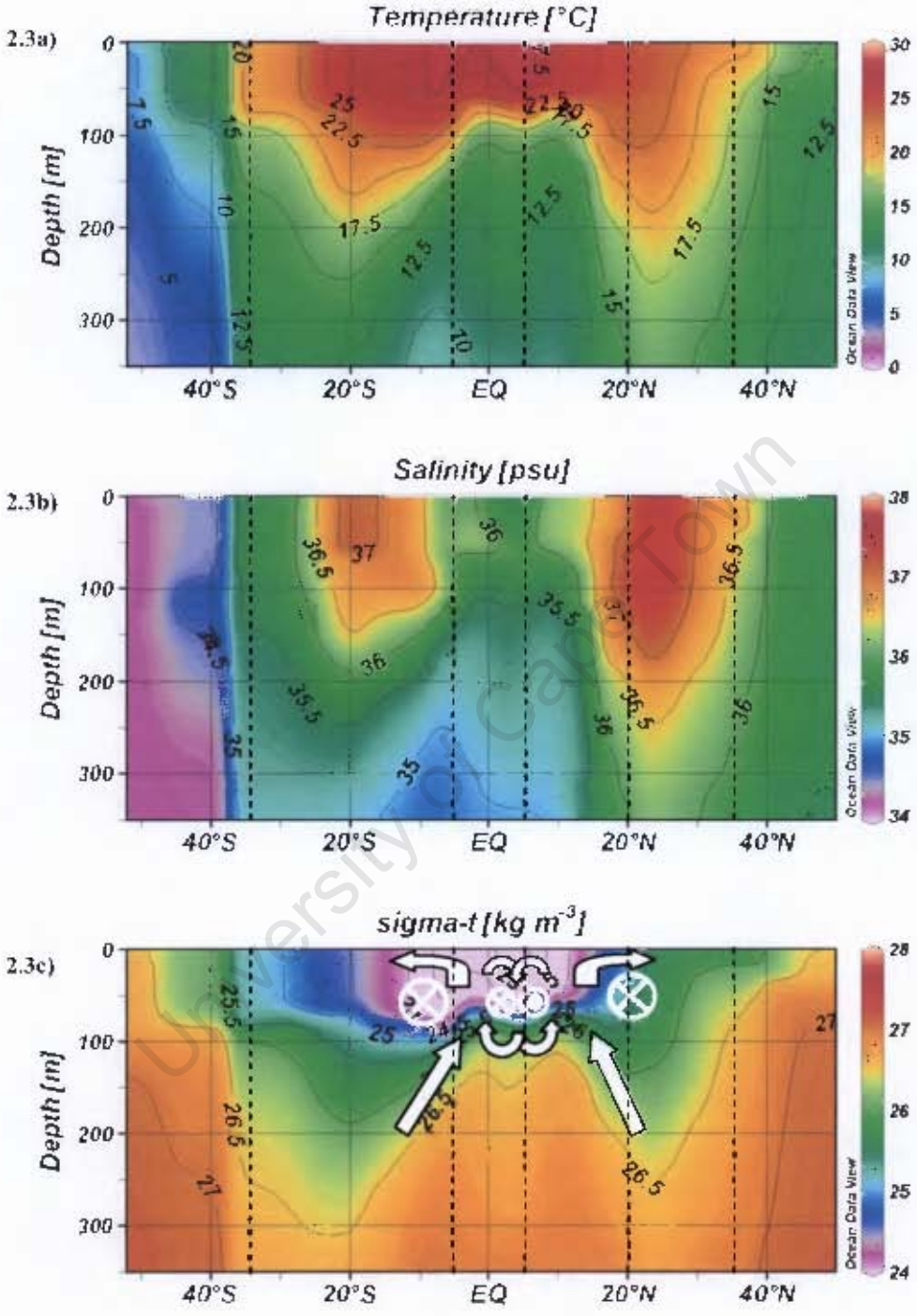

Figure 2.3. General hydrography as observed on AMT 12 with a) temperature, b) salinity and c) density. Temperate (35°- 50°N and 35°-50°S), oligotrophic (20°-35°N and 5°-35°S), equatorial (5°S-5°N) and upwelling (5°-20°N) domains are indicated by vertical dashed lines. The approximate locations and current patterns (white arrows and symbols in c) of the equatorial current system are shown. SEC: South Equatorial Current; EEC: Equatorial Counter Current; NEC: North Equatorial Current. See text for more details.

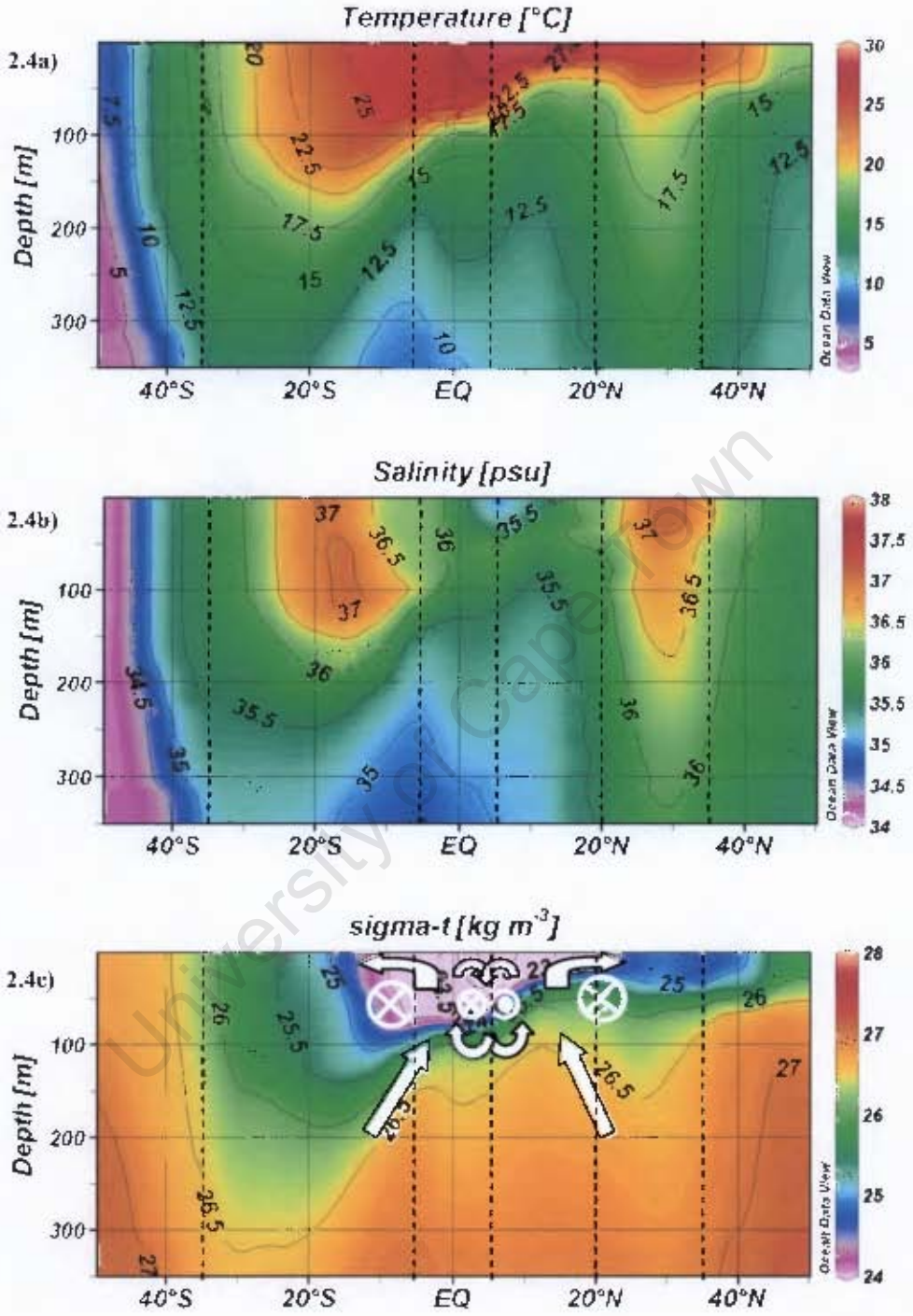

Figure 2.4. General hydrography as observed on AMT 13 with a) temperature, b) salinity and c) density. Temperate (35°- 50°N and 35°-50°S), oligotrophic (20°-35°N and 5°-35°S), equatorial (5°S-5°N) and upwelling (5°-20°N) domains are indicated by vertical dashed lines. The approximate locations and current patterns (white arrows and symbols in c) of the equatorial current system are shown. SEC: South Equatorial Current; EEC: Equatorial Counter Current; NEC: North Equatorial Current. See text for more details.

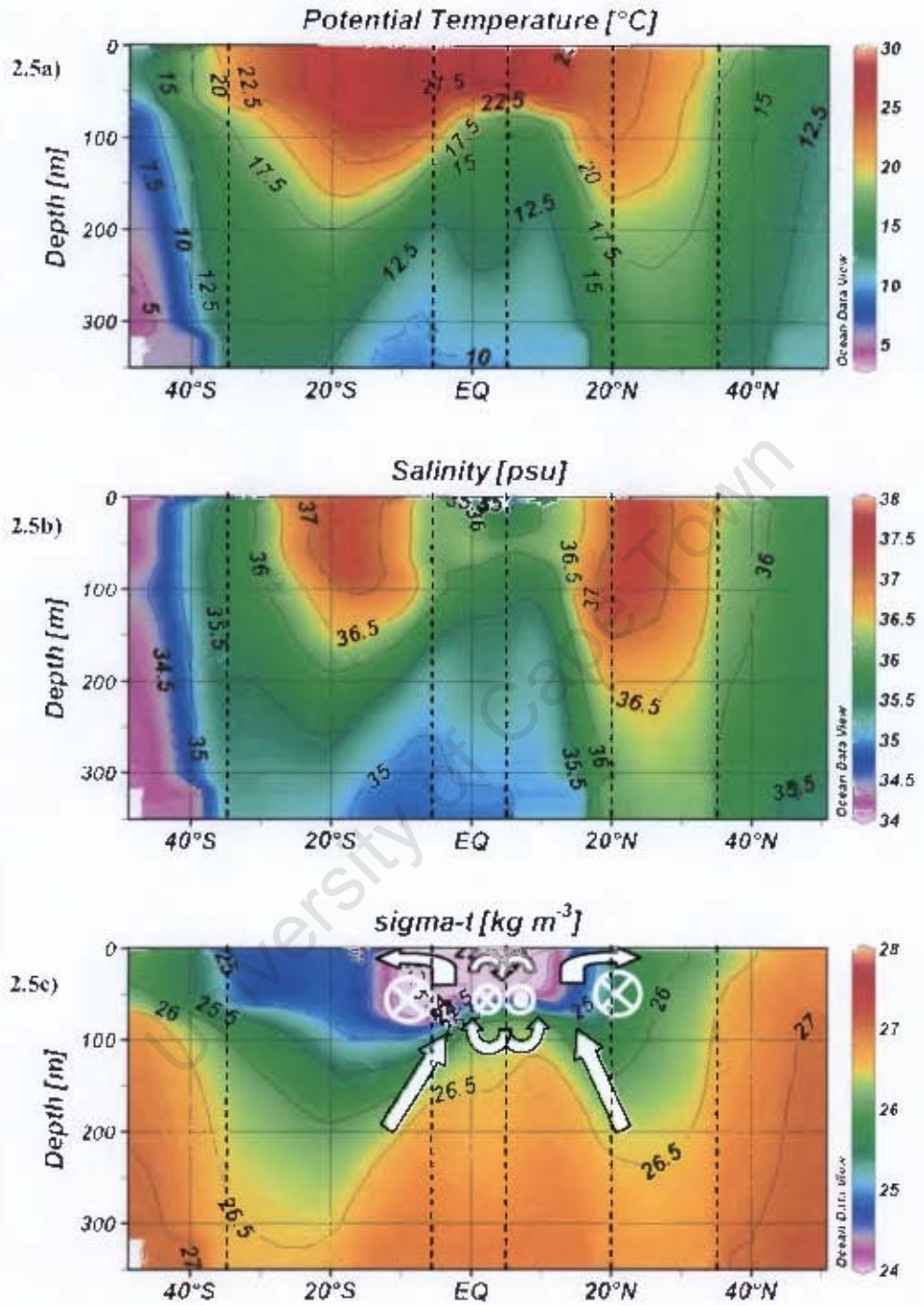

Figure 2.5. General hydrography as observed on AMT 14 with a) temperature, b) salinity and c) density. Temperate (35°- 50°N and 35°-50°S), oligotrophic (20°-35°N and 5°-35°S), equatorial (5°S-5°N) and upwelling (5°-20°N) domains are indicated by vertical dashed lines. The approximate locations and current patterns (white arrows and symbols in c) of the equatorial current system are shown. SEC: South Equatorial Current; EEC: Equatorial Counter Current; NEC: North Equatorial Current. See text for more details.

Within the ocean gyres, salinity increased from high latitudes towards the subtropics, reflecting the balance between evaporation and precipitation (Aiken and Bale, 2000) (Figures 2.3b, 2.4b, 2.5b). Within the tropics, however there was a decrease in salinity due to high rainfall associated with the inter-tropical convergence zone (ITCZ). The southern subtropical front was well represented in the southern hemisphere with a strong gradient in salinity at ~40° S, but less so at the STF in the northern hemisphere where smaller gradients were seen over a larger special scale.

Sea surface density across the three transects ranged from 22 kg m^{-3} just north of the equator to ~27 kg m^{-3} at the southern end of the AMT 12 cruise track and the northern extremity of AMT 14 (see Figures 2.3c, 2.4c, 2.5c). There was a general shoaling of the pycnocline towards the north in all three transects. A layer of less dense surface water extended further north in AMT 13 with the opposite being true for AMT 12 and AMT 14 with a low density surface layer extending further south.

2.3.2 Ambient chemical environment

Latitudinal variations in the nitracline depth followed those of the thermocline (Figures 2.6a, 2.7a, 2.8a). Surface waters were nitrate depleted (<30 μmol l^{-1}) while the 1 μmol l^{-1} nitracline was typically found between 100-150 m in the centre of the gyres. Shallower surface mixed layer depths (<75 m) and increased nutrient concentrations in subsurface waters occured across the equator and north of the equator, reflecting the effects of upwelling associated with the equatorial divergence at ~0° and the northern boundary of the North Equatorial Counter Current (NECC) at ~10°N (Aiken and Bale, 2000). During AMT 13 (Figure 2.7a), the increased subsurface NO_3 persisted further north and an outcropping of the 1 μmol l^{-1} nitracline was evident between 15° and 20°N, consistent with the cooling of subsurface waters indicating the proximity of the coastal upwelling area off NW Africa. In temperate latitudes at the northern and southern ends of the transect, the reduction in temperature and SML depths coincided with an increase in NO_3 concentrations.

During AMT 12 and 13 (Figure 2.6a, 2.7a) the low surface nitrate conditions in the northern temperate region persisted to 50°N whereas on AMT 14 (Figure 2.8a), the 1 μmol l^{-1} nitracline outcroped at ~39°N, increasing surface nitrate concentrations in the

temperate North Atlantic. Similarly, the 1 μmol l^{-1} nitracline outcroped at ~35°S on AMT 12 and AMT 13 compared to ~40°S on AMT 14. The highest surface nitrate concentrations were always found south of the SCC.

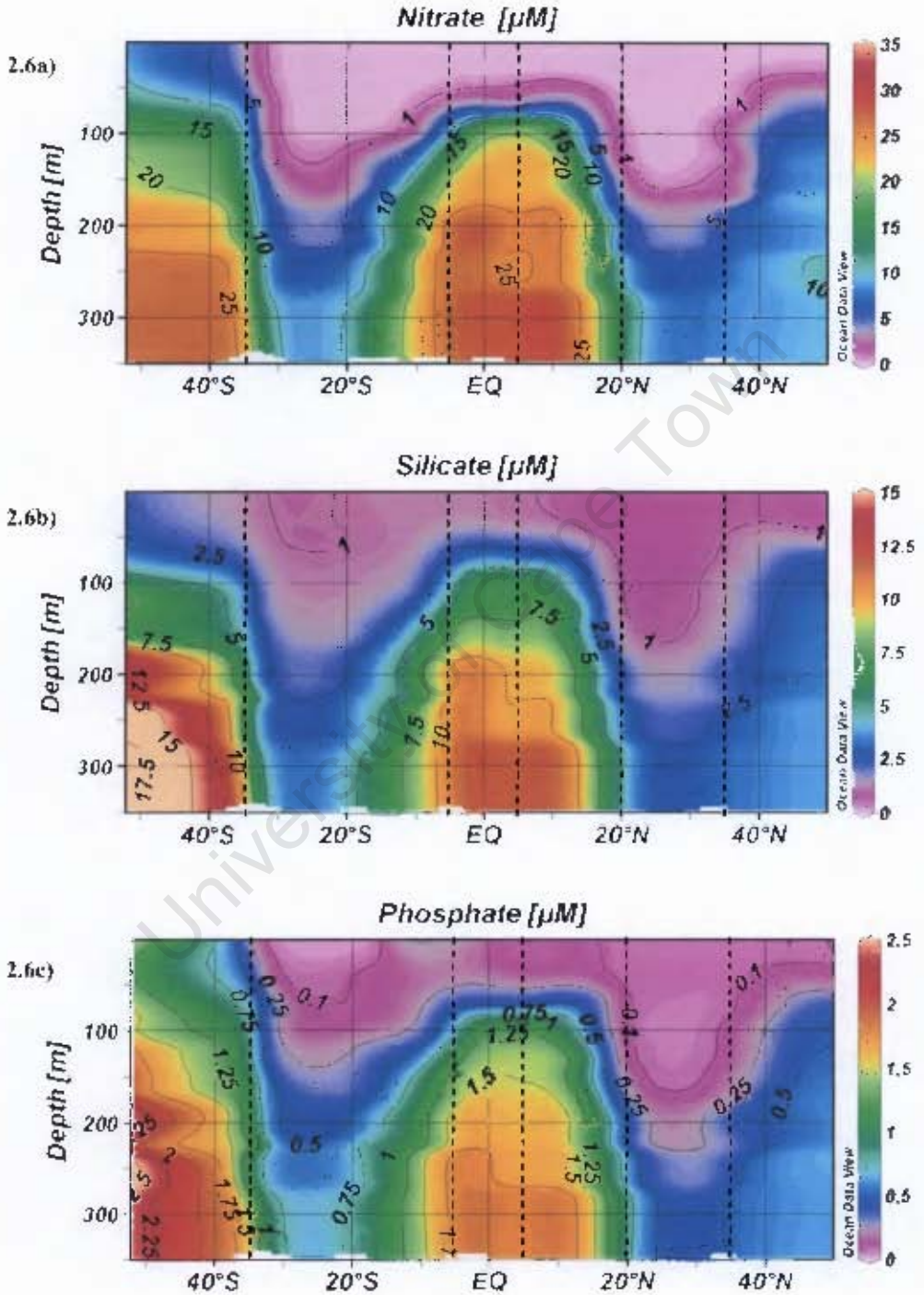

Figure 2.6. Ambient nutrient concentrations as measured during AMT 12 for a) nitrate b) silicate and c) phosphate. Temperate (35°- 50°N and 35°-50°S), oligotrophic (20°-35°N and 5°-35°S), equatorial (5°S-5°N) and upwelling (5°-20°N) domains are indicated by vertical dashed lines.

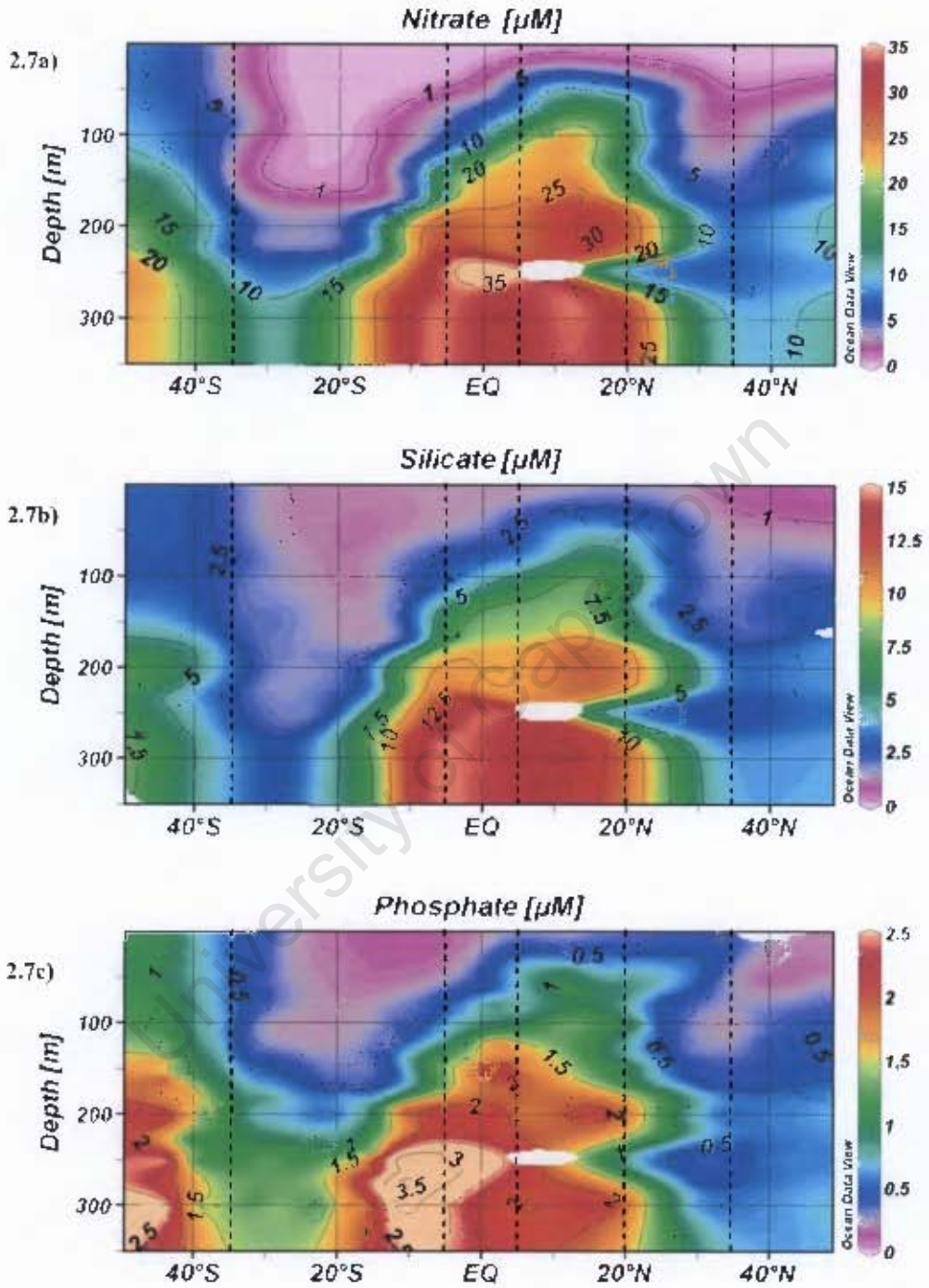

Figure 2.7. Ambient nutrient concentrations as measured during AMT 13 for a) nitrate b) silicate and c) phosphate. Temperate (35°- 50°N and 35°-50°S), oligotrophic (20°-35°N and 5°-35°S), equatorial (5°S-5°N) and upwelling (5°-20°N) domains are indicated by vertical dashed lines.

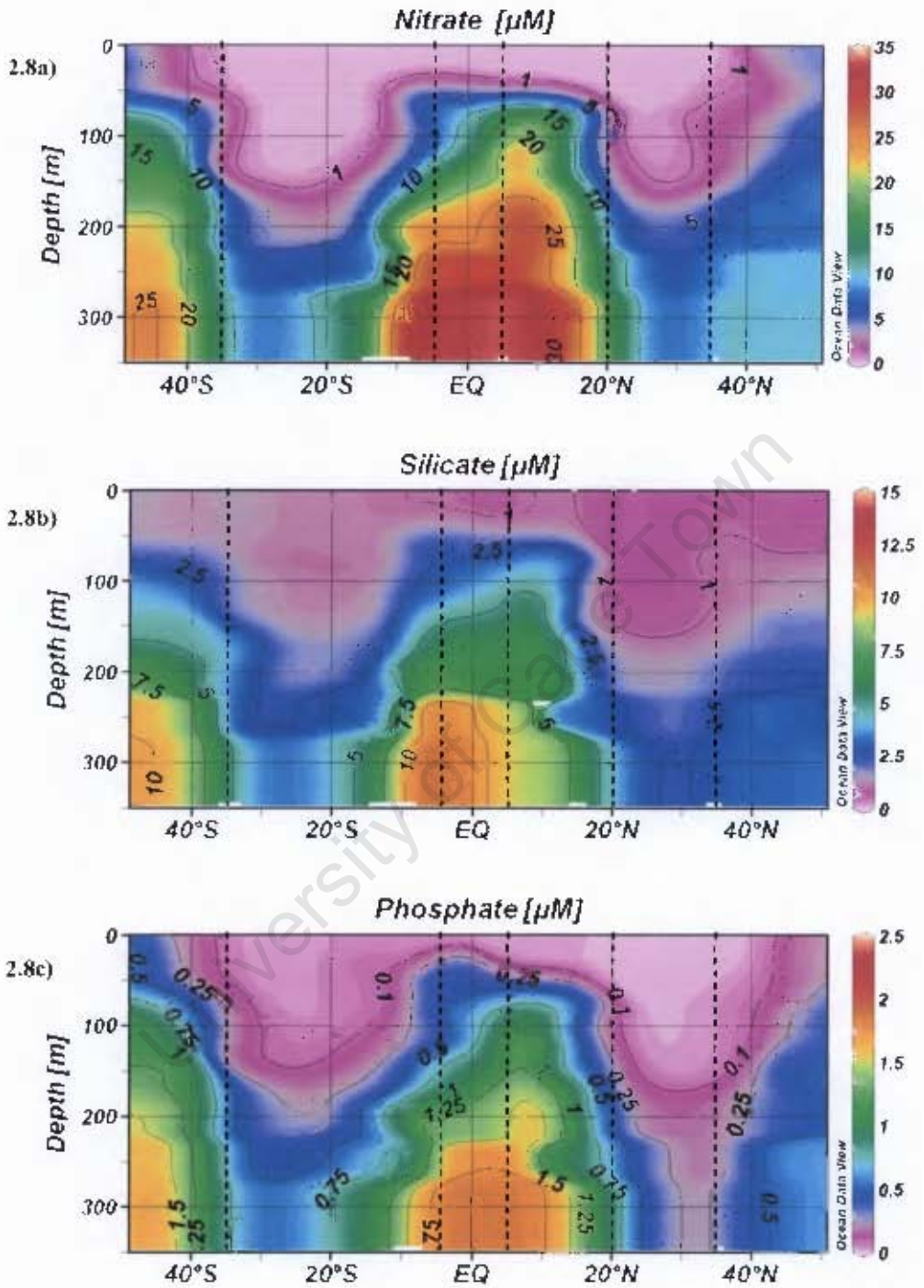

Figure 2.8. Ambient nutrient concentrations as measured during AMT 14 for a) nitrate b) silicate and c) phosphate. Temperate (35°- 50°N and 35°-50°S), oligotrophic (20°-35°N and 5°-35°S), equatorial (5°S-5°N) and upwelling (5°-20°N) domains are indicated by vertical dashed lines.

Silicate (SiO_2) and phosphate (PO_4) concentrations showed a similar distribution to NO_3 with extremely low surface concentrations that increase with depth. On AMT 12 and AMT 14, surface silicate concentrations were lower (<1 μmol l^{-1}) in the northern gyre and extended to deeper depths (~170 m) than in the southern gyre (Figure 2.6b, 2.7b). AMT 13 alternatively had lower silicate concentrations extending to greater depth in the southern gyre but higher surface Si concentrations that reached >2.5 μmol l^{-1} south of 40°S (Figure 2.7b). Again the Mauritanian upwelling system was well represented with high subsurface concentrations of ~5 μmol l^{-1} at 18°N. Phosphate concentrations (see Figures 2.6-2.8c) were lowest in surface waters of the northern gyre on AMT 14 (<<0.1 μmol l^{-1}) while the highest surface concentrations (~1.25 μmol l^{-1}) were found at the southern extremities of AMT 12, where a strong frontal boundary in phosphate concentrations was evident between 30-50°S.

2.3.3 Chlorophyll-a and diagnostic pigments

Surface chlorophyll-a concentrations were generally <0.1 mg m^{-3} in surface waters, particularly in the centres of the northern and southern subtropical gyres (see Figures 2.9a-c). Chlorophyll-a concentrations increased with depth to form a basin-scale subsurface chlorophyll-a maximum (DCM). No consistent relationship was found between the depth of the DCM and the MLD (Poulton et al., 2006b) however the depth of the DCM was closely related to the depth of the 1 μmol l^{-1} nitracline and was deepest (180 m) in the southern central gyre on AMT 13. An inverse relationship is known to exist between the depth of the DCM and its intensity (Herbland and Voituriez, 1979) and was evident on AMT with shallower DCM's in the equatorial, upwelling and temperate regions having higher chlorophyll concentrations (0.2-0.5 mg m^{-3}) than the extremely deep maxima in the centres of the gyres (0.05-0.1 mg m^{-3}). In the highly stratified gyre centres, the deep surface mixed layer had very low chlorophyll concentrations (<0.05 mg m^{-3}). In the temperate latitudes, chlorophyll-a concentration displayed some seasonal changes. In the northern temperate region during boreal spring (AMT 12 and AMT 14), chlorophyll-a concentrations were slightly higher (0.6-0.8 mg m^{-3}) than in boreal autumn (<0.5 mg m^{-3}), reflecting the late stages of the North Atlantic spring bloom (Figures 2,9a, 2.9c). Similarly, in the southern temperate region, highest chlorophyll-a concentrations (0.5 mg m^{-3}) were found during the austral spring (AMT 13) (Figure 2.9b).

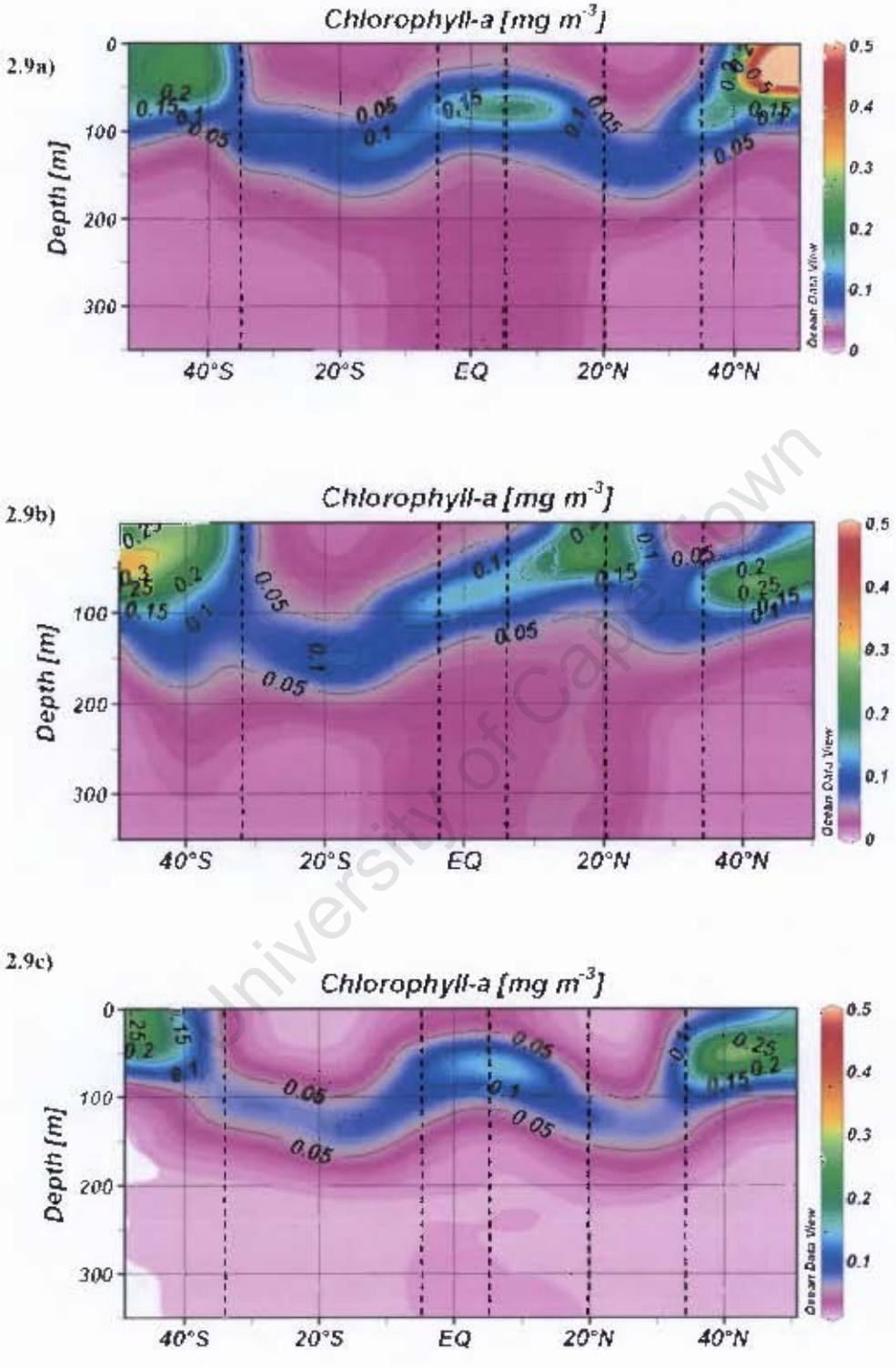

Figure 2.9. Total flourometric chlorophyll-a sections as measured for a) AMT 12 b) AMT 13 and c) AMT 14. Temperate (35°- 50°N and 35°-50°S), oligotrophic (20°-35°N and 5°-35°S), equatorial (5°S-5°N) and upwelling (5°-20°N) domains are indicated by vertical dashed lines.

In the southern temperate region there was a shoaling of the DCM, with high chlorophyll-a concentrations extending to the surface in contrast to the northern temperate region on AMT 13 and AMT 14 where the highest chlorophyll-a concentrations were subsurface. The NW African coastal upwelling on AMT 13, displayed a marked increase in chlorophyll-a, with concentrations reaching 0.5 mg m^{-3} (Figure 2.9b).

The distribution of diagnostic pigments (DP) provided information concerning the size distribution of the phytoplankton community (Figures 2.10, 2.11, 2.12). Diagnostic pigments integrated to the 1% light depth show that microphytoplankton (Micro/DP) represented <10% of total diagnostic pigments throughout the tropical and subtropical Atlantic, except in association with upwelled waters off NW Africa during AMT 13 where they contributed 34% to the total (Figures 2.11a-c). In the temperate fringes of the subtropical gyres, the percentage of microphytoplankton contribution to total pigments increased, particularly during the spring where maximum contributions reached 30-40% in the northern hemisphere spring (AMT 12, 14) compared to ~20% in northern hemisphere autumn (AMT 13) and a maximum of ~30% in the southern hemisphere spring (AMT 13) compared to ~10% in the southern hemisphere autumn (AMT12, AMT 14). From the diagnostic pigment sections, it is clear that on AMT 13 the increase in microphytoplankton off the NW coast of Africa and in the southern temperate waters (Figure 2.11a) was concentrated in surface waters. The increase in percentage microphytoplankton in the northern temperate regions on AMT 12 and AMT 14 tended to be focused in the subsurface 50-100 m (Figures 2.10a, 2.12a). Despite the increase in chlorophyll-a concentrations in the equatorial region (Figures 2.9a-c), there was no significant change in the contribution of the various diagnostic pigment indices (Figures 2.13a-c).

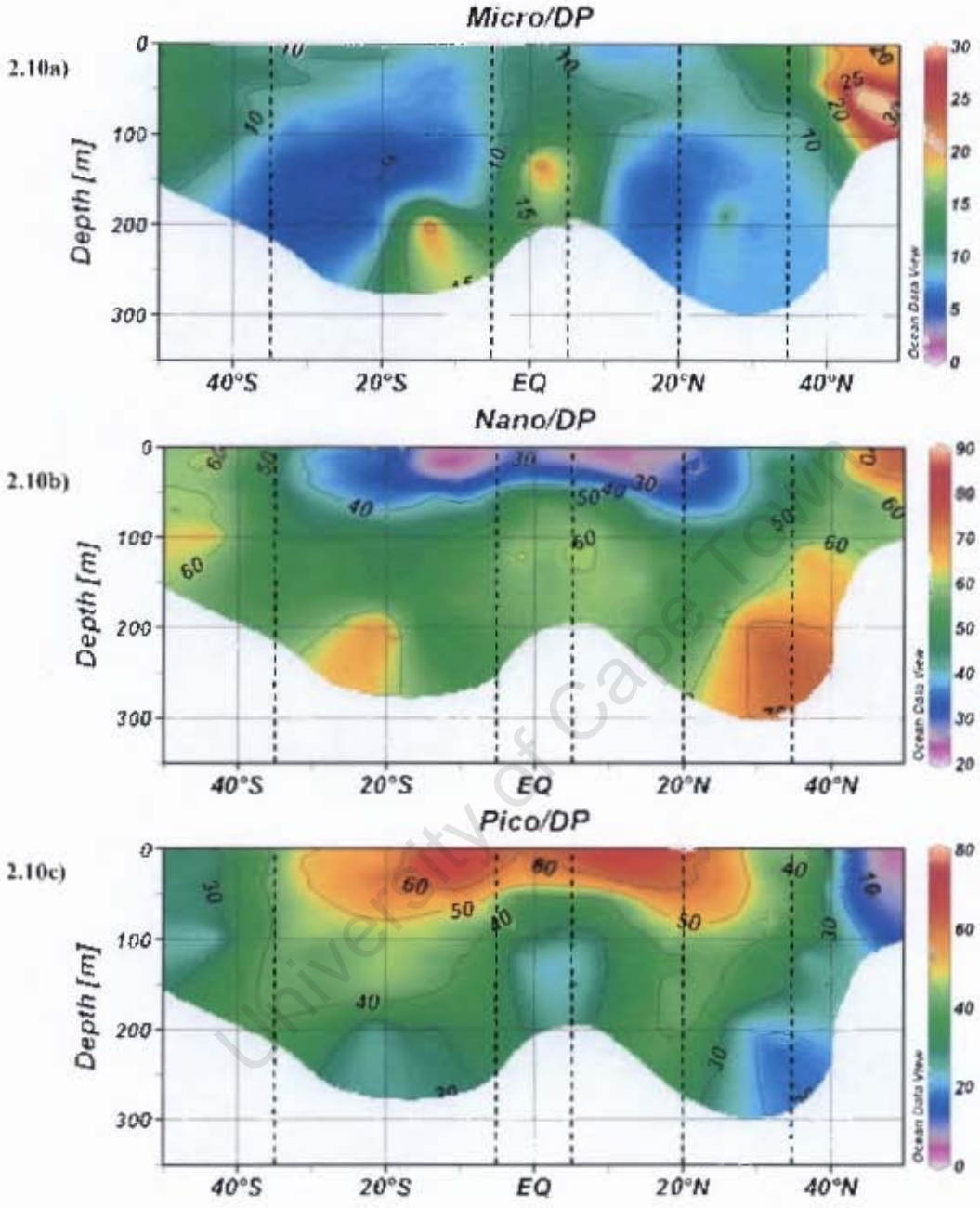

Figure 2.10. Sections of diagnostic pigment indices on AMT 12 for a) micro/DP b) nano/DP and c) pico/DP. Temperate (35°- 50°N and 35°-50°S), oligotrophic (20°-35°N and 5°-35°S), equatorial (5°S-5°N) and upwelling (5°-20°N) domains are indicated by vertical dashed lines.

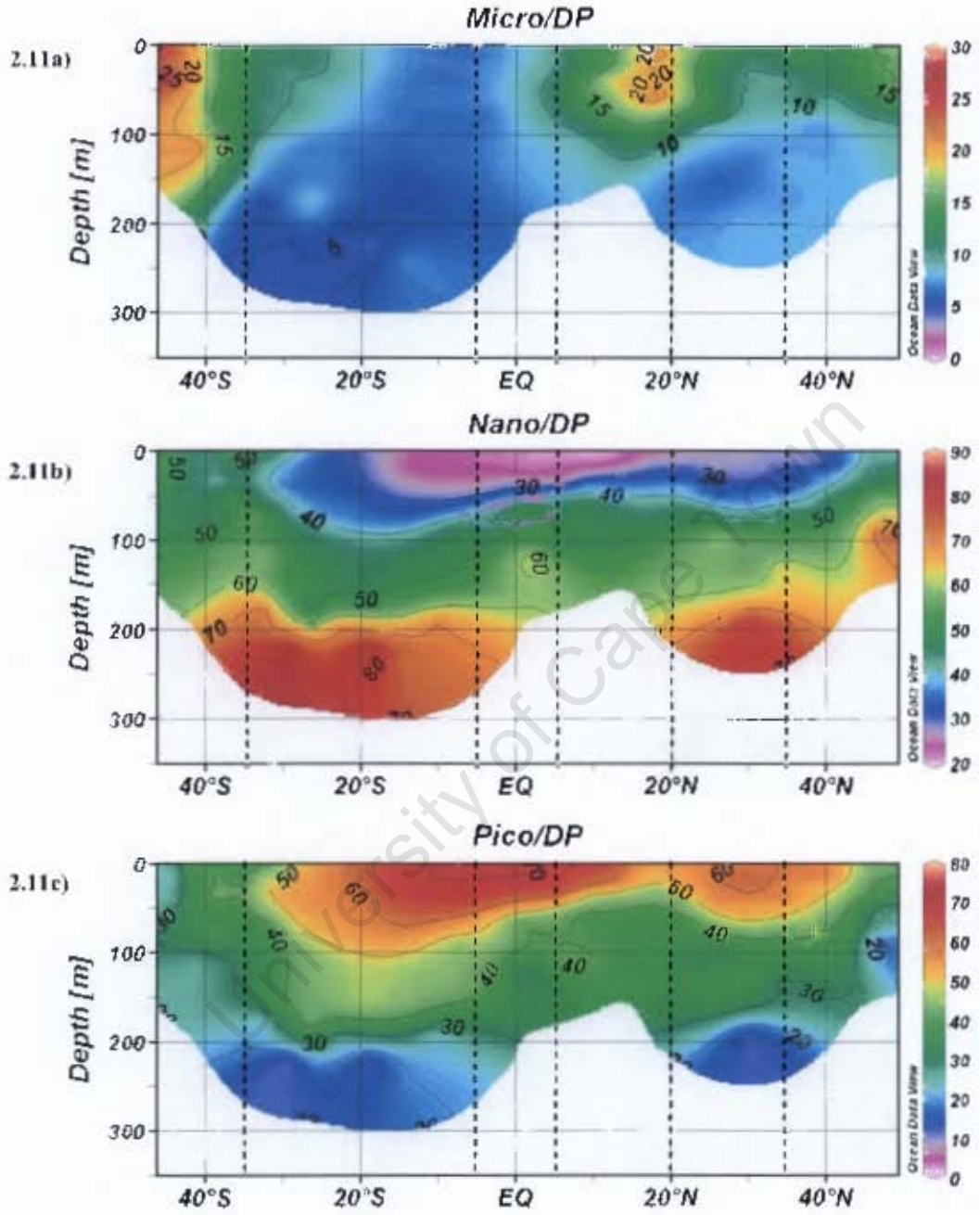

Figure 2.11. Sections of diagnostic pigment indices on AMT 13 for a) micro/DP b) nano/DP and c) pico/DP Temperate (35°- 50°N and 35°-50°S), oligotrophic (20°-35°N and 5°-35°S), equatorial (5°S-5°N) and upwelling (5°-20°N) domains are indicated by vertical dashed lines.

2.12a)

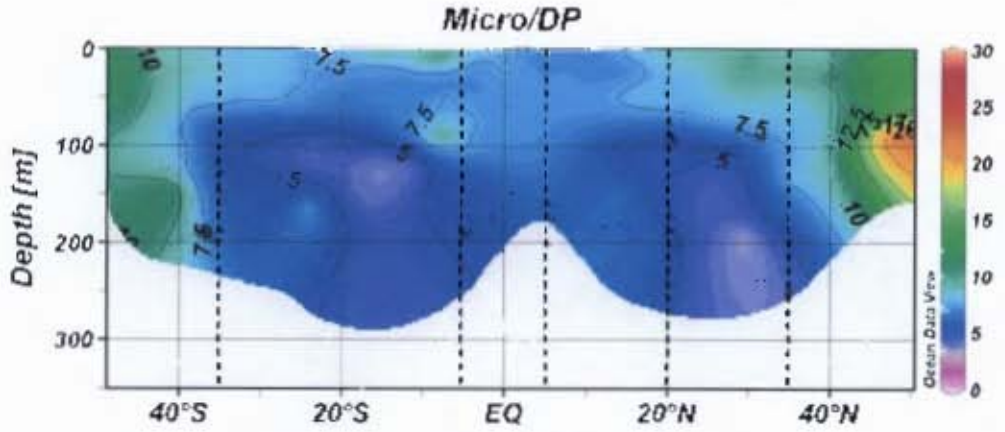

2.12b)

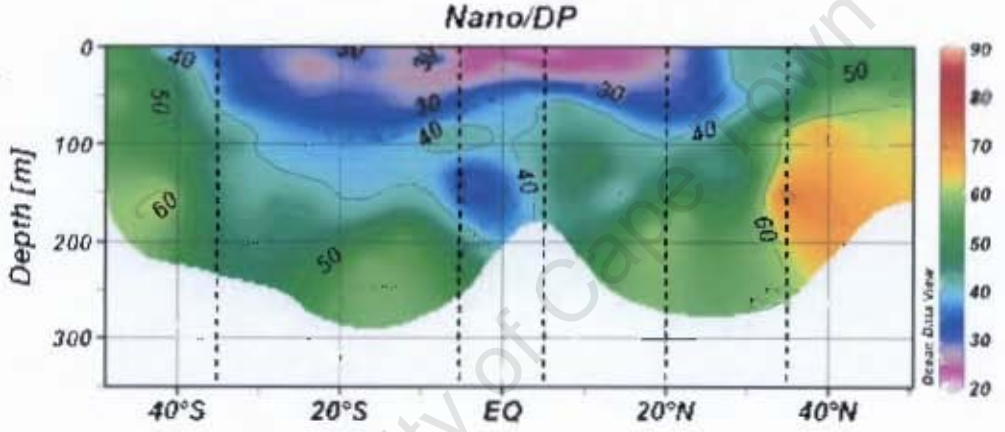

2.12c)

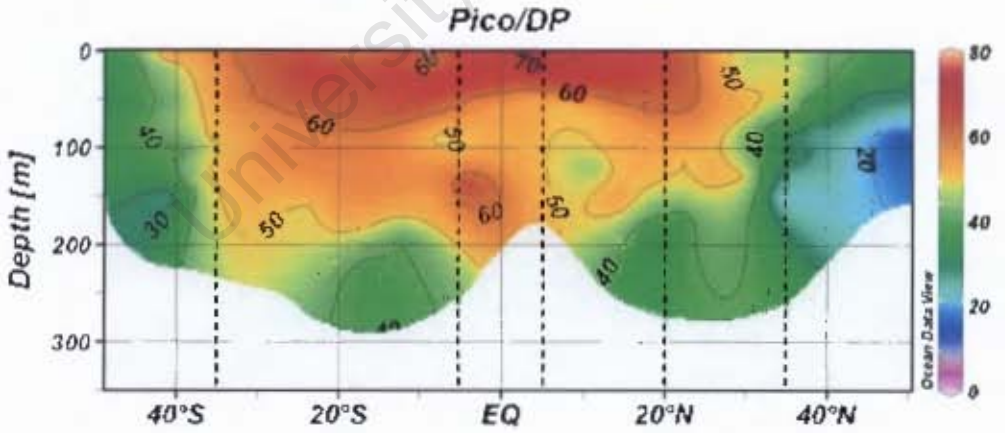

Figure 2.12. Sections of diagnostic pigment indices on AMT 14 for a) micro/DP b) nano/DP and c) pico/DP. Temperate (35°- 50°N and 35°-50°S), oligotrophic (20°-35°N and 5°-35°S), equatorial (5°S-5°N) and upwelling (5°-20°N) domains are indicated by vertical dashed lines.

Nanophytoplankton were the major contributors to total diagnostic pigments in both the northern and southern temperate regions on all three cruises (Figures 2.13a-c). Their distribution through the water column ranged between surface and subsurface maxima (Figures 2.10b, 2.11b, 2.12b). Picophytoplankton formed the dominant size fraction throughout the tropical and subtropical Atlantic on both AMT 13 and AMT 14 (~45-80%) (Figures 2.13b,c) and for most of AMT 12 (Figure 2.13a), although nanophytoplankton on occasion contributed more to total pigments. Above 100 m, picophytoplankton were the dominant size fraction in the tropical and subtropical regions, contributing 50-80% of total pigments (Figures 2.10c, 2.11c, 2.12c). Deeper in the water column (>200 m) in the gyre centres, nanophytoplankton dominated, making up >50% of the total pigments (Figures 2.10b, 2.11b, 2.12b).

2.3.4 Primary production

Rates of primary production decreased with depth at all latitudes throughout all three transects (Figures 2.14a-c). The DCM thus represented a chlorophyll maximum rather than a productivity maximum. Extremely low production rates characterised the central subtropical gyres (0.2-0.3 mmol C m^{-3} d^{-1}) and deep water (<0.1 mmol C m^{-3} d^{-1}). Primary production rates were highest (>0.8 mmol C m^{-3} d^{-1}) in surface waters of the northern temperate region during AMT 12 and AMT 14 and in southern temperate surface waters during AMT 13. Equally high fixation rates were associated with the Mauritanian upwelling system on AMT 13, while secondary peaks in surface production were associated with the equatorial upwelling region (~0.5-0.7 mmol C m^{-3} d^{-1}) and south of 40°S on AMT 14 (~0.5 mmol C m^{-3} d^{-1}). The seasonal variation in primary productivity was evident from the rates of carbon fixation integrated to the 1% light level (Figure 2.15) where higher rates of integrated production characterised the southern subtropical gyre and temperate waters during spring (AMT 13) and the northern hemisphere during spring on AMT 12 and AMT 14. Slightly higher rates of production were associated with the equatorial region and high productivity region off the NW coast of Africa on AMT 13.

2.13a)

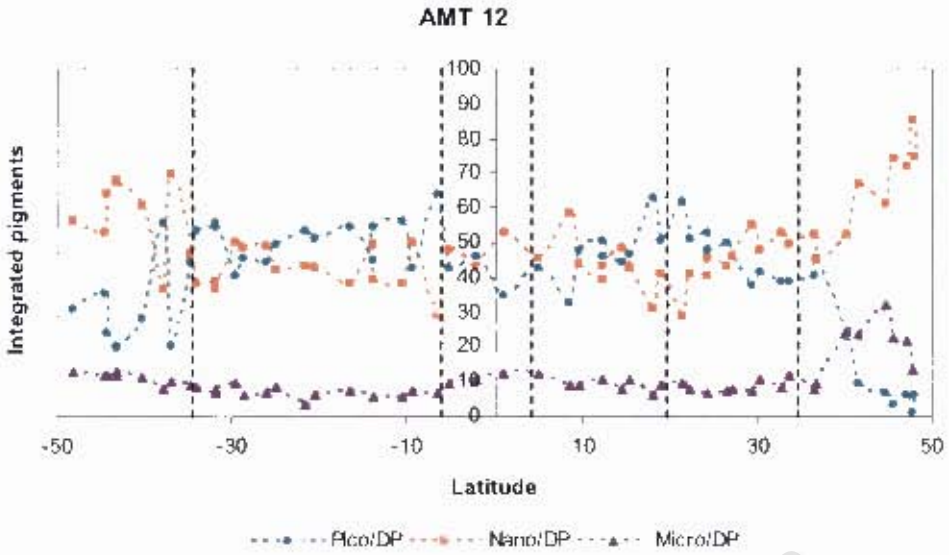

2.13b)

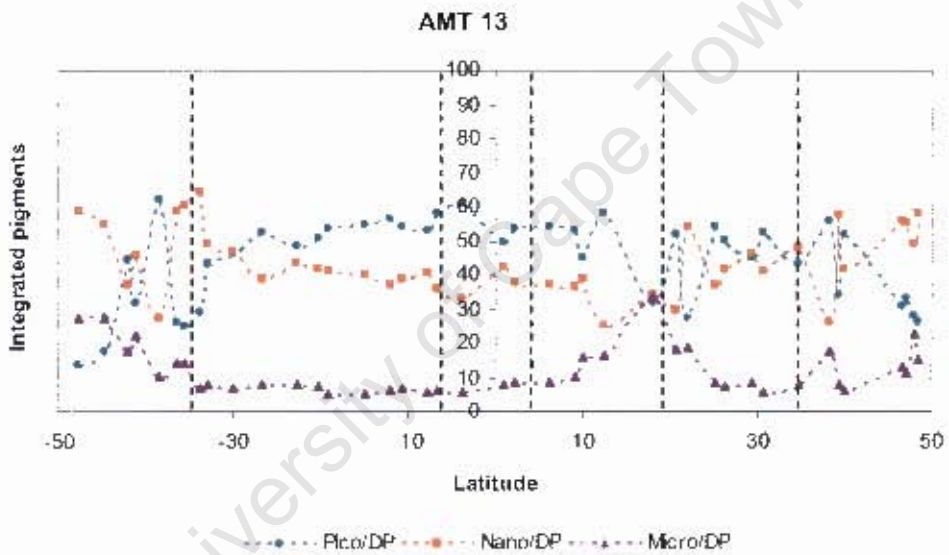

2.13c)

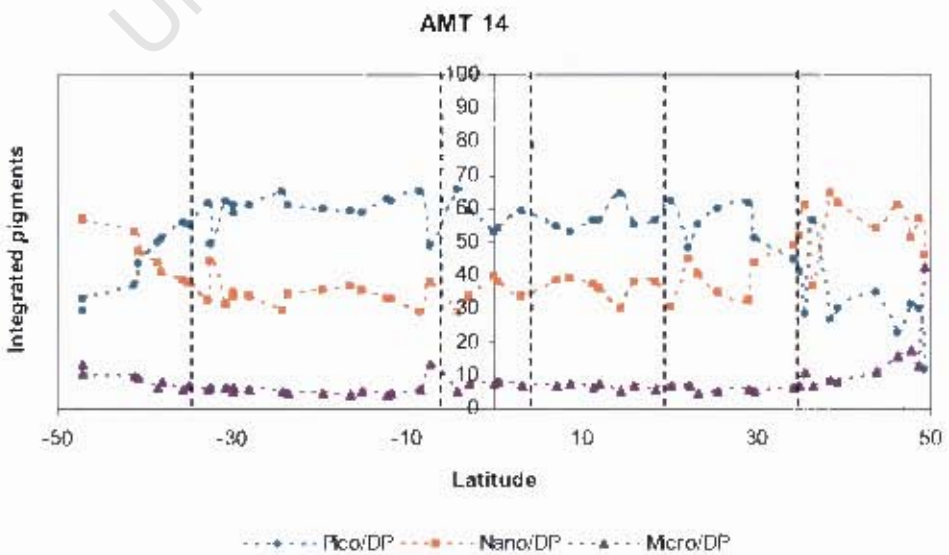

Figure 2.13. Diagnostic pigment indices integrated to the 1% light depth for a) AMT 12 b) AMT 13 and c) AMT 14. Temperate (35°- 50°N and 35°-50°S), oligotrophic (20°-35°N and 5°-35°S), equatorial (5°S-5°N) and upwelling (5°-20°N) domains are indicated by vertical dashed lines.

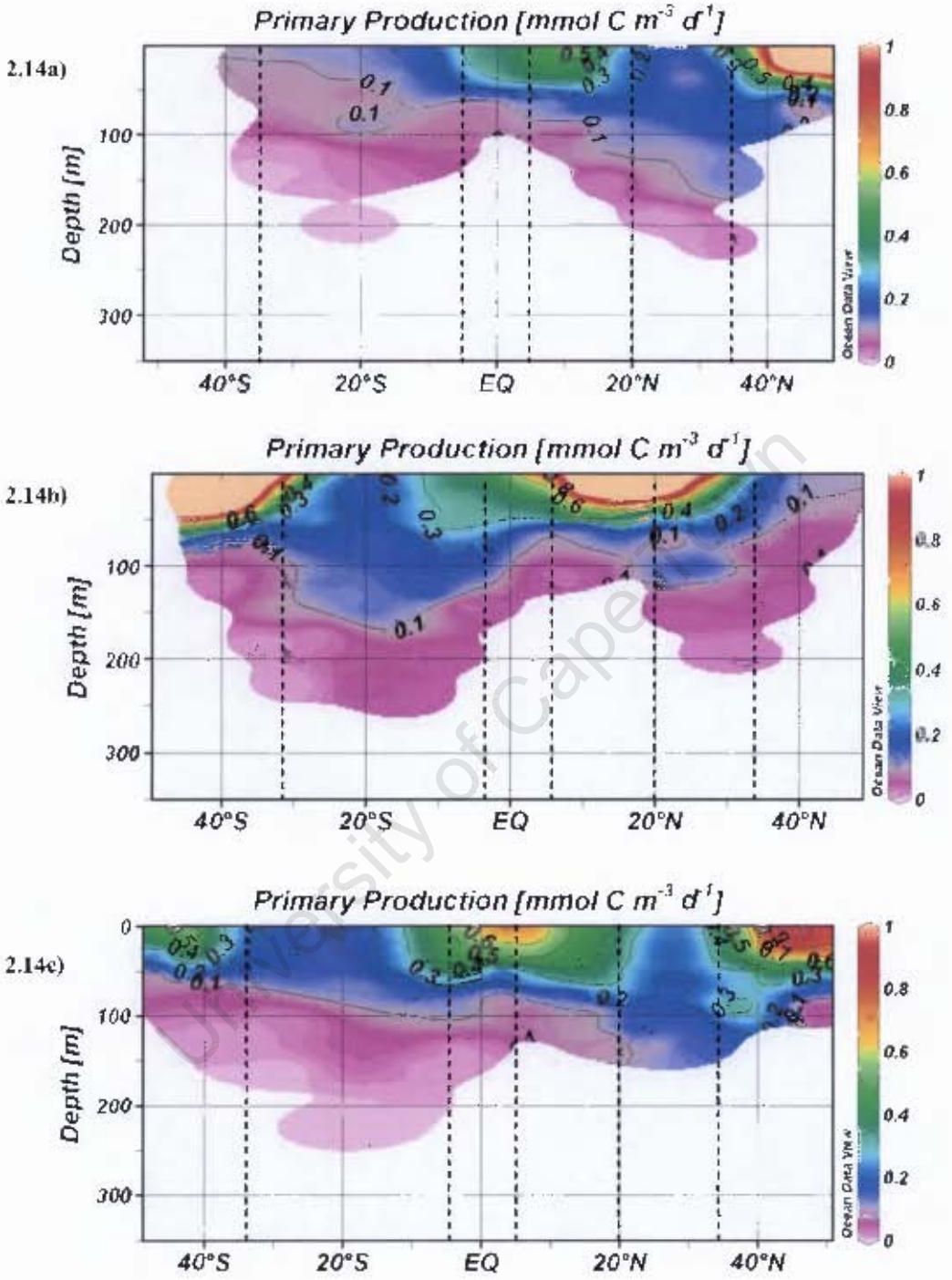

Figure 2.14. Sections of daily rates of carbon fixation for a) AMT 12, b) AMT 13 and c) AMT 14. Temperate (35°- 50°N and 35°-50°S), oligotrophic (20°-35°N and 5°-35°S), equatorial (5°S-5°N) and upwelling (5°-20°N) domains are indicated by vertical dashed lines.

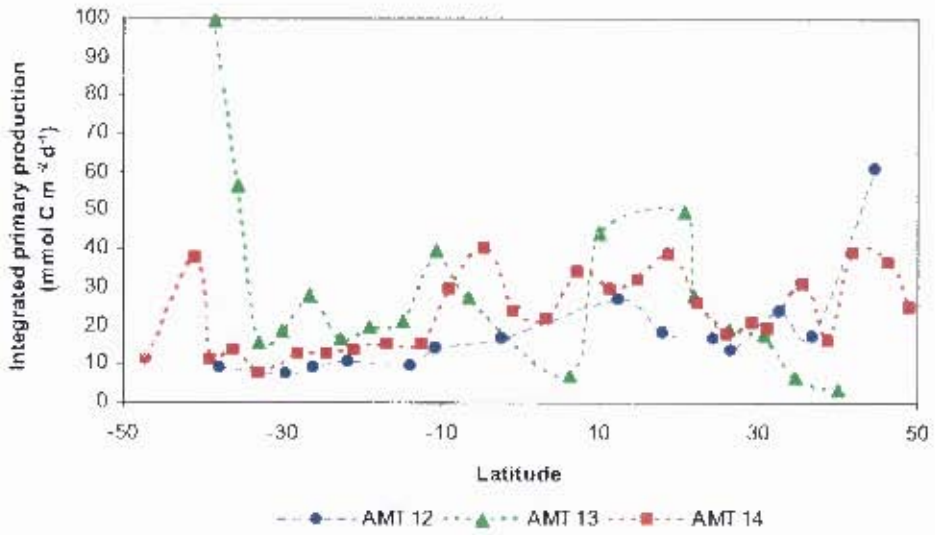

Figure 2.15. Daily integrated carbon fixation rates to the 1% light level for AMT 12, AMT 13 and AMT 14

2.3.5 Nitrate uptake

In the tropical and subtropical Atlantic, nitrate uptake (ρNO_3) rates in surface waters were extremely low (<0.025 mmol m^{-3} d^{-1}) and reflect the very low concentrations of NO_3 found here (Figures 2.16a,b). In the central gyres, ρNO_3 rates increased with depth due to increased nitrate concentrations originating from the nutricline and reached maximum rates (>0.04 mmol m^{-3} d^{-1}) at ~150 m in the gyre centres and ~70 m in the equatorial upwelling region. Maximum ρNO_3 uptake rates for AMT 12 (Figure 2.16a) were found in the surface 50 m south of 40°S whereas on AMT 14 (Figure 2.16b) the highest uptake rates were north of 40°N and extended to 70 m. An increase in subsurface uptake rates was also evident in the equatorial upwelling region. The increase in uptake reflects the increase in ambient nitrate concentrations in these waters. Subsurface uptake rates over the whole of the AMT 14 transect tended to be somewhat higher than during AMT 12. Daily rates of ρNO_3 uptake integrated to the 0.1% light level for AMT 12 and AMT 14 are shown in Figure 2.17a. Integrated rates of ρNO_3 uptake on AMT 14 were on average (mean = 12.30 $\pm$ 11.44 mmol m^{-2} d^{-1}) substantially higher (by ~five-fold) than on AMT 12 (mean = 2.40 $\pm$ 3.01 mmol m^{-2} d^{-1}).

When Redfield stoichiometry was applied (Redfield et al., 1963) to the 0.1% light level integrated ρNO_3 uptake rates, carbon-based new production estimates exceeded carbon fixation rates (Painter et al., in press). They suggested that the high ρNO_3 rates in the lower euphotic zone (1% and 0.1%) exceeded the immediate ρNO_3 requirements necessary to support local particulate NO_3 production. The metabolic processes responsible for these high ρNO_3 rates at depth are unclear but may include auto- and heterotrophic uptake as well as perhaps a degree of dark autotrophic ρNO_3 that is independent of the carbon uptake rate (Painter et al., in press). Consequently Painter et al. (in press) reduced the integration depth to the 14% light depth (the deepest sampling depth where the influence of the nitracline could conclusively be ruled out), allowing estimates of new production that were then lower than 'new' carbon fixation rates. Figure 2.17b shows integrated ρNO_3 uptake rates to the 14% light level with average uptake rates during AMT 14 (mean = 1.54 ± 1.48 mmol m^{-2} d^{-1}) being almost three times higher than those of AMT 12 (mean = 0.57 ± 0.51 mmol m^{-2} d^{-1}).

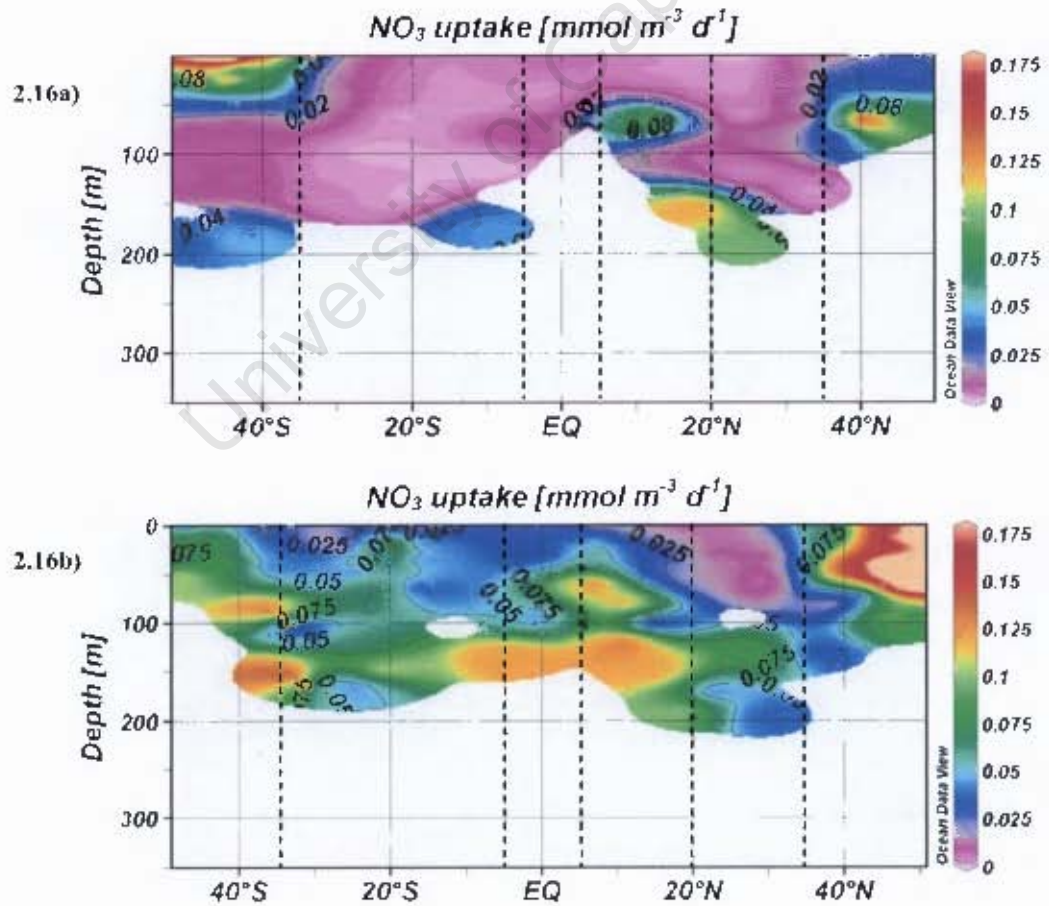

Figure 2.16. Sections of daily rates of NO_3 uptake for a) AMT 12, and b) AMT 14. Temperate (35°- 50°N and 35°-50°S), oligotrophic (20°-35°N and 5°-35°S), equatorial (5°S-5°N) and upwelling (5°-20°N) domains are indicated by vertical dashed lines.

2.17a)

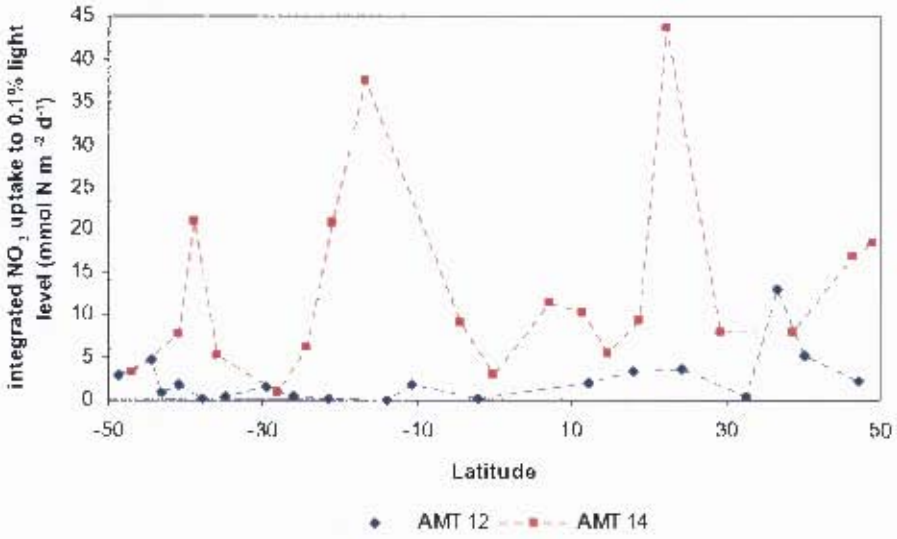

2.17b)

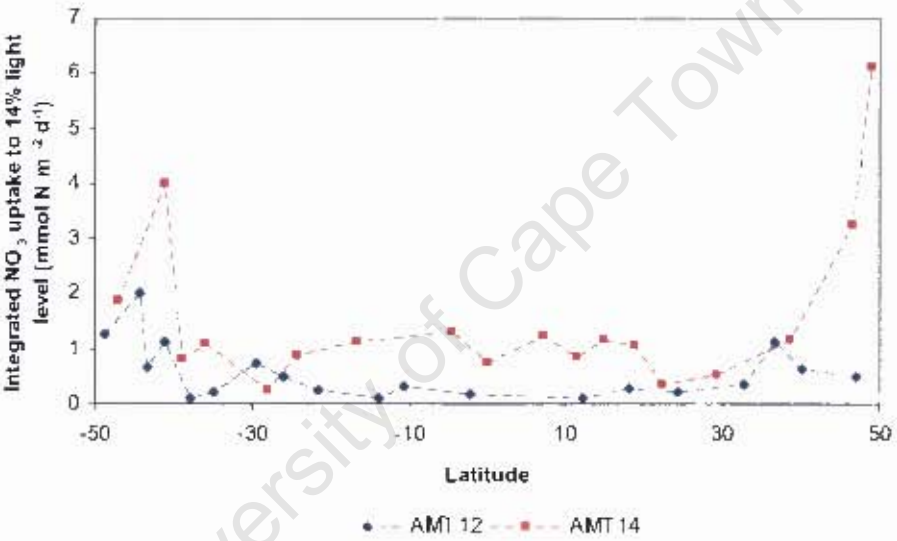

Figure 2.17. Daily rates of NO_3 uptake for AMT 12 and AMT 14 integrated to a) the 0.1% light depth and b) the 14% light depth

2.3.6 Characterisation of ecological domain

Taking account of the hydrography and biogeochemistry (Figures 2.3-2.16) the sampling environment was partitioned into 4 ecological domains: temperate (35°-50°N and 35°-50°S), oligotrophic (20°-35°N and 5°-35°S), equatorial (5°S-5°N) and upwelling (5°-20°N). The defining characteristics for each environment were drawn from Marañón et al. (2001). The temperate ecological domain was sampled at higher latitudes where the seasonal thermocline was weak or absent, there was an increase in subsurface NO_3 and surface chlorophyll-a was >0.05 mg m^{-3} (Figures 2.3-2.9).

Integrated diagnostic pigments averaged over the temperate region (Figures 2.18a-c) revealed a phytoplankton community dominated by nanophytoplankton (54%) and the highest percentage DP of microphytoplankton (15%). Oligotrophic regions were defined by a well developed thermocline >60 m, an upper mixed layer concentration of NO_3 <0.05 μM, surface chlorophyll <0.04 mg m^{-3} and a deep chlorophyll maximum (~100 m). The equatorial region was characterised by an uplifted thermocline and nitracline and a shallower DCM (~70 m) of higher chlorophyll concentration (>0.08 mg m^{-3}) than the central subtropical gyres. Finally, the upwelling regions of which there are two. Firstly, the upwelling region north of the equator, defined by a shallow upper mixed layer (60 m) and a chlorophyll maximum (>0.1 mg m^{-3}) located at ca 60 m, where NO_3 was >1 μM. The second is the upwelling region off the coast of NW Africa where SML depths were very shallow (~30 m) and chlorophyll concentrations (>0.15 mg m^{-3}) extended to the surface. The diagnostic pigments for all three regions (oligotrophic, equatorial and upwelling) revealed a similar community size structure distribution that was dominated by picophytoplankton (~50%) followed by ~40% nanophytoplankton and ~10% microphytoplankton (Figures 2.18a-c). The upwelling region in AMT 13 (Figure 2.18b) had a slightly higher percentage of microphytoplankton than AMT 12 and AMT 14, due to the upwelling off NW Africa.

2.3.7 Profiles of total ^{234}Th

Figures 2.19 (a-z) present depth profiles of ^{234}Th from AMT 12, 13 and 14, separated into 4 ecological domains to reveal several differences. The total ^{234}Th activities (dpm l^{-1}) and POC concentrations (μmol l^{-1}) are available in Tables 2.3a-c.

Temperate - All thorium profiles show clear ^{234}Th deficits in surface waters, with total ^{234}Th activities of ~2 dpm l^{-1} compared to ^{238}U activities of 2.5 dpm l^{-1} (Figures 2.19a-f). In the southern temperate region (Figures 2.19a, b), substantial disequilibria were evident in the top 60 m with equilibrium being reached at 100 m. At AMT 12 (Figure 2.19a) the particulate thorium maximum at 54 m coincided with the minimum in dissolved thorium, indicating intense scavenging. Intense scavenging was also seen in the northern temperate surface waters of AMT 13 (Figure 2.19d). However at this station a strong ^{234}Th remineralisation peak was also observed at 200 m.

2.18a)

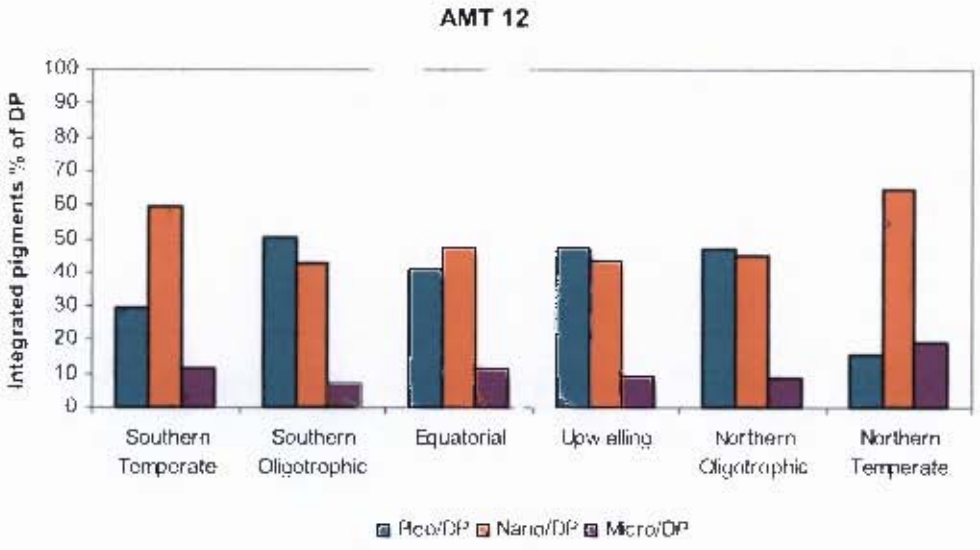

2.18b)

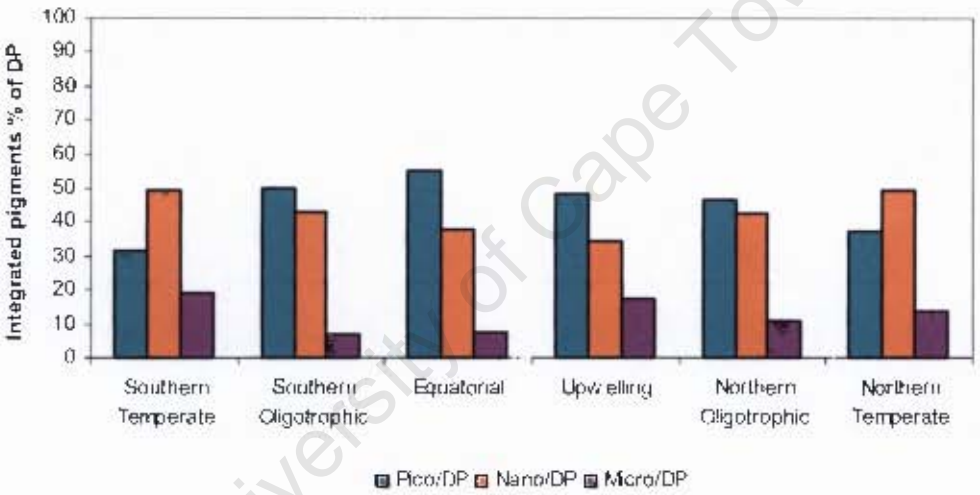

2.18c)

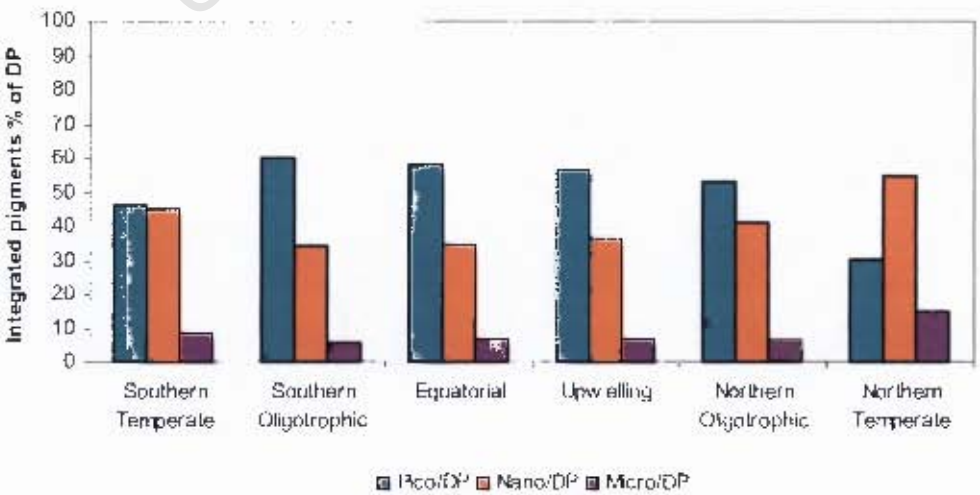

Figure 2.18. Diagnostic pigment indices integrated to the 1% light level and averaged over the ecological domains.

A similar subsurface remineralisation peak was observed at AMT12 (Figure 2.19c). At both stations total ^{234}Th was in equilibrium with ^{238}U at 100 m where regeneration and rapid export of particles balance each other. For the northern temperate region on AMT 14, one station showed a very intense disequilibrium that extended to 270 m (Figure 2.19e), while at the other station, the thorium deficit was only evident in the surface waters and equilibrium was regained by 90 m (Figure 2.19f). At 250 and 350 m this station tended toward a thorium excess however due to the relatively high analytical uncertainties was still regarded as being in equilibrium with uranium.

The Southern oligotrophic gyre - AMT 12 profiles (Figures 2.19g, h) showed a small thorium deficiency in surface waters that extended to 150 m. These stations had subsurface peaks in both particulate and dissolved thorium. Total ^{234}Th profiles on AMT 14 show small and hardly detectable radioactive disequilibria, with an extremely small subsurface disequilibrium at ~50 m depth. Equilibrium was reached between 120 and 300 m (Figures 2.19l-n) and for one profile (Figure 2.19l), there was a slight ^{234}Th excess at 300 m. On AMT 13 Figure 2.19k showed significant deficiency of total thorium with equilibrium being regained at ~100 m. Figures 2.19i,j on the other hand showed low ^{234}Th removal from surface waters. Minimum and maximum subsurface peaks in dissolved and particulate thorium coincide at 100 m indicating thorium scavenging. Below this depth, both profiles tended towards total ^{234}Th excess, of which the dissolved thorium fraction comprised (89-95%) of the total thorium.

The Northern oligotrophic gyre - During AMT 12 (Figure 2.19o) and AMT 13 (Figures 2.19p-r), total ^{234}Th was only slightly lower than ^{238}U, indicating slow rates of thorium removal from surface waters. The majority of profiles from AMT 12 and 13 show low particulate thorium in the surface waters that increased with depth, indicating an absence of particle scavenging from surface waters. Subsurface peaks in particulate thorium coincided with very high concentrations of dissolved thorium that together comprise the total thorium excess. For AMT 14, (Figures 2.19s,t) total ^{234}Th was in equilibrium with ^{238}U within analytical uncertainties throughout the water column, indicating very slow rates of particle export.

Equatorial - Profiles from equatorial stations were more varied and reflect the dynamic environment of this region where relatively large changes can take place over comparatively small space scales. Equatorial stations showed enhanced thorium removal from surface waters compared to the surrounding oligotrophic regions. The equatorial stations from AMT 12 (Figure 2.19u) and AMT 14 (Figure 2.19w) showed clearly detectable disequilibria in the topmost 200 m with equilibrium being reached at ~150 and ~300 m respectively. Figure 2.19u had a pronounced peak in both particulate and dissolved thorium just below the equilibrium depth that leads to a large thorium excess at 200 m. AMT 13 (Figure 2.19v) had a minimum in particulate and maximum in dissolved thorium at the surface. Very little thorium removal was seen throughout the water column and only a slight excess was observed at 300 m. There were relatively low concentrations of dissolved ^{234}Th at 500 m.

Upwelling - On AMT 12 and 13, the upwelling stations (Figure 2.19x,y) revealed a shallow export layer with equilibrium depths of ~60 m, below which there was a subsurface remineralisation of thorium at 100 to 200 m. Both stations also had low dissolved thorium at 500 m. On AMT 14 (Figure 2.19z) there was some evidence for a deficit in total ^{234}Th at 80 m with equilibrium being regained at 200 m. From 200 m downwards, the total ^{234}Th profile tended toward disequilibrium. However, total ^{234}Th activities did not differ from ^{238}U activities within analytical uncertainties.

Southern temperate

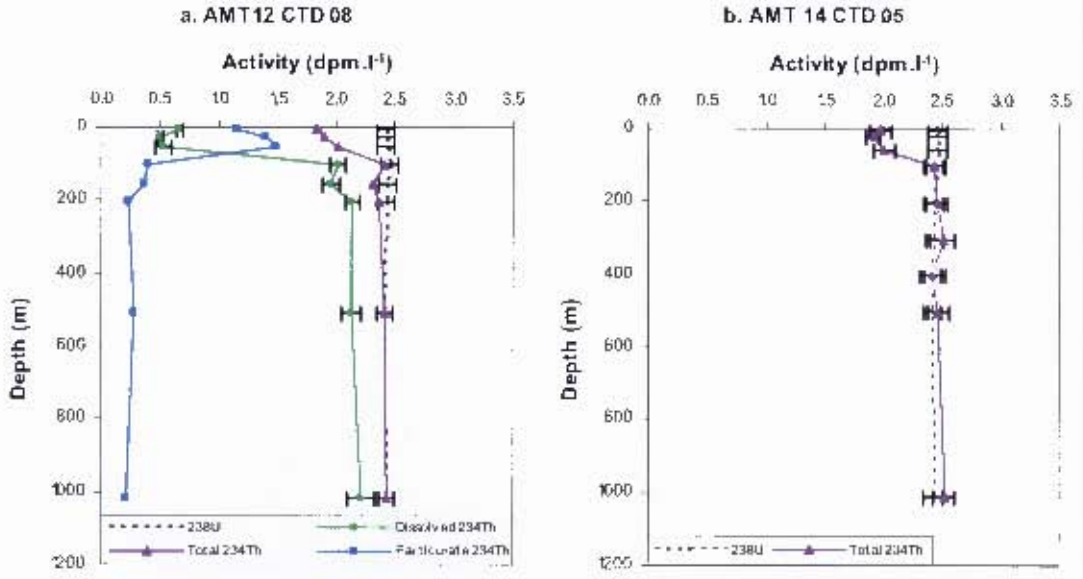

Northern temperate

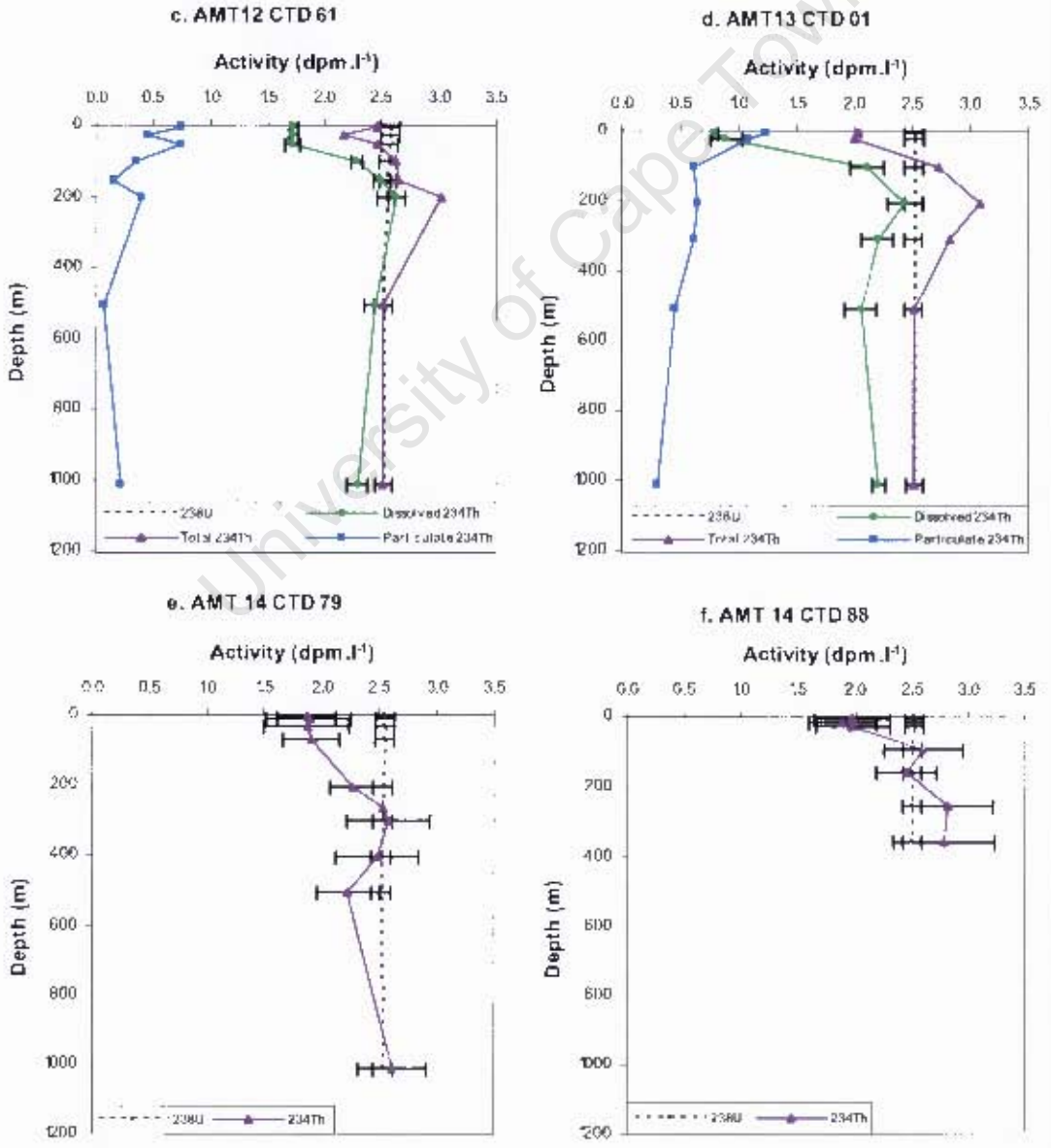

Figure 2.19. Vertical profiles of particulate, dissolved and total ^{234}Th and ^{238}U (dpm l^{-1}). Profiles are grouped into four ecological domains; temperate, oligotrophic, equatorial and upwelling. Error bars on total ^{234}Th data (AMT 14) indicate ± 1SD of propagated overall uncertainties (see text for details). Error bars on ^{238}U indicate ± 2SD (3.3%).

Southern oligotrophic

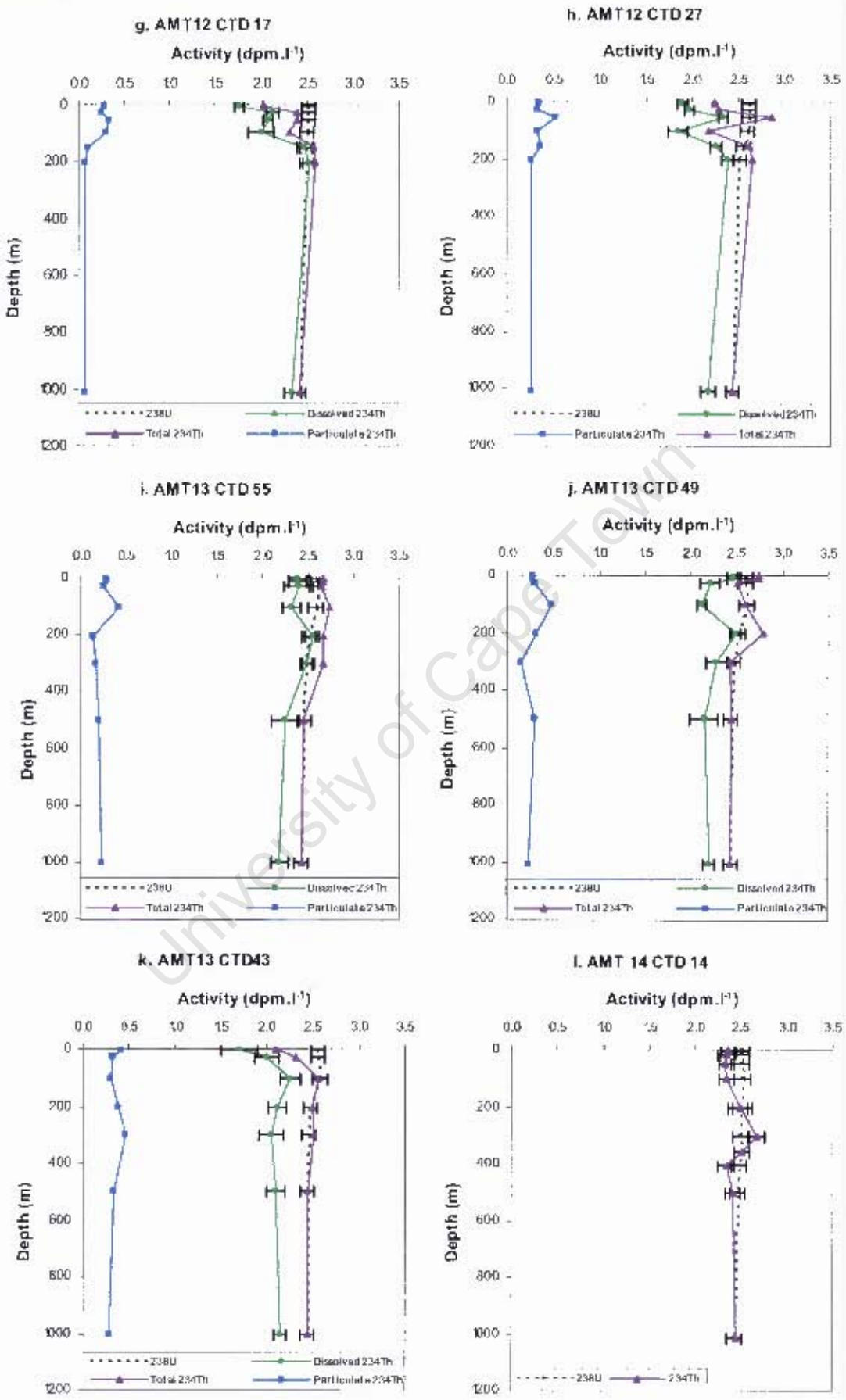

Figure 2.19. Vertical profiles of particulate, dissolved and total ^{234}Th and ^{238}U (dpm l^{-1}). Profiles are grouped into four ecological domains; temperate, oligotrophic, equatorial and upwelling. Error bars on total ^{234}Th data (AMT 14) indicate ± 1SD of propagated overall uncertainties (see text for details). Error bars on ^{238}U indicate ± 2SD (3.3%).

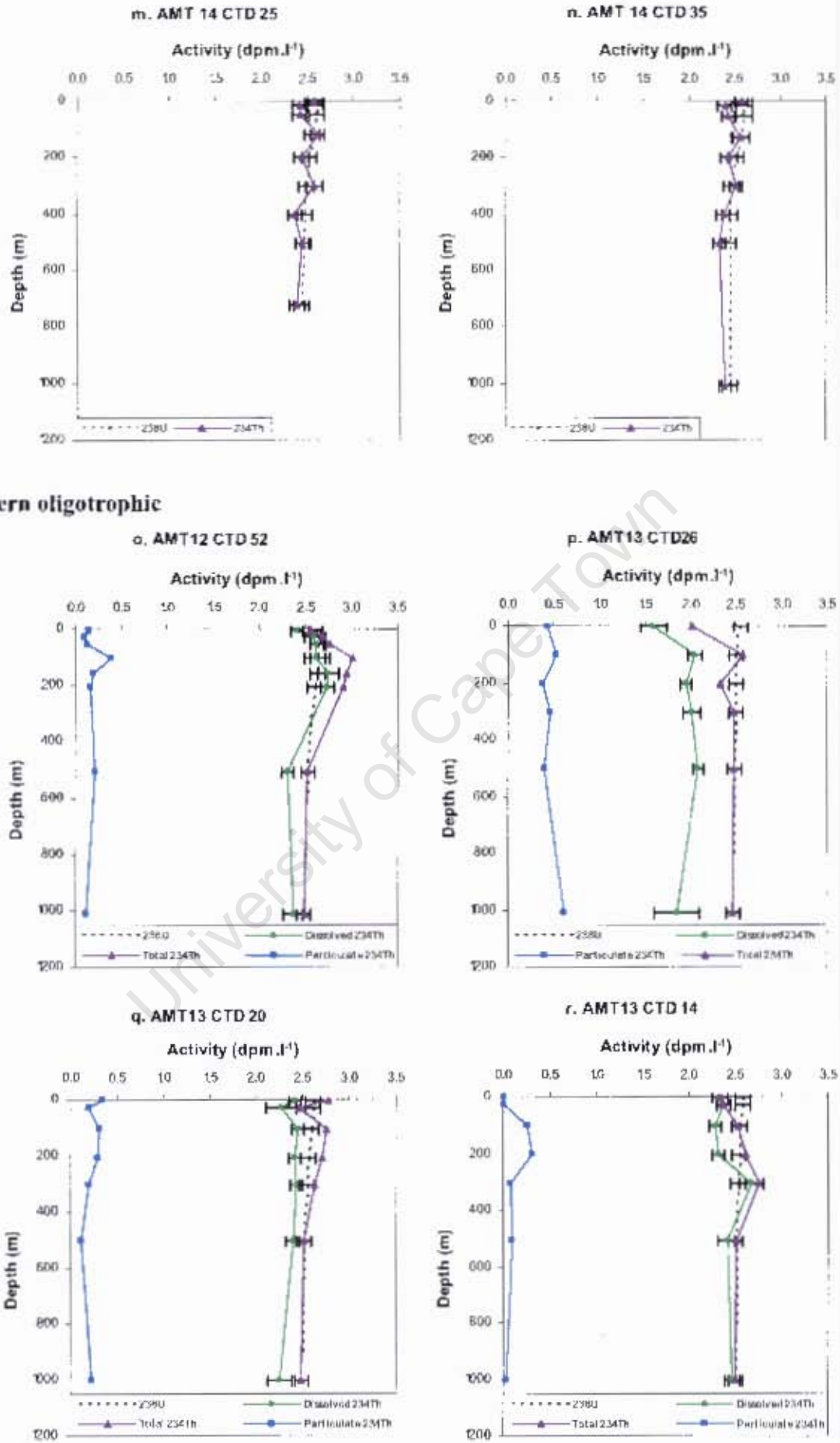

Figure 2.19. Vertical profiles of particulate, dissolved and total ^{234}Th and ^{238}U (dpm l^{-1}). Profiles are grouped into four ecological domains; temperate, oligotrophic, equatorial and upwelling. Error bars on total ^{234}Th data (AMT 14) indicate ± 1SD of propagated overall uncertainties (see text for details). Error bars on ^{238}U indicate ± 2SD (3.3%).

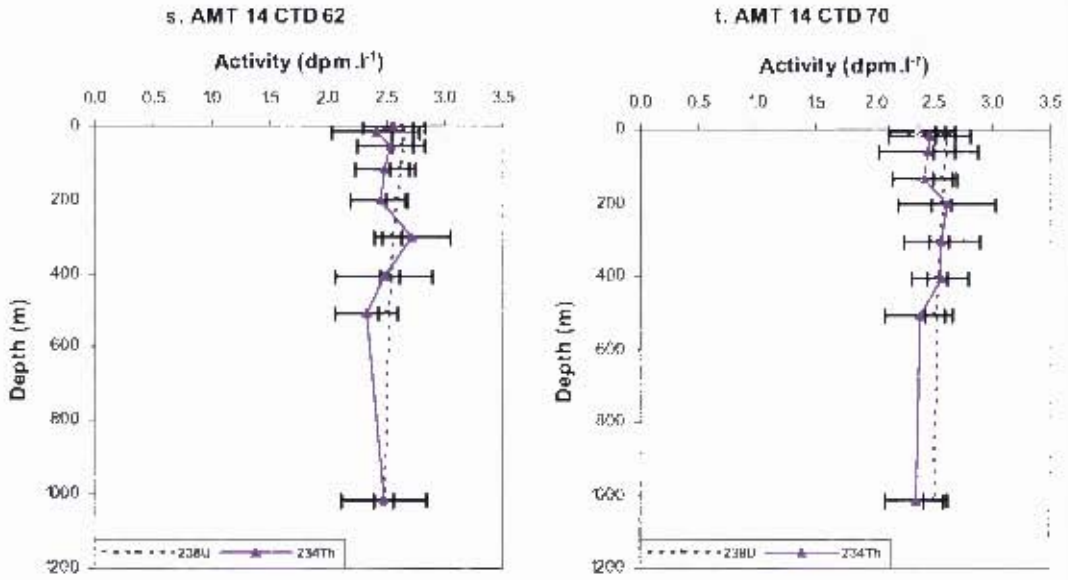

Equatorial

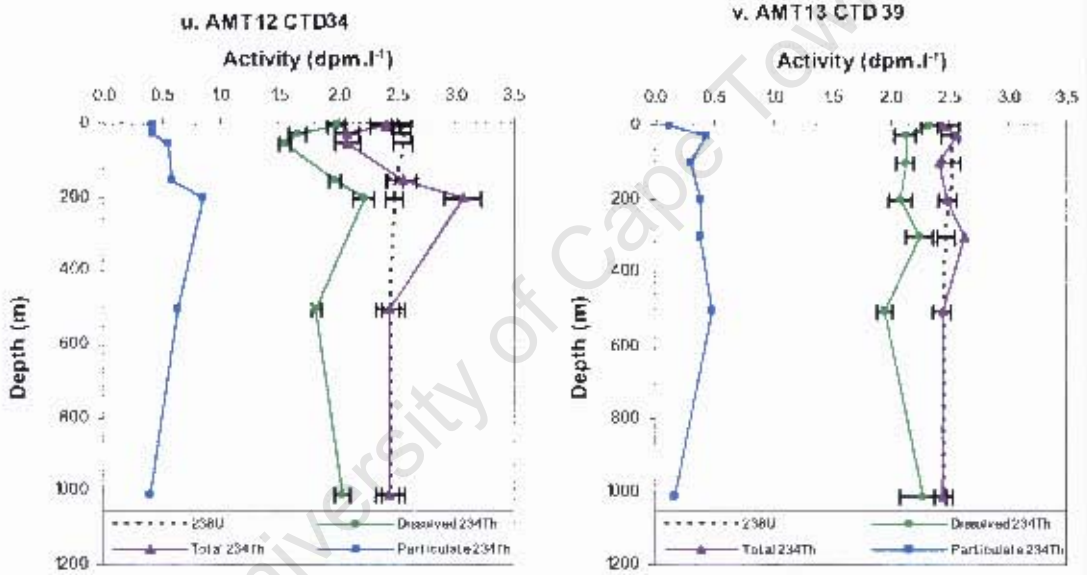

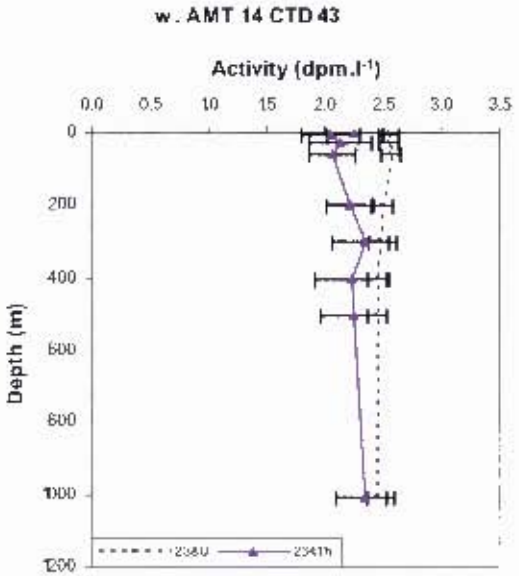

Figure 2.19. Vertical profiles of particulate, dissolved and total ^{234}Th and ^{238}U (dpm l^{-1}). Profiles are grouped into four ecological domains; temperate, oligotrophic, equatorial and upwelling. Error bars on total ^{234}Th data (AMT 14) indicate ± 1SD of propagated overall uncertainties (see text for details). Error bars on ^{238}U indicate ± 2SD (3.3%).

Upwelling

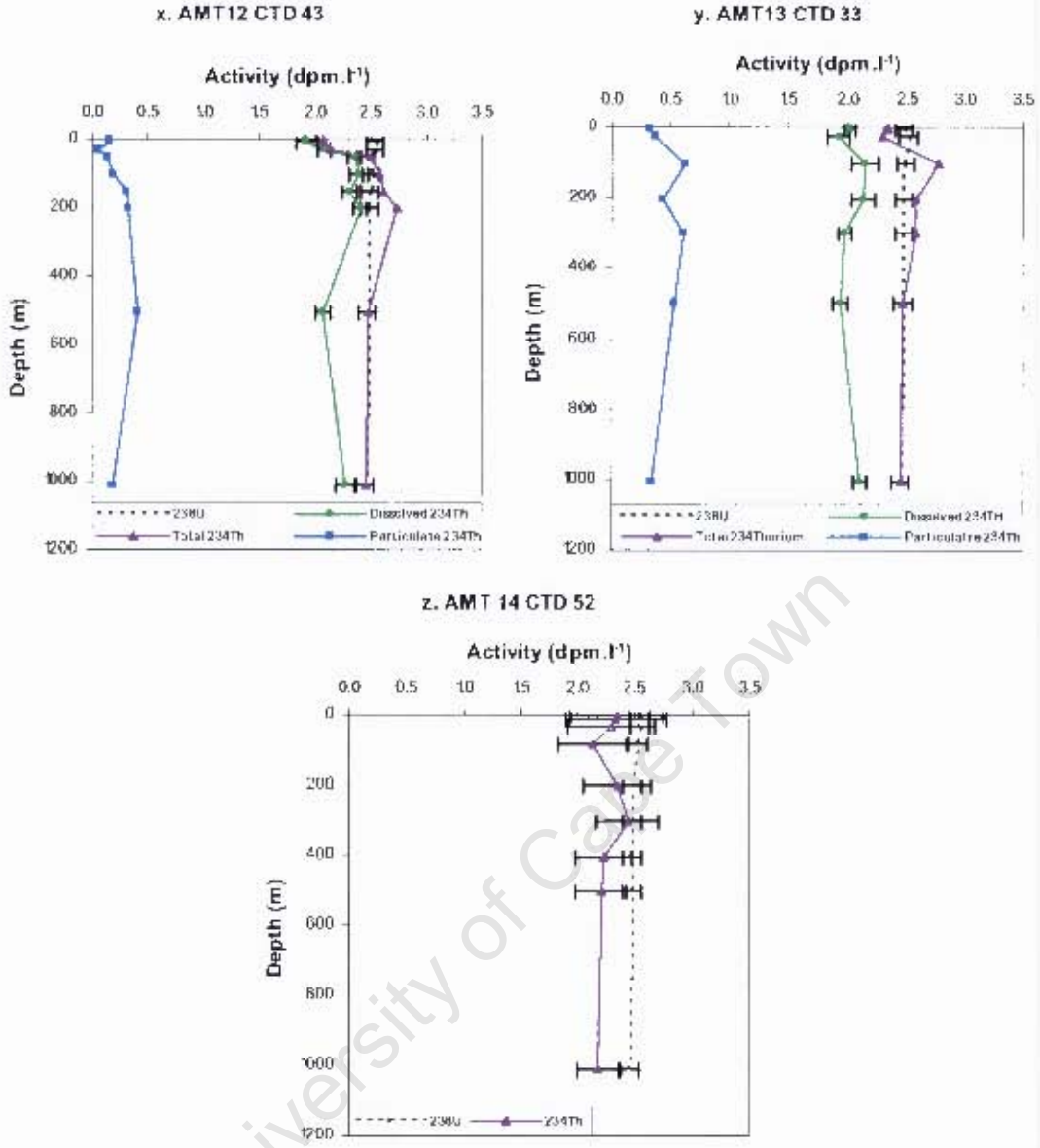

Figure 2.19. Vertical profiles of particulate, dissolved and total ^{234}Th and ^{238}U (dpm l^{-1}). Profiles are grouped into four ecological domains; temperate, oligotrophic, equatorial and upwelling. Error bars on total ^{234}Th data (AMT 14) indicate + 1SD of propagated overall uncertainties (see text for details). Error bars on ^{238}U indicate ± 2SD (3.3%).

Table 2.3a. ^{238}U, particulate and dissolved ^{234}Th activities and particulate organic carbon (POC) concentrations for AMT 12.

AMT 12

Station ID	Depth (m)	^{238}U (dpm l^{-1})	Part.^{234}Th (dpm l^{-1})	Diss.^{234}Th (dpm l^{-1})	±1SD (dpm l^{-1})	Depth (m)	POC (μM)
CTD 08	7	2.42	1.16	0.67	0.02		
	28	2.42	1.40	0.50	0.02		
	54	2.42	1.48	0.53	0.07		
	104	2.45	0.39	2.02	0.06		
	154	2.43	0.36	1.95	0.07		
	205	2.42	0.22	2.14	0.06		
	509	2.41	0.28	2.13	0.08		
	1016	2.43	0.21	2.21	0.11		
CTD 17	7	2.51	0.28	1.75	0.05		
	26	2.51	0.26	2.13	0.07		
	51	2.51	0.33	2.07	0.05		
	98	2.50	0.29	2.01	0.14		
	152	2.49	0.09	2.47	0.08		
	203	2.49	0.07	2.51	0.06		
	1011	2.42	0.07	2.34	0.09		
CTD 27	7	2.61	0.35	1.89	0.05		
	27	2.61	0.33	1.96	0.05		
	51	2.61	0.52	2.34	0.06		
	103	2.59	0.33	1.84	0.10		
	153	2.55	0.36	2.26	0.07		
	203	2.51	0.26	2.39	0.06		
	1010	2.44	0.27	2.17	0.08		
CTD 34	7	2.54	0.41	1.99	0.07	10	7.12
	26	2.55	0.41	1.66	0.07	20	4.50
	51	2.55	0.54	1.54	0.05	35	3.45
	151	2.48	0.58	1.97	0.05	74	7.06
	202	2.48	0.85	2.22	0.09	120	5.79
	504	2.44	0.63	1.82	0.05		
	1010	2.45	0.41	2.04	0.07		
CTD 43	7	2.55	0.15	1.93	0.09	25	4.62
	26	2.55	0.05	2.09	0.06	50	3.23
	51	2.46	0.14	2.36	0.06	100	1.90
	101	2.51	0.19	2.39	0.09	150	3.31
	151	2.49	0.30	2.31	0.06	200	3.14
	201	2.49	0.32	2.41	0.06	500	3.47
	504	2.47	0.40	2.07	0.06	1000	2.04
	1011	2.46	0.18	2.28	0.08		
CTD 52	7	2.61	0.15	2.41	0.06	18	3.96
	28	2.64	0.11	2.58	0.10	37	2.54
	53	2.63	0.14	2.62	0.08	60	2.79
	103	2.63	0.39	2.62	0.14	140	1.95
	154	2.63	0.20	2.74	0.11	190	2.25
	204	2.59	0.17	2.74	0.07		
	506	2.52	0.22	2.30	0.06		
	1013	2.48	0.11	2.37	0.10		
CTD 61	7	2.58	0.74	1.72	0.04	10	3.58
	27	2.58	0.44	1.72	0.04	20	3.18
	51	2.56	0.75	1.72	0.07	36	3.00
	101	2.55	0.35	2.28	0.05	85	4.03
	153	2.55	0.15	2.50	0.08	120	1.95
	204	2.54	0.40	2.63	0.07		
	508	2.51	0.07	2.44	0.09		
	1012	2.51	0.22	2.29	0.09		

Table 2.3b. ^{238}U, particulate and dissolved ^{234}Th activities and particulate organic carbon (POC) concentrations for AMT 13

AMT 13

Station ID	Depth (m)	^{238}U (dpm l^{-1})	Part.^{234}Th (dpm l^{-1})	Diss.^{234}Th (dpm l^{-1})	±1SD (dpm l^{-1})	POC (µM)	Station ID	Depth (m)	^{238}U (dpm l^{-1})	Part.^{234}Th (dpm l^{-1})	Diss.^{234}Th (dpm l^{-1})	±1SD (dpm l^{-1})	POC (µM)
CTD 01	5	2.51	1.23	0.80	0.02	8.06	CTD 39	2	2.50	0.11	2.33	0.07	2.92
	22	2.51	1.09	0.90	0.14	5.23		28	2.50	0.43	2.13	0.09	3.65
	103	2.51	0.61	2.10	0.15	3.86		102	2.51	0.29	2.12	0.07	1.42
	203	2.51	0.65	2.43	0.14	2.18		204	2.49	0.38	2.09	0.10	1.93
	305	2.51	0.61	2.20	0.14	2.12		304	2.47	0.38	2.24	0.12	2.43
	506	2.51	0.46	2.05	0.13	1.90		506	2.44	0.48	1.95	0.07	2.50
	1012	2.52	0.30	2.21	0.06	1.79		1012	2.45	0.17	2.28	0.20	1.97
CTD 14	2	2.57	0.00	2.33	0.08	5.15	CTD 43	2	2.55	0.41	1.70	0.20	3.92
	27	2.57	0.00	2.37	0.06	2.07		27	2.55	0.31	2.00	0.14	4.99
	103	2.55	0.26	2.28	0.06	2.03		101	2.58	0.30	2.25	0.11	2.28
	204	2.54	0.30	2.31	0.13	2.44		201	2.47	0.37	2.11	0.10	2.16
	303	2.53	0.09	2.68	0.09	1.20		301	2.46	0.46	2.05	0.14	1.95
	507	2.50	0.10	2.41	0.08	1.29		497	2.44	0.34	2.10	0.10	1.80
	1005	2.50	0.04	2.46	0.12	1.13		1001	2.44	0.28	2.15	0.07	1.23
CTD 20	2	2.61	0.35	2.42	0.07	2.45	CTD 49	12	2.59	0.27	2.47	0.07	3.25
	27	2.61	0.20	2.27	0.16	nd		24	2.59	0.30	2.21	0.11	2.98
	103	2.59	0.30	2.45	0.07	2.59		103	2.61	0.48	2.11	0.05	nd
	202	2.56	0.29	2.41	0.06	1.49		203	2.52	0.31	2.49	0.06	2.09
	302	2.54	0.19	2.43	0.06	1.35		303	2.47	0.15	2.28	0.12	1.64
	502	2.51	0.12	2.39	0.07	0.80		502	2.44	0.29	2.14	0.16	1.74
	999	2.48	0.22	2.26	0.13	1.35		1010	2.44	0.24	2.20	0.06	2.11
CTD 26	2	2.55	0.43	1.59	0.14	5.60	CTD 55	10	2.60	0.28	2.39	0.10	2.99
	103	2.50	0.54	2.05	0.09	1.28		28	2.60	0.26	2.40	0.16	3.07
	203	2.49	0.37	1.95	0.06	1.70		103	2.59	0.42	2.31	0.10	2.91
	304	2.50	0.47	2.02	0.10	1.43		203	2.51	0.13	2.54	0.08	2.40
	504	2.48	0.40	2.09	0.05	1.18		304	2.49	0.17	2.49	0.06	1.65
	1007	2.47	0.61	1.86	0.25	1.18		498	2.45	0.20	2.26	0.15	1.46
CTD 33	4	2.48	0.33	2.02	0.05	4.90		1002	2.43	0.24	2.19	0.10	5.62
	26	2.52	0.37	1.93	0.10	3.71							
	102	2.49	0.62	2.15	0.11	1.21							
	203	2.48	0.44	2.14	0.09	nd							
	303	2.48	0.60	1.98	0.05	0.93							
	502	2.47	0.52	1.95	0.06	0.57							
	1005	2.45	0.34	2.11	0.06	1.25							

Table 2.3c. ^{238}U and total (particulate + dissolved) ^{234}Th activities and particulate organic carbon (POC) concentrations for AMT 14. nd indicates not determined.

AMT 14

Station ID	Depth (m)	^{238}U (dpm l^{-1})	Total ^{234}Th (dpm l^{-1})	±1SD (dpm l^{-1})	POC (μM)	Station ID	Depth (m)	^{238}U (dpm l^{-1})	Total ^{234}Th (dpm l^{-1})	±1SD (dpm l^{-1})	POC (μM)
CTD 05	7	2.46	1.97	0.09	12.43	CTD 52	3	2.54	2.34	0.4	4
	21	2.46	1.91	0.06	nd		10	2.54	2.33	0.43	3.19
	61	2.46	2	0.09	nd		35	2.54	2.3	0.38	3.65
	101	2.45	2.42	0.09	5.82		81	2.52	2.13	0.29	3.77
	202	2.43	2.45	0.09	8.3		202	2.48	2.34	0.3	1.62
	303	2.43	2.51	0.11	nd		303	2.47	2.44	0.27	1.5
	403	2.42	2.41	0.11	2.77		404	2.48	2.23	0.25	1.82
	506	2.42	2.46	0.09	4.05		504	2.47	2.21	0.23	1.79
	1011	2.43	2.52	0.09	3.65		1011	2.46	2.18	0.19	1.52
CTD 14	6	2.51	2.36	0.08	2.77	CTD 62	2	2.64	2.57	0.27	2.95
	14	2.51	2.34	0.09	6.79		17	2.64	2.41	0.38	3.33
	47	2.51	2.33	0.07	3.6		51	2.64	2.54	0.29	4.34
	101	2.52	2.35	0.08	2.8		116	2.62	2.49	0.26	2.78
	203	2.5	2.49	0.13	1.28		203	2.58	2.44	0.24	1.49
	303	2.49	2.67	0.08	1.22		303	2.56	2.72	0.32	1.05
	405	2.48	2.34	0.08	1.47		405	2.54	2.48	0.42	1.03
	502	2.46	2.41	0.09	0.77		505	2.52	2.33	0.27	0.98
	1011	2.43	2.44	0.09	2.98		1012	2.48	2.49	0.37	1.3
CTD 25	5	2.59	2.57	0.1	2.15	CTD 70	3	2.6	2.37	0.24	2.72
	17	2.59	2.42	0.09	nd		18	2.6	2.48	0.35	1.63
	48	2.6	2.41	0.07	2.61		57	2.6	2.46	0.42	1.96
	121	2.55	2.61	0.08	2.31		132	2.59	2.43	0.28	2.59
	199	2.52	2.44	0.08	2.05		203	2.57	2.62	0.41	2.6
	302	2.49	2.57	0.09	1.33		304	2.56	2.57	0.32	1.27
	403	2.48	2.36	0.07	1.02		404	2.54	2.57	0.24	1.65
	503	2.46	2.44	0.08	2.67		505	2.53	2.38	0.29	0.98
	723	2.43	2.39	0.08	1.36		1013	2.5	2.35	0.26	1.3
CTD 35	1	2.6	2.57	0.07	3.14	CTD 79	3	2.55	1.87	0.25	2.7
	16	2.6	2.4	0.07	3.47		10	2.55	1.89	0.37	4.31
	55	2.6	2.43	0.07	4.03		31	2.54	1.87	0.37	5.12
	128	2.57	2.56	0.1	2.5		71	2.54	1.9	0.24	nd
	200	2.51	2.44	0.09	1.64		203	2.53	2.26	0.19	2.03
	300	2.46	2.51	0.07	1.2		304	2.52	2.58	0.37	1.64
	401	2.45	2.37	0.07	1.06		405	2.52	2.48	0.35	1.29
	502	2.44	2.34	0.07	5.56		506	2.51	2.23	0.27	1.36
	1009	2.45	2.39	0.07	3.81		1013	2.54	2.62	0.3	1.55
CTD 43	2	2.55	2.256	0.24	4.52	CTD 88	3	2.51	1.97	0.33	4.95
	8	2.55	2.048	0.24	3.41		18	2.51	1.89	0.29	5.11
	27	2.55	2.129	0.26	3.43		28	2.51	1.98	0.32	4.73
	58	2.57	2.067	0.2	5.78		93	2.51	2.6	0.35	2.79
	200	2.49	2.212	0.19	3.31		155	2.51	2.46	0.26	3.47
	300	2.47	2.344	0.27	1.78		255	2.51	2.82	0.4	1.86
	402	2.45	2.226	0.32	1.58		355	2.5	2.78	0.44	nd
	503	2.45	2.248	0.28	1.11						
	1009	2.45	2.343	0.25	1.6						

2.4 Discussion

Before discussing the latitudinal distributions of ^{234}Th-derived POC export, the ^{234}Th scavenging model is described (section 2.4.1) and evaluated (section 2.4.2) followed by a latitudinal description of ^{234}Th fluxes (section 2.4.3). In section 2.4.4, the approach adopted to calculate POC export is described, including a brief discussion of particulate POC/^{234}Th ratios crucial for this approach as well as an interpretation of the latitudinal distribution of open-ocean POC export. Section 2.4.5 follows with a discussion of estimates of POC export efficiency determined by the ratio of ^{234}Th-derived POC export to ^{14}C-derived primary production.

2.4.1 ^{234}Th scavenging model

The total ^{234}Th activity balance in a given parcel of water can be described by the following equation:

$$\partial A_t / \partial t = [A_U - (A_p + A_d)] \lambda - P + V = (A_U - A_t) \lambda - P + V \qquad (1)$$

where $\partial A_t / \partial t$ (dpm m^{-3} d^{-1}) is the temporal rate of change in total ^{234}Th activity A_t (dpm m^{-3}), A_p is particulate ^{234}Th activity (dpm m^{-3}), A_d is dissolved ^{234}Th activity (dpm m^{-3}), A_U is the uranium activity (dpm m^{-3}), λ is the decay constant for ^{234}Th (0.02876 d^{-1}), P is the net loss of ^{234}Th on sinking particles (dpm m^{-3} d^{-1}), and V is the sum of advective and diffusive terms (dpm m^{-3} d^{-1}).

The net loss of ^{234}Th on sinking particles is given by

$$P = (A_U - A_t) \lambda - \partial A_t / \partial t + V \qquad (2)$$

Single activity profiles obtained during this study lack information on spatio-temporal variability and necessitate the assumption of steady state on a time scale of up to a few weeks. As limited sampling opportunities did not allow multiple measurements at each station, activity gradients in time or space cannot be assessed. The data therefore do not allow estimation of horizontal and vertical advective contributions to thorium

sinking fluxes, but they are assumed to be insignificant compared to scavenging rates and export on sinking particles. (An exception is the tropical open-ocean upwelling regime; see below).

A steady state has to be assumed, i.e., $\partial A_t / \partial t = 0$, and the calculated ^{234}Th flux is assumed to be constant over the mean life of ^{234}Th (34.8 days). Moreover, advection and diffusion are neglected as being small relative to the other terms. Finally, equation (1) assumes that vertical processes control the uptake and removal of ^{234}Th from the water column and that lateral transport is unimportant. In which case Equation (1) simplifies to a one-dimensional (vertical) system:

$$P = (A_U - A_t)\,\lambda \qquad (3)$$

To calculate ^{234}Th flux from the surface into the deep ocean, the activity profile of total ^{234}Th is integrated from the sea surface to depth, *z*, where radioactive equilibrium was reached:

$$P = \lambda \int_0^z (A_U - A_t)dz \qquad (4)$$

A steady-state approach essentially assumes a constant flux over periods of days to weeks determined by the ^{234}Th decay and residence times. This assumption provides adequate resolution of ^{234}Th fluxes in many settings (Tanaka et al., 1983; Wei and Murray, 1991; Moran and Buesseler, 1993; Buesseler et al., 2001a). However, non-steady state effects are important during periods of significant ^{234}Th drawdown, such as during phytoplankton blooms and post-bloom conditions (Buesseler et al., 1992b, Buesseler et al., 1998, Buesseler et al., 2001a; Cochran et al., 1997). For a more in-depth discussion on the assumptions involved in the steady-state approach see section 4.4.5.1.

The effect of upwelling on the thorium balance (V in equation [1]) is significant in regions of high upwelling velocity, such as the equatorial Pacific (Buesseler et al., 1995; Bacon et al., 1996; Dunne and Murray, 1999), where estimated fluxes were 25-35% higher when upwelling was considered (Buesseler et al., 1995), and the north-

western Arabian Sea during the Southwest Monsoon (Buesseler et al., 1998). Horizontal processes affecting the intensity of thorium scavenging are found to only be important in continental margins and decrease offshore (e.g. Cochran et al., 1995; Gustafsson et al., 1998; Benitez-Nelson et al., 2000, Charette et al., 2001).

In general, upwelling in the north and south subtropical gyres is not well developed so its contribution to ^{234}Th flux estimates is assumed to be small. However, at the equator, in the upwelling region north of the equator and in the NW African coastal upwelling region, additional thorium brought into the euphotic zone by upwelling should be considered. However, as this term has been ignored because of a lack of physical measurements of upwelling rates and a lack of repeat stations to overcome non steady-state, it is likely that ^{234}Th and subsequent POC flux estimates for these regions may represent lower limits.

2.4.2 Evaluation of the ^{234}Th flux approach

Thorium-234 has been used as a natural particle tracer in some coastal, continental-margin and open-ocean environments of the Atlantic before (e.g. Buesseler et al., 2001a; Charette and Moran, 1999; Charette et al., 2001,Cochran et al., 1995, 2000; Hall et al., 2000; Miller and Sværen, 2003; Rutgers van der Loeff et al., 1997, 2002; Smith et al., 2004). However, still relatively little is known about its dynamics in the open-ocean setting and in the central gyres in particular. By focusing on the open-ocean environment between ~50°N and ~50°S, this unique study crosses a range of ecosystems from sub-polar to tropical and upwelling systems to oligotrophic mid-ocean gyres. Export of POC from the surface into the deep ocean is believed to be low in the subtropical gyres, particularly in their central areas. Due to the small magnitude of this export, it is difficult to measure and associated uncertainties are high. The actual importance of the subtropical gyres for carbon sequestration is therefore not well constrained. This study adds directly measured and quasi-integrative (time scale of weeks) POC flux estimates in the centres and fringes of both the North and South Atlantic gyres. Results from this study therefore improve the assessment of export variability in the subtropical gyres and constrains the gyres' significance for carbon sequestration in the global context.

Cumulative ^{234}Th depletion for each station was integrated from the sea surface to the depth where secular equilibrium was first reached. Surface fluxes estimated from the steady state model ranged from 0-1138 dpm m^{-2} d^{-1} for AMT 12, from 0-1131 dpm m^{-2} d^{-1} for AMT 13 and from 0-3332 dpm m^{-2} d^{-1} for AMT 14 (Tables 2.4a,b,c). Such values characterise net particle export. However, at many stations, particularly in the subtropical gyres, there was a detectable subsurface thorium excess. As ^{234}Th excess is considered an indicator of remineralisation processes in the mesopelagic zone, these results imply that relative to particle export, shallow remineralisation was at times significant. Evaluating the significance of remineralisation relative to particle export was determined by integrating the subsurface thorium excess to the re-equilibration depth. For many of the stations on AMT 12 and AMT 13 however, this depth range was not very well resolved by the sampling intervals so that the exact depth at which equilibrium was regained is not known. Nevertheless, as the thorium excess is not expected to extend to 500 m, excess activity was integrated to the deepest point of thorium excess (~200 or ~300 m) and thus the data represent lower limits (see Tables 2.4a,b). The net export flux was calculated by subtracting the subsurface ^{234}Th excess from the surface ^{234}Th deficit.

If physical terms are negligible and steady-state assumed, release of ^{234}Th at depth, due to particle remineralisation should be equal to or lower than ^{234}Th scavenged by sinking particles, so that ^{234}Th excess at depth is equal to or lower than integrated ^{234}Th deficit in the upper water column (Savoye et al., 2006). On several CTD's from AMT 12 and AMT 13, the integrated ^{234}Th excess was greater than the surface ^{234}Th deficit (see Tables 2.4a,b). Similar remineralisation peaks (i.e. negative ^{234}Th fluxes) below depths of 150 m were found in the North Pacific Subtropical Gyre by Benitez-Nelson et al. (2001). After correction for radioactive decay, these mesopelagic peaks in ^{234}Th excess were shown to represent high ^{234}Th export events from the upper 150 m in the preceding months. A study by Savoye et al. (2004) in the Southern Ocean also found two significantly negative ^{234}Th fluxes at 300m. A reoccupation of one of these sites allowed a non-steady state estimation of the 100 m ^{234}Th flux which confirmed that the steady-state assumption was invalid. They concluded that negative flux at depth implies steady-state assumptions were invalid when physical terms are negligible (Savoye et al., 2006). In this study, if the subsurface excess was greater than the surface deficit, the net export was depicted as zero in the figures and tables.

Surface and net fluxes along the three AMT transects are shown in Figures 2.20a-c. As particulate ^{234}Th activities for AMT 12 and AMT 13 were calculated using a correction based on the assumption of equilibrium at 500 and 1000 m, it is not possible to calculate uncertainties for total ^{234}Th activities on these two cruises (see Methods). This was not the case for AMT 14. However CTD stations 43, 52, 79 and 88 (AMT 14) had unusually high uncertainties in the ^{234}Th data (see Methods) which made an accurate assessment of the depth at which equilibrium was reached more difficult. This translates into an enhanced uncertainty on estimated ^{234}Th/^{238}U disequilibria and consequently ^{234}Th and POC fluxes. In particular the subsurface thorium excess calculation at station CTD 14 needs to be considered with caution as there is only one data point providing evidence for ^{234}Th excess. Nevertheless, given typical vertical scales of particulate, biological and biogeochemical gradients in the surface ocean, the vertical sampling resolution was sufficiently high to capture the main features of the total ^{234}Th profile and therefore arrive at reliable steady-state ^{234}Th and POC export estimates.

2.4.3 ^{234}Th fluxes

Overall, there are clear spatial trends in ^{234}Th flux patterns along the three transects (Figures 2.20a,b,c). Minimum surface ^{234}Th removal occurred in the centres of the oligotrophic gyres and ranged from 0 to 752 dpm m^{-2} d^{-1}. Additional thorium removal was associated with the upwelling region north of the equator (226-1556 dpm m^{-2} d^{-1}) and within the Mauritania upwelling system (1131 dpm m^{-2} d^{-1}). Enhanced thorium fluxes were found in the equatorial upwelling region and ranged from 215 to 2956 dpm m^{-2} d^{-1}. This at least signified that ^{234}Th export exceeded the potential for ^{234}Th introduction by upwelling. In temperate regions, relatively high yet variable ^{234}Th fluxes occurred, and surface ^{234}Th fluxes ranged from 392 to 3332 dpm m^{-2} d^{-1}. As the extent of disequilibrium is correlated with biological productivity (particle production) both spatially (Coale and Bruland, 1985, 1987; Bruland and Coale, 1986), and temporally, (Buesseler et al., 2001a), low measured fluxes in the gyres centres were consistent with low productivity dominated by the microbial loop (Marañón et al., 2001). Similarly, higher rates of particle flux are expected from the equatorial upwelling and temperate regions that have more variable physical forcing to supply

vertical nutrient fluxes can support higher rates of primary productivity and senescence by larger cells.

Seasonal variation between the two oligotrophic gyres was also evident in all three cruises. AMT 12 and AMT 14 showed more enhanced particle removal from surface waters in austral autumn in the southern oligotrophic gyre (mean = 671 $\pm$ 2.8 and 513 $\pm$ 216 dpm m^{-2} d^{-1} respectively) compared to boreal spring in the northern oligotrophic gyre (mean = 0 dpm m^{-2} d^{-1}). AMT 13 showed a similar seasonal pattern with higher particle removal in autumn in the northern gyre (mean = 534 $\pm$ 544 dpm m^{-2} d^{-1}) compared to spring in the southern gyre (mean = 205 $\pm$ 300 dpm m^{-2} d^{-1}). Higher particle flux in autumn compared to spring is the result of seasonal changes in the structure of the water column affecting the depth of the nutrient depleted upper mixed layer. Spring is the beginning of the high productivity season when the expression in export is not yet developed. Whereas autumn follows the high productivity summer season and as export lags production, the high flux results for autumn can be attributed to the summer growth period.

During AMT 14 in the northern temperate region (~38.7°N and ~20°W, CTD 79) a high ^{234}Th flux rate of 3332 dpm $m^{-2}d^{-1}$ was found. Although this is well within the range of fluxes found during the spring bloom in the NABE, which for the end of May (19-30th) ranged from 1050 dpm m^{-2} d^{-1} at 35 m to 5060 dpm m^{-2} d^{-1} at 150 m (Buesseler et al., 2001a), it was nonetheless surprising as primary production rates for this station were low (16.5 mmol C m^{-2} d^{-1}). Although such a high flux was only sampled once, it may not be unique given the sparse spatial coverage of sampling at ~250 km intervals during AMT cruises. It is quite possible therefore that episodic or patchy events were underestimated if occurring at relatively short temporal or spatial scales. The high ^{234}Th flux found at this station could have been associated with a short-lived bloom triggered by nutrient injection into surface waters. Some evidence for this was found in cooler surface water temperatures (17°C) indicative of localised upwelling and an outcropping of the 1 µmol l^{-1} nitracline at ~38°N (Figure 2.8a). In response, this station had the highest chlorophyll concentrations (0.55 µg l^{-1}) which peaked at 50 m, significantly shallower than the DCM usually characteristic of this region (Figure 2.9c). However, low associated productivity (16.54 mmol C m^{-2} d^{-1})

suggests NO_3, Si, P, and/or Fe limitation associated with the end of the bloom or an underestimate of productivity.

2.20a)

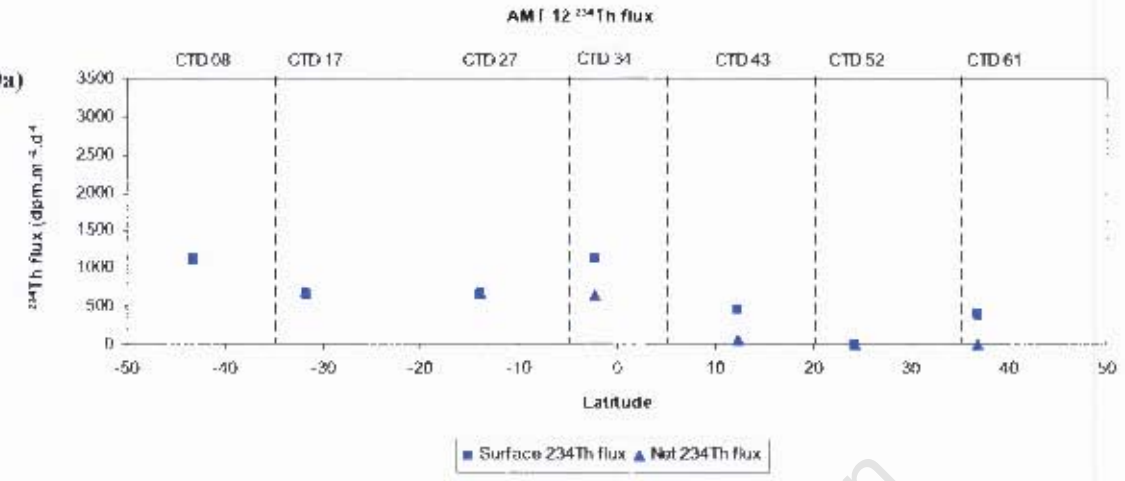

2.20b)

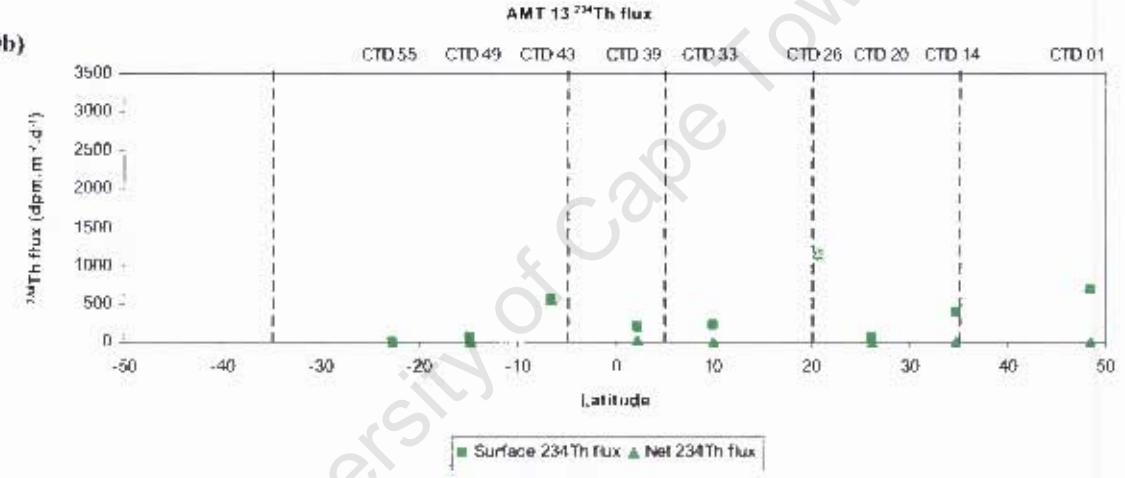

2.20c)

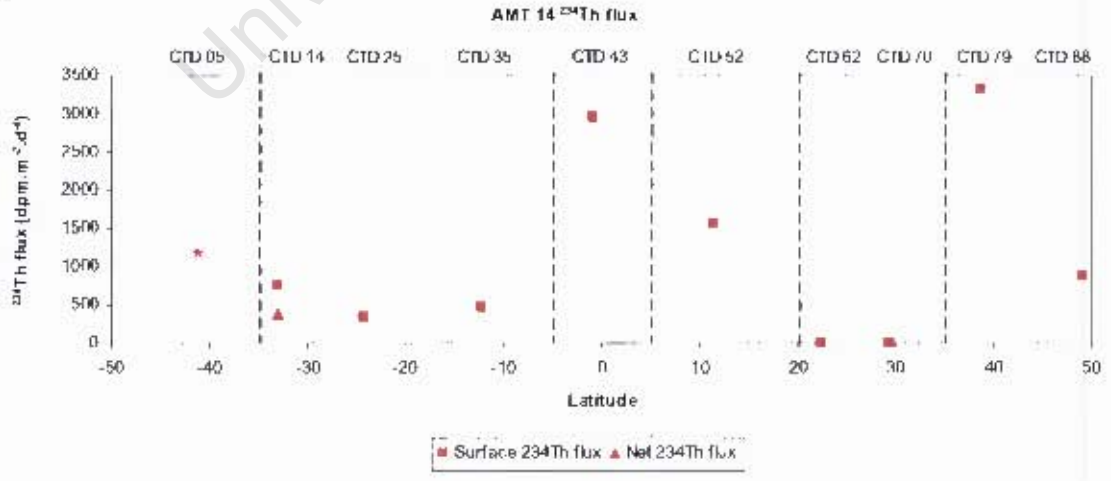

Figure 2.20: ^{234}Th fluxes (dpm m^{-2} d^{-1}) along the AMT 12 a), AMT 13 b) and AMT 14 c) transects. Two flux estimates for several stations are shown: the upper flux estimate (surface flux) results from the integrated surface disequilibrium with an $^{234}Th/^{238}U$ activity ratio<1; the lower flux estimate (net flux) is the upper estimate corrected for the integrated disequilibrium with a $^{234}Th/^{238}U$ activity ratio >1. See text for more details. CTD identifiers and biogeographical domains are indicated on each diagram.

Table 2.4. Compilation of surface, subsurface (layer of ^{234}Th excess) and net ^{234}Th fluxes (see section 2.4.2 for a detailed exlanation), depths at which radioactive equilibrium was reached and where SAPS were deployed, POC/^{234}Th ratios of the >0.7 and >50μm particles, surface and net POC export for a) AMT 12, b) AMT 13 and c) AMT 14

a) **AMT 12**

Station Number	Surface ^{234}Th Flux (dpm m^{-2}d^{-1})	Surface Equilibrium Depth (m)	Subsurface ^{234}Th Excess (dpm m^{-2}d^{-1})	Subsurface Equilibrium Depth (m)	Net ^{234}Th Flux (dpm m^{-2}d^{-1})	SAPS Depth (m)	POC : ^{234}Th ratio > 0.7μm (μmol dpm^{-1})	POC : ^{234}Th ratio > 50 μm (μmol dpm^{-1})	Surface POC export (mmol C m^{-2}d^{-1})	Net POC export (mmol C m^{-2}d^{-1})
CTD 08	1138	104	-	-	1138	100		27.4	31.2	31.2
CTD 17	669	152	-	-	669	100		6.5	4.3	4.3
CTD 27	673	153	-	-	673	100		2.0	1.4	1.4
CTD 34	1132	151	474	> 202	658	100	2.7	3.4	3.8	2.2
CTD 43	463	51	396	> 201	67	100	0.7	5.1	2.4	0.3
CTD 52	0	-	1374	> 204	0	100	0.8	2.9	0	0
CTD 61	392	79	426	> 204	0	100	1.2	1.5	0.6	0

b) **AMT 13**

Station Number	Surface ^{234}Th Flux (dpm m^{-2}d^{-1})	Surface Equilibrium Depth (m)	Subsurface ^{234}Th Excess (dpm m^{-2}d^{-1})	Subsurface Equilibrium Depth (m)	Net ^{234}Th Flux (dpm m^{-2}d^{-1})	POC : ^{234}Th ratio > 0.7μm (μmol dpm^{-1})	‡ Minimum POC : ^{234}Th ratio > 50 μm (μmol dpm^{-1})	‡ Maximum POC : ^{234}Th ratio > 50 μm (μmol dpm^{-1})	Mean Surface POC export +/- range (mmol C m^{-2}d^{-1})	Net POC export /- range (mmol C m^{-2}d^{-1})
CTD 55	0	-	< 1611	>304	0	1.42	2.30	5.88	0	0
CTD 49	66	103	702	303	0	0.80	1.90	4.87	0.22 +/- 0.10	0
CTD 43	549	101	-	-	549	0.87	2.10	5.38	2.05 +/- 0.90	2.05 +/- 0.90
CTD 39	215	204	< 197	>304	18	0.50	1.39	3.55	0.53 +/- 0.23	0.04 +/- 0.02
CTD 33	226	59	722	203	0	0.44	1.04	2.65	0.42 +/- 0.18	0
CTD 26	1131	304	-	-	1131	0.59	1.17	3.00	2.36+/- 1.03	2.36 +/- 1.03
CTD 20	67	63	839	302	0	0.89	2.07	5.30	0.25 +/- 0.11	0
CTD 14	403	103	< 445	>303	0	0.80	1.90	4.85	1.36 +/- 0.60	0
CTD 01	680	103	< 2409	>305	0	0.97	3.37	8.62	4.08 +/- 1.79	0

c) **AMT 14**

Station Number	Surface ^{234}Th Flux (dpm m^{-2}d^{-1}) ± error	Surface Equilibrium Depth (m)	Subsurface ^{234}Th Excess (dpm m^{-2}d^{-1}) ± error	Subsurface Equilibrium Depth (m)	Net ^{234}Th Flux (dpm m^{-2}d^{-1}) ± error	SAPS Depth (m)	POC : ^{234}Th ratio > 0.7μm (μmol dpm^{-1}) ± error	POC : ^{234}Th ratio > 50 μm (μmol dpm^{-1}) ± error	Surface POC export (mmol C m^{-2}d^{-1}) ± error	Net POC export (mmol C m^{-2}d^{-1}) ± error
CTD 05	1174 ± 347	101	-	-	1174 ± 347	100	2.40 ± 0.26	6.0 ± 0.7	7.0 ± 2.2	7.0 ± 2.2
CTD 14	752 ± 592	203	386 ± 574	360	367 ± 825	100	1.19 ± 0.13	7.5 ± 0.9	5.6 ± 4.5	2.7 ± 6.2
CTD 25	333 ± 426	121	-	-	333 ± 426	140	0.88 ± 0.09	7.6 ± 0.8	2.5 ± 3.2	2.5 ± 3.2
CTD 35	455 ± 443	128	-	-	455 ± 443	140	0.93 ± 0.10	7.2 ± 0.8	3.3 ± 3.2	3.3 ± 3.2
CTD 43	2956 ± 1403	300	-	-	2956 ± 1403	100	2.33 ± 0.26	8.4 ± 0.9	24.8 ± 12.0	24.8 ± 12.0
CTD 52	1556 ± 1470	202	-	-	1556 ± 1470	100	1.53 ± 0.23	9.8 ± 2.1	15.2 ± 14.7	15.2 ± 14.7
CTD 62	0	-	-	-	0	160	0.84 ± 0.10	14.8 ± 1.6	0	0
CTD 70	0	-	-	-	0	160	1.00 ± 0.15	6.3 ± 4.8	0	0
CTD 79	3332 ± 1394	265	-	-	3332 ± 1394	100	1.86 ± 0.25	12.2 ± 6.6	40.7 ± 27.9	40.7 ± 27.9
CTD 88	884 ± 865	93	-	-	884 ± 865	100	1.08 ± 0.16	6.0 ± 1.0	5.3 ± 5.3	5.3 ± 5.3

‡ Minimum and maximum ranges of POC/^{234}Th ratios for the >50μm particles were estimated from AMT 12 and AMT 14 respectively based on the proportional increase of the >50μm POC/^{234}Th ratio compared to the >0.7μm POC/^{234}Th ratio. See text for details.

It is quite possible to uncouple low productivity and high ^{234}Th flux rates because of the 12-24 hr time scale of production measurements relative to longer time-averaged (~35 days) ^{234}Th flux measurements. This implies that the high ^{234}Th flux rates measured here could well represent export from a previous bloom. Further evidence to support this hypothesis comes from eight day and 13 data point averaged SeaWiFS chlorophyll estimates obtained at 36.7°N, the position of CTD 79 (see Figure 2.21). Chlorophyll concentrations were obtained for a six month period straddling the sampling date for CTD 79. These data clearly reveal a chlorophyll bloom in the region ~2 weeks prior to sampling that could account for the high ^{234}Th flux rates. This argument is also supported by Teira et al. (2005), who relate high surface chlorophyll to high productivity in the eastern north Atlantic subtropical gyre.

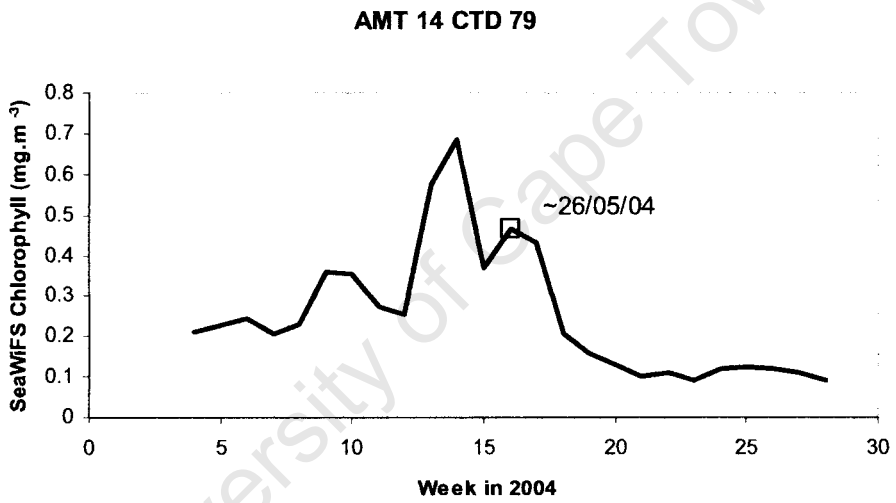

Figure 2.21. SeaWiFs-derived chlorophyll concentrations for AMT 14 - CTD 79 presented as a time history for weeks 4-28 in 2004. The approximate sampling date for CTD 79 (26 May 2004) is indicated by an open square.

These arguments highlight the possible differences in ^{234}Th fluxes when using steady state vs. non steady state models. With increasing ^{234}Th inventories ($\partial A_{tot} / \partial t > 0$), for example during post bloom conditions, steady state removal time estimates for ^{234}Th will be too short and ^{234}Th export estimates will be too large (Buesseler et al., 1992a). The historical information of this site suggests that it was sampled in post bloom conditions and it is therefore possible that the calculated ^{234}Th flux is overestimated.

2.4.4 Estimating POC export flux

To translate ^{234}Th flux into POC export, the POC/^{234}Th ratio of sinking particles (>50 μm) was measured by *in situ* filtration on AMT 12 and AMT 14 and estimated on AMT 13 by scaling up the POC/^{234}Th ratio of the 0.7μm particles (see Methods). If the removal flux of ^{234}Th is driven by local production and export of organic matter on rapidly settling particles, and as the large particles (>50 μm) sampled for the POC/^{234}Th ratio represent the dominant bulk of particles carrying both POC and ^{234}Th into the deep ocean (Bishop et al., 1977, Clegg and Witfield, 1990), POC fluxes can be calculated as:-

$$\text{POC flux} = (\text{POC/Th})_L \, P \qquad (5)$$

Where $(\text{POC/Th})_L$ is the ratio of POC to ^{234}Th on particles rapidly sinking out of the euphotic zone and P is the net loss of ^{234}Th on sinking particles (dpm m^{-3} d^{-1}) (e.g., Cochran et al., 2000; Buesseler et al., 2001a).

Surface and net POC fluxes at each station are derived from surface and net thorium fluxes using the same POC/^{234}Th ratio (see Table 2.4). To propagate errors for the POC/^{234}Th ratios and the POC flux results, a $\pm$ 10% uncertainty for the SAPS-derived POC concentrations was assumed. This is higher than the analytical uncertainty and is meant to reflect the uncertainty due to spatial variability on the relevant horizontal scale of meters to hundreds of meters (ship moving/drifting while sampling). A similar uncertainty due to spatial variability was reported by Turnewitsch and Springer (2001) for particle-associated (>0.4 μm) ^{234}Th. The high uncertainties in the POC export data for AMT 14 result from enhanced errors in some of the ^{234}Th activity data and/or small disequilibria with consequently higher uncertainties. Nevertheless, the uncertainties of POC export fluxes of this study fall within the range of uncertainties published so far (e.g., Buesseler et al., 1992a; Schmidt et al., 2002; Buesseler et al., 2005).

2.4.4.1 POC/^{234}Th ratios

The POC/^{234}Th ratio of particles varies significantly with location and time because of changes in primary and secondary productivity, plankton community structure, export production, particle size distribution, particle aggregation/disaggregation and food web dynamics (Lee et al., 1993; Buesseler et al., 1995, 2006; Bacon et al., 1996; Murray et al., 1996; Charette and Moran, 1999; Burd et al., 2000; Moran et al., 2003; Buesseler et al., 2006; Santschi et al., 2006). As calculated carbon fluxes are sensitive to variable POC/ ^{234}Th ratios, these need carefull consideration. The reasons for this variability are however not well understood. Potential causes include: the lifetime of the particles in the surface with respect to sinking, the surface to volume ratio of particles, biasis during particle collection and differential binding to specific substance classes (Passow et al., 2006).

Figures 2.22a,b show profiles of POC/^{234}Th from >0.7 µm particles for AMT 13 and AMT 14. POC/^{234}Th ratios for the >0.7 µm particles from AMT 12 are not plotted as the bottle depths sampled for POC did not correspond to the bottle depths sampled for ^{234}Th. It was felt that interpolating the values to obtain a profile of >0.7 µm POC/^{234}Th ratios would not have been sufficiently scientifically accurate (the CTD POC and ^{234}Th data for AMT 12 are however available in Table 2.3a). Profiles of the POC/^{234}Th ratios from the >0.7 µm particles for AMT 13 and AMT 14 show an overall decrease with depth. This is expected if preferential carbon losses, such as mechanical particle breakdown and remineralisation of carbon exceed the decrease of ^{234}Th activity on sinking particles (see for example, Fig 12 in Bacon et al., 1996). A noticeable difference in the POC/^{234}Th profiles of the two cruises is that on AMT 14 there was a slight subsurface increase in the POC/^{234}Th ratio at 50-100 m superimposed on the overall decreasing trend with depth (Figure 2.22b), whereas on AMT 13, the POC/^{234}Th ratio decreased steadily from the surface to 300 m (Figure 2.22a). In general, phytoplankton growth is expected to dominate in the euphotic layers and grazing and bacterial remineralisation to become more important at depth in aphotic waters. This should be reflected in high surface POC/^{234}Th ratios and lower POC/^{234}Th ratios at depth. This is particularly evident from the AMT 13 ^{234}Th profiles which often show thorium excess at 100-300 m indicative of intense remineralisation. A similar subsurface maxima in POC/^{234}Th ratios at depth (50-70 m) was found by

Speicher et al. (2006) in the Tyrrhenian Sea, which coincided with the depth of the DCM. Although the mechanism for the DCM-related variability in POC/^{234}Th ratios was unclear they suggested that a change in phytoplankton cell density or species composition at the DCM could be responsible, as ^{234}Th-binding sites and seawater ligand characteristics are influenced by the phytoplankton community (Guo et al., 2002a; Santschi et al., 2003; Passow et al., 2006). In this study however, the subsurface peak in POC/^{234}Th ratios (AMT 14) did not appear to be related to the DCM and only coincided on four of the stations sampled. Although the cause of the subsurface peak in POC/^{234}Th ratios on AMT 14 is unclear, such an increase at 50/100 m implies higher phytoplankton growth and POC concentrations and/or lower particulate ^{234}Th activities at that depth compared to AMT 13. POC concentrations in the 50-100 m depth range were indeed higher on AMT 14 compared to AMT 13 or AMT 12 (Figures 2.23a-c), in particular in the northern subtropical gyre and southern temperate region, implying either higher rates of particle formation (by phytoplankton production) and/or reduced particle removal either by sedimentation and/or grazing.

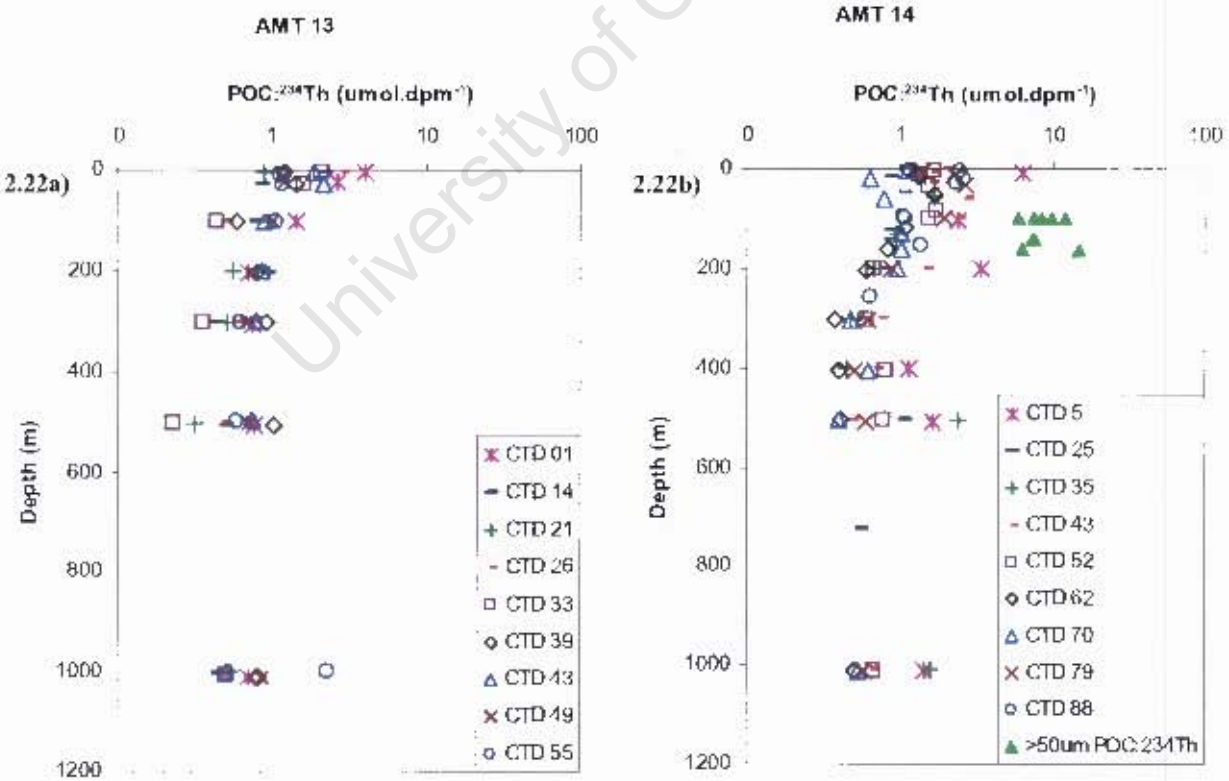

Figure 2.22. Depth profiles of POC/^{234}Th ratios for the >0.7 µm particles from a) AMT 13 and b) AMT 14 POC/^{234}Th ratios of the >50 µm particles from AMT 14 are indicated by solid green triangles on b)

A feature of the AMT 14 subsurface maximum in POC/^{234}Th ratios at 100 m (mean = 1.8 $\pm$ 0.6 µmol dpm^{-1}) is that it significantly (t = 3.75, n = 13, P <0.0025) exceeds this ratio at 100 m on AMT 13 (mean = 0.8 $\pm$ 0.3 µmol dpm^{-1}) with the result that the estimated >50 µm POC/^{234}Th ratios for AMT 13 are much lower and this translates into a lower mean POC flux for AMT 13. Low POC/^{234}Th ratios reflect both lower average POC values and thorium excess that together characterise high remineralisation rates. Conversely, the elevated POC flux at 100 m observed on AMT 14 implies particle production at depth to drive higher export measured there. Overall however, POC/^{234}Th variability is much greater in surface waters than at depth, indicating that biological processes controlling the POC/^{234}Th ratio typically decrease below the euphotic zone (~200 m) (Buesseler, 1998).

The POC/^{234}Th ratio from AMT 12 and AMT 14 of the >0.7 µm particles at the depth of the SAPS ranged from 0.74-2.75 µmol dpm^{-1} (mean = 1.40), whereas the POC/^{234}Th ratio of the >50µm particles collected from the SAPS ranged from 1.5-27.4 µmol dpm^{-1} (mean = 7.91) (Figure 2.22b; Table 2.4a,c). As ^{234}Th is assumed to adhere to particle surfaces and POC to be determined by particle volume, these results of increasing POC/^{234}Th ratio with increasing particle size are anticipated and consistent with previous studies (see review by Buesseler et al., 2006) in the mid Atlantic (Charette and Moran, 1999), the Arabian Sea (Buesseler et al., 1998), the Ross Sea (Cochran et al., 2000) and the Labrador Sea (Moran et al., 2003).

POC/^{234}Th ratios for the >50 µm particles from AMT 12 were generally much lower than for AMT 14 (Figure 2.24). These trends suggest that for AMT 12 there were either higher rates of carbon remineralisation or an increase in heterotrophic grazing compared to AMT 14. However, as the depth-integrated biomass of meso-zooplankton, nano- and micro-zooplankton was consistent between cruises (see Figure.8 San Martin et al., 2006), this suggests similarity in heterotrophic grazing pressure and implies instead that increased particle remineralisation in the >50 µm particle fraction was a more likely contributor to lower POC/^{234}Th ratios on AMT 12. Furthermore, POC/^{234}Th ratios derived from *in situ* SAPS pumps on AMT 14 were relatively high (6-14.8 µmol dpm^{-1}) compared to recent studies in the equatorial Pacific where >53 µm POC/^{234}Th ratios ranged from <0.5 to 6.5 µmol dpm^{-1}

(Buesseler et al., 1995, Bacon et al., 1996, Murray et al., 1996). However the AMT 14 POC/^{234}Th ratios fit into the range found by Charette and Moran (1999) in the southern subtropical and equatorial Atlantic whose >53 µm POC/^{234}Th ratios between 50 and 110 m averaged at 24 ± 12.2 µmol dpm^{-1}.

High latitudes and productive coastal waters tend to be dominated by the export of large cells and elevated POC/^{234}Th ratios compared to oligotrophic settings dominated by small particles and typically lower POC/^{234}Th ratios (Buesseler et al., 2006). Although none of the ecological domains sampled on the AMT transects were dominated by large cells, the temperate fringes of the gyres were characterised by an increase in the percentage contribution of microphytoplankton, particularly in spring where they numerically contributed 30-40% and there was a shift in the dominant size fraction from pico- to nanophytoplankton (Figures 2.10, 2.11, 2.12). This change in the community size structure was however not evident in the POC/^{234}Th ratios which showed no obvious latitudinal trends (Figure 2.24). A possible reason for this was an increase in zooplankton abundance and their mean size (337-550 µm) in the temperate regions of the transect (San Martin et al., 2006). An increase in large zooplankton populations increases the contribution of faecal pellets to POC flux which have a low POC/^{234}Th ratio due to preferential carbon losses (Buesseler et al., 2006). Increased grazing and carbon export as faecal pellets may therefore compensate for the increase in the size structure of the phytoplankton community and possibly accounts for the lack of increase in the POC/^{234}Th ratios in the temperate ecological domain.

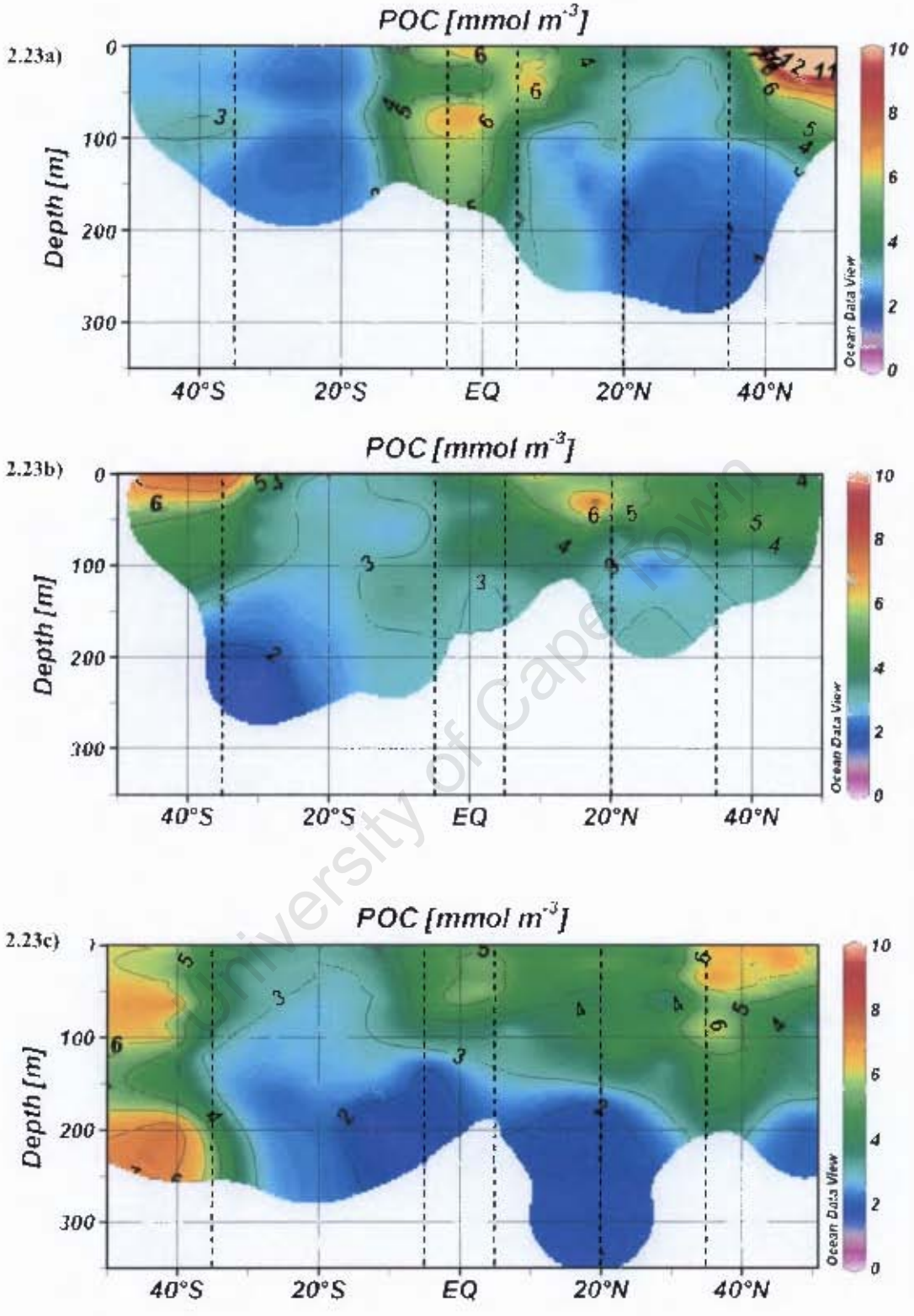

Figure 2.23. Particulate organic carbon concentrations for a) AMT 12, b) AMT 13 and c) AMT 14. Temperate (35°- 50°N and 35°-50°S), oligotrophic (20°-35°N and 5°-35°S), equatorial (5°S-5°N) and upwelling (5°-20°N) domains are indicated by vertical dashed lines.

2.24

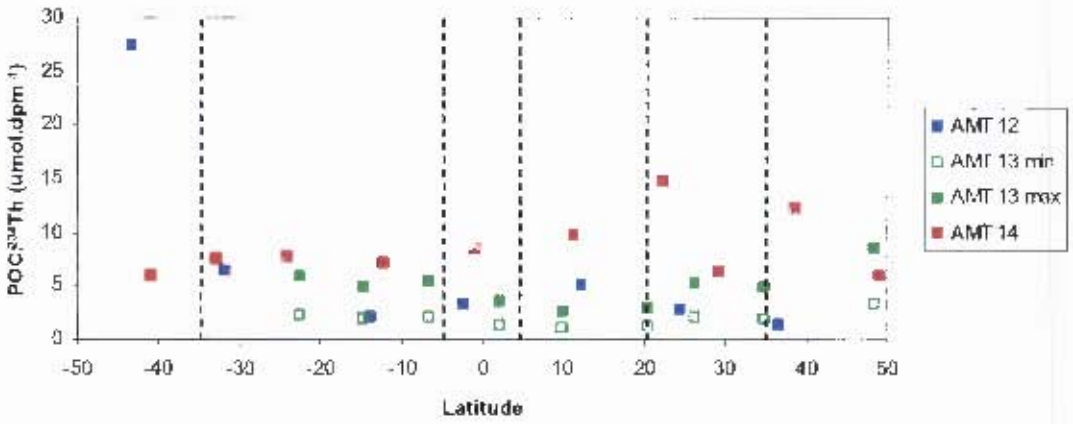

Figure 2.24. Latitudinal distribution of POC/^{234}Th ratios for the >0.50 µm particles from AMT 12, AMT 13 and AMT 14. Minimum and maximum estimates for the AMT 13 >50 µm POC/^{234}Th ratio are based on the increase in POC:^{234}Th ratio with particle size from the >0.7 µm to the >50 µm measured on AMT 12 and AMT 14 respectively. See text for details. Temperate (35°- 50°N and 35°-50°S), oligotrophic (20°-35°N and 5°-35°S), equatorial (5°S-5°N) and upwelling (5°-20°N) domains are indicated by vertical dashed lines.

2.4.5 POC export

The latitudinal distribution of POC export during AMT 12, 13 and 14 are plotted in Figures 2.25a-c. At stations where the remineralisation excess exceeded the surface ^{234}Th flux, there was an apparent net POC export flux of zero. The majority of POC flux results for both the northern and southern gyres are low. On many of the stations, particularly during AMT 12 and AMT 13, there was a large subsurface ^{234}Th excess, resulting in a substantial reduction in net versus surface POC flux results. Since ^{234}Th excess is a strong indicator of remineralisation processes in the mesopelagic zone, these results imply that relative to particle export, particle break up and remineralisation were significant in both the northern and southern subtropical gyres.

In the centre of the oligotrophic gyres, POC fluxes were low, but increased over the equator and at the northern and southern fringes of the gyres; comparing well with other ^{234}Th based POC export studies carried out in the Atlantic Ocean, as illustrated in Figure 2.26. These include 1) The JGOFS spring bloom study at the Antarctic Polar Front (APF) (Rutgers van der Loeff et al., 1997), 2) The subtropical and equatorial study by Charette and Moran (1999), 3) the Bermuda Atlantic Time Series study (BATS) (Michaels et al., 1994) and 4) the JGOFS North Atlantic Bloom Experiment (NABE) (Buesseler et al., 1992a). These direct measurements of POC export have

been plotted against modelled estimates of export at ~100 m depth from the Princeton general circulation model (GCM) by Charette and Moran (1999). This is a phosphorus-based model of nutrient cycling that was developed in conjunction with a GCM to evaluate the roles of dissolved and sinking particulate phases in the downward transport of organic matter in the ocean (Najjar et al., 1992). The horizontal resolution of the model is 3.75° in longitude by roughly 4.5° in latitude. The model simulations provide annually averaged values of POC export for a given location. By contrast, the AMT ^{234}Th based POC export data provide quasi-integrative export estimates for the few weeks prior to sampling. Despite this difference in time scales, the ^{234}Th-derived estimates fit the GCM predicted data remarkably well throughout the transect. POC flux estimates on AMT 12 and AMT 13 are generally lower than the Princeton GCM estimates in the equatorial and subtropical convergence region (~35°N), although they do fall within the range measured by Charette and Moran (1999). The POC flux results from this study can also be compared with annual mean export estimates presented by Falkowski et al. (1998; Fig. 2) derived from remotely sensed chlorophyll fluorescence. Despite the different approaches and time scales, the AMT export estimates agree very well with the values from Falkowski et al. (1998).

The latitudinal patterns of surface POC export flux found during AMT are described below (Figure 2.25a,b,c). For AMT 13 the mid point in the range of estimated fluxes is referred to.

Oligotrophic gyres - Lowest surface POC export fluxes were found in the oligotrophic gyres, ranging from 0 to 1.36 mmol C m $^{-2}$ d^{-1} in the northern gyre (mean 0.3 $\pm$ 0.6) and from 0 to 5.6 mmol C m $^{-2}$ d^{-1} in the southern gyre (mean 2.9 $\pm$ 1.9). Low POC export rates such as these characterise tightly coupled regeneration based microbial food webs (Buesseler, 1998).

Equatorial and Upwelling - Enhanced POC export fluxes of the equatorial region (0.53-24.8 mmol C m $^{-2}$ d^{-1} mean 10.3 $\pm$ 12.5) and the upwelling region north of the equator (0.4-15.2 mmol C m $^{-2}$ d^{-1} mean 6.0 $\pm$ 8.0) are comparable to those of Charette and Moran (1999) for the equatorial Atlantic whose POC export flux ranged from 0 to 42.9 mmol C m $^{-2}$ d^{-1} (mean 19 $\pm$ 17). However, the model calculations for ^{234}Th

export neglect advection, which may be important due to upwelling of water enriched in ^{234}Th. For example, in the equatorial Pacific, Buesseler et al. (1995) found that ^{234}Th fluxes were 25-35% higher when upwelling was considered. As a result therefore, the estimates of POC export in these regions may represent lower limits. Similarly, the flux estimates in the upwelling region of the NW coast of Africa on AMT 13 (CTD 39) are likely to be underestimated. Of particular interest at this station was the comparatively low POC export (2.36 mmol C m^{-2} d^{-1}), despite significantly higher ^{234}Th flux (1131 dpm m^{-2} d^{-1}) than at any other station on this cruise. This is due to the extremely low POC/^{234}Th ratio of the >0.7 μm particles at 100 m (0.59 μmol dpm^{-1}), most likely due to this stations' proximity to the NW African coast upwelling system which is strongly influenced by atmospheric mineral dust inputs associated with plumes originating from the Sahara Desert (Baker et al., 2003). It is possible that such land-derived material would have a lower carbon content than *in situ* biologically derived particles such as phytoplankton, while the dust itself scavenges thorium, so lowering the POC/^{234}Th ratio.

Temperate latitudes - Temperate regions exhibited high POC export flux compared to the surrounding oligotrophic regions and ranged from 0.6 to 40.7 mmol C m^{-2} d^{-1} (mean = 14.1 $\pm$ 17.4). As the temperate ecological domain is characterised by detectable nitrate and increased chlorophyll concentrations, higher POC fluxes are expected. The southern temperate station sampled on AMT 12 (CTD 08) was situated at the southern edge of the southern gyre and likely to be influenced by the South Subtropical Convergence (SSC). This station had a particularly high POC flux of 31.2 mmol C m^{-2} d^{-1}. Although the ^{234}Th flux was relatively high (1138 dpm m^{-2} d^{-1}) it was the exceptionally high POC/^{234}Th ratio of the >50 μm size fraction (27.4 μmol dpm^{-1}) that exerted the strongest influence on the POC export at this station. As POC/^{234}Th ratios are expected to increase with particle size (a result of an increase in volume/surface area), such high POC/^{234}Th ratios suggest a community strongly influenced by larger cells (e.g. diatoms), which due to their high sinking velocities play an important role in the sequestration of carbon to the deep ocean (Buesseler et al., 2006). This explanation however seems unlikely when examining the microphytoplankton abundance in Figure 2.10a.

2.25a)

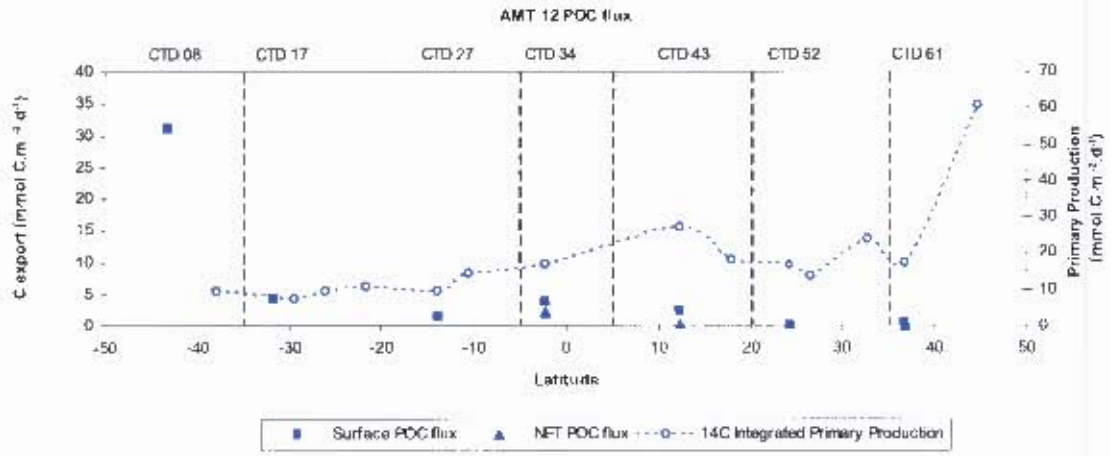

2.25b)

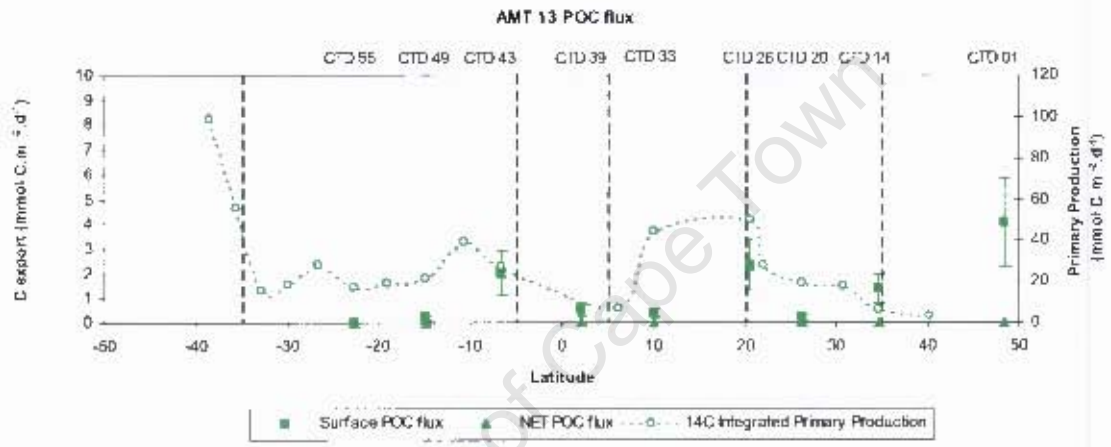

2.25c)

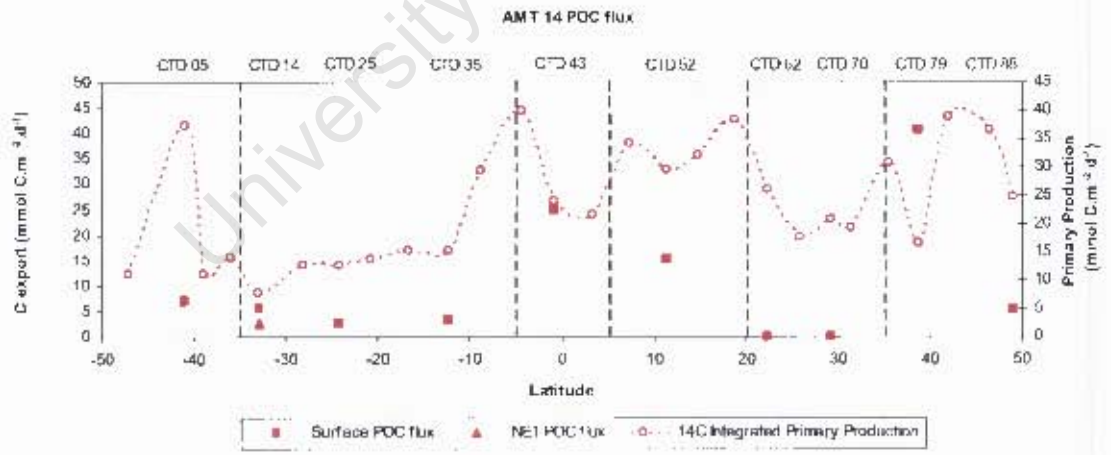

Figure 2.25. Primary production estimates (mmol C m^{-2} d^{-1}), surface (squares) and net (triangles) POC fluxes (mmol C m^{-2} d^{-1}) along the AMT 12 a) AMT 13 b) and AMT 14 c) transects. AMT 13 POC flux estimates are based on a range of >50 µm POC/^{234}Th ratios derived from the >0.7 POC/^{234}Th ratios of AMT 13 and the increase in POC/^{234}Th ratio with particle size measured on AMT 12 and AMT 14. The midpoint has been plotted as a solid marker and the range is represented by error bars. See text for details.

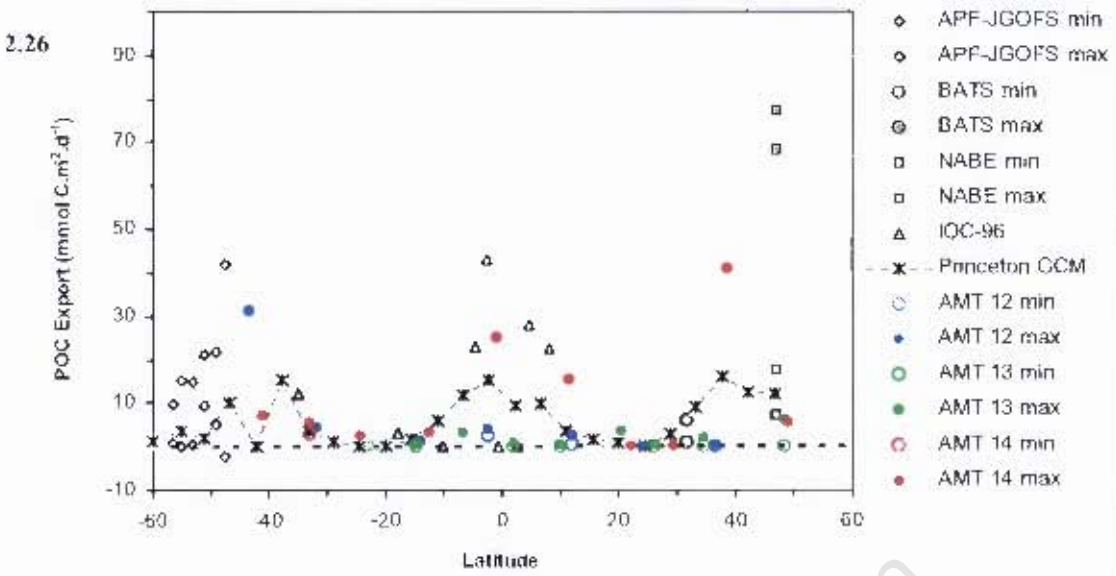

Figure 2.26: Compilation of POC export fluxes in the Atlantic between 60°N and 60°S calculated using the Princeton GCM (Charette and Moran, 1999) and the ^{234}Th tracer approach and plotted versus latitude. All flux estimates were obtained for within the depth range of 75-200 m. Surface flux estimates for the water layer showing a ^{234}Th activity deficit from this study are represented by solid blue circles (AMT 12), green circles (AMT 13) and red circles (AMT 14). Open circles for AMT 12, 13 and 14 represent the net thorium flux in which the surface thorium flux has been corrected for presence of a detectable ^{234}Th activity excess at depth. Grey triangles represent the IOC 1996 study integrated to ~100 m (Charette and Moran, 1999). The other grey and white symbols indicate upper and lower estimates, respectively, from the APF-JGOFS (diamonds; Rutgers van der Loeff et al., 1997), the BATS (circles: Michaels et al., 1994; Buesseler, 1998) and the NABE (squares: Buesseler et al., 1992). The NABE estimates are plotted for fluxes at 75 m (upper grey and white squares) and 100 m (lower grey and white squares) depth. The horizontal dashed line indicates zero flux.

2.4.6 The ThE ratio

When considering oceanic carbon cycling, an important parameter is the ratio of POC export to total primary production, analogous to the f ratio (Eppley and Peterson, 1979). Buesseler et al. (1998) defined the ratio of ^{234}Th derived POC export to primary production as the "*ThE*" ratio. Low *ThE* <10% is consistent with a small ^{234}Th/^{238}U disequilibrium (Buesseler, 1998) and expected from tightly coupled food webs, where nutrients are efficiently recycled via the microbial loop and/or small zooplankton, characteristic of oligotrophic regimes (Karl, 1999). By contrast, high *ThE* ratios typify regions that have an efficient biological pump based on relatively large and rapidly sinking particles such as diatoms (Buesseler et al., 1998).

One would therefore expect *ThE* ratios from the north and south Atlantic gyres to be <10%. At four of the stations *ThE* ratios (based on surface POC flux and euphotic

zone primary production) were zero and imply that virtually all primary production was recycled within the euphotic zone. All four stations occurred in the oligotrophic gyres during autumn, three in the northern oligotrophic on AMT 12 (CTD 52) and AMT 14 (CTD 62,70) and one in the southern oligotrophic during AMT 13 (CTD 55). The majority of the remaining *ThE* ratios from AMT 12 and AMT 13 were <10% and consistent with low $^{234}Th/^{238}U$ disequilibria and/or low POC/^{234}Th ratios that result in low POC fluxes (Figure 2.27; Tables 2.4a,b,c). Many of these stations also had large subsurface thorium excess indicative of intense remineralisation that accounts for low export efficiencies and low POC/^{234}Th ratios. However, *ThE* ratios of <10% were not always the case and intermediate but comparatively high *ThE* ratios (20-50%) were common on AMT 14 in the southern and northern temperate region (CTD's 05, 88), in the southern oligotrophic gyre (CTD 35) and within the upwelling region north of the equator (CTD 52). Similarly high *ThE* ratios (~20%) were found in the southern oligotrophic and equatorial region on AMT 12 (CTD 34) and in the northern oligotrophic on AMT 13 (CTD 14) (Figure 2.27; Tables 2.4a-c).

2.27

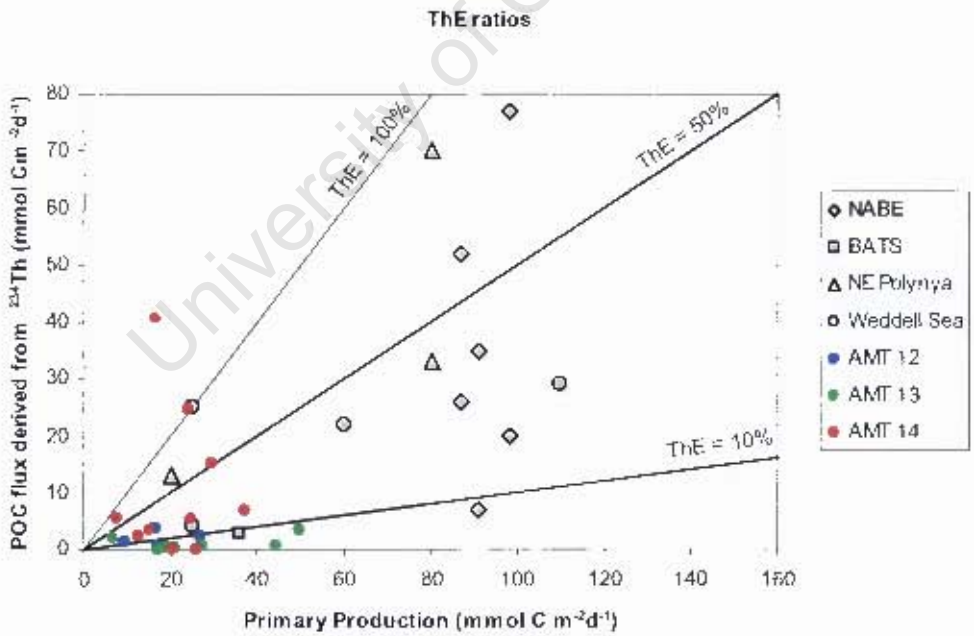

Figure 2.27: Compilation plot of *ThE* ratios [^{14}C derived primary production (mmol C $m^{-2}d^{-1}$) versus POC flux (mmol C $m^{-2}d^{-1}$) derived from the ^{234}Th approach]. Lines of *ThE* – 100%, 50% and 10% are drawn for comparison to data from Buesseler (1998 Fig 1). *ThE* for this study are based on surface POC export fluxes (as opposed to net fluxes) and are represented by blue circles (AMT 12), green circles (AMT 13) and red circles (AMT 14). The other studies are represented by grey diamonds from the NABE (Buesseler et al., 1992a); open squares from BATS (Michaels et al., 1994, Buesseler, 1998); open triangles from the NE Polynya, Greenland (Cochran et al., 1995, 1997) and open circles from the Weddell Sea / Polar Front (Rutgers van der Loeff et al., 1997).

As argued earlier, station CTD 79 (northern temperate) on AMT 14 was considered to be in a post bloom phase and uncoupled from time-averaged POC export. The exceedingly high *ThE* ratio (246%) at this station was therefore not entirely unexpected. Such uncoupling has been recorded previously in the NABE (Buesseler et al., 1992a), the Arabian Sea (Buesseler et al., 1998) and the Ross Sea (Cochran et al., 2000) resulting in high export ratios of >30-50% and up to 79% during the NABE (Figure 2.27). The high *ThE* value for CTD 79 was three times this, suggesting that intense decoupling occurred, pointing to the occurrence of pulsed high export events that could easily be missed by instantaneous sampling but captured by temporally quasi-integrating tracers such as ^{234}Th. Such events could be driven by atmospheric deposition of iron and nitrogen in the northern gyre (Baker et al., 2003) or by pulsed inputs of nutrients from the deep ocean. As station CTD 79 is within the northern oligotrophic/temperate transition zone (Mouriño et al., 2004), it is likely to be characterised by significant mesoscale activity (Garcon et al., 2001; Mouriño et al., 2003) that deliver episodic nutrient pulses from depth (Karl, 1999), as well as Saharan dust inputs that together can result in episodic productivity and POC flux events (Platt and Harrison, 1985; Karl et al., 1996). Assuming these results and arguments are representative, these ^{234}Th based POC flux data challenge the conventional idea that subtropical gyres are unimportant carbon sinks. At the very least, the boundaries of the gyres may behave like trap-doors for carbon flux into the deeper ocean.

2.4.7 Inter cruise comparisons

When comparing inter inter-annual variability between cruises such as those carried out on the AMT programme it is important to remember that limitations inherent in the sampling strategy mean that a highly heterogeneous ocean is randomly under sampled and that inter-cruise differences may reflect the "noise" inherent in the system as apposed to actual differences in the biogeochemistry of the system. Recent studies that examine data from AMT 12, 13 and 14 find only minor changes in inter-annual variability between the three cruises (see Robinson et al., 2006 for an overview). There was relatively little difference in the chlorophyll-a concentrations (Figure 2.9a,b,c) or size distributions of the phytoplankton community (Figures 2.10-2.13) (see also Poulton et al., 2006b). Heywood et al. (2006) also found no significant variation in concentrations of *Prochlorococcus* spp. or *Synecococcus* spp. Carbon

fixation rates between cruises also showed only minor insignificant differences (Figure 2.15) (Poulton et al., 2006b). Yet despite these similarities in phytoplankton community structure and primary production rates, POC fluxes for the entire AMT 14 transect (mean = 10.44 $\pm$ 13.07) were higher than those of AMT 12 (mean = 6.2 $\pm$ 11.11) and significantly higher than those of AMT 13 (mean = 1.25 $\pm$ 1.36; $t = 2.09$, $n = 17$, $P < 0.05$).

Is there any evidence to support elevated POC fluxes for AMT 14 despite no apparent increases in productivity or changes in community structure? Ambient NO_3 concentrations were higher at all depths during AMT 14 compared to AMT 12 and higher at all stations north of 35°S on AMT 13. Within the oligotrophic subtropical latitudes (40°S – 40°N) mean NO_3 concentrations for the four sampled irradiance horizons (97, 55, 33 and 14%) on AMT 14 were 74-152% higher than those of AMT 12 and 90-600% higher than those of AMT 13 (Painter et al., in press). In the absence of other limiting factors, the relationship between NO_3 concentration and NO_3 uptake is often linear at concentrations of up to 70 nmol l^{-1} (Rees et al., 1999). Thus the higher integrated NO_3 uptake rates measured on AMT 14 compared to AMT 12 (Figure 2.17a,b) may conceivably be explained simply as a function of increasing NO_3 concentration (Painter et al., in press). Nevertheless, the significance of this is that higher nitrate concentrations and correspondingly higher nitrate uptake rates have classically been considered to be closely related to higher export production (Dugdale and Goering, 1967), consistent with the measurements of elevated POC fluxes derived from the ^{234}Th measurements on AMT 14. Although this argument and conclusion is attractive, extreme care must be taken not to regard this as new production in the sense of Dugdale and Goering, 1967) as recent evidence (Fernandez and Raimbault, in press and Yool et al., in press) shows >70% of the nitrate available in surface waters of subtropical gyres is in fact regenerated nitrate due to nitrification that was hitherto thought to be confined to aphotic waters. This in itself leads to gross over-estimates of nitrate uptake by virtue of isotopic dilution, an effect that has long been known for calculations of ammonium uptake that require correction for ammonium regeneration (Glibert et al., 1982a,b).

Despite this, the nitrate concentration data and its implications for new and export production need to be considered carefully. An explanation for elevated nitrate

concentrations and nitrate uptake rates was provided by Painter et al. (in press) who suggested that an interaction between the depth of the mixed layer and the distance to the nitracline in conjunction with variations in the cross nitracline flux of NO_3 may account for the increase in ambient NO_3 observed on AMT 14. Painter et al. (in press) suggested that the increase in NO_3 concentrations appear to promote a nutrient preference shift within the phytoplankton community rather than causing an increase in primary production rates.

A major difficulty in reconciling these observations of increased nitrate concentrations and increased nitrate uptake rates with increased POC export is that there is no measurable and corresponding increase in carbon fixation (Poulton et al. 2006b). Phytoplankton typically take up N and fix C in a manner that sustains the intracellular Redfield stoichiometry, although exceptions to this are known where 'luxury' or 'dark' uptake of N is undertaken by motile cells within the nitracline region in the absence of C fixation (Villareal et al., 1999), particularly within strongly stratified regions where surface (euphotic layer) nitrate is limiting. During the daylight period, when such cells rise in the water column, carbon fixation may proceed and C:N stoichiometry is re-established using the stored N pool. However, the problem encountered during AMT 14 is that the apparent nitrate uptake at the 0.1-1% depth was very substantial while there was no measured C fixation, so much so that intracellular Redfield stoichiometry was perturbed to unbelievably and unrealistically high values. Therefore, the more likely explanation for elevated nitrate uptake at that depth is due to nitrification that renders the uptake results meaningless.

Overall then, it remains unclear why there are elevated nitrate concentrations during AMT 14 and speculation about nitrification, differential inter-cruise vertical mixing of NO_3 and apparent increased nitrate uptake (and supposed export from 'new' production) remain unconvincing and untested. However, the elevated rates of POC flux deduced from the ^{234}Th measurements appear to be robust and there is no sound reason to doubt these thorium-derived POC fluxes unless or until contrary evidence emerges to refute these flux measurements.

There remains however the question of whether the AMT 12 and AMT 13 POC flux rates were underestimated because of some weaknesses in the corrections for the

contaminated filters. However, the export trends and values for both AMT 12 and 13 are internally consistent and also reflect the general biological and physical signals for these two transects. In particular, the strong evidence for high POC remineralisation rates during AMT 12 and AMT 13 and its absence during AMT 14 would itself mean that higher rates of POC flux should be expected for AMT 14 relative to that for AMT 12 and AMT 13; placing the comparative values in appropriate and realistic perspective.

2.5 Summary and conclusions

Fluxes of POC from the surface water column into the deep Atlantic ocean between ~50°S and ~50°N have been estimated using the natural tracer ^{234}Th. There is general agreement between POC flux results and the range of fluxes determined by previous studies in the Atlantic Ocean. Lowest POC export was associated with the central subtropical gyres and characterise tightly coupled regeneration based microbial food webs. Enhanced POC export typified the equatorial divergence and the open-ocean upwelling region north of the equator. These regions were characterised by shallower surface mixed layers and increased NO_3 in subsurface waters. Increased POC export was also found at higher latitudes where higher productivity was supported by increased nutrient supply from the deep ocean (Palter et al., 2005). High fluxes at the poleward edges of the oligotrophic gyres probably resulted from episodic nutrient loading processes associated with submesoscale features.

Estimates of instantaneous primary production (PP) were compared with ^{234}Th derived POC export, the latter bearing information from the past few weeks. Low *ThE* <10% is typical of subtropical regimes where nutrients are efficiently recycled via the microbial loop and therefore expected from the north and south Atlantic gyres. At four stations in the oligotrophic gyres *ThE* were zero implying the recycling of virtually all primary production within the euphotic zone. The majority of *ThE* ratios from AMT 12 and AMT 13 were <10% and consistent with low ^{234}Th/^{238}U disequilibria. Many of these stations also had a large subsurface thorium excess indicative of intense remineralisation that accounts for low export efficiencies. However, *ThE* ratios <10% were not always the case and intermediate but

comparatively high *ThE* ratios (20-50%) were found on AMT 12 and AMT 13 and common on AMT 14 where two stations had very high *ThE* >100%. Such high *ThE* ratios suggest uncoupling of primary production and export estimates due to the different time scales of the approaches. Moreover, this uncoupling points to the occurrence of pulsed high export events that could be easily missed by instantaneous sampling but traced by temporally quasi-integrating tracers such as ^{234}Th. Similarly, transient peaks in ^{234}Th excess that exceed surface deficits imply that the system was not in steady-state over the half life of thorium but that higher export events had occurred in the months prior to station sampling (Benitez-Nelson et al., 2001). These results confirm that carbon export in the oligotrophic centres of the gyres is low; however when looking at the North and South Atlantic gyres as a whole and particularly at the gyre's northern and southern fringes, the data suggests that carbon sequestration can be substantial and that spatio-temporal variability in these areas of the world's oceans needs to be considered more fully in the context of global oceanic carbon sequestration.

Relatively little difference was found between phytoplankton community structure and primary production rates between the three cruises, yet POC fluxes for the entire AMT 14 transect were higher than those of AMT 12 and AMT 13. AMT 14 also had higher nitrate concentrations and correspondingly higher nitrate uptake rates which have classically been considered to be closely related to higher export production (Dugdale and Goering, 1967) and consistent with elevated POC fluxes on this cruise. However a major difficulty in reconciling these observations is that there was no measurable and corresponding increase in carbon fixation. It is possible that the increase in ambient NO_3 promotes a nutrient preference shift within the phytoplankton community rather than causing an increase in primary production (Painter et al., in press), but more likely that the elevated nitrate uptake is due to nitrification (Fernandez and Raimbault, in press and Yool et al., in press). The reasons for higher nitrate concentrations, increased nitrate uptake and elevated POC flux on AMT 14 despite no increase in primary production or change in community structure remain unclear but provide a good focus for future research.

3 Variable export fluxes and efficiencies for calcite, opal and organic carbon in the Atlantic Ocean: the ballast effect in action?

3.1 Introduction

The capacity of the biological carbon pump to transfer atmospheric CO_2 into the deep ocean is dependent upon the efficiency of particulate organic carbon export, and the degree of remineralisation as particles sink (Sarmiento et al., 2004b). The fate of particulate matter produced within the euphotic zone is governed by competition between dissolution/remineralisation and export, with a return to the solution phase being enhanced by long residence times in the upper ocean. Strong correlations observed in the deep ocean between the vertical fluxes of particulate organic carbon (POC) and of inorganic material (calcite, opal, clay) have been used to suggest that mineral phases may enhance the export and survival of organic matter as it sinks into the deep ocean (the 'ballast effect'), by increasing the density and sinking speeds of particle aggregates (Klaas and Archer, 2002), and by providing some protection from remineralisation (Armstrong et al., 2002). However the processes underlying these correlations are not well understood and the contrary has also been suggested whereby organic aggregates scavenge non-sinking mineral material, in which case the flux of POC may determine the flux of minerals to the deep-sea and not the reverse (Passow, 2004; Passow and De La Rocha, 2006). Rapid sinking of material will prevent significant dissolution of opal and calcite and remineralisation of organic carbon (Ragueneau et al., 2000). However, dissolution in the upper ocean may preclude the efficient export of inorganic, and associated organic material (Nelson et al., 1995; Milliman et al., 1999; Feely et al., 2002).

Realistic modelling of the biological pump and the oceanic pathways for atmospheric CO_2 sequestration (Sarmiento et al., 2004b) depend on developing an improved understanding of the mechanisms of particle formation and rates of remineralisation/dissolution, and their variability with respect to depth and regional hydrography (Buesseler et al., 2001a; Cochran et al., 2000, Ragueneau et al., 2006). Although there are relatively few measurements of biomineral formation, dissolution within the upper ocean (<1 km) a substantial proportion (~50-80%) of the calcite and

opal produced in the euphotic zone is now the accepted paradigm (Nelson et al., 1995; Milliman et al., 1999; Feely et al., 2002). Opal dissolution is mediated by low, undersaturated concentrations of silicate relative to particulate concentrations (Nelson et al., 1995) and bacterial action (Passow, 2004; Bidle and Azam, 1999), while calcite dissolution is thought to be mediated by localised acidic conditions, as found within the guts of zooplankton (Harris, 1994; Pond et al., 1995; Hansen et al., 1996; Jansen and Wolf Gladrow, 2001), and in microenvironments during aggregate formation (faecal pellets, marine snow) (Milliman et al., 1999). A comparison of measurements of primary production and biomineralisation in the subtropical Atlantic with published sediment trap data (Poulton et al., 2006a) indicated that the proportion of organic carbon associated with mineralising phytoplankton production was greater than that exported to the deep sea, that calcite (the major biomineral) had a turnover time (~3 d) within the euphotic zone, comparable to that of the phytoplankton, and that ~70% of the calcite being formed was dissolved in the upper 2-3 km of the ocean. Clearly the nature of the association between particulate organic carbon and mineral material both within and below the euphotic zone is fundamental to understanding how organic carbon export is controlled. In the euphotic zone, ballasting may result from a physical association during biomineral and organic carbon formation (cellular), grazing (packaging) or sinking (aggregation) (Passow, 2004). In the previous chapter POC export and POC export efficiencies were examined along three transects (AMT 12, AMT 13 and AMT 14) in the north and south Atlantic gyres. In this chapter measurements of POC production and export are combined with measurements of biomineral production and export made on AMT 14 (Figure 3.1) in order to examine: (i) whether the strong correlations observed between particulate and biomineral fluxes in deep (>2 km) sediment trap data (e.g. Klaas and Archer, 2002) are evident at shallower euphotic water depths; and (ii) if the export efficiencies (*ThE* = surface production/ export flux) of the different particle types are related.

Export efficiencies of POC, calcite and opal are determined by comparing surface production rates of organic carbon (i.e. photosynthetic rates) and biomineral phases (calcification, silicification) (from Poulton et al., 2006), to shallow (<100 m) particulate export fluxes of organic carbon, calcite and opal. High organic carbon export can result from low productivity systems with efficient export (little remineralisation) or from high productivity systems with inefficient export (extensive

remineralisation) (Francois et al., 2002). Thus in order to examine the relationships between biomineral and organic carbon export, it is necessary to consider both the magnitude of export and the amount of export relative to surface production as expressed by the export efficiency (*ThE*). Due to the paucity of stations sampled along the AMT 14 transect (n = 10), it is not possible to characterise large-scale regional patterns of export, instead, the relationship between production and export at the time of sampling is examined within the context of what is known of the phytoplankton community present.

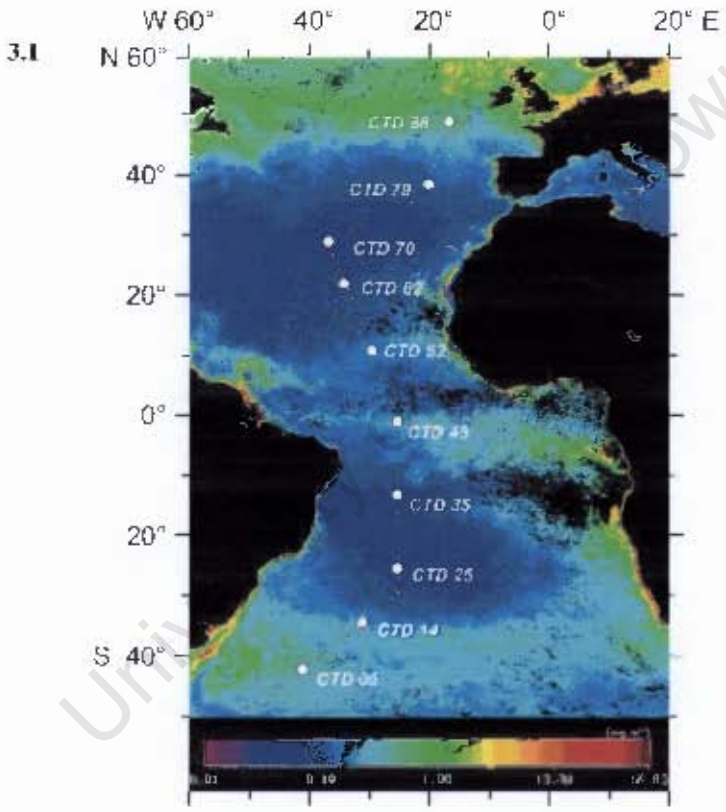

Figure 3.1. Cruise track and positions of export sampling stations for the May 2004 Atlantic Meridional Transect (AMT 14). Cruise track is overlaid on a monthly sea surface chlorophyll (mg m^{-3}) composite. Note station positions relative to surface chlorophyll concentrations: (i) higher chlorophyll temperate waters in both hemispheres (CTD 88, CTD 05; 49.00°N, 41.04°S), (ii) relatively high chlorophyll waters in both the northern (CTD 79; 38.67°N) and southern (CTD 14; 32.97°S) subtropical convergences; (iii) intermediate chlorophyll concentrations for equatorial stations (CTD 43, CTD 52; 0.94°S, 11.40°N); and (iv) low chlorophyll concentrations in the northern (CTD 62, CTD 70; 22.33°N, 29.30°N) and southern (CTD 35, CTD 25; 12.28°S, 24.23°S) subtropical gyres.

3.2 Sampling and methods

3.2.1 Standing stocks of particulate material

For particulate organic carbon methods see section 2.2.2 in the previous chapter. Particulate inorganic carbon (PIC) measurements were made on 1 litre seawater samples filtered onto 0.45 μm cellulose nitrate filters, rinsed with a 0.02 mol potassium tetraborate solution, extracted in 2% nitric acid and analysed using Inductively Coupled Plasma Atomic mass Spectrometry (ICP – AOES). Relative standard deviation (RSD) between replicate PIC measurements was ~14%. Biogenic silica (BSi) measurements were made on 1litre seawater samples filtered onto 0.4 μm polycarbonate filters, stored at -20°C, digested in 0.2 mol sodium hydroxide, neutralised with 0.1 mol hydrochloric acid (Brown et al., 2003) and analysed using a ATI Unicam 8625 UV/VIS spectrometer. RSD between replicate samples was ~13%.

3.2.2 Particulate production and export measurements

The small volumes (<0.3 l^{-1}) used for production measurements undersample large and rare mineralising plankton (foraminifera, pteropods, radiolarians), whereas SAPS sampling of the sinking particulate material (average 1500 litres) better samples such organisms. This difference in sampling volumes implies that export estimates may include some additional calcite and opal production relative to surface measurements of calcification and silicification. However, large calcifiers and silicifiers are relatively rare in subtropical waters (Baumann et al., 2004) and hence such additional sources of calcite and opal are regarded as minimal. On deck simulated *in situ* phytoplankton organic and biomineral production measurements were made at 5 light depths (97, 55, 33, 14, and 1% incident irradiance) as determined from *in situ* CTD data. For this study, the surface productive layer (euphotic zone) is defined as spanning from the surface to the depth of 1% incident irradiance. As the energy for calcification comes from photosynthesis, little dark calcification is thought to occur, and silicification is fuelled by respiration. Daily rates of calcification (and photosynthesis) are thus considered to include only the light period and silicification

to include both light and dark periods. For methods on primary production measurements see section 2.2.4 in the previous chapter.

3.2.3 Calcification

Calcification measurements were made following the 'Micro-Diffusion Technique' (MDT) (Balch and Kilpatrick, 1996; Balch et al., 2000). For MDT, water samples (3 light) were spiked with 60-80-Ci 14C-labelled sodium bicarbonate and incubated alongside photosynthesis samples. Incubations were terminated by filtering onto 0.2 μm (later 0.4 μm) polycarbonate filters and thoroughly washed with fresh filtered seawater before placing in pony vials. A gas tight septum and micro-pot containing a 2'- Polyethylamine soaked glass-fibre filters were attached to each pony vial and a small gauge syringe was used to inject 1 ml of 1% phosphoric acid into the filter at the bottom of the vial. After the samples had equilibrated (20-24 hrs), the septa were removed and the micropots (with glass-fibre filters) placed in fresh pony vials and liquid scintillation cocktail added. Sample activities were counted in a liquid scintillation counter. The mean RSD for calcification measurements was ~31% (3-72%). Formalin blank measurements were made at a five stations and a cruise average was applied to all measurements. The MDT determines both inorganic (acid labile) and organic (non-acid labile) particulate carbon fixation (Balch and Kilpatrick, 1996; Balch et al., 2000). The mean RSD for MDT measurements of photosynthesis was ~16% (2-45%). A comparison of the photosynthesis measurements from the MDT and the standard productivity protocol showed good agreement (model II regression, $y = 1.19MDT - 0.01$, $r^2 = 0.85$, $p<0.001$, $n = 48$). All references to organic carbon production are from standard photosynthesis measurements (not MDT measurements).

3.2.4 Silicification

Daily measurements of silicification were made following the measurements of Brzinski and Phillips (1997) and Brown et al. (2003). Water samples (3 light) from 4-5 light depths were spiked with 0.05 μCi of a high specific activity (2 μCi ml^{-1}) ^{32}Si-labelled silic acid tracer and incubated in 250 ml polycarbonate bottles for 24 hrs alongside samples for photosynthesis and calcification. Incubations were terminated

by filtering onto 0.4 μm polycarbonate filters and washed with filtered seawater. Filters were digested with 0.2 mol sodium hydroxide at 85°C for 1 hr. Liquid scintillation cocktail was added after the filters had cooled and analysed using a liquid scintillation counter with a dual window 60 minute counting protocol on return to the National Oceanography Centre (NOC), UK (Brown et al., 2003). Counting efficiency in the assigned windows was calibrated using ^{32}Si and ^{32}P spikes (Brzezinski and Phillips, 1997; Brown et al., 2003). Spike activity was determined by diluting an aliquot of ^{32}Si stock with artificial seawater and counting three replicates in liquid scintillation cocktail. The mean RSD for silicification measurements was 28% (2-89%).

3.2.5 Export measurements

Export of POC, calcite and opal were calculated from water column $^{234}Th/^{238}U$ disequilibria (e.g. Buesseler, 1998). Estimates of methodological errors for export fluxes are calculated based on propagated methodological uncertainties (full details in section 2.2.6) and an RSD for particulate measurements of 15%. See previous chapter for details on measurements of ^{234}Th flux (Section 2.4.1). Ratios of particulate ^{234}Th to POC (range 6-15, mean 8.6 ± 2.9), calcite (0.07-0.82, mean 0.42 ± 0.25) and opal (0.01-0.25, mean 0.10 ± 0.07) were determined on large (>50 μm), rapidly sinking particles derived from SAPS filtrations. In order to calculate opal and calcite fluxes these ratios were multiplied by the thorium flux as was done for the POC flux calculations in section 2.2.4. Inherent in the calculations of export fluxes is the use of a single value for ^{234}Th disequilibrium for the different types of particulate material. Thus, it could be argued that any underlying relationship between export fluxes can result from a relationship between POC, opal and/or calcite concentrations within large exported particles and not from the fluxes themselves. However, as no statistically significant relationships were found between the POC/^{234}Th ratio and either of the calcite/^{234}Th ($r = 0.41$, $n = 10$, $p>0.05$) or opal/^{234}Th ($r = 0.41$, $n = 10$, $p>0.05$) ratios on the large particles, the observed relationships between the different export fluxes (Figure 3.5a) are considered to be valid.

At several stations ($n = 6$), there were significant discrepancies between estimated particulate export from the euphotic zone and estimates from the water column over

which ^{234}Th disequilibrium was estimated (the export layer). Euphotic zone estimates were on average ~55% (± 21%) lower than export layer estimates at all except one station. The exception was at CTD 14 (32.97°S) where a subsurface thorium excess at ~300 m resulted in higher euphotic zone estimates than export layer estimates. The general discrepancy observed between euphotic zone and export layer estimates indicates that particulate scavenging of ^{234}Th also occurs below the euphotic zone. To calculate export efficiencies (export/production; *ThE* after Buesseler et al., 1998) for the different particle types, the integration depth of the steady state ^{234}Th disequilibria model was limited to the depth of the euphotic zone, so that export and production were integrated over the same depth range.

3.3 Results and discussion

3.3.1 Particulate material

Generally, POC, PIC and BSi concentrations were highest at or above the 1% irradiance level (Figures 3.2a-c). Highest POC (>4-6 mmol C m^{-3}) concentrations were found around the equator, at 22°N, 35°N and in northern temperate waters, highest PIC concentrations (>0.1 mmol C m^{-3}) were in northern and southern temperate waters, and at 30°N, while highest BSi concentrations (>0.06-1 mmol Si m^{-3}) were found around the equator, at 40°S, between 15-20°N and north of 32°N (Figure 3.2c). Generally, the lowest concentrations of POC, PIC and BSi were observed in the euphotic zone of the subtropical gyres; <3 mmol C m^{-3} for POC, <0.06 mmol C m^{-3} for PIC and <0.04 mmol Si m^{-3} for BSi (Figures 3.2a-c). Relatively high concentrations of POC (>5 mmol C m-3) and PIC (>0.1 mmol C m-3) were also found below the euphotic zone (Figures 3.2a,b), mainly in southern temperate waters (>40°S), and suggest that material was being lost from the euphotic zone (Figures 3.2a,b). In the case of BSi, high concentrations (>0.1 mmol Si m^{-3}) were found at depth around the equator (3°N), along the margins of the northern subtropical gyre, and in the northern hemisphere (Figure 3.2c).

3.2a)

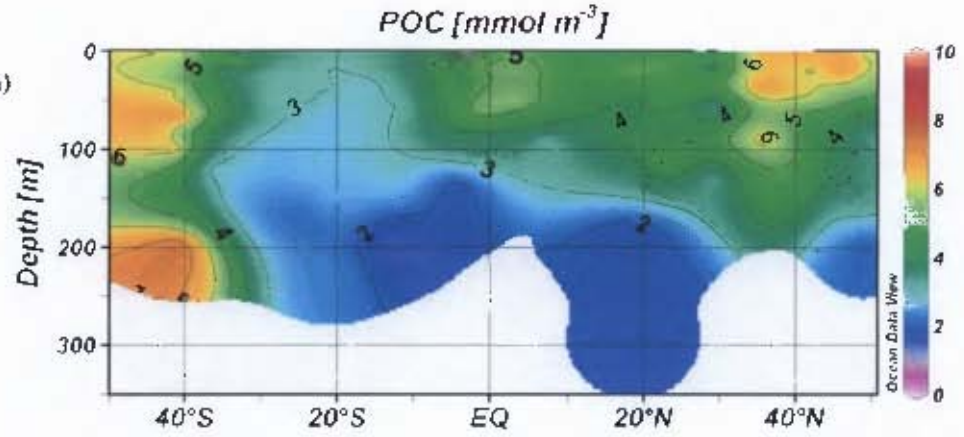

3.2b)

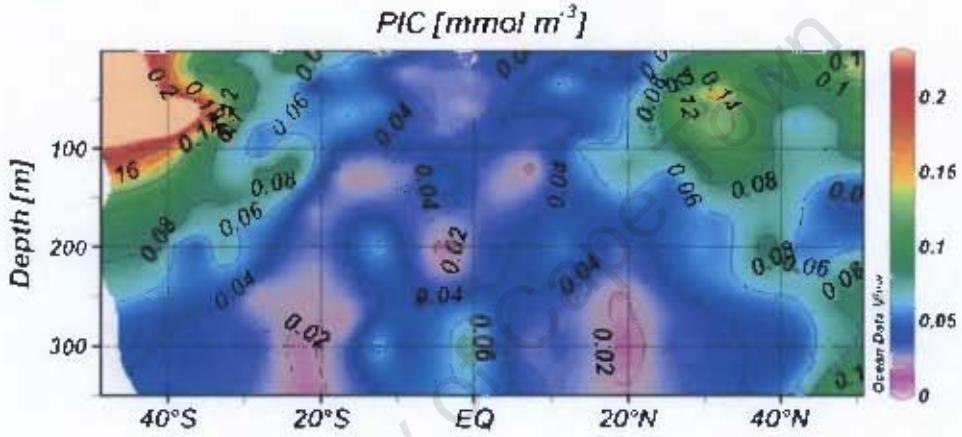

3.2c)

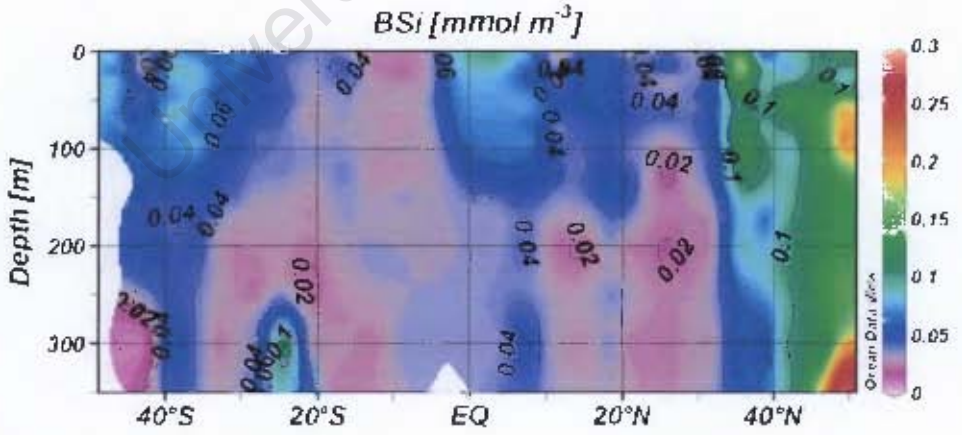

Figure 3.2 Ambient nutrient concentration as measured during AMT 14 for a) particulate organic carbon (POC), b) calcite (PIC) and c) biogenic silica (BSi)

3.3.2. Production, export and export efficiencies

Rates of primary production decreased with depth at all latitudes and were highest around the equator and in temperate waters and lowest in the central gyres (see Figure 2.13c chapter 2). Rates of calcification and silicification were highly variable between stations and with depth (Figure 3.3), reflecting the natural patchiness in distribution of coccolithophores and diatoms (Venrick, 1982; Balch and Kilpatrick, 1996; Nelson and Brzezinski, 1997).

Calcification was the dominant process except in subsurface equatorial waters and in the northern subtropical convergence. At most stations calcification decreased with depth, a consequence of the light dependency of calcification, whereas silicification frequently increased or remained constant with depth reflecting its dependence on dissolved silicate concentrations, and on respiration as opposed to photosynthesis as an energy source (Figure 3.3) (Martin-Jézéquel et al., 2000; Claquin et al., 2002; Poulton et al., 2006a).

3.3

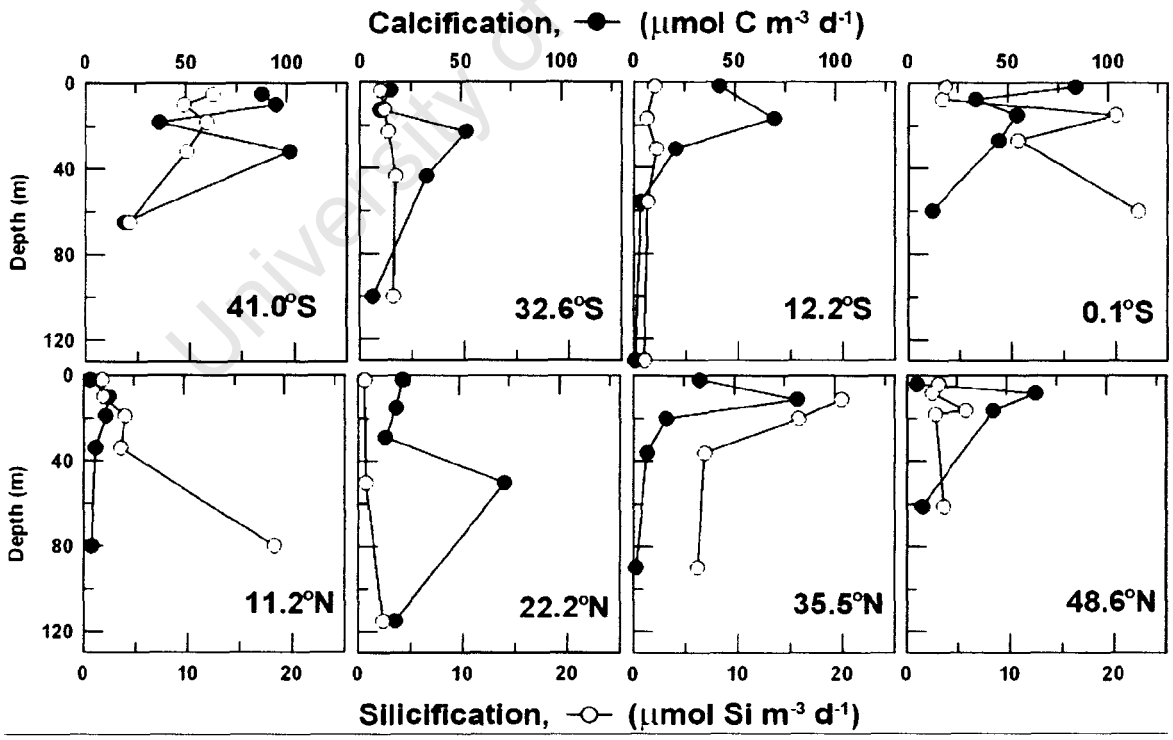

Figure 3.3. Depth profiles of calcification (closed circles) and silicification (open circles) for selected stations during AMT 14. Figure sourced from Poulton et al. (2006a).

The magnitude of (molar) export fluxes for the different particulate materials (Figure 3.4) were higher for organic carbon (range 2.53-11.76 mmol C m^{-2} d^{-1}) than for calcite (0.03-0.61 mmol C m^{-2} d^{-1}) or opal (0.01-0.24 mmol Si m^{-2} d^{-1}) (Table 3.1). Calcite export fluxes were generally less than an order of magnitude higher than opal fluxes (Table 3.1). CTD 79 (38.67°N) with the highest organic carbon flux (11.76 mmol C m^{-2} d^{-1}) was also the station with the highest biomineral fluxes (0.61 mmol C m^{-2} d^{-1} for calcite and 0.24 mmol Si m^{-2} d^{-1}) (Table 3.1).

In agreement with deep sediment trap data (e.g. Klaas and Archer, 2002), there appear to be linear relationships between organic carbon, calcite (Figure 3.5a) and opal fluxes (Figure 3.5b). However, these relationships are not as obvious if the high export station CTD 79 (38.67°N) is ignored. Although a relationship between calcite and organic carbon flux remains, no relationship is now observed between opal and organic carbon flux (Figure 3.5). It is also unclear from these relationships (Figure 3.5) whether the range of magnitude of organic carbon/biomineral export observed in this study represents efficient export from unproductive regions or inefficient export from highly productive systems (Francois et al., 2002). Rather, an understanding of the regional and general export efficiencies (*ThE*) for the different particulate types is required.

The export efficiencies (*ThE*) of all three particulate phases were highly variable (Figure 3.4) and ranged from 0.1 to 0.7 for POC, from 0.05 to 1.51 for opal and from 0.02 to 0.79 for calcite (Table 3.1). The mean values of *ThE* for the three phases (Table 3.1) were however similar (0.26 for calcite, 0.31 for opal, and 0.29 for organic carbon), suggesting that similar processes determine the efficiencies of mineral and organic carbon export. However, when *ThE* values for the three phases are compared on a station by station basis (Figures 3.5c,d) they appear unrelated (over the euphotic zone) in a way that is not predictable from surface rates of primary productivity (Figure 3.4; Table 3.1) and it becomes clear that such averages mask considerable variability (spatial and/or temporal) in the processes that determine *ThE* (Figure 3.4; Table 3.1).

Table 3.1 Compilation of station positions, euphotic zone depths (1% light level), estimates of particulate organic carbon (POC), calcite and opal production, export fluxes and export efficiencies. Calculated errors for export fluxes are based on accounting for methodological uncertainties (see Methods chapter 2.2.6.1). NA indicates not available.

Station Number	Latitude	Euphotic Depth	**Production**			**Export**			**Export efficiencies *(ThE)***		
			POC	Calcite	Opal	POC	Calcite	Opal	POC	Calcite	Opal
	deg N	(m)	(mmol m^{-2} d^{-1})			(mmol m^{-2} d^{-1})					
CTD 05	-41.04	65	37.42	4.54	0.59	5.36 ± 1.86	0.39 ± 0.13	0.02 ± 0.01	0.14	0.09	0.04
CTD 14	-32.97	103	13.18	2.47	0.3	3.69 ± 2.87	0.11 ± 0.08	0.04 ± 0.03	0.28	0.04	0.13
CTD 25	-24.23	122	12.72	nd	0.15	2.53 ± 3.26	0.10 ± 0.13	0.02 ± 0.02	0.20	nd	0.12
CTD 35	-12.28	130	15.25	1.97	0.21	3.29 ± 3.25	0.05 ± 0.05	0.01 ± 0.01	0.22	0.02	0.05
CTD 43	-0.94	59	24.01	2.38	0.84	6.33 ± 3.58	0.34 ± 0.19	0.01 ± 0.01	0.26	0.14	0.01
CTD 52	11.40	81	29.52	0.52	0.6	6.26 ± 6.81	0.41 ± 0.45	0.08 ± 0.09	0.21	0.79	0.14
CTD 62	22.33	115	25.95	4.44	0.14	0	0	0	0	0	0
CTD 70	29.30	132	20.70	1.19	0.15	0	0	0	0	0	0
CTD 79	38.67	50	16.49	0.88	0.16	11.76 ± 5.15	0.61 ± 0.27	0.24 ± 0.11	0.71	0.70	1.51
CTD 88	49.00	28	24.74	1.25	0.16	2.84 ± 2.33	0.03 ± 0.03	0.08 ± 0.06	0.11	0.03	0.48
Mean (S.D.)						5.26 (3.03)	0.26 (0.21)	0.06 (0.08)	0.27 (0.19)	0.26 (0.34)	0.31 (0.51)

The majority of stations showed higher *ThE* for organic carbon than for calcite or opal (Figures 3.5c,d; Table 3.1), and only at CTD 79 (38.67°N) (Figures 3.5c,d; also see Table 3.1) was high *ThE* for organic matter comparable to or higher than values for either biomineral. Comparison of biomineral to organic carbon ratios for material synthesised in the euphotic zone to those of exported material provides a proxy for the relative changes in the characteristics of exported particles (Figure 3.6) (Brown et al., 2006). At most stations, these ratios show that there is relatively more dissolution of biominerals in the euphotic zone than remineralisation of organic carbon although there is considerable variability between stations (Figure 3.6).

Station to station differences in export fluxes and *ThE* values for organic carbon, calcite and opal highlight regional variability in the form and control of particle export, which in turn is most likely related to differences in the composition and dynamics of the planktonic ecosystems over the AMT transect.

Comparison of both the magnitude of export fluxes and the export relative to surface production (*ThE*) for organic carbon, calcite and opal show that: (i) although linear relationships appear to characterise the relationship between absolute fluxes of organic carbon, calcite and opal, there is significant regional variability and high biomineral fluxes are not always related to high organic carbon fluxes particularly with respect to opal (Figure 3.5b); and (ii) although average *ThE* were similar for the three particulate types, there is considerable station by station difference. Such regional disparity in export fluxes and *ThE* are likely to be related to regional patterns in hydrography and planktonic ecosystem structure and are examined in the context of these factors in the next section.

3.3.3 Regional variability of export flux and export efficiency

A variety of hydrographic provinces and ecosystems are sampled by the AMT transect, and these include the stratified oligotrophic subtropical gyres, tropical equatorial upwelling waters, seasonally variable subtropical convergences and seasonally mixed temperate waters at either end of the transect (Robinson et al., 2006). Surface and upper ocean (<50 m) chlorophyll-a concentrations are low (<0.10 mg m^{-3}) within both subtropical gyres of the Atlantic Ocean, with elevated

chlorophyll-a concentrations (>0.3 mg m^{-3}) associated with the equatorial upwelling (10°S-15°N), and seasonally in the subtropical convergences and temperate waters of both hemispheres (Figure 3.1)(Robinson et al., 2006). Generally, small picophytoplankton (<2 μm) dominate both biomass and organic carbon production throughout the AMT transect (Zubkov et al., 1998; Marañón et al., 2000; Poulton et al., 2006b), although there are slight increases in biomass and production by larger phytoplankton cells in equatorial upwelling waters (Perez et al., 2005a) and in temperate waters during (northern) spring (Tarran et al., 2006). The grazer community is more variable over the AMT transect, with nanoflagellate (2-20 μm) and microzooplankton (20-200 μm) grazers dominant in the subtropical gyres, while mesozooplankton (>200 μm) biomass and grazing pressure increases in equatorial and temperate waters (Huskin et al., 2001; Isla et al., 2004).

Low rates of calcification and silicification were characteristic of the subtropical gyres (Figure 3.4) and highlight the low biomass of coccolithophores and diatoms (Nelson et al., 1995; Haider and Thierstein, 2001). Particulate export from CTD 62 and CTD 70 in the northern subtropical gyre (22.33°N, 29.30°N) was negligible in so far as detection limits of the thorium technique allowed, implying full remineralisation/ dissolution of material synthesised in the upper ocean at the time of sampling. At CTD's 35, 25 and 14 in the southern subtropical gyre (12.28°S, 24.23°S, 32.97°S), low *ThE* for calcite (0.02-0.04), opal (0.05-0.13) and organic carbon (0.20-0.28) also suggest that a large proportion of surface production was retained in the upper ocean. A comparison of biomineral to organic carbon ratios for surface production and exported material for stations in the southern subtropical gyre (Figure 3.6) both indicate preferential dissolution of mineral material (opal, calcite) relative to organic carbon.

Efficient nanoflagellate and microzooplankton grazing, as well as bacterial activity, are likely to enhance silica dissolution in subtropical surface waters by exposing individual diatom frustules to under-saturated surface water silica concentrations (Nelson et al., 1995; Passow et al., 2003; Ragueneau et al., 2006) and facilitating intracellular or aggregate associated calcite dissolution (Hansen et al., 1996; Milliman et al., 1999). Dominance of the community by small cells, with slow sinking rates, may also promote the dissolution of calcite and opal by increasing their residence time

in surface waters. The biological pump in the subtropical gyres is therefore thought to be characterised by an active microbial loop and efficient recycling of biomineral and organic carbon production.

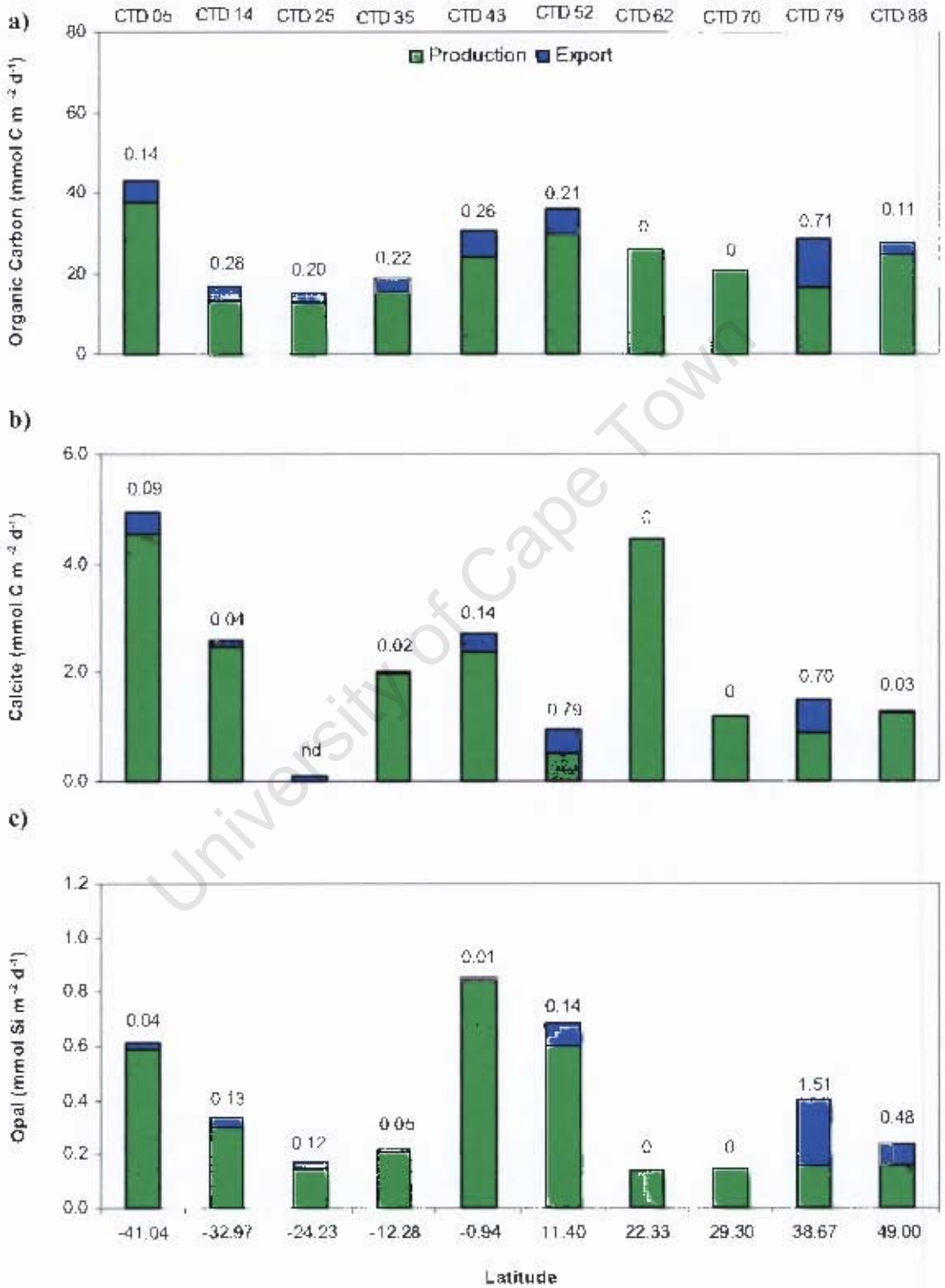

Figure 3.4 Euphotic zone integrated (molar) rates of production (bottom green bars) and export (top blue bars) for (a) organic carbon (mmol C m^{-2} d^{-1}), (b) calcite (mmol C m^{-2} d^{-1}), and (c) opal (mmol Si m^{-2} d^{-1}). The ratio of export to production (export efficiency) for each particle type is provided. Nd indicates not determined. CTD station numbers are provided above. Note that export fluxes from stations in the northern subtropical gyre (CTD 62, CTD 70) were below the detection limits of the ^{234}Th technique.

By contrast at CTD's 43 and 52 in equatorial waters of the Atlantic Ocean (0.94°S, 11.40°N), elevated nutrient concentrations due to localised upwelling (Longhurst, 1993; Perez et al., 2005a) cause increases in chlorophyll concentrations (Figure 3.1) (Robinson et al., 2006) and increased rates of organic production (Figure 3.4c) (Marañón et al., 2000; Poulton et al., 2006a). However, due to strong grazing pressure by meso- and microzooplankton, there is little change in the size structure of the phytoplankton community (Perez et al., 2005a). Nevertheless, increases in the integrated rates of calcification and silicification (Figures 2b,c) (Poulton et al., 2006a) imply that although picoplankton dominate, larger phytoplankton cells must also be present but that these are efficiently grazed (and exported) by the high mesozooplankton biomass found in equatorial waters (Huskin et al., 2001; Isla et al., 2004). Export efficiencies were high for calcite (0.14-0.79) and organic carbon (0.21-0.26) but low for opal (0.01-0.14) in equatorial waters (Figure 3.4; Table 3.1). A comparison of biomineral to organic carbon ratios of surface production and export implies preferential organic carbon remineralisation relative to calcite dissolution and preferential opal dissolution relative to carbon remineralisation (Figure 3.6).

Significant dissolution of opal in equatorial waters (Figure 3.6b) is likely to be mediated by enhanced mesozooplankton grazing (Huskin et al., 2001; Isla et al., 2004), which exposes individual diatom frustules to relatively low ambient silicate concentrations (Nelson et al., 1995) and also increases the number of broken diatom frustules (Roman and Rublee, 1980), thereby preparing them for subsequent colonization by bacteria (Ragueneau et al., 2006). High calcite *ThE* (0.79) at CTD 52 in the northern equatorial station (11.40°N) was associated with relatively low *ThE* for organic carbon (0.21), which implies that there was no enhanced organic carbon *ThE* associated with relatively high calcite *ThE*. There are several mechanisms that may have been responsible for this. For example, if equatorial mesozooplankton were selectively feeding on the productive coccolithophores as opposed to the dominant picophytoplankton community, they would be producing calcite rich faecal pellets and calcite export would be promoted. Other mechanisms may include spatio-temporal variability in production and export caused by mesoscale eddies, characteristic of low latitude current systems (Longhurst, 1993; Perez et al., 2005a). Observations of high calcite *ThE* in the equatorial Atlantic also explains previous observations of high

equatorial calcification rates coupled with low standing stocks of calcite (Poulton et al., 2006a).

CTD's 05 and 79 in the subtropical convergences of the Atlantic Ocean (41.04°S, 38.67°N) are sites of seasonally enhanced biomass (Figure 3.1), production (Figure 3.4), and seasonal differences in the plankton community (Marañón et al., 2000; Robinson et al., 2006). During AMT 14 (May 2004), early autumn conditions of enhanced mixing, low irradiance and moderate nutrient concentrations characterised the southern subtropical convergence while the northern subtropical convergence was experiencing late spring conditions of reduced mixing, high irradiance but reduced nutrient concentrations (Marañón et al., 2000; Robinson et al., 2006).

At CTD 05 in the southern subtropical convergence (41.04°S), calcite, opal and organic carbon production were all high, whereas *ThE* values were all very low (0.09, 0.04 and 0.14, respectively) (Figure 3.4; Table 3.1). However, at CTD 79 in the northern subtropical convergence (38.67°N), reverse trends were found with calcite, opal and organic carbon production all being relatively low, whereas their *ThE* values were among the highest values found in this study (0.70, 1.51, and 0.71, respectively) (Figure 3.4; Table 3.1). A comparison of the biomineral to organic carbon ratio for surface production and export also showed different patterns in the two subtropical convergences (Figure 3.6). In the southern subtropical convergence (CTD 14; 32.97°S) there was preferential dissolution of both calcite and opal relative to organic carbon remineralisation, whereas in the northern subtropical convergence (CTD 79; 38.67°N) there was preferential organic carbon remineralisation relative to opal dissolution, and to a lesser extent, calcite dissolution (Figure 3.6). However, as these trends arise from rather few data points, these observations cannot be confirmed as characteristic seasonal or regional indices.

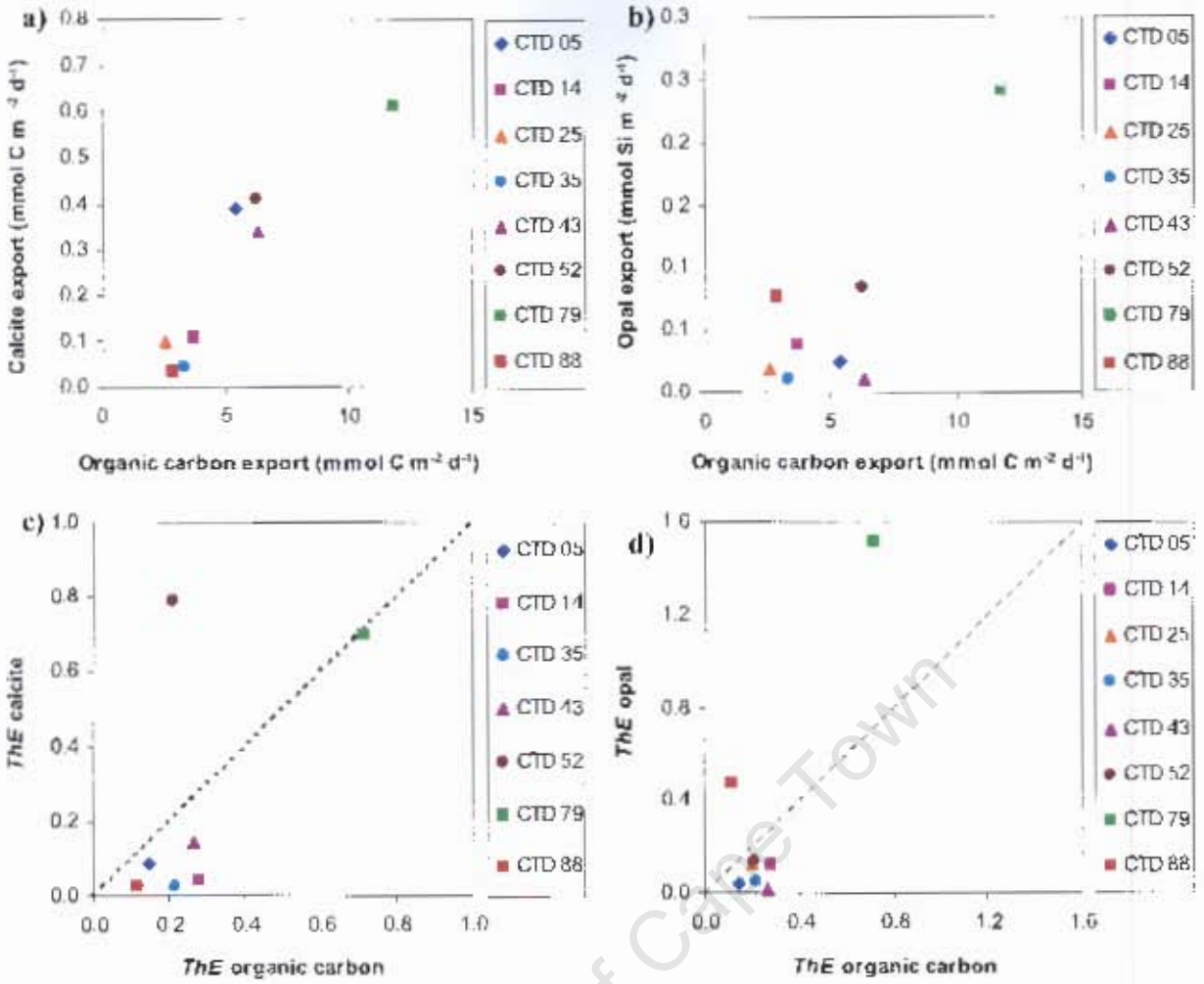

Figure 3.5 Comparison of export fluxes (mmol m^{-2} d^{-1}) and export efficiencies (export/production) for calcite, opal and particulate organic carbon: (a) calcite and particulate organic carbon fluxes, (b) opal and particulate organic carbon fluxes, (c) calcite and particulate organic carbon export efficiencies (*ThE*), and (d) opal and particulate organic carbon export efficiencies (*ThE*). Dashed lines (c,d) represent a 1:1 line.

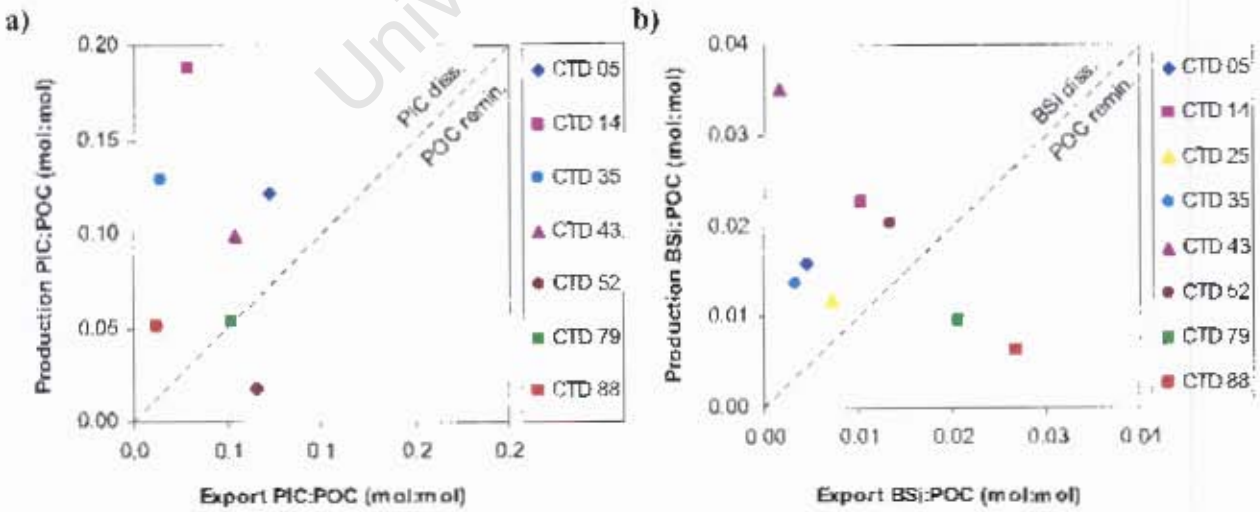

Figure 3.6. Relative changes in the molar ratios of particulate material composition between surface production and export: (a) calcite to particulate organic carbon (calcite:organic carbon), and (b) opal to particulate organic carbon (opal: organic carbon). Values above the 1:1 (dashed lines) line indicate relative mineral dissolution, while values below the 1:1 line indicate organic carbon remineralisation.

Nevertheless, differences in *ThE* and relative biomineral dissolution / organic carbon remineralisation patterns between the two subtropical convergences may be caused by seasonal differences in the temporal coupling of production and export. In the northern subtropical convergence, material being exported may represent the remnants of the spring bloom community settling out of the water column as low nutrient conditions develop. Thorium-based measurements of export integrate over relatively long timescales (~31 days; Buesseler et al., 1998) compared to relatively instantaneous measurements of primary production (<1 day). Elevated *ThE* may therefore result from significant temporal decoupling between export and primary production. Indeed, averaged SeaWiFS chlorophyll-a estimates obtained for this station clearly reveal elevated chlorophyll-a concentrations in the region ~2 weeks prior to our *in situ* sampling which suggests that the high ^{234}Th flux rate measured here could represent export from a previous episode of elevated productivity (see section 2.4.3; Figure 2.20).

In contrast, consistently low *ThE* in the southern subtropical convergence suggest that the autumnal bloom may not have progressed to the export phase due to continuing high nutrient conditions at the time of sampling (Figure 2.7; Chapter 2). Spatial decoupling of production and export may also be important in the patterns observed in the northern subtropical convergence, as both convergences are strongly influenced by mesoscale physical instabilities (Garcon et al., 2001; Mouriño et al., 2003), with stations close to 38.67°S (35.5°N, 41.6°N) having high diatom and coccolithophore cell densities (Poulton, unpublished results; T. Adey, pers. comm.) and high rates of calcification and silicification (Poulton et al., 2006a).

It is likely that seasonal export from the northern subtropical convergence is due to large aggregates which sink much faster (~100 m d^{-1}) than the timescale for significant biotic dissolution of calcite (Jansen et al., 2002), or opal (Hill, 1992; Alldredge and Jackson, 1995), although there is evidence of organic carbon remineralisation relative to opal dissolution (Figure 3.6b). In these conditions, it is possible for sinking material to scavenge other particulate material present in the water column (i.e. calcite, opal and other phytoplankton cells) (Passow and La Roche, 2006) to further enhance *ThE* for all components.

High opal *ThE* (0.48) relative to calcite (0.03) and organic carbon (0.11) was sampled at CTD 88 in the northern temperate waters (49.00°N) indicating that material exported at this time contained little calcite or organic carbon. Comparison of the ratio of opal to organic carbon in material produced in the surface relative to that exported (Figure 3.6b) showed relatively more organic carbon remineralisation than opal dissolution. These differences may result from (i) a phytoplankton community that is dominated by opal export originating from heavily-silicified nutrient-stressed diatoms (Hutchins and Bruland, 1998; Timmermans et al., 2004), (ii) from significant remineralisation of organic carbon as material is re-packaged and/or sinks or (iii) from the export of predominantly aggregated diatoms as the net impact of aggregation is a lowering of opal dissolution (Moriceau et al., 2007), whereas organic carbon is being utilised by bacteria within the aggregates (Smith et al., 1992).

3.4 Conclusion

The relationship observed between integrated euphotic zone calcite and organic carbon export fluxes (Figure 3.5a) and the similarities in average *ThE* for the different particle types (Table 3.1) suggests a mechanistic relationship between efficient organic carbon and biomineral export.

However, when the relationship is viewed on a regional basis this agreement breaks down (Figures 3.5c,d; see also Figure 3.4 and Table 3.1). Similarly, a comparison of the biomineral to organic carbon ratio of surface production and exported material generally suggests preferential calcite or opal dissolution relative to organic carbon remineralisation (Figure 3.6). It is suggested that regional patterns of export and *ThE* for calcite, opal and organic carbon (Figure 3.4) and relative differences in calcite/opal dissolution versus organic carbon remineralisation (Figure 3.6) result from variability in the mechanisms controlling export. These may include latitudinal and seasonal differences in planktonic ecosystem structure, physical forcing and the degree of spatial/temporal coupling of surface production and export.

As calcite dominates ballasting material in the subtropical Atlantic ocean (Francois et al., 2002; Poulton et al., 2006a), a good relationship exists between calcite and

organic carbon fluxes (Figure 3.5a) rather than between opal and organic carbon fluxes (Figure 3.5b). However, the lack of a distinct relationship between *ThE* for calcite, opal and organic carbon (Figure 3.5c,d) implies that efficient organic carbon export from the productive euphotic zone may not always be enhanced by *ThE* of biominerals. Instead, efficient particulate export from the euphotic zone may be more dependent on the characteristics of the planktonic community composition (e.g. size spectra, taxa) and ecology (e.g. physiology, grazing pressure). Nevertheless, at one station in the northern subtropical convergence, the highest organic carbon fluxes were associated with high biomineral export and high organic carbon *ThE* was associated with high biomineral *ThE* (Table 3.1). Therefore, important exceptions to the general pattern of decoupling between organic carbon and biomineral fluxes exist, which may significantly influence annual export.

At several stations (CTD's 05, 14, 25, 35, 43), *ThE* for organic carbon (0.14-0.28) was higher than that for calcite (0.02-0.14) or opal (0.01-0.13) (Table 3.1) which is the reverse of *ThE* patterns observed in deep sediment traps, where only ~1-2% of surface organic carbon production reaches the deep sea (Sarmiento et al., 2004b) compared to ~30-50% of minerals (see Table 3 in Poultan et al., 2006a). These patterns imply significant remineralisation of organic carbon relative to biominerals below the euphotic zone as particles sink and/or scavenge biomineral material as they settle (Passow and De La Rocha, 2006), such that opal and calcite are 'chemically' decoupled from organic carbon during sinking leading to an increase in the biomineral to organic carbon ratio with depth. The potential for effective ballasting of the remaining organic carbon therefore increases with depth, which may account for the observation of a 'ballast effect' in sediment trap material (Klaas and Archer, 2002).

4 A time-series study of surface and deep-water carbon export in the northeast Atlantic Ocean

4.1 Introduction

The downward flux of particulate material from the upper mixed layer of the ocean has a major effect on biogeochemical processes in the oceans and on the earth system, directly bearing on the ability of the ocean to sequester carbon dioxide from the atmosphere. Particle flux necessarily decreases with increased depth as the material is remineralised or dissolves, but our ability to predict the rate at which this flux decreases with depth remains uncertain. However, it is important that we gain a better understanding of this as the depth at which material is remineralised or dissolved determines the time before it is once again able to contribute to the biogeochemistry of the surface ocean and hence be relevant in air sea interactions.

Carbon remineralised above the depth of winter mixing (200-800 m depending on location) can affect air sea fluxes within a year of its remineralisation. It is only after deposition beyond the depth of winter mixing that such carbon is separated from the atmosphere for climatically significant periods of time (100's to 1000's of years) (Lampitt and Antia, 1997). Furthermore, from a benthic perspective, sedimentation of phytodetritus from the euphotic zone to the deep sea is considered one of the most important sources of energy for deep-sea ecosystems (Billett et al., 1983; Fowler and Knauer, 1986), which controls the distribution, dynamics and metabolism of deep-sea benthic organisms (Danovaro et al., 1999; Graf, 1989; Soltwedel et al., 1996).

Inter-annual changes in upper ocean planktonic community structure can affect the mass flux (Boyd and Newton, 1995), or may simply affect the composition of sedimenting material, while the mass flux remains constant (Deuser et al., 1995). Seasonal variability in particulate flux and the composition of the settling material are also influenced by biogeochemical processes in the water column and by hydrographic conditions that may advect material to, or away from, the site of interest. For example, Lampitt et al. (2001) estimated that particles trapped at 1000 m may have originated from up to 60 km from the sampling site and those sampled at 3000 m up to 130 km away. Understanding the effect of these processes on fluxes to

the deep sea and clarifying the relationship between surface production and deep water export are crucial to our understanding of ocean-atmosphere and pelagic–benthic coupling.

It is generally accepted that where high rates of productivity are supported by new nutrients (high f-ratios; Eppley and Peterson, 1979), losses via sedimentation will be a large proportion of the production measured. Furthermore, environments dominated by highly variable physical forcing such as mid-latitude wind mixing or insolation and high latitude sea-ice advance and retreat, should also lose a larger proportion of primary production than in more stable tropical or subtropical environments (Lampitt and Antia, 1997). However, our understanding of temporal and spatial variability in the oceans is severely limited by under-sampling as ship-based measurements rarely provide long-term data sets or large scale coverage. While satellite imagery can provide basin-scale estimates of phytoplankton biomass and productivity, moorings and sediment traps offer a useful method to monitor parts of the ocean on a long-term basis, therefore providing long timescale records (months to years) of particle fluxes averaged over ocean areas of hundreds of square kilometres. Sediment trap records can also provide information on surface-water processes although interpretation of the data is complicated by the complexity of the trajectories of sinking particulate matter (Gust et al., 1994) and the selective loss of material during sinking due to organic matter degradation and mineral dissolution (e.g. Armstrong et al., 2002).

Long-term studies of the northeast Atlantic deep ocean (49°N, 16.5°W) have been addressed by ongoing research over the Porcupine Abyssal Plain (PAP) observatory since 1989. The PAP study site (Figure 4.1) has become a major focus for interdisciplinary scientific research and monitoring; examining complex oceanic processes from surface waters to the seafloor by recording a suite of biological, chemical and physical measurements. In this Chapter, data collected from 5 cruises carried out between 2003 and 2006 (Tables 4.1a-e) examine:

i) the link between surface phytoplankton production and particle export.

ii) the spatial and temporal variability of surface and deep water processes that regulate particle flux.

Measurements of chlorophyll-a concentrations, primary production and new production are compared to export measurements to assess the relationship between NO_3 uptake (high f-ratios), carbon flux, and efficient carbon export (high *ThE*). In addition, measurements of particle export collected from moored sediment traps at 3000 m are compared to surface particle export derived from the $^{234}Th/^{238}U$ disequilibrium approach and from direct measurements using drifting PELAGRA sediment traps.

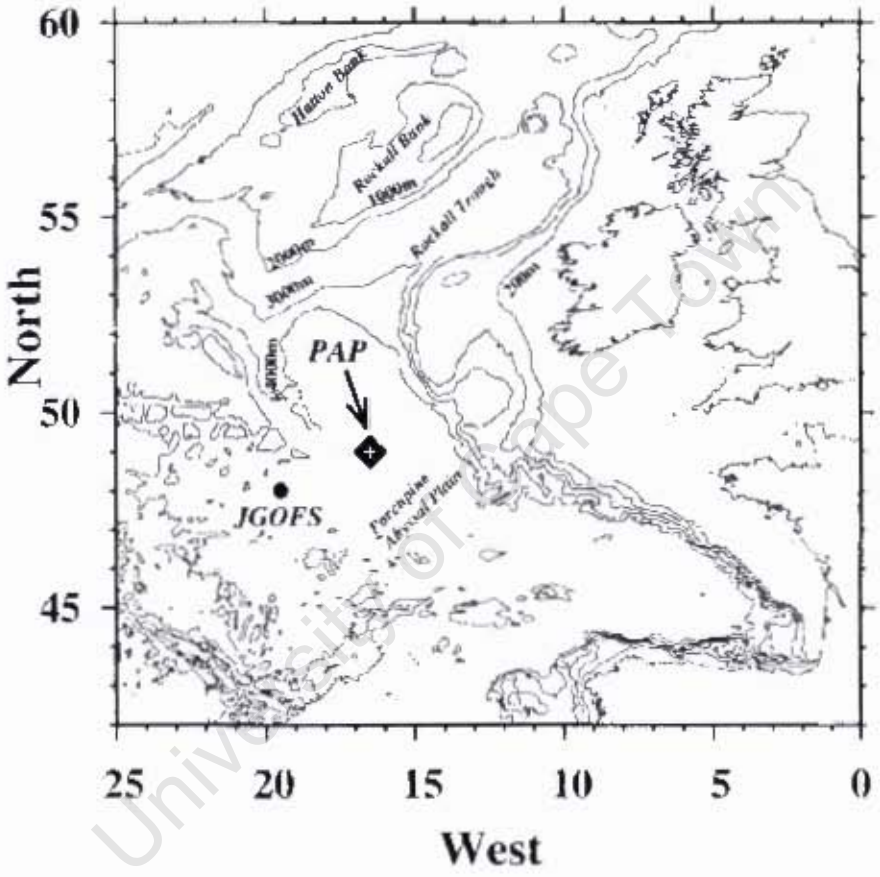

Figure 4.1. Map showing the location of the Porcupine Abyssal Plane observatory PAP and of the JGOFS site at which the North Atlantic Bloom Experiment (NABE) was carried out. Figure reproduced from Lampitt et al. (2001).

4.2 Study region

The PAP observatory is situated at approximately 49°N 16.5°W (Figure 4.1) near the centre of the North Atlantic Drift (NADR) province according to Longhurst, (1998). The PAP site is at the centre of an extensive area of flat abyssal plain (Billett and Rice, 2001) which is in contrast to the NABE experiment where rough topography

enhances spatial variability in the benthic environment, making interpretation of the data problematic. The PAP site lies to the south of the main stream of the North Atlantic Current and is subject to return flows coming from the west and northwest. An intermittent stream of cyclonic and anticyclonic mesoscale eddies cross the site, extending sometimes several thousand meters into the water column. Currents in the lower part of the water column tend to flow northward (Vangriesheim et al., 2001) and only in the upper water column is this general trend less predictable and occasionally, as in 1998, the flow reverses and flows southwards. Currents within 150 m of the seabed are typically 15 cm s^{-1} and always <20 cm s^{-1} (Lampitt et al., 2001; Vangriesheim et al., 2001), ensuring that sediment traps are likely to perform highly efficiently (Baker et al., 1988).

Strong seasonal variability controls the biology of the region that in winter experiences very low chlorophyll concentrations as a result of deep mixing to 800 m driven by convective overturning. Throughout the winter there are however short periods of stability when the mixed layer may only be a few tens of meters thick. With warming in spring (April), the water column becomes more stable and an upper mixed layer of about 50 m is established leading to a major phytoplankton bloom. Following surface nutrient depletion, a subsurface chlorophyll maximum typically develops and persists throughout the late spring and summer period.

Hovmoller plots of satellite derived sea surface chlorophyll for the region 47°-51°N and 14.5°-18.5°W over the last 10 years (Figure 4.2) illustrate the seasonal variability, with high chlorophyll concentrations associated with the development of the spring bloom followed by low chlorophyll concentrations and high cloud cover in winter. The inter annual variability in the strength of the bloom is also apparent and of particular interest is the unusually low chlorophyll concentrations in the spring of the past three years (2004-2006) which coincides with the time of this study.

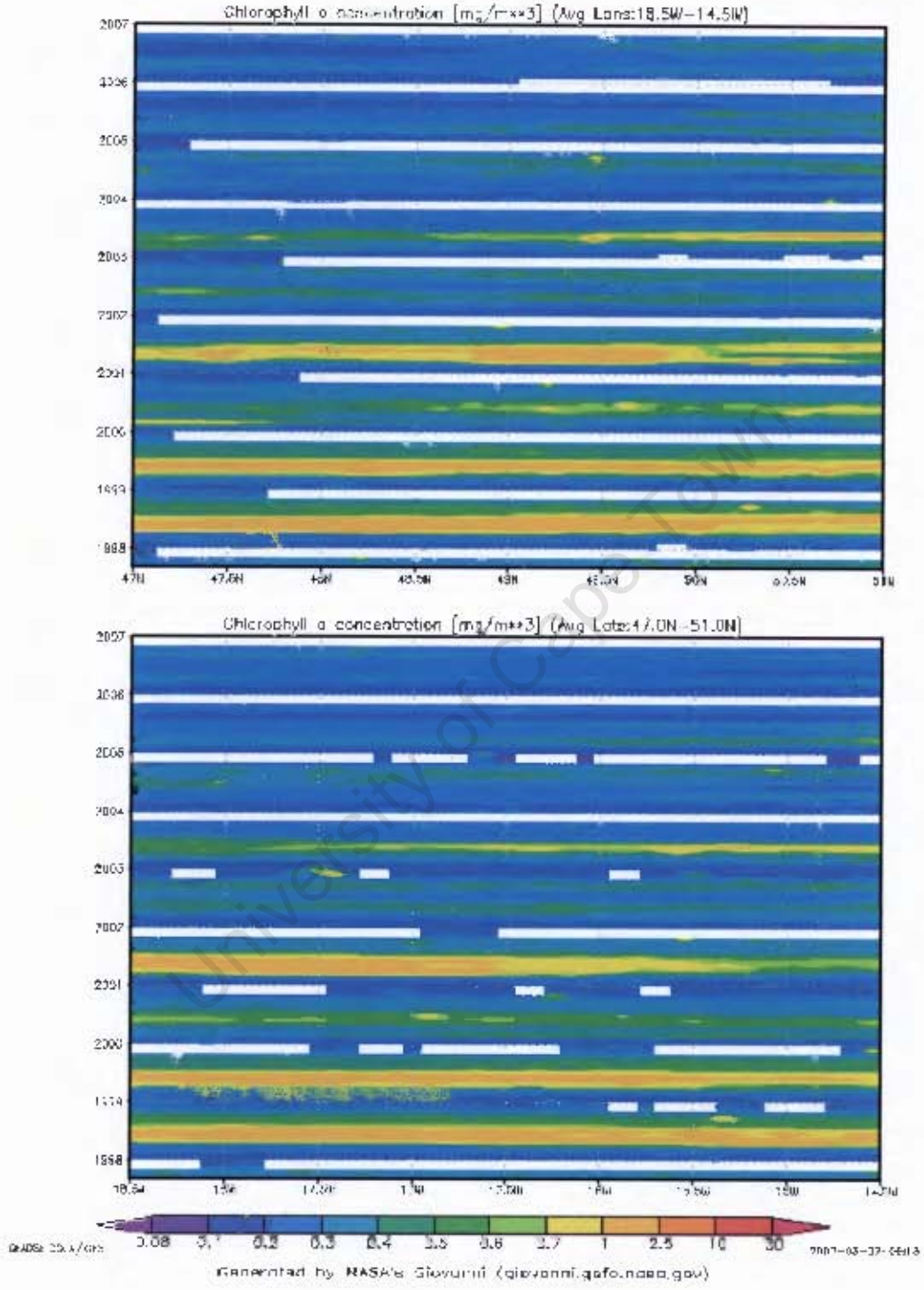

Figure 4.2. Hovmoller plots of SeaWiFs surface chlorophyll-a concentration (mg m^{-3}) from monthly composites of 9km products for the region 47°-51°N and 14.5°-18.5°W from 1997 to 2007.

Table 4.1. Cruise and sampling ID, sampling dates and station positions for a) primary and new production stations, b) ^{234}Th stations, where stations 405, 409, 56525, 15689, 18797 and 18707 were deep water repetition stations for calculation of the counting efficiency and testing the reproducibility of the method. The remaining ^{234}Th stations were profile stations, c) Stand Alone Pumping Systems – SAPS stations, d) PELAGRA neutrally buoyant sediment trap stations and e) 3000 m moored sediment trap stations. See section 3.3.5 for details on SAPS and PELAGRA depths

a) Primary Production and ^{15}N CTD's

Cruise	Sampling Date	Station ID	Latitude (deg N)	Longitude (deg W)
P 300	2003/07/06	405	41.70	22.12
P 300	2003/07/10	415		
P 300	2003/07/12	426	48.99	16.43
AMT 14	2004/05/29	CTD 88	49.00	16.39
CD158	2004/06/19	56503	48.85	16.50
CD158	2004/06/21	56510	49.00	15.51
CD158	2004/06/22	56516	48.81	16.73
CD158	2004/06/23	56520	48.97	16.50
CD158	2004/06/25	56529	48.83	16.59
D 295	2005/07/07	15686	49.05	16.42
D295	2005/07/07	15689	49.04	16.67
D 295	2005/07/11	15701	49.01	16.55
D 296	2005/07/16	15706	48.95	16.50
D 296	2005/07/18	15714	49.02	16.62
D 296	2005/07/20	15720	48.84	16.52
D306	2006/06/25	17703	48.83	16.50
D306	2006/06/26	17803	48.83	16.50
D306	2006/06/27	17903	49.03	16.15
D306	2006/06/28	18003	48.84	16.49
D306	2006/06/29	18103	48.83	16.50
D306	2006/06/30	18203	48.83	16.50
D306	2006/07/01	18303	48.84	16.50
D306	2006/07/02	18403	48.85	16.50
D306	2006/07/03	18503	48.83	16.50
D306	2006/07/04	18603	48.83	16.50
D306	2006/07/05	18703	48.83	16.50

b) ^{234}Th CTD's

Cruise	Sampling Date	Station ID	Latitude (deg N)	Longitude (deg W)
P 300	2003/07/06	405	41.70	22.12
P 300	2003/07/08	409	48.99	16.54
P 300	2003/07/12	426	48.99	16.43
P 300	2003/07/13	432	49.00	16.45
AMT 14	2004/05/29	CTD 88	49.00	16.39
CD 158	2004/06/19	56503	48.85	16.50
CD 158	2004/06/21	56511	49.00	16.51
CD 158	2004/06/22	56516	48.81	16.73
CD 158	2004/06/23	56520	48.97	16.50
CD 158	2004/06/24	56525	48.99	16.50
CD 158	2004/06/25	56529	48.83	16.59
D 295	2005/07/07	15686	49.05	16.42
D 295	2005/07/07	15689	49.04	16.77
D 295	2005/07/11	15701	49.01	16.55
D 296	2005/07/16	15706	48.95	16.50
D 296	2005/07/18	15714	49.02	16.62
D 296	2005/07/20	15720	48.84	16.52
D 306	2006/06/26	17705	48.83	16.50
D 306	2006/06/29	18005	48.84	16.53
D 306	2006/07/01	18205	48.83	16.50
D 306	2006/07/06	18707	48.81	16.50

c) SAPS

Cruise	Sampling Date	Station ID	Latitude (deg N)	Longitude (deg W)
P 300	2003/07/11	419	49.00	16.45
P 300	2003/07/11	419	49.00	16.45
AMT 14	2004/05/29	CTD 88	49.00	16.39
CD 158	2004/06/21	56513	49.00	16.45
D 296	2005/07/18	15713	49.03	16.62
D 306	2006/06/29	18011	48.83	16.50
D 306	2006/07/01	18211	48.83	16.50
D 306	2006/07/07	18806	48.83	16.51

d) PELAGRA

Cruise	Sampling Date start	Sampling Date end	Station ID	Lat. start (deg N)
P 300	2003/07/12	2003/07/13	429	48.95
CD 158	2004/06/24	2004/06/25	56522	49.00
D 296	2005/07/18	2005/07/20	15716	48.86
D 306	2006/07/02	2006/07/06	183003	48.86
D 306	2006/07/02	2006/07/06	183004	48.86

e) Moored Traps

Cruise	Sampling Date start	Sampling Date end	Station ID	Latitude (deg N)
P 300	2003/07/06	2004/05/23	430	49.00
CD 158	2004/06/16	2005/07/24	56526	49.04
D 306	2005/07/17	2006/07/06	183012	49.03

4.3 Materials and methods

The five cruises to the PAP site that will be discussed in this Chapter are as follows:

1) The Poseidon cruise in July 2003 (P300),
2) The AMT 14 transect that sampled over the PAP site (CTD 88) in May 2004,
3) The Charles Darwin cruise in June 2004 (CD158),
4) The Discovery cruise in July 2005 (D295/296)
5) The Discovery cruise in June/July 2006 (D306).

To make inter-annual comparisons more equitable, biological and biogeochemical measurement protocols at the PAP site were designed to be consistent. However, there were differences in the way that measurements were made on some of the cruises. Where these differences are significant, they are highlighted.

4.3.1 Chlorophyll-a and nutrients

Phytoplankton were recovered by filtering 250-500 ml of seawater through glass fibre filters (Whatman GF/F) and chlorophyll-a pigment was extracted in 90% acetone at -20°C overnight. Total chlorophyll was measured fluorometrically on board ship using a TD-700 Turner Designs fluorometer, calibrated with fresh chlorophyll standard (Sigma, UK) in 90% acetone (4°C, 18-20 hrs) and set up to measure chlorophyll-a in the presence of chlorophyll-b following Welschmeyer (1994).

Samples for macronutrients (NO_3 + NO_2, PO_4 and Si) were taken from stainless CTD casts and usually analysed on-board using a Skalar San Plus autoanalyser. Where ammonium and urea measurements were also made (in association with ^{15}N experiments), the manual protocols followed by Lucas et al., (in press) were adopted. On occasion (July 2005, D295/6), nutrient samples were frozen at -20°C and analysed on the Skalar San Plus autoanalyser back at the National Oceanography Centre, Southampton (NOC).

4.3.2 Primary production

On every cruise (see Table 4.1a for station details), daily rates of carbon fixation (mmol C m^{-3} d^{-1}) were estimated in a consistent manner from the incorporation of radio-labelled sodium bicarbonate ($NaH^{14}CO_3$) into particulate material. Four seawater samples (three light and one dark) were collected from six light depths (97, 55, 33, 14, 4.4 and 1% surface irradiance) and inoculated with ~10 µCi $NaH^{14}CO_3$ in acid rinsed polycarbonate bottles (70 ml). The samples were then incubated from dawn to dusk (~12 hours) in deck incubators that simulated *in situ* light depths. Light gradients were established in large Perspex incubation tubes wrapped appropriately with Lee Misty Blue and Grey neutral density filters. The incubator tubes were cooled with a through-flow of surface (7 m) seawater. Incubations were terminated by filtration (<200 mbar) onto 0.2 µm polycarbonate filters, rinsed with filtered sea water and acid-fumed overnight to remove residual inorganic ^{14}C. After this, filters were placed in 7 ml "pony" vials and 5 ml Ultima Gold scintillation cocktail was added to each vial. To determine the exact activity of the ^{14}C label, 100 µl of ^{14}C stock was added to 10 ml Carbasorb (CO_2 trapping agent), and from that, 10 x 100 µl aliquots were placed in 7 ml vials and 5 ml Permafluor cocktail was added. Total DPM activity of samples and standards were measured on a Wallac liquid scintillation counter.

4.3.3 New production and regenerated production

Concurrent with ^{14}C measurements (see Table 4.1a for station details), three water samples were taken for analyses of new and regenerated production; one each for nitrate, ammonium and urea uptake. Two litre samples were decanted into rinsed polycarbonate bottles and inoculated with 100 µl from stock solutions of $K^{15}NO_3$, $^{15}NH_4Cl$ and $CO(^{15}NH_2)_2$ respectively. The volume of ^{15}N spike in each case was adjusted to represent ~10% of the ambient substrate concentration. Bottles were incubated for ~10 hours alongside the primary production experiments, and terminated by filtering onto 25 mm ashed GF/F filters. Ammonium regeneration experiments were conducted simultaneously with the ammonium uptake experiments to correct NH_4 uptakes for NH_4 re-cycling. A second 2 l bottle was spiked with 100 µl of $^{15}NH_4Cl$ as for the uptake experiments, but this was immediately filtered through a

25 mm (ashed) Whatman GF/F filter to collect 900 ml filtrate to derive the ^{14}N:^{15}N isotopic ratio at time zero (Ro). Exactly 1.0 ml NH_4Cl solution (0.5349 g l^{-1}) was added to each bottle as a "carrier" prior to freezing the samples at –20°C. At the end of the NH_4 uptake filtration, 900 ml filtrate was recovered to measure ^{15}N isotopic dilution by excreted NH_4, carrier was added as before and the sample (Rt) also frozen as before. All filters were stored at –20°C prior to analysis at NOC on a Europa elemental analyser coupled to a GV Isoprime mass spectrometer (GV Instruments, Manchester, UK).

In June/July 2006 (D306) ammonium and urea uptake were not measured, however dual-labelled ^{13}C-bicarbonate uptake measurements were made concurrently with light and dark $^{15}NO_3$ uptake (ρNO_3) measurements. Incubations were conducted at the same light depths in 2 l polycarbonate bottles. Light and dark bottles were inoculated with both ^{15}N (0.1 µmol $K^{15}NO3$ / 100 µl) and ^{13}C spikes (4.2507 g sodium bicarbonate / 100 ml Milli Q water) to achieve ^{15}N and ^{13}C enrichments of ~10 and 4% respectively. After incubation, samples were filtered onto ashed GF/F filters; that were stored frozen (at -20°C) prior to measuring ^{15}N and ^{13}C enrichment on the mass spectrometer at NOC as before.

Estimates of carbon-based new production were obtained from ρNO_3*6.625 (Redfield et al., 1963; Eppley, 1989; Dugdale et al., 1992) and expressed as mmol C m^2 d^{-1}. A 12 hour daylight period of ρNO_3 was assumed to be representative of the autotrophic period of carbon fixation and was therefore used to convert from hourly to daily rates. However, since dark ρNO_3 is known (e.g. Cochlan et al., 1991), these uptake rates must be viewed as minimum daily rates. Furthermore, recent evidence for extensive nitrification in surface waters (Fernandez and Raimbault, in press; Yool et al., in press) may significantly over-estimate "new" production because of high rates of regenerated nitrate production.

4.3.4 Total ^{234}Th

Samples for thorium analysis were collected from the CTD at four stations in July 2003 (P300), one station in May 2004 (AMT 14), six stations in June 2004 (CD158),

six stations in July 2005 (D295/6) and four stations in June/July 2006 (D306) (Table 4.1b). Ten litre water samples were collected from the CTD bottle rosette from 8-10 depths to a maximum depth of either 500 or 1000 m. The sampling distribution was concentrated in the surface 100 m where a significant export of thorium on settling particles is expected to result in radioactive disequilibrium. To extract total ^{234}Th (dissolved + particulate) from the water, a medium-volume technique was used based on procedures described by Rutgers van der Loeff and Moore (1999), Buesseler at al. (2001b), Turnewitsch and Springer (2001), and Rutgers van der Loeff et al. (2006) (see section 2.2.6 of this thesis for details). The counting efficiency was determined by assuming that total ^{234}Th was in radioactive equilibrium with its parent ^{238}U at depth. On P300 (July 2003) the counting efficiency was calculated from 8 replicate samples at 1474 m taken from CTD405. The mean counting efficiency was 0.271 $\pm$ 0.009 cpm dpm^{-1} (mean $\pm$ 1SD). On AMT 14 the mean counting efficiency was 0.34 $\pm$ 0.03 cpm dpm^{-1} (mean $\pm$ 1SD) (see section 2.2.6.1 for details). On CD158 (June 2004) the counting efficiency was calculated from 6 replicate samples at 1000 m from CTD56525 together with the 500 m samples from the remaining 5 CTD's. The mean counting efficiency for these stations was 0.260 $\pm$ 0.006 cpm.dpm^{-1} (mean $\pm$ 1SD). On D295/6 (July 2005), the counting efficiency was calculated from 5 replicate samples from 1000 m, a 2500 m and a 3500 m sample on CTD15689 together with the 500 m samples from the remaining CTD's. The mean counting efficiency was 0.265 $\pm$ 0.009 (mean $\pm$ 1SD). On D306 the counting efficiency was calculated from 5 replicate samples at 1000 m from CTD 18707 together with the 500 m and 1000 m samples from the remaining three CTD's. The mean counting efficiency was 0.268 $\pm$ 0.010 (mean $\pm$ 1SD).

4.3.5 The large particulate pool

SAPS

The large particulate material fraction used to calculate the POC/^{234}Th ratio of the sinking particulate pool was collected in two ways. In the first instance, large particles >50 μm were collected by filtering large volumes of sea water through a 50 μm (P300 >70 μm) nylon mesh (293 mm diameter) using battery operated *in situ* pumps (Stand Alone Pumping Systems – SAPS). On most cruises the pumps were placed at 100 m, considered to be the base of the export layer and in accordance with the majority of

$^{234}Th/^{238}U$ based export studies. On P300 (July 2003) however, two pumps were placed at 85 m and 95 m and the averaged POC/^{234}Th ratio at ~90 m was used to calculate POC flux. On D306 (June/July 2006), three SAPS stations at 100 m were sampled during the cruise (Table 4.1c). An average POC/ ^{234}Th ratio from the three SAPS stations was used to calculate POC fluxes on this cruise. Once on board, the sample on the mesh was re-suspended using thorium-free filtered sea water and split into fractions using a 'Fulsom' splitter. One fraction was filtered onto pre-combusted 25 mm GF/F filters and stored frozen for subsequent POC analysis while another fraction was filtered onto 142 mm diameter (0.8 μm pore size) polycarbonate filters for ^{234}Th analysis (see section 2.2.7 for details).

PELAGRA

Alternatively, sinking particulates were collected using neutrally buoyant PELAGRA traps set at 180 m over 1 day on CD158 (June 2004), at 120 m over 2 days on D295/6 (July 2005) and from 150 m and 250 m over 4 days on D306 (June/July 2006) (Table 4.1d). Prior to each deployment of PELAGRA, a CTD was deployed to ascertain the temperature and salinity and therefore *in situ* water density. This allows accurate calculation of the ballast required for each trap at a specified depth. PELAGRA sample cups were filled with 500 ml of preservative solution (formalin, brine and sodium tetraborate) to fix organic material and to prevent particle dissolution during trap deployment. Samples collected by the PELAGRA traps were split with a 'Fulsom' splitter and filtered onto 142 mm 0.8 μm polycarbonate filters for ^{234}Th analyses and onto pre-combusted and pre-weighed 47 mm GFF filters for POC analysis. POC/^{234}Th ratios of the material collected in the trap were used to calculate the PELAGRA based POC flux from the ^{234}Th flux. For D306 (June 2006), the mean POC/^{234}Th ratio of the 150m and 250m trap was used. The POC flux measured directly by each trap was calculated as a function of POC concentration / (collection area of the trap * time [days]) that each trap spent at the selected depth. To minimise the uncertainties associated with comparisons of flux data from different depths (100 m for ^{234}Th fluxes and 150-300 m for PELAGRA fluxes), POC fluxes measured directly by PELAGRA traps were scaled to a standard flux at 100 m according to the equation (deep flux = surface flux/(deep depth/shallow depth)$^{0.858}$) derived by Martin et al. (1987) which describes the decrease of POC flux with depth.

Moored traps

Measurements of downward flux of particulate material below 3000 m at the PAP observatory has been in progress since 1989, although not continuously. Since 2003, moorings have been deployed with McLane time series sediment traps at 3000 and 4700 m (only data from the 3000 m traps will be dealt with in this chapter) (Table 4.1e). The JGOFS protocol was adopted for sample handling (Newton et al., 1994) and fluxes of organic carbon were determined as previously described by Newton et al. (1994) for 1989/99 material, and as described by Kiriakoulakis et al. (2001) and Ragueneau et al. (2001) for the 1992–1999 material.

4.4 Results

4.4.1 Nutrients

Profiles of ambient NO_3 show extremely low concentrations in the surface 25 m in July 2003 (P300 <0.26 μmol l^{-1}) and July 2005 (D295/6 <0.74 μmol l^{-1}), below which concentrations increased rapidly to a maximum of ~8 and ~9 μmol l^{-1} at 100 m (Figures 4.3a and 4.3d respectively). Higher surface nitrate concentrations were observed in May 2004 (AMT 14) and of all cruises exhibited the highest surface NO_3 concentrations of ~5.5 μmol l^{-1} which extended to 30 m (Figure 4.3b), while in June 2004 (CD158) substantial NO_3 concentrations above 40 m (~2-5 μmol l^{-1}; Figure 4.3c) were also apparent. In June/July 2006 (D306), NO_3 concentrations in the surface 15 m ranged from 0.3-2 μmol l^{-1}, below which concentrations steadily increased to ~5-7 μmol l^{-1} at 45-60 m (Figure 4.3e).

Integrated NO_3, $Si(OH)_4$ and PO_4 concentrations to the 0.1% light depth and averaged for each cruise are shown in Figure 4.4 and Table 4.2. Nutrient concentrations for AMT 14 are however only integrated to the 14% light depth, consistent with the integration depth of ρNO_3 measurements (Painter et al., in press). Integrated NO_3 concentrations were variable, ranging from 543 mmol m^{-2} in June 2004 (CD158), to 137 mmol m^{-2} in June/July 2006 (D306). Similarly, $Si(OH)_4$ concentrations varied from 128 mmol m^{-2} in June 2004 (CD158) to 23 mmol m^{-2} in June/July 2006 (D306), but were especially low in May 2004 (AMT 14) where concentrations in the surface

30 m were below the detection limit. PO_4 concentrations ranged from 9 to 37 mmol m^{-2}

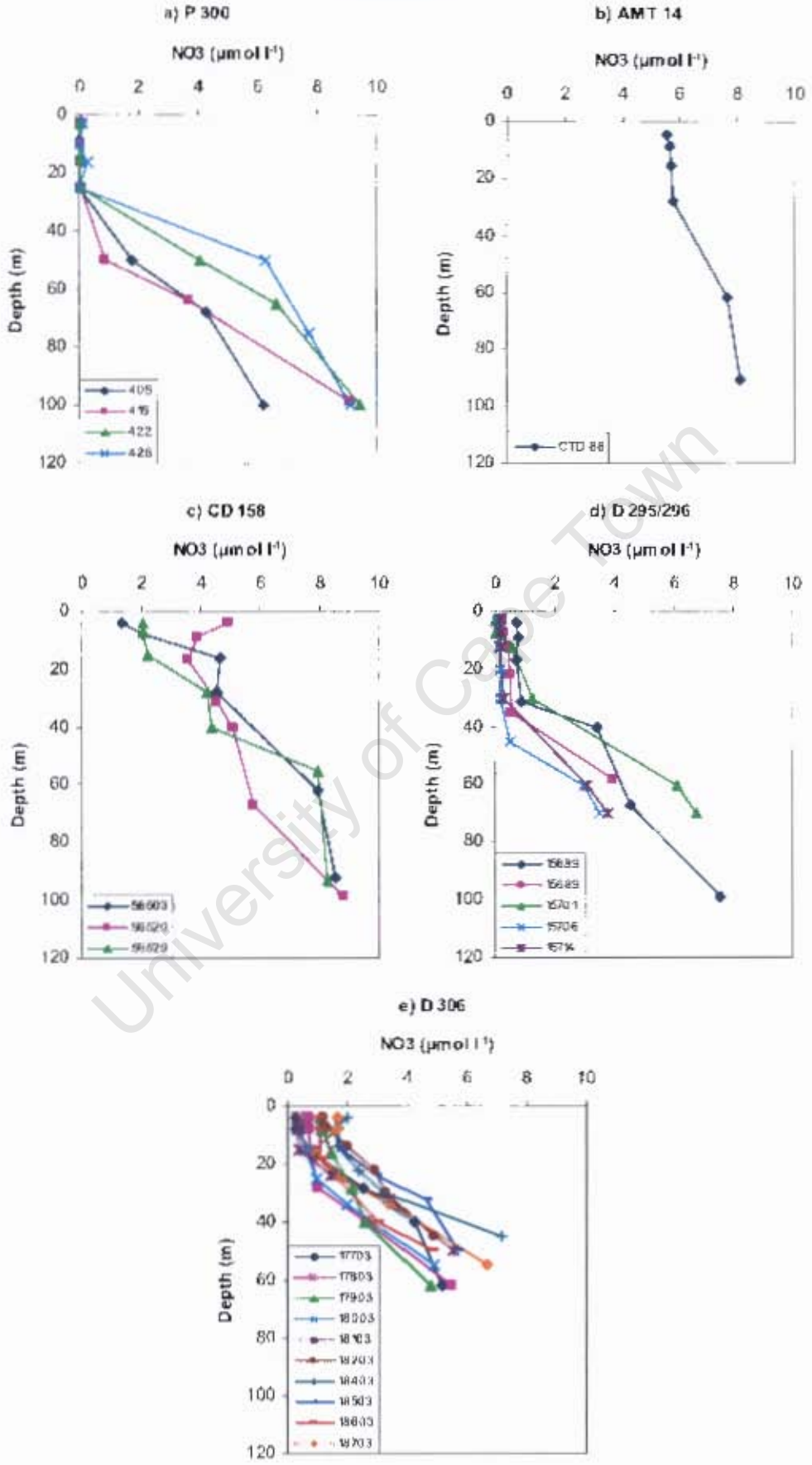

Figure 4.3. Profiles of ambient NO_3 (µmol l^{-1}) for a) P300 in July 2003 b) AMT 14 in May 2004 c) CD158 in June 2004 d) D295/6 in July 2005 and e) D306 in June/July 2006. Box numbers represent CTD casts.

Table 4.2. NO_3, $Si(OH)_4$ and PO_4 concentrations (mmol m^{-2}) integrated to the 0.1% light depth. Nutrient concentrations for AMT 14 are also integrated to the 14% light depth, consistent with the integration depth of nitrate uptake measurements. See text for details. Means ± SD where appropriate.

Cruise	Station ID	Integrated NO_3 (mmol m^{-2})	Integrated $Si(OH)_4$ (mmol m^{-2})	Integrated PO_4 (mmol m^{-2})
P 300	405	244.17	103.63	18.94
	415	267.82	58.80	25.47
	422	414.31	98.73	32.56
	426	467.21	118.05	31.33
Mean		348.38	94.80	27.07
± 1SD		109.27	25.36	6.25
AMT 14	CTD 88	611.89	46.13	38.05
		† 155.37	† 0.28	† 8.69
CD 158	56503	553.27	147.87	33.01
	56520	552.71	98.66	36.50
	56529	525.66	138.71	36.52
Mean		543.88	128.41	35.34
± 1SD		15.78	26.17	2.02
D 295/6	15686	332.60	118.06	23.99
	15689	66.02	19.33	5.76
	15701	191.78	71.76	12.89
	15706	66.75	20.18	7.69
	15714	90.94	33.84	7.49
Mean		149.62	52.63	11.56
± 1SD		114.63	42.31	7.44
D 306	177003	170.55	35.32	12.99
	178003	133.17	8.76	8.25
	179003	150.14	14.53	12.08
	180003	99.49	10.12	7.55
	181003	113.18	19.89	11.41
	182003	125.90	23.19	8.22
	184005	141.35	36.57	9.00
	185003	169.01	26.38	11.13
	186004	103.22	10.61	6.74
	187004	163.59	46.61	13.72
Mean		136.96	23.20	10.11
± 1SD		26.46	12.94	2.45

† Integrated to the nitracline 14% light depth

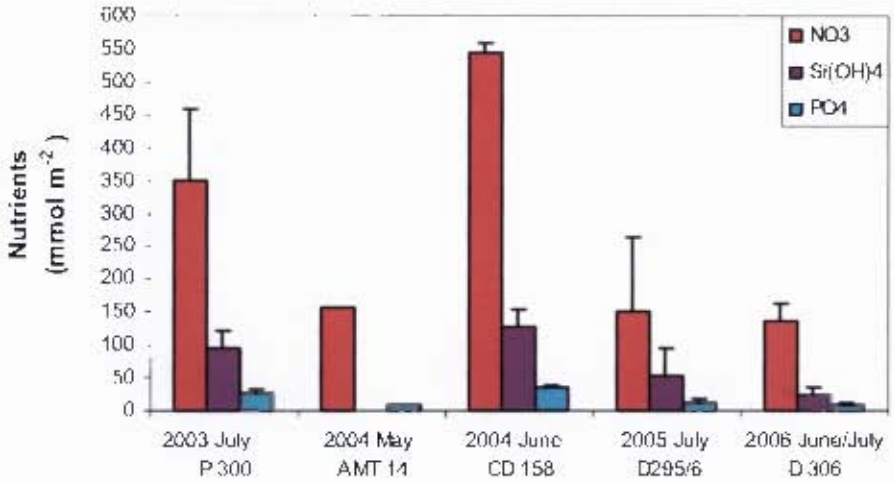

Figure 4.4. Ambient concentrations of nitrate (NO_3), silicate ($Si(OH)_4$) and phosphate (PO_4) integrated to the 0.1% light depth (14% on AMT 14) and averaged over each cruise. Error bars represent mean ± 1SD.

4.4.2 Chlorophyll-a

Typical chlorophyll profiles (Figures 4.5a-e) showed low concentrations (~0.2-0.5 mg m^{-3}) in surface waters (above 25 m) and a characteristic deep chlorophyll maximum (DCM) between ~30-65 m. However, chlorophyll-a profiles in June/July 2006 (D306) (Figure 4.5e) showed an unusually wide range in surface concentrations from ~0.3 to 1.3 mg m^{-3}, but again with a subsurface DCM at ~30 m. Chlorophyll concentrations in June 2004 (CD 158) were atypical in their absence of a DCM and decreased from the surface (~0.5 mg m^{-3}) with depth (Figure 4.5c).

Chlorophyll-a concentrations integrated over the euphotic zone and averaged for each cruise (Figure 4.6, Table 4.3) showed lowest concentrations in May 2004 (AMT 14) of 7.31 mg m^{-2} but rose to highest recorded concentrations (32.34 ± 3.34 mg m^{-2}) just a month later in June 2004 (CD158). Similarly high concentrations (28.51 ± 15.84mg m^{-3}) were recorded in June/July 2006 (D306) while intermediate concentrations were recorded in July 2003 (P300) (17.01 ± 4.31 mg m^{-3}) and in July 2005 (D295/6) (22.34 ± 5.47 mg m^{-3}).

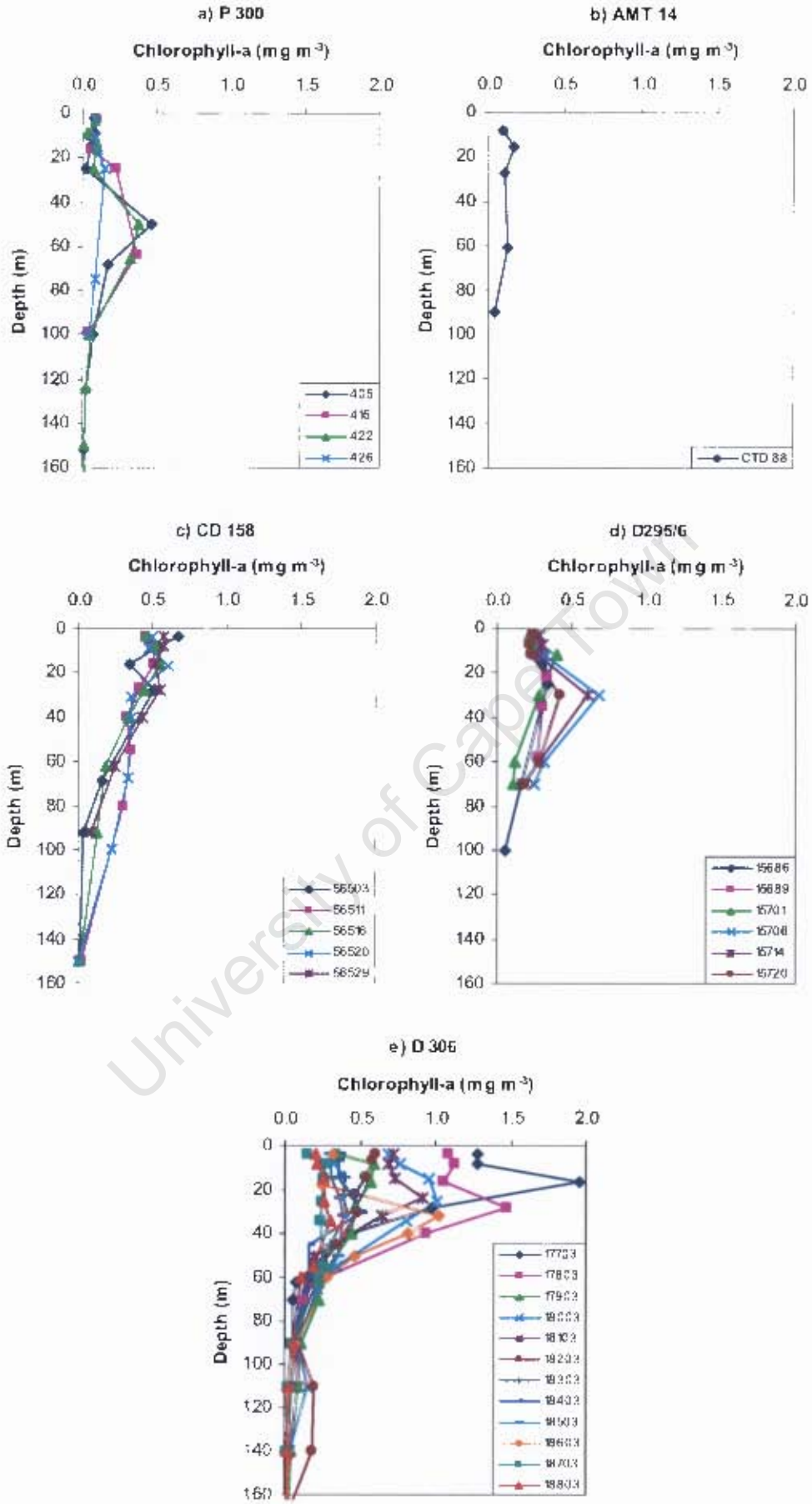

Figure 4.5. Profiles of chlorophyll-a (mg m^{-3}) for a) P300 in July 2003, b) AMT 14 in May 2004, c) CD158 in June 2004, d) D295/6 in July 2005 and e) D306 in June/July 2006. Box numbers represent CTD casts.

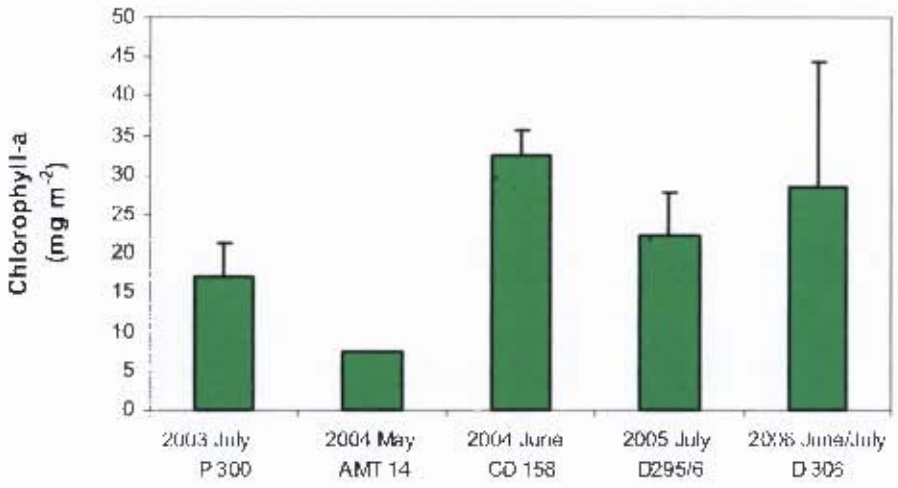

Figure 4.6. Chlorophyll concentrations (mg m^{-2}) integrated to the 0.1% light depth and averaged over each cruise. Error bars represent mean ± 1SD.

4.4.3 Primary production, new production and f-ratios

Daily rates of carbon fixation integrated to the 0.1% light depth in July 2003 (P300) ranged from 19.00 to 40.17 mmol m^{-2} d^{-1} (Table 4.3) and collectively had the lowest cruise averaged primary production of 28.88 ± 6.95 mmol C m^{-2} d^{-1} (Figure 4.7). Similarly low rates of primary production (28.75 mmol C m^{-2} d^{-1}) were recorded in May 2004 during AMT 14 (Table 4.3). However, to compare primary production to new production, carbon fixation rates for AMT 14 were integrated to the 14% light depth (14.23 mmol C m^{-2} d^{-1}) and plotted in Figure 4.7. Higher rates of integrated primary production were associated with the subsequent three cruises (CD158, D295/6, D306) in June 2004 (74.91 ± 25.27 mmol C m^{-2} d^{-1}), July 2005 (89.31 ± 3.51 mmol C m^{-2} d^{-1}) and June/July 2006 (88.19 ± 37.16mmol C m^{-2} d^{-1}) respectively (Figure 4.7 and Table 4.3.).

In June 2004 (CD158), too little ^{15}N spike was added to the incubation bottles and the subsequent NO_3, NH_4 and urea uptake rates were therefore unreliable and almost certainly too low. However it was assumed that the ^{15}N based f-ratios for these samples ($\rho NO_3/(\rho NO_3+\rho NH_4+\rho Urea)$ were still valid (Table 4.3). Based on this assumption, carbon based new production was derived from: C-based NP = total PP * f-ratio (Table 4.3).

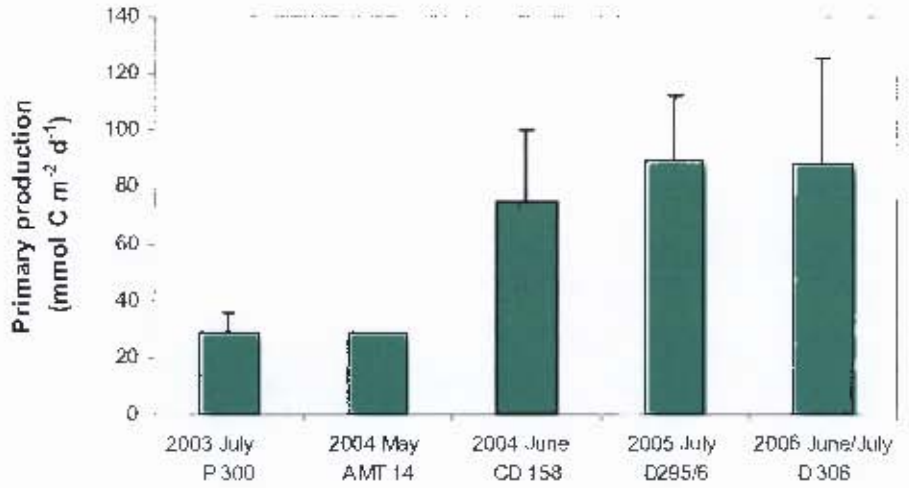

Figure 4.7. Daily rates of carbon fixation (mmol C m^{-2} d^{-1}) integrated to the 0.1% light depth (14% on AMT 14) and averaged over each cruise. Error bars represent mean ± 1SD.

When Redfield stoichiometry was applied (Redfield et al., 1963) to the 0.1% light depth, integrated NO_3 uptake rates on AMT 14 (May 2004), carbon-based new production estimates (ρNO_3 * Redfield ratio of 6.625) exceeded ^{14}C derived carbon fixation rates (Painter et al., in press) (Table 4.3). Because of suspected dark NO_3 uptake and/or nitrification, Painter et al. (in press) consequently reduced the integration depth to the 14% light depth where the influence of dark uptake and nitrification associated with the nutricline could largely be ruled out. This resulted in estimates of new production that were then lower and consistent with ^{14}C carbon fixation rates (see section 2.3.5). However, for CTD88 on AMT 14 at the PAP site, the f-ratio based on new production and primary production integrated to the 14% light level still gave an unrealistically high f-ratio of 2.85 (Table 4.3). Given the unreasonably high f-ratios, combined with the abnormal influence of the nitracline on this cruise (Painter et al., in press) and the likelihood of overestimating NO_3 uptake in the subtropical gyres due to nitrification (Yool et al., in press), the f-ratio for this station was instead based on $(\rho NO_3)/(\rho NO_3+\rho NH_4+\rho Urea)$ and integrated to the 14% light level (Table 4.3). As with CD158, the product of the AMT 14 f-ratio and primary production produced a more reasonable carbon based new production rate. F-ratios for the remaining three cruises were calculated from integrated carbon based new production [(ρNO_3 * 6.625)/(integrated total primary production)].

Integrated carbon based new production estimates (Table 4.3) averaged over each cruise (Figure 4.8) show a similar scenario to that of primary production with lowest integrated rates occurring in July 2003 (P300) and in May 2004 (AMT 14) (6.45 ± 2.34 and 3.27 mmol C m^{-2} d^{-1} respectively) compared to much higher rates on the subsequent three cruises (CD158, D295/6, D306) in June 2004 (24.57 ± 9.41 mmol C m^{-2} d^{-1}), July 2005 (19.20 ± 7.90 mmol C m^{-2} d^{-1}) and June/July 2006 (25.64 ± 10.83 mmol C m^{-2} d^{-1}) respectively (Figure 4.8 and Table 4.3).

The resultant f-ratios (NP/total PP) (Table 4.3) showed a somewhat different pattern to either of the uptake rates with slightly higher f-ratios in June 2004 (CD158; 0.34 ± 0.11) and in June/July 2006 (D306; 0.29 ± 0.06) and similarly low f-ratios in July 2003 (P300; 0.22 ± 0.10), May 2004 (AMT 14; 0.23) and July 2005 (D295/6; 0.23 ± 0.09).

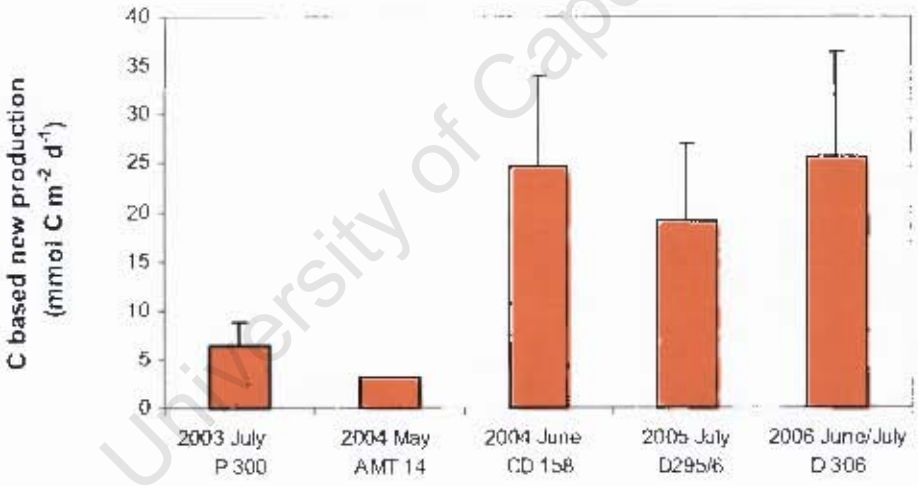

Figure 4.8. Daily rates of carbon based new production (mmol C m^{-2} d^{-1}) integrated to the 0.1% light depth (14% on AMT 14) and averaged over each cruise. Error bars represent mean ± 1SD.

Table 4.3. Compilation of chlorophyll-a, (mg m^{-2}), carbon based new production (mmol C m^{-2} d^{-1}), and primary production (mmol C m^{-2} d^{-1}) integrated to the 0.1% light depth. f-ratios calculated from C-based NP/total PP unless otherwise stated. See methods for details.

Cruise	Station ID	Integrated Chlorophyll-a (mg m^{-2})	Int C based new production (mmol C m^{-2} d^{-1})	Int 14C PP (mmol C m^{-2} d^{-1})	Integrated f-ratio
P 300	405	17.64	9.72	27.35	0.36
P 300	411			31.58	
P 300	415	21.09	4.38	40.17	0.11
P 300	422	19.46		19.00	
P 300	426	9.85	5.26	26.30	0.20
Mean		17.01	6.45	28.88	0.22
± 1SD		4.31	2.34	6.95	0.10
AMT 14	CTD 88	7.31	122.57	28.75	4.26
			† 40.61	† 14.23	† 2.85
			‡ 3.27		* 0.23
CD158	56503	30.05	‡ 16.41	56.59	* 0.29
CD158	56510	31.12	‡ 19.97	41.76	* 0.48
CD158	56516	29.16	‡ 34.38	88.57	* 0.39
CD158	56520	37.34	‡ 16.95	83.37	* 0.20
CD158	56529	34.01	‡ 35.16	104.24	* 0.34
Mean		32.34	24.57	74.91	0.34
± 1SD		3.34	9.41	25.27	0.11
D 295/6	15686	21.92	23.84	80.69	0.30
D 295/6	15689	17.10	14.54	52.02	0.28
D 295/6	15701	16.29	11.01	100.42	0.11
D 295/6	15706	30.25	16.15	103.65	0.16
D 295/6	15714	27.05	32.87	109.74	0.30
D 295/6	15720	21.42	16.80		
Mean		22.34	19.20	89.31	0.23
± 1SD		5.47	7.90	23.51	0.09
D 306	17703	55.01	25.96	128.32	0.20
D 306	17803	59.49	53.22	174.37	0.31
D 306	17903	27.10	29.83	99.53	0.30
D 306	18003	41.78	18.71	101.46	0.18
D 306	18103	31.86	23.56	91.64	0.26
D 306	18203	22.08	22.08	73.64	0.30
D 306	18303	16.41		61.06	
D 306	18403	16.99	20.42	56.47	0.36
D 306	18503	17.18	16.88	56.61	0.30
D 306	18603	27.51	29.70	75.32	0.39
D 306	18703	13.14	16.05	51.63	0.31
D 306	18803	13.57			
Mean		28.51	25.64	88.19	0.29
± 1SD		15.84	10.83	37.16	0.06

† integrated to the nitricline 14% light depth

* f ratio calculated from $(\rho NO_3)/(\rho NO_3 + \rho NH_4 + \rho Urea)$

‡ carbon based new production calculated from f ratio $(\rho NO_3)/(\rho NO_3 + \rho NH_4 + \rho Urea)$ * primary production

4.4.4 Profiles of total ^{234}Th

Figure 4.9 presents profiles of total ^{234}Th activity from five cruises carried out at the PAP site between 2003 and 2006. The total ^{234}Th and ^{238}U activities for each sample are available in Tables 4.4a-e. Both profiles from July 2003 (P300) (Figures 4.9a,b) show substantial disequilibrium in the surface 25m with ^{234}Th activities of ~1 dpm.l^{-1} compared to ^{238}U activities of ~2.5 dpm.l^{-1}. ^{234}Th activities increased below 25 m and equilibrium was regained at 75 and 100 m. The May 2004 (AMT 14) station (Figure 4.9c) showed a clear thorium deficit in the topmost 30 m and equilibrium was reached at 93 m. At 250 and 350 m this station tended toward thorium excess, but due to the relatively high analytical uncertainties, was still considered in equilibrium with uranium. ^{234}Th profiles in June 2004 (CD158) (Figures 4.9d-h) show clearly detectable disequilibria in surface waters with ^{234}Th activities ranging from ~1.6-2.0 dpm.l^{-1}. Profiles show some variability, with equilibrium depths ranging from ~50 to ~100 m. Both profiles from July 2005 (D295) have surface as well as subsurface ^{234}Th minima at 68 m (Figure 4.9i) and 30 m (Figure 4.9j) although for one station (CTD15701) (Figure 4.9j), there was a slight ^{234}Th excess at ~61 m with equilibrium being regained at ~71 m. All three profiles (Figures 4.9k-m) from later in July 2005 (D296) show similar distributions of ^{234}Th, with low activities (~1.5 dpm.l^{-1}) in the surface ~12 m, below which activities steadily increased to reach equilibrium at ~100 m. The first profile on D306 (CTD 17705; Figure 4.9n) had slightly higher surface ^{234}Th activities (1.62 dpm.l^{-1}) than the subsequent three profiles (Figures 4.9o-q; 1.15, 1.33 and 1.28 dpm.l^{-1}), ^{234}Th activities increased steadily on all four profiles to reach equilibrium between 92 and 103 m. CTD 17705 (Figure 4.9n) showed a slight ^{234}Th excess at 152 m with equilibrium being regained at 186 m. The profile tended toward another excess at 301 m however was considered to be in equilibrium with ^{238}U within analytical uncertainties. Similarly the profile of CTD18205 (Figure 4.9p) tended toward a slight disequilibrium at 152 m but was also in equilibrium within analytical uncertainties.

P 300

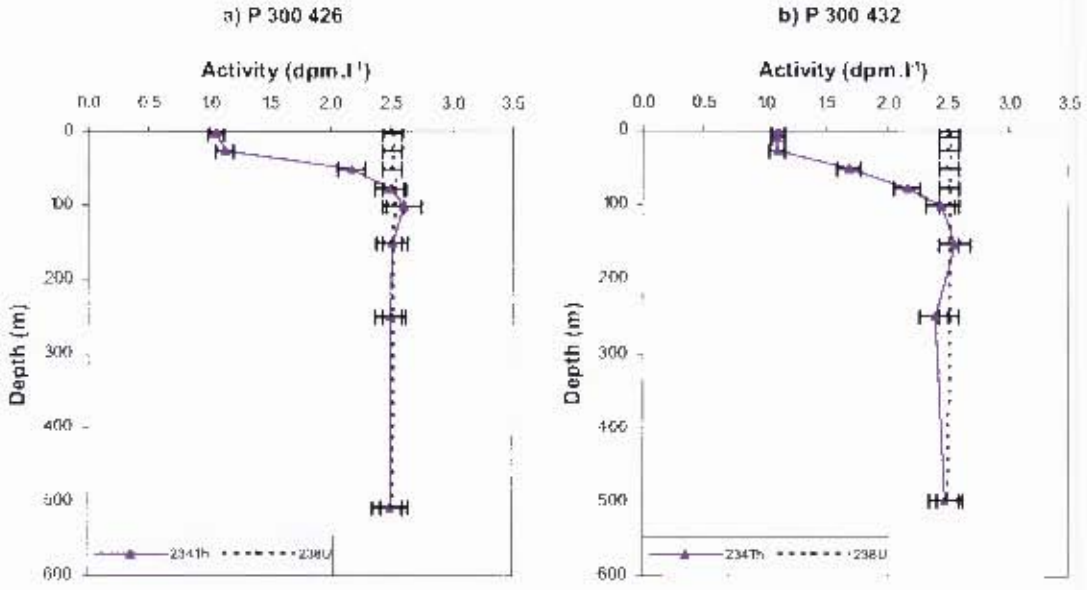

AMT 14

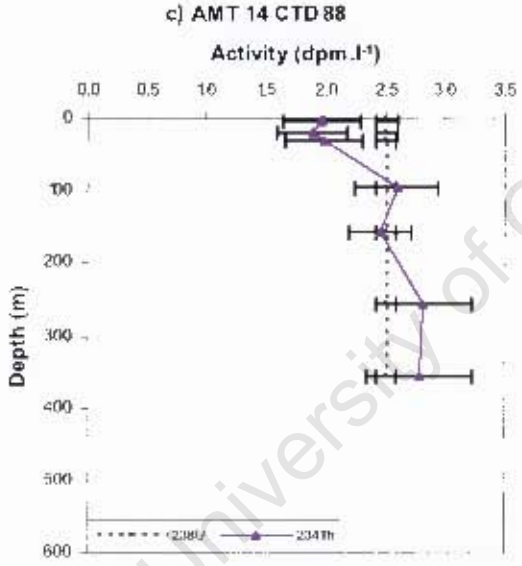

Figure 4.9. Vertical profiles of total ^{234}Th and ^{238}U activities (dpm l^{-1}) for a-b) P300 in July 2003 and c) AMT 14 in May 2004. Error bars on total ^{234}Th data indicate + 1SD of propagated overall uncertainties. Error bars on ^{238}U indicate ± 2SD (3.3%).

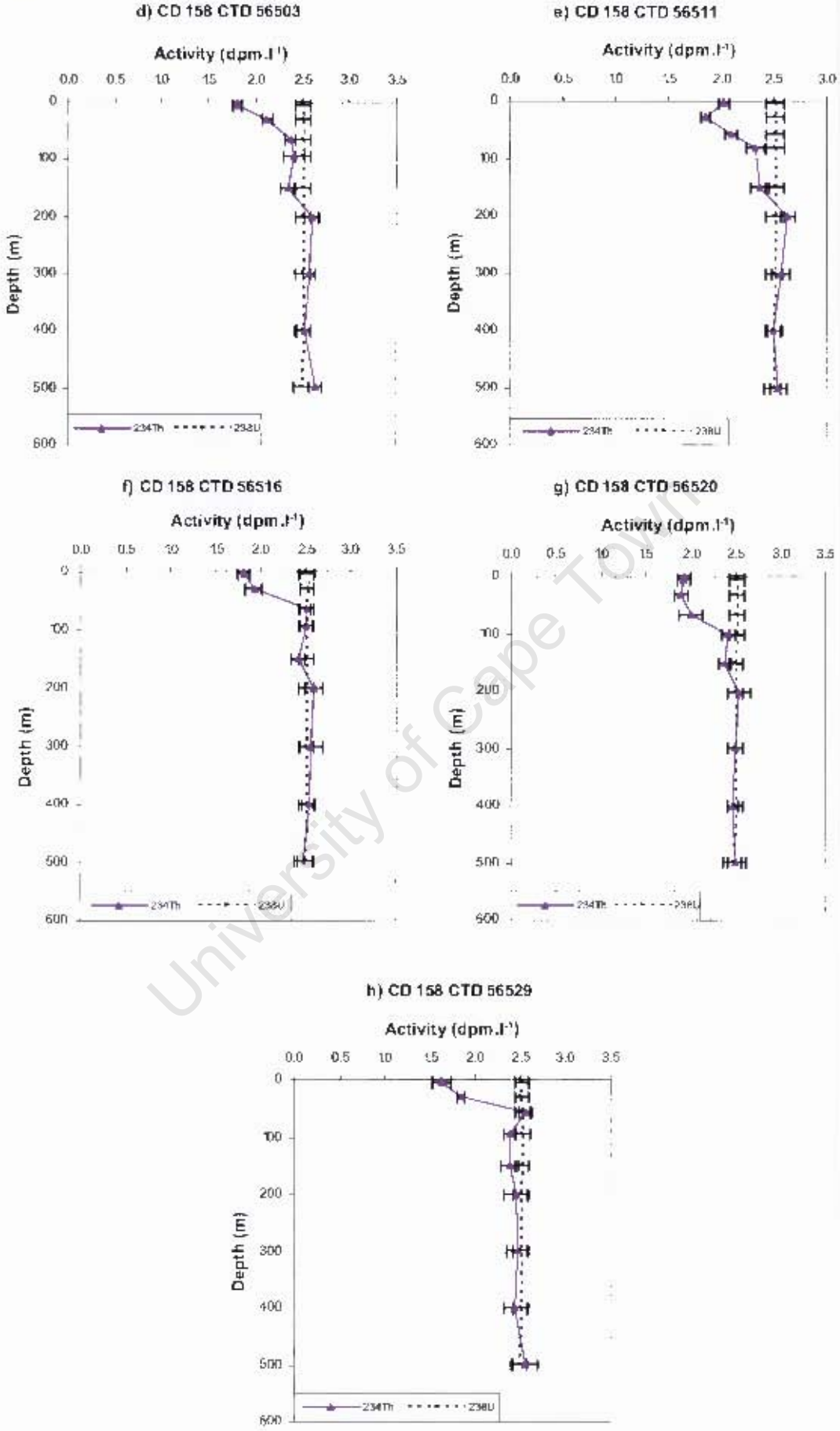

Figure 4.9 continued. Vertical profiles of total ^{234}Th and ^{238}U activities (dpm l^{-1}) for d-h) CD158 in June 2004. Error bars on total ^{234}Th data indicate ± 1SD of propagated overall uncertainties. Error bars on ^{238}U indicate ± 2SD (3.3%).

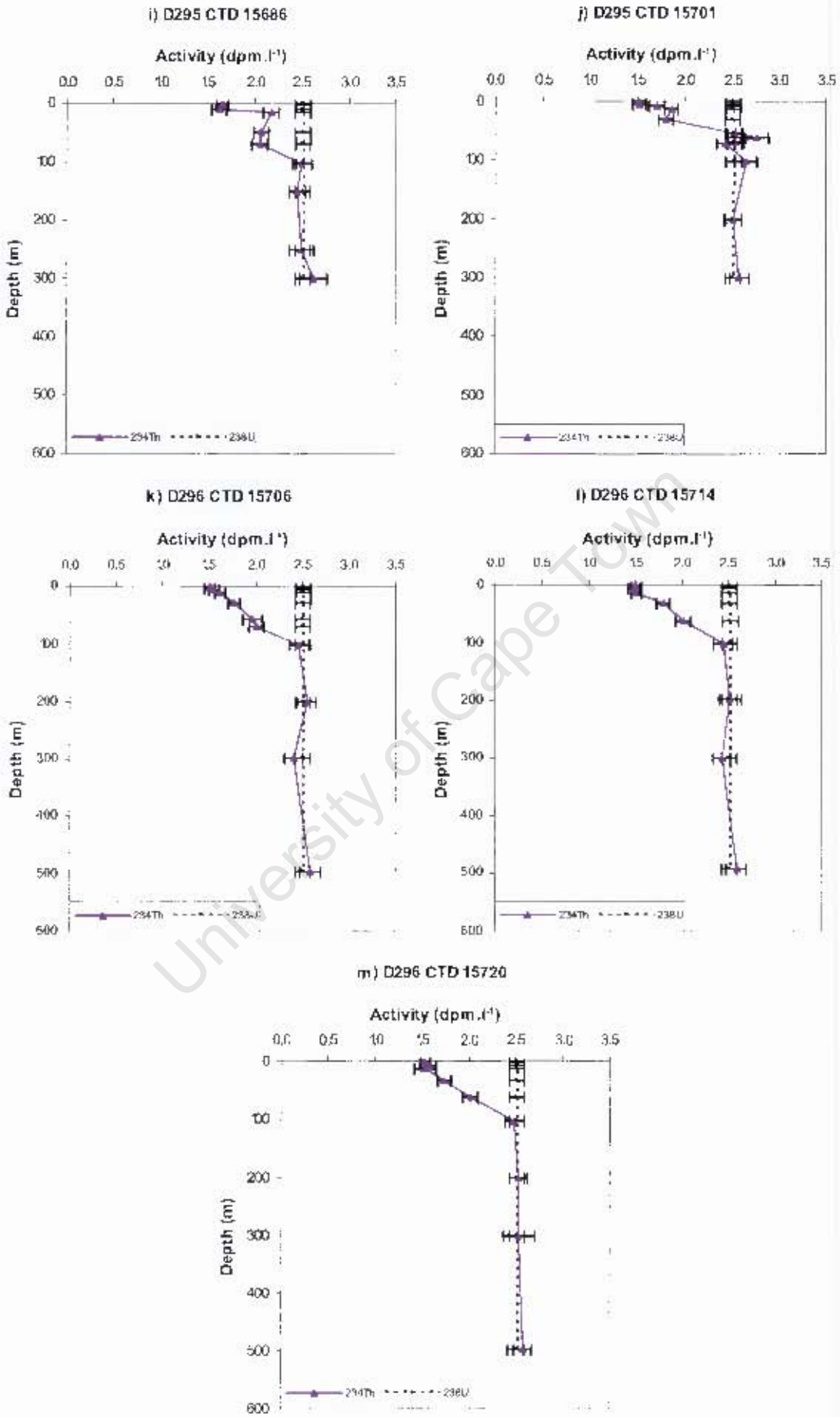

Figure 4.9 continued. Vertical profiles of total ^{234}Th and ^{238}U activities (dpm l^{-1}) for i-m) D295/6 in July 2005. Error bars on total ^{234}Th data indicate ± 1SD of propagated overall uncertainties. Error bars on ^{238}U indicate ± 2SD (3.3%).

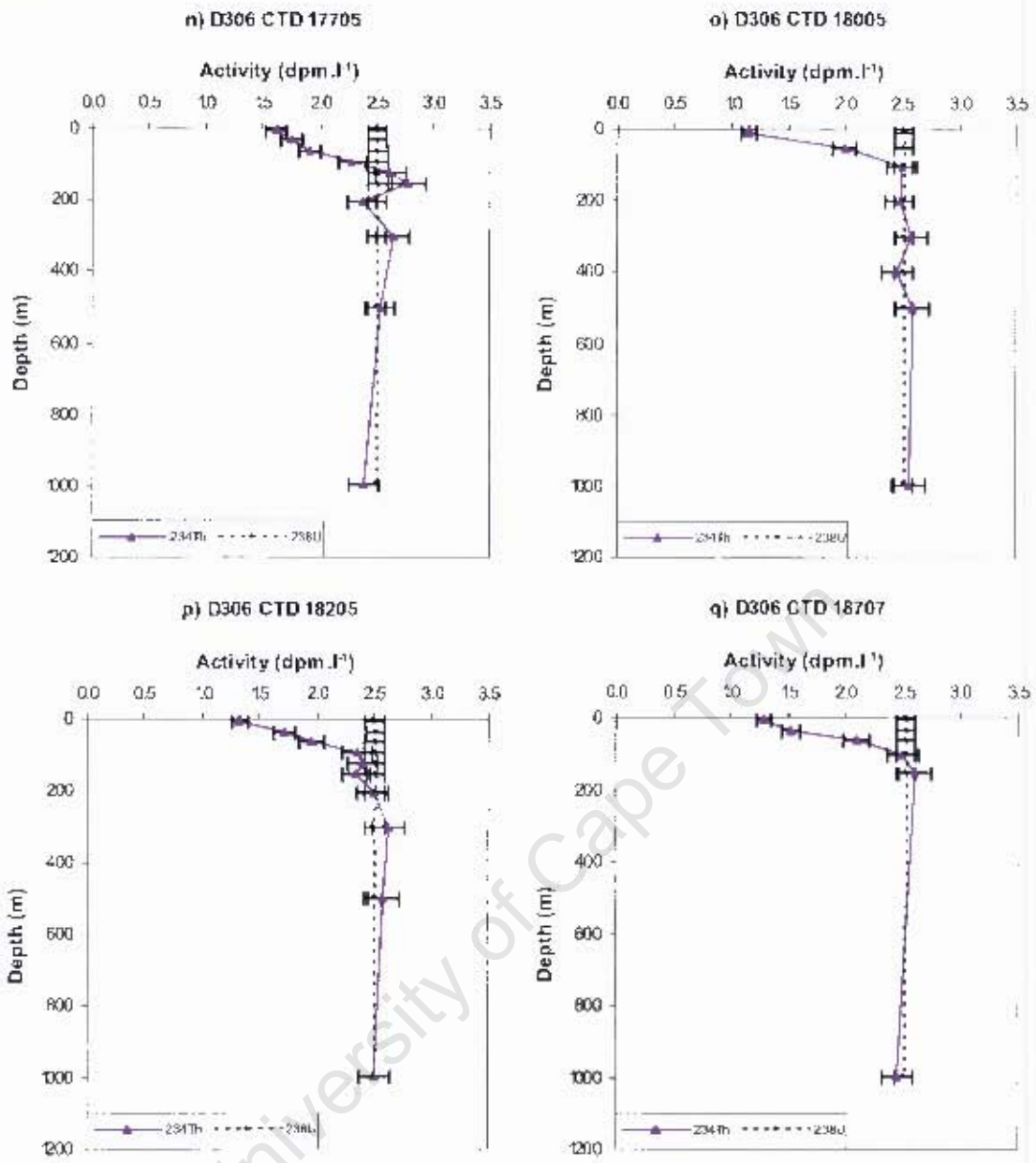

Figure 4.9 continued. Vertical profiles of total ^{234}Th and ^{238}U activities (dpm l^{-1}) for n-q) D306 in June/July 2006. Error bars on total ^{234}Th data indicate ± 1SD of propagated overall uncertainties. Error bars on ^{238}U indicate ± 2SD (3.3%).

Table 4.4. ^{238}U and total ^{234}Th activities for a) P300 (June 2003), b) AMT 14 (May 2004) and c) CD158 (June 2004). All ^{234}Th and ^{238}U data are reported in disintegrations per minute per litre (dpm l^{-1}). Uncertainties for total ^{234}Th are $\pm$ 1SD of propagated overall uncertainties. ^{238}U was calculated from salinity.

a) Poseidon 300

Station ID	Depth (m)	^{238}U (dpm.l^{-1})	Total ^{234}Th (dpm.l^{-1})	1SD (dpm.l^{-1})
426	3	2.51	1.05	0.06
	25	2.51	1.13	0.07
	50	2.51	2.18	0.11
	75	2.52	2.49	0.13
	100	2.52	2.60	0.14
	150	2.51	2.51	0.13
	249	2.51	2.49	0.13
	508	2.50	2.49	0.14
432	9	2.51	1.10	0.06
	25	2.51	1.09	0.06
	49	2.51	1.68	0.10
	75	2.52	2.17	0.11
	100	2.51	2.44	0.12
	151	2.51	2.56	0.13
	250	2.51	2.40	0.12
	499	2.50	2.48	0.13

b) AMT 14

Station ID	Depth (m)	^{238}U (dpm.l^{-1})	Total ^{234}Th (dpm.l^{-1})	1SD (dpm.l^{-1})
CTD 88	3	2.51	1.97	0.33
	18	2.51	1.89	0.29
	28	2.51	1.98	0.32
	93	2.51	2.60	0.35
	155	2.51	2.46	0.26
	255	2.51	2.82	0.40
	355	2.50	2.78	0.44

c) CD 158

Station ID	Depth (m)	^{238}U (dpm.l^{-1})	Total ^{234}Th (dpm.l^{-1})	1SD (dpm.l^{-1})
56503	6	2.50	1.81	0.05
	30	2.51	2.12	0.05
	64	2.51	2.37	0.06
	94	2.51	2.40	0.11
	151	2.51	2.34	0.07
	201	2.51	2.60	0.07
	301	2.50	2.57	0.06
	400	2.50	2.52	0.07
	499	2.49	2.63	0.06
56511	4	2.51	2.02	0.05
	28	2.51	1.84	0.05
	55	2.51	2.10	0.06
	80	2.51	2.33	0.08
	150	2.51	2.36	0.09
	200	2.51	2.63	0.07
	301	2.50	2.56	0.09
	400	2.50	2.50	0.07
	501	2.49	2.54	0.08
56516	3	2.51	1.81	0.07
	28	2.51	1.92	0.09
	62	2.51	2.50	0.06
	92	2.51	2.50	0.07
	151	2.50	2.41	0.08
	201	2.50	2.58	0.10
	301	2.50	2.56	0.13
	399	2.50	2.53	0.08
	498	2.49	2.48	0.10
56520	5	2.51	1.92	0.06
	31	2.51	1.89	0.08
	67	2.51	2.00	0.12
	101	2.51	2.42	0.08
	151	2.50	2.38	0.07
	202	2.50	2.54	0.12
	300	2.50	2.50	0.09
	400	2.50	2.47	0.06
	499	2.49	2.49	0.13
56529	4	2.51	1.62	6.39
	28	2.51	1.84	2.54
	55	2.51	2.55	2.73
	93	2.51	2.38	2.76
	150	2.51	2.38	3.91
	200	2.51	2.45	5.08
	300	2.50	2.46	4.56
	400	2.50	2.44	4.99
	499	2.49	2.55	5.39

Table 4.4 continued. ^{238}U and total ^{234}Th activities for d) D295/6 (July 2005) and e) D306 (June/July 2006). All ^{234}Th and ^{238}U data are reported in disintegrations per minute per litre (dpm l^{-1}). Uncertainties for total ^{234}Th are $\pm$ 1SD of propagated overall uncertainties. ^{238}U was calculated from salinity.

d) D 295/296

Station ID	Depth (m)	^{238}U (dpm.l^{-1})	Total ^{234}Th (dpm.l^{-1})	1SD (dpm.l^{-1})
15686	4	2.51	1.65	0.07
	10	2.51	1.63	0.08
	15	2.51	2.17	0.08
	49	2.52	2.07	0.09
	68	2.52	2.05	0.08
	102	2.52	2.50	0.10
	151	2.52	2.46	0.09
	250	2.52	2.49	0.13
	300	2.51	2.62	0.14
15701	4	2.51	1.52	0.07
	8	2.51	1.70	0.08
	13	2.51	1.85	0.08
	30	2.51	1.80	0.08
	61	2.52	2.76	0.13
	71	2.52	2.43	0.09
	101	2.52	2.64	0.11
	200	2.51	2.51	0.09
	300	2.51	2.57	0.10
15706	3	2.51	1.50	0.06
	6	2.51	1.54	0.06
	12	2.51	1.61	0.06
	30	2.51	1.76	0.07
	58	2.51	1.97	0.10
	71	2.51	2.01	0.08
	101	2.51	2.46	0.10
	200	2.51	2.55	0.11
	299	2.51	2.41	0.10
	497	2.51	2.58	0.11
15714	3	2.51	1.51	0.06
	6	2.51	1.49	0.06
	12	2.51	1.51	0.06
	32	2.51	1.80	0.08
	62	2.51	2.01	0.08
	101	2.51	2.44	0.11
	196	2.51	2.51	0.12
	299	2.51	2.43	0.09
	491	2.51	2.58	0.11
15720	3	2.51	1.53	0.06
	8	2.51	1.57	0.08
	13	2.51	1.54	0.12
	32	2.51	1.74	0.07
	62	2.51	2.02	0.08
	102	2.51	2.48	0.10
	200	2.51	2.53	0.09
	299	2.51	2.54	0.16
	497	2.51	2.58	0.10

e) D 306

Station ID	Depth (m)	^{238}U (dpm.l^{-1})	Total ^{234}Th (dpm.l^{-1})	1SD (dpm.l^{-1})
17705	7	2.51	1.62	0.09
	33	2.51	1.75	0.09
	63	2.51	1.91	0.10
	92	2.51	2.29	0.12
	122	2.51	2.62	0.14
	152	2.51	2.79	0.15
	202	2.51	2.38	0.13
	301	2.51	2.65	0.14
	500	2.50	2.54	0.14
	996	2.50	2.39	0.13
18005	11	2.51	1.15	0.06
	52	2.51	1.99	0.11
	102	2.51	2.49	0.13
	200	2.51	2.48	0.13
	300	2.51	2.58	0.14
	399	2.51	2.45	0.13
	499	2.50	2.59	0.14
	997	2.50	2.56	0.14
18205	6	2.51	1.33	0.07
	34	2.51	1.72	0.09
	63	2.51	1.96	0.10
	93	2.51	2.35	0.13
	123	2.51	2.39	0.13
	153	2.51	2.35	0.12
	202	2.51	2.49	0.13
	302	2.50	2.63	0.14
	500	2.50	2.58	0.14
	997	2.50	2.50	0.13
18707	7	2.51	1.28	0.07
	33	2.52	1.52	0.08
	63	2.52	2.09	0.11
	103	2.52	2.49	0.13
	153	2.52	2.60	0.14
	998	2.50	‡ 2.44	‡ 0.13

‡ values averaged from 5 replicate samples at 998m

4.4.5 Shallow water fluxes

4.4.5.1 ^{234}Th flux

The variability in ^{234}Th fluxes within each cruise (Standard Deviation between ^{234}Th fluxes /mean ^{234}Th flux) ranged from 12% of the mean total flux in June/July 2006 (D306) to 27% in July 2005 (D295/6). This variability was very similar to the range of percentage errors (1SD/mean * 100) (Table 4.5) of the calculated thorium fluxes that ranged between 15 and 33% (Figure 4.10). Variability within each cruise was therefore not considered significant and a steady-state was assumed for the duration of the cruises.This assumption was further justified by the short sampling interval between stations within each cruise (typically 1-5 days apart and a maximum 13 days between the first and last station on D306) (Table 4.1c), which is shorter than the characteristic time scale of thorium decay (mean life: 34.8 days). (An unlikely and intense non steady state condition would be required to significantly impact the thorium budget on such a short time scale.) In addition to analytical uncertainty observed short-term (within-cruise), variability in the shape of total ^{234}Th profiles and resulting steady-state fluxes is probably caused by passing internal waves or due to transient effects resulting from changes in the wind/air pressure field. The repeated within-cruise sampling dampens the impact of such variability and is believed to provide a representative average picture of total ^{234}Th distribution in the study area for the cruise duration.

It needs to be stressed though, that there is no direct information available on the history of the ^{234}Th signals during the weeks before sampling. There is the possibility that the sampled snapshot is part of a non-steady state situation on a time scale of a few weeks, the characteristic time scale of ^{234}Th. As will be shown below a composite picture of the biogeochemical parameters of this study suggests that a pre-bloom condition was sampled at the end of May 2004 (AMT 14) and a post-bloom condition in July 2003/5 (P300 and D295/6), whereas a bloom peak and an the early stage of a bloom decline were probably sampled in June 2004 (CD158) and June/July 2006 (D306), respectively. This supports the notion that the PAP site is part of a temporally highly dynamic region and that non-steady states are likely. However, as time series data covering the characteristic time scale of ^{234}Th (mean life: 34.8 d) are not

available, a steady-state approach was used to calculate ^{234}Th export fluxes. In general, when a total ^{234}Th inventory is decreasing (at the onset of a bloom with more intense scavenging and particle settling) steady-state estimates of ^{234}Th export will be too low, and with increasing ^{234}Th inventory (for example during post-bloom conditions) steady-state estimates of ^{234}Th export will be too high. In other words, over a complete bloom cycle steady-state estimates of export flux will tend to underestimate the true magnitude of flux variability. This caveat needs to be kept in mind when interpreting and discussing the ^{234}Th and POC export fluxes.

For the ^{234}Th flux calculations, it was also assumed that net ^{234}Th transport into or out of the sampled station due to horizontal advection of total ^{234}Th activity gradients and due to vertical turbulent diffusivity was negligible. Due to the absence of strong upwelling gradients, the net upwelling (vertical advection) is not expected to play an important role in the surface ocean of the PAP area. Moreover, given typical vertical total ^{234}Th activity gradients and assuming a maximum range of vertical turbulent diffusivities in and near the pycnocline of the Northeast Atlantic of (0.1-1 cm s^{-2}), net turbulent diffusive upward transport of total ^{234}Th into the euphotic zone should only amount to a maximum of 10-100 dpm m^{-2} d^{-1} mostly rendering this transport term small relative to the downward flux of ^{234}Th on settling particles [(1000 dpm m^{-2} d^{-1}); see Figure 4.10)]. There is only indirect information to scrutinize the validity of the assumption of a negligible role of lateral advection. T/S plots for stations within each cruise (Figure 4.11) suggest that the same body of surface water was not always sampled. Moreover, particularly during the month before cruise P300 (July 2003) and during the month before the PAP site was sampled on cruise AMT 14 (end of May 2004), there were comparatively pronounced horizontal gradients on a spatial scale of ~10 km in remotely sensed surface chlorophyll near the PAP site (Figure 4.16). These chlorophyll gradients could also have been reflected in concomitant gradients of particle dynamics, and hence, ^{234}Th dynamics. If such gradients existed and were laterally advected through the sampling site, a model approach without an advection term would lead to erroneous ^{234}Th export estimates. Therefore, the poorly constrained impact of lateral advection adds an unknown level of uncertainty to our ^{234}Th flux estimates. This caveat also needs to be kept in mind when interpreting and discussing the ^{234}Th and POC export fluxes.

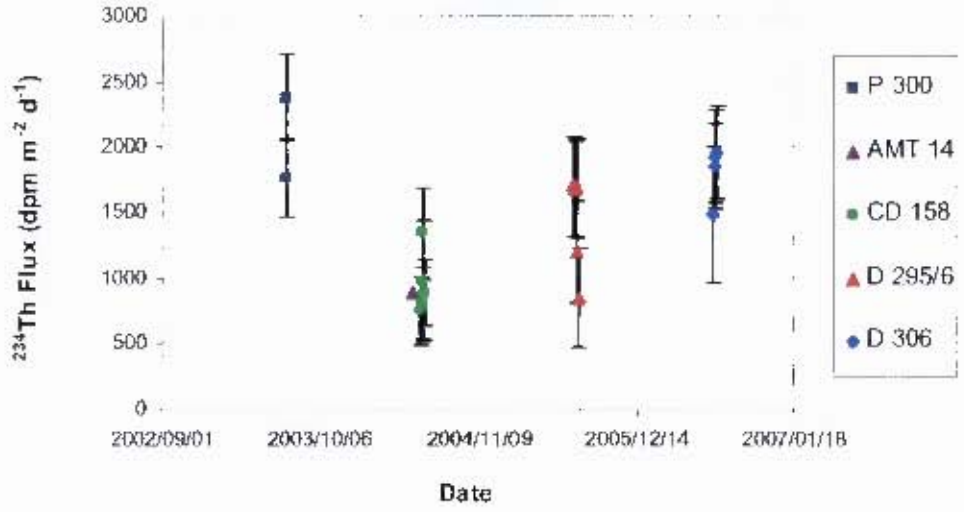

Figure 4.10. Steady state ^{234}Th fluxes (dpm m^{-2}d^{-1}) measured on each cruise between 2003 and 2006. Error bars on fluxes indicate ± 1SD of propagated overall uncertainties.

^{234}Th fluxes estimated from the steady state model are shown in Table 4.5. ^{234}Th fluxes were calculated from water column ^{234}Th/^{238}U disequilibria (e.g. Buesseler, 1998), integrated from the sea surface to the depth at which secular equilibrium was regained. Surface equilibrium depths ranged from 55-105 m (Table 4.5). In June/July 2006 (D306) one station (CTD 17705) had a detectable subsurface thorium excess at 152 m (Figure 4.9n). This excess (313 dpm m^{-2} d^{-1}) was integrated from 112 m to the depth at which equilibrium was regained (186 m) and subtracted from the surface ^{234}Th flux (1797 dpm m^{-2} d^{-1}) to give a net flux of 1484 dpm m^{-2} d^{-1} (Table 4.5). Thorium fluxes averaged for each cruise are shown in Figure 4.12 and Table 5.4. Lowest fluxes were found in May and June 2004 (AMT 14, CD158) of 884 ± 865 and 957 ± 320 dpm m^{-2} d^{-1} respectively, while the highest of 2076 ± 431 dpm m^{-2} d^{-1} was found in July 2003 (P300). Intermediate fluxes of 1427 ± 385 and 1808 ± 220 dpm m^{-2} d^{-1} were found in July 2005 (D295/6) and June/July 2006 (D306).

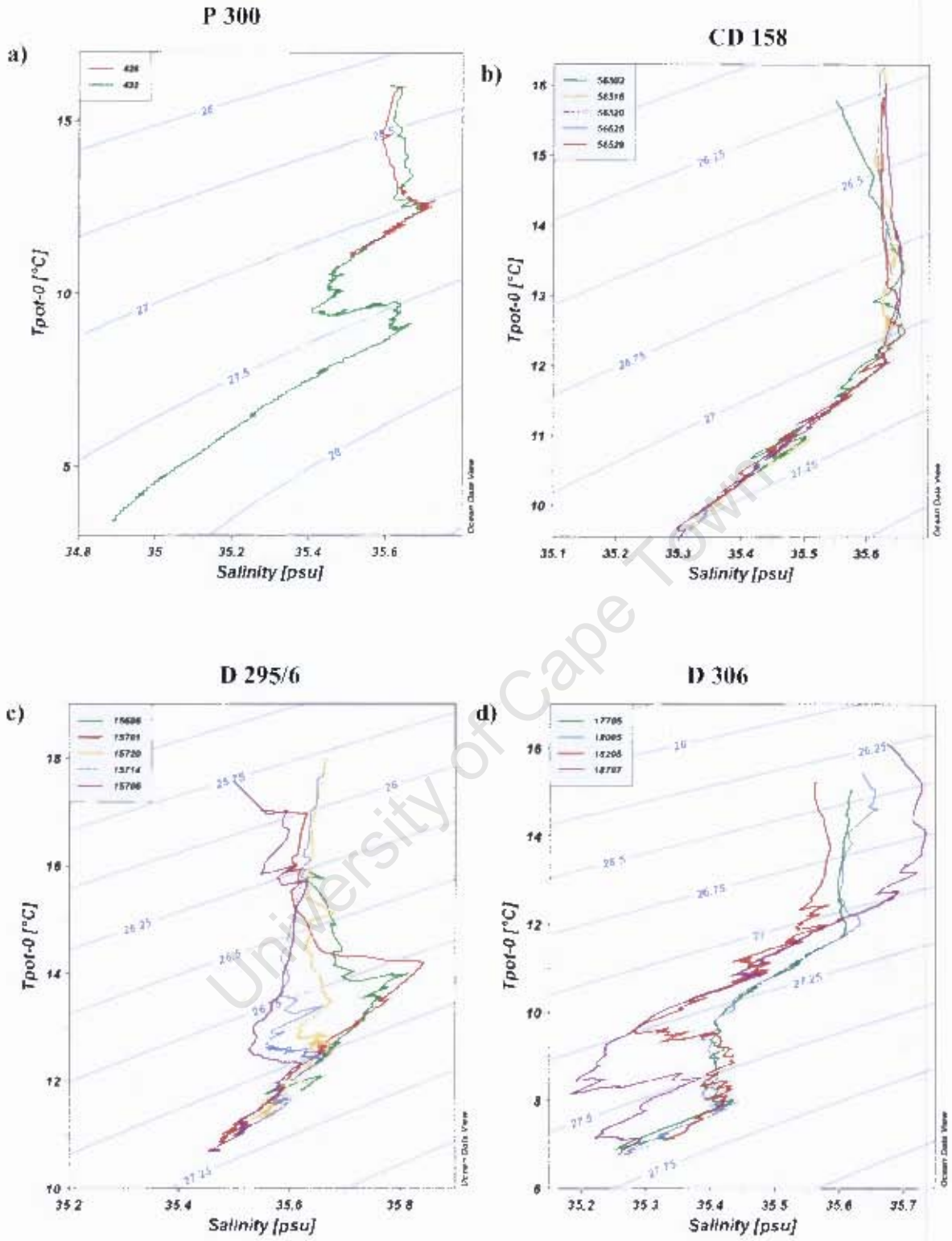

Figure 4.11. Potential temperature (°C) versus salinity (psu) for the thorium stations on a) P300 in July 2003 b) CD158 in June 2004 c) D295/6 in July 2005 and d) D306 in June/July 2006.

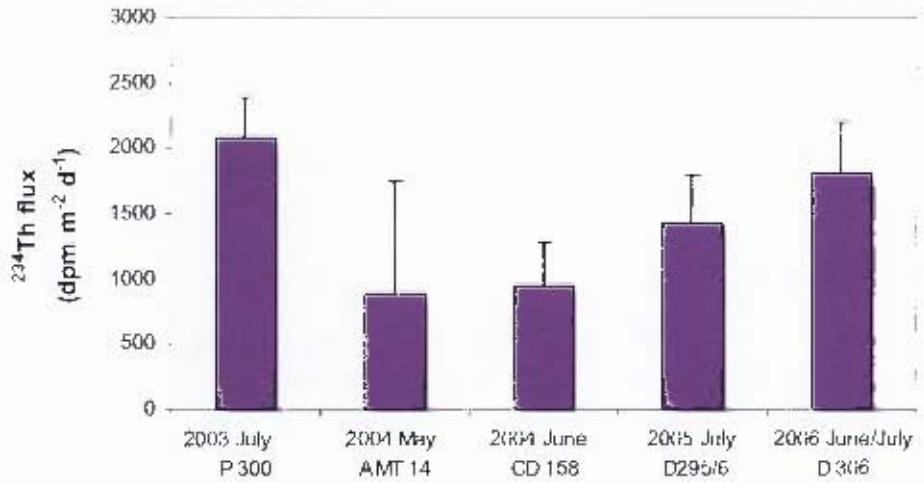

Figure 4.12. ^{234}Th fluxes (dpm m^{-2} d^{-1}) averaged over each cruise. Error bars represent the mean 1SD for each cruise propogated from overall analytical uncertainties.

4.4.5.2 POC flux

POC export was calculated from ^{234}Th flux*POC/^{234}Th ratio of the settling particles (see section 2.4.1 and 2.2.4 for details). The POC/^{234}Th ratios of settling particles were calculated from both the >50 µm particles collected from the SAPS pumps and from the particles that settled into the PELAGRA traps on all except the AMT 14 cruise where no PELAGRA was available (Table 4.5). POC/^{234}Th ratios were generally quite low, ranging from ~3 to ~6 µmol dpm^{-1} in July 2003 (P300), May 2004 (AMT 14), July 2005 (D295/6) and for the SAPS POC/^{234}Th ratio only in June/July 2006 (D306). Higher POC/^{234}Th ratios were found in PELAGRA (~13 µmol dpm^{-1}) in June/July 2006 (D306) and in both SAPS and PELAGRA in June 2004 (CD158) (~53 µmol dpm^{-1} and 25 µmol dpm^{-1} respectively) (Table 4.5).

The high POC/^{234}Th ratios for June 2004 (CD158) translate into high POC fluxes, in particular for the SAPS POC flux (50.93 ± 12.36 mmol C m^{-2} d^{-1}) relative to the PELAGRA POC flux (23.69 ± 5.75 mmol C m^{-2} d^{-1}) (Table 4.5; Figure 4.13). Conversely, the POC flux derived from PELAGRA in June/July 2006 (D306) was much higher (23.55 ± 2.87 mmol C m^{-2} d^{-1}) than that derived from the SAPS POC/^{234}Th ratio (5.85 ± 0.71 mmol C m^{-2} d^{-1}). POC fluxes were similarly low for P300 in July 2003 (6.34 ± 1.32 and 3.72 ± 0.77 for SAPS and PELAGRA respectively) and D295/6 in July 2005 (5.81 ± 1.57 and 6.16 ± 1.66 for SAPS and

PELAGRA respectively. (Figure 4.13, Table 4.5). Measured PELAGRA trap POC fluxes were lower than ^{234}Th based modelled fluxes in June 2004 (CD158) (13.88 mmol C m^{-2} d^{-1}) and July 2005 (D295/6) (1.49 mmol C m^{-2} d^{-1}), intermediate in June/July 2006 (D306) (9.52 mmol C m^{-2} d^{-1}) and similar in July 2003 (P300) (4.70 mmol C m^{-2} d^{-1}).

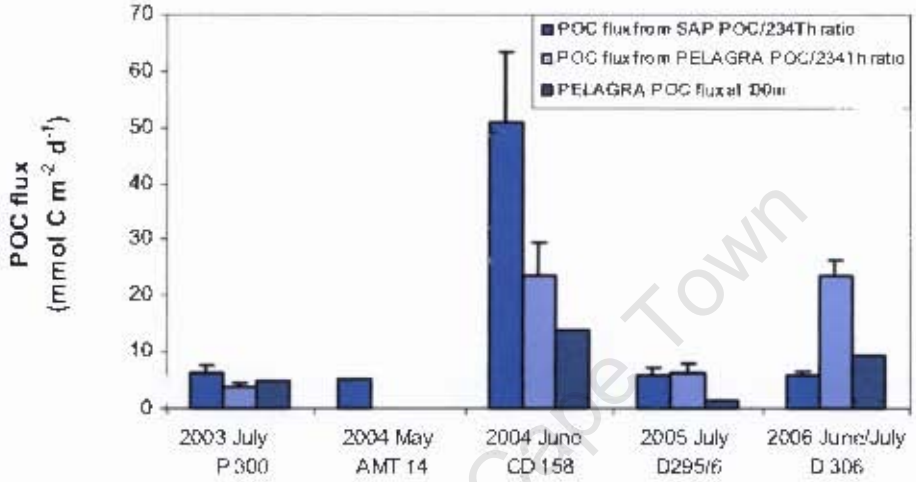

Figure 4.13. POC fluxes (mmol C m^{-2} d^{-1}) calculated using the POC/^{234}Th ratios from SAPS pumps and PELAGRA traps averaged over each cruise. Error bars represent the mean standard deviation (± 1SD). The dark blue bars represent the POC flux collected by the PELAGRA deployments adjusted to 100m according to Marin et al. (1978).

4.4.6 Deep-sea fluxes

Due to malfunctioning of the most recent 2005/6 trap deployments, a full set of samples was not collected by the 3000 m trap between 4th and 18th of June/July 2006 and between 28th August 2005 and 9th May 2006. Nevertheless, strong intra- and inter-annual variability in mass fluxes delivered to the sediment trap at 3000 m is observed over the previous 15 year time series (Figure 4.14). Downward particle flux consistently increases at the start of April, followed by a decrease at the end of October, with maximum fluxes associated with the summer season (Lampitt et al., 2001). Dry weight fluxes from 2003-2005 showed similar inter-annual variability in the timing and magnitude of major flux events. However, unlike flux measurements from the previous years (1989-1999), the peak in particle flux for 2003 was observed earlier in the year, reaching a maximum at the end of April. Summer fluxes for 2003-2005 also appeared somewhat lower than in previous years.

Table 4.5. Compilation of ^{234}Th fluxes, depths at which radioactive equilibrium was reached, POC/^{234}Th ratios from SAPS and PELAGRA and POC export calculated from both the SAPS and PELAGRA POC/^{234}Th ratios. Means ± SD where appropriate.

a) **P 300 - July 2003**

Station Number	Net ^{234}Th Flux (dpm $m^{-2}d^{-1}$)	1SD (dpm $m^{-2}d^{-1}$)	Equilibrium Depth (m)	POC : ^{234}Th ratio > 70 µm (µmol dpm^{-1})	SAPS POCexport (mmol C $m^{-2}d^{-1}$)	POC : ^{234}Th PELAGRA (µmol dpm^{-1})	PELAGRA POC export (mmol C $m^{-2}d^{-1}$)
426	1771	296	75	* 3.05	5.41	1.79	3.17
432	2381	336	100		7.27		4.27

b) **AMT 14 - May 2004**

Station Number	Net ^{234}Th Flux (dpm $m^{-2}d^{-1}$)	1SD (dpm $m^{-2}d^{-1}$)	Equilibrium Depth (m)	POC : ^{234}Th ratio > 50 µm (µmol dpm^{-1})	SAPS POCexport (mmol C $m^{-2}d^{-1}$)
CTD 88	884	865	93	6.0	5.3

c) **CD 158 - June 2004**

Station Number	Net ^{234}Th Flux (dpm $m^{-2}d^{-1}$)	1SD (dpm $m^{-2}d^{-1}$)	Equilibrium Depth (m)	POC : ^{234}Th ratio > 50 µm (µmol dpm^{-1})	SAPS POCexport (mmol C $m^{-2}d^{-1}$)	POC : ^{234}Th PELAGRA (µmol dpm^{-1})	PELAGRA POC export (mmol C $m^{-2}d^{-1}$)
56503	755	261	64	53.22	40.19	24.75	18.69
56511	978	458	69		52.08		24.22
56516	815	276	62		43.35		20.16
56520	1344	352	101		71.54		33.27
56529	892	253	55		47.48		22.08

d) **D295/296 - July 2005**

Station Number	Net ^{234}Th Flux (dpm $m^{-2}d^{-1}$)	1SD (dpm $m^{-2}d^{-1}$)	Equilibrium Depth (m)	POC : ^{234}Th ratio > 50 µm (µmol dpm^{-1})	SAPS POCexport (mmol C $m^{-2}d^{-1}$)	POC : ^{234}Th PELAGRA (µmol dpm^{-1})	PELAGRA POC export (mmol C $m^{-2}d^{-1}$)
15686	1704	378	101	3.65	6.94	4.31	7.35
15701	1685	369	101		6.86		7.27
15706	1689	375	102		6.88		7.29
15714	1203	381	102		4.90		5.19
15720	853	384	68		3.47		3.68

e) **D 306 - June/July 2006**

Station Number	Net ^{234}Th Flux (dpm $m^{-2}d^{-1}$)	1SD (dpm $m^{-2}d^{-1}$)	Equilibrium Depth (m)	POC : ^{234}Th ratio > 50 µm (µmol dpm^{-1})	SAPS POCexport (mmol C $m^{-2}d^{-1}$)	POC : ^{234}Th PELAGRA (µmol dpm^{-1})	PELAGRA POC export (mmol C $m^{-2}d^{-1}$)
17705	§ 1484	524	186	‡ 3.24	4.80	† 13.03	19.34
18005	1929	358	105		6.24		25.13
18205	1856	329	93		6.01		24.18
18707	1962	356	103		6.35		25.56

* mean from 85m and 95m SAPS

‡ mean from three 100m SAPS

†mean from 150m and 250m PELAGRA

§ Net ^{234}Th flux calculated from surface ^{234}Th flux - subsurface ^{234}Th excess

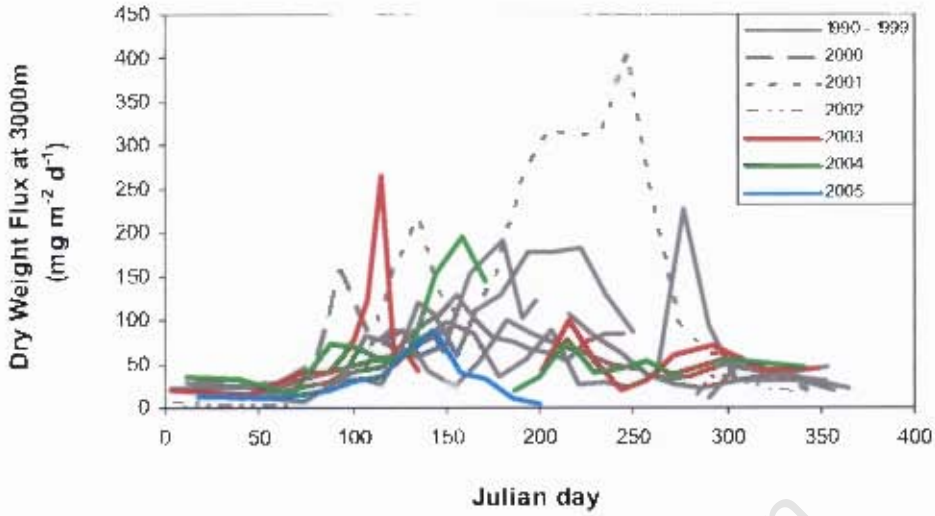

Figure 4.14. Dry weight flux (mg m^{-2} d^{-1}) collected from the 3000m sediment trap for the years 1990 to 2002 marked in grey and the years 2003 to 2005 marked in colour. Data for 1990 -1999 from Lampitt et al., 2001; data for 2003-2005 personal communication R. Lampitt.

POC fluxes in 2003 (Figure 4.15) peaked in mid April (17 mg C m^{-2} d^{-1}) and from the dry mass flux plot (Figure 4.14), we can assume the peak had ended by the beginning of May. Two smaller peaks in POC flux were seen at the beginning of August and in mid October (6 and 7 mg C m^{-2} d^{-1} respectively). In 2004, the POC flux peaked at the beginning of June (14 mg C m^{-2} d^{-1}) with two similar secondary peaks at the beginning of August and at the end of October (6 and 8 mg C m^{-2} d^{-1}). An additional secondary peak was also found earlier in 2004 in mid April (~6 mg C m^{-2} d^{-1}).

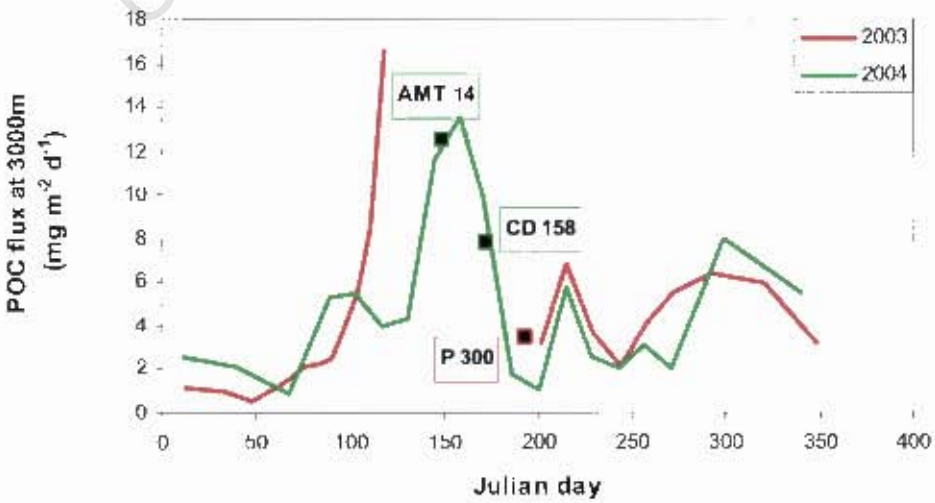

Figure 4.15. POC flux collected by the 3000m sediment trap for the years 2003 (red) and 2004 (green). The time of the cruises which took place in these years are marked on the graph. I. Salter personal communication.

4.5 Discussion

The aim of the ensuing discussion is to establish the relationship between surface phytoplankton production and particle export and to examine the spatial and temporal variability of surface and deep water processes that regulate particle flux. To achieve this, measurements of chlorophyll-a concentrations, primary production and new production are compared to export measurements to assess the relationship between NO_3 uptake (high f-ratios) and measured export and export efficiency (high *ThE* ratios). Furthermore, measurements of particle export collected from moored sediment traps at 3000 m are compared to surface particle export derived from the $^{234}Th/^{238}U$ disequilibrium approach.

It is widely believed that the magnitude and composition of settling material reflects the biology and biogeochemistry of the euphotic zone and the rates of remineralisation and dissolution of the material as it sinks through the water column (Jickells et al., 1996). Inter-annual changes in upper ocean productivity and community structure may also have an effect on the total mass flux (Boyd and Newton, 1995), or may simply affect the composition of sedimenting material, while the mass flux remains constant (Deuser, et al., 1995). Alternatively (or in concert), any affect on the composition of sedimenting material can affect sinking speeds and the remineralisation / dissolution rates of settling particles, thereby also affecting the total mass flux at depth. It is generally accepted that in environments dominated by highly variable physical forcing, vertical nutrient fluxes support high rates of productivity by larger phytoplankton cells (e.g. diatoms) that are later grazed by mesozooplankton. Such ecosystems are characterised by a short food chain with minimal respiratory carbon losses and efficient export of carbon to the ocean interior by the rapid sinking of large diatoms and faecal pellets (Falkowski et al., 1998; Tremblay et al., 2000). Alternatively, in more stable environments where the supply of new nutrients to the euphotic zone is limited, ecosystems tend to be dominated by smaller nano- and picophytoplankton and microzooplankton grazers (the 'microbial loop') with low or negligible sinking rates. Such ecosystems are characterised by many steps in the food chain and efficient recycling of organic matter in surface waters (Azam, 1998) and provide only weak biological CO_2 draw-down or a net CO_2 source to the atmosphere (Karl, 1999). One would therefore expect to find that where

primary production is dominated by new production, high f-ratios will be associated with high and efficient surface and deep water organic carbon export. Conversely, where primary production is dominated by regenerated nutrients, low f-ratios are expected to be linked to low and inefficient surface and deep-water carbon export.

Comparing rates of phytoplankton production with rates of export is however often problematic due to frequently incompatible spatial and temporal measurement scales. Episodic and spatially variable surface-water events may be poorly represented by near-instantaneous *in situ* surface-water production measurements compared to ^{234}Th flux and sediment trap measurements which integrate over much longer time and space scales. To overcome this problem, the relationship between *in situ* surface chlorophyll and productivity was combined with satellite derived chlorophyll data to estimate primary productivity over similar time and space scales to those of the flux measurements (see for example Venables et al., in press; Seeyave et al., in press Lucas et al., in press).

4.5.1 Relevant time and space scales

^{234}Th model fluxes and floating sediment traps collect an average particle flux which has a horizontal length scale related to the kinetic energy field above the trap and the particle sinking speed. According to Buesseler et al. (1992a), based on the analysis of Siegel et al. (1990), ^{234}Th model fluxes and trap fluxes at 150 m should be considered as averages over horizontal scales of 10s to 100s of kilometres. Given a mean residual current speed at the PAP site of 9 cm s^{-1} (Lampitt et al., 2001) over the mean life of thorium of 31 days (Buesseler, 1998), a given body of water can travel a distance of up to 240 km. However as this distance is unlikely to be in a straight line, 240 km should be considered a higher estimate for the relevant spatial scale of ^{234}Th flux.

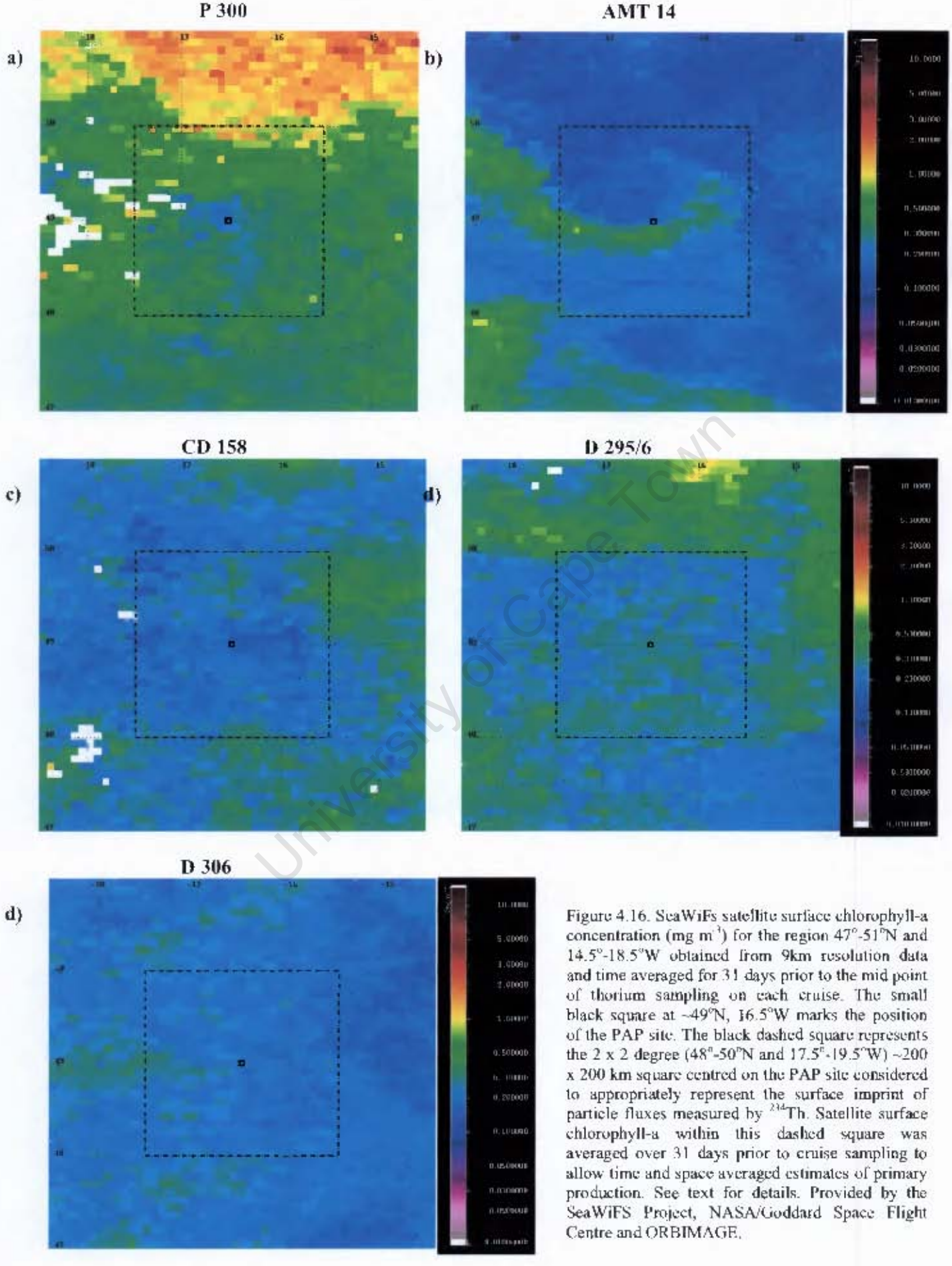

Figure 4.16. SeaWiFs satellite surface chlorophyll-a concentration (mg m^{-3}) for the region 47°-51°N and 14.5°-18.5°W obtained from 9km resolution data and time averaged for 31 days prior to the mid point of thorium sampling on each cruise. The small black square at ~49°N, 16.5°W marks the position of the PAP site. The black dashed square represents the 2 x 2 degree (48°-50°N and 17.5°-19.5°W) ~200 x 200 km square centred on the PAP site considered to appropriately represent the surface imprint of particle fluxes measured by ^{234}Th. Satellite surface chlorophyll-a within this dashed square was averaged over 31 days prior to cruise sampling to allow time and space averaged estimates of primary production. See text for details. Provided by the SeaWiFS Project, NASA/Goddard Space Flight Centre and ORBIMAGE.

Composites of satellite derived surface chlorophyll for the 31 days prior to each cruise (Figures 4.16a-e) and Hovmoller plots of surface chlorophyll (Figure 4.2) for the years 2003-2006 (both over 47°-51°N and 14.5-18.5°W) illustrate the typical spatial scales of variability in the vicinity of the PAP site. Images of 2 x 2 degrees or approximately a 200 x 200 km square (48°-50°N and 17.5°-19.5°W) centred on the PAP site incorporate the main biological features associated with this region and are therefore considered to appropriately represent the surface imprint of particle fluxes measured by ^{234}Th.

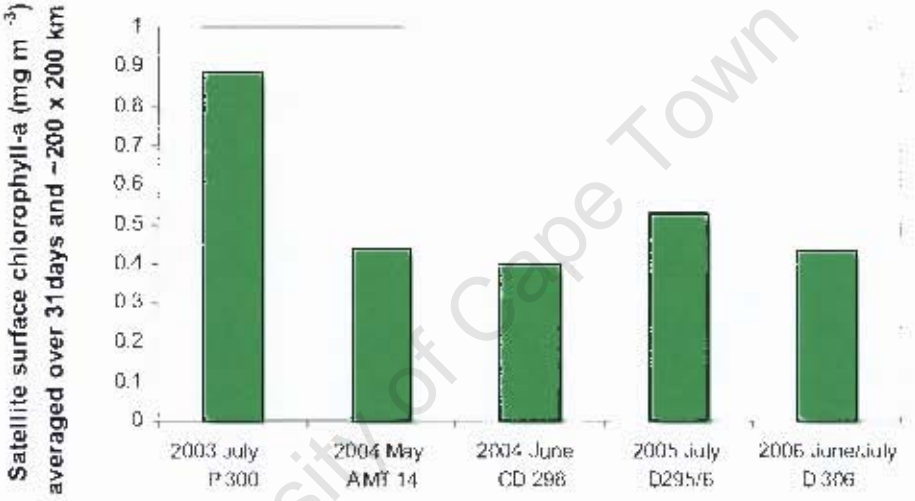

Figure 4.17. SeaWiFs satellite surface chlorophyll-a concentrations (mg m^{-3}) obtained from 9km resolution data and averaged for the region 47°-51°N and 14.5°-18.5°W over 31 days prior to the mid point of thorium sampling on each cruise.

4.5.2 Surface phytoplankton biomass and production

Surface SeaWiFS chlorophyll concentrations from 9 km pixels were averaged over the selected time and space scales; 31 days prior to the mid point of thorium sampling and covering 48°-50°N and 17.5°-19.5°W (Figures 4.16a-e) to give an averaged surface chlorophyll concentration for each cruise (Figure 4.17). Time and space averaged chlorophyll-a concentrations were highest in July 2003 (0.89 mg m^{-3}), similar to those from 2004-2006 which ranged from 0.40-0.53 mg m^{-3} (Figure 4.17).

Based on the relationship between *in situ* measured surface chlorophyll-a concentrations and integrated primary production measurements (Figure 4.18; r = 0.75, n = 25 P >0.01), time and space averaged primary production estimates (integrated over the euphotic zone) were calculated for each of the 5 cruises (Figure 4.19). To estimate an error on these calculations, an attempt was made to compare satellite estimates of surface chlorophyll at the PAP site for the same day as sampling *in situ* surface chlorophyll concentrations. However, only 7 out of the of the 27 days sampled for *in situ* chlorophyll had satellite chlorophyll estimates due to cloud or lack of overpass; too few data points to permit a relationship and error estimates for satellite derived primary production. Satellite derived primary production rates were highest in June 2003 (118.27 mmol C m^{-2} d^{-1}) and similar for the remaining 4 cruises (2004-2006) ranging from 75.2 to 86.4 mmol C m^{-2} d^{-1} (Figure 4.19).

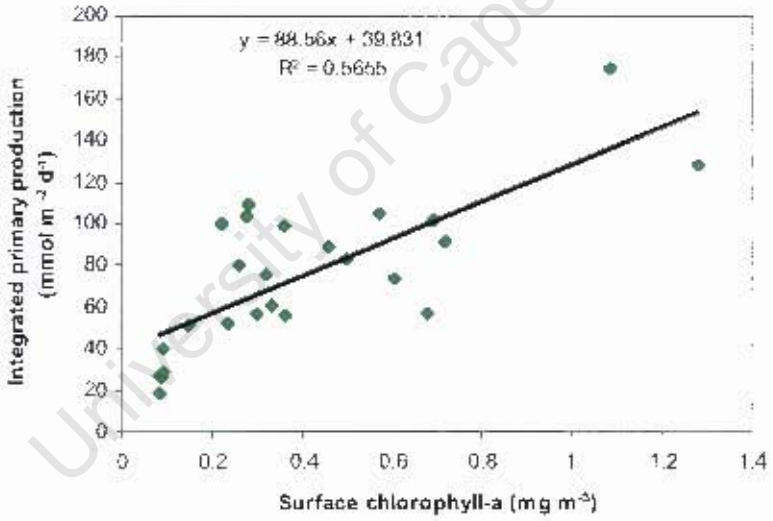

Figure 4.18. The relationship between *in situ* measured surface chlorophyll (mg m^{-3}) and integrated (0.1% light depth) carbon fixation (mmol m^{-2} d^{-1}). (r = 0.75, P <0.001, n – 25). Data are taken from all PAP site cruises between 2003-2006.

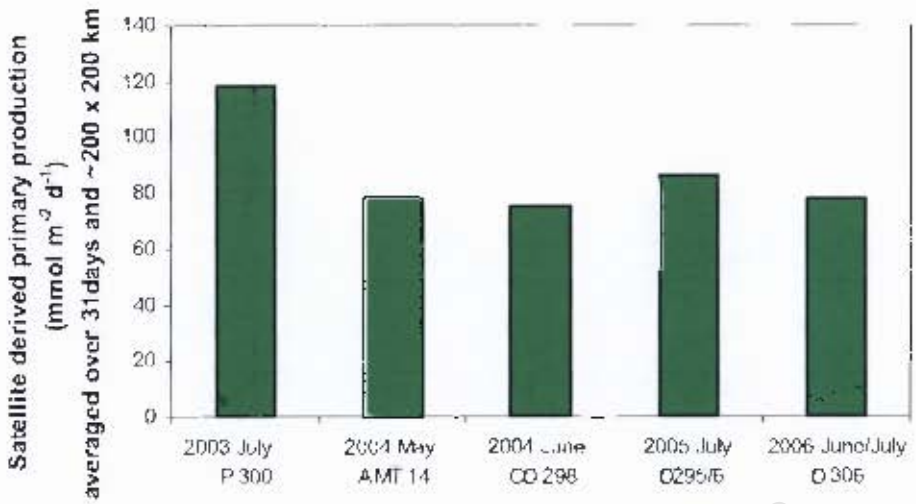

Figure 4.19. Satellite derived integrated (0.1% light depth) primary production (mmol C m^{-2} d^{-1}) averaged over 47°-51°N; 14.5°-18.5°W and 31 days prior to the mid point of sampling.

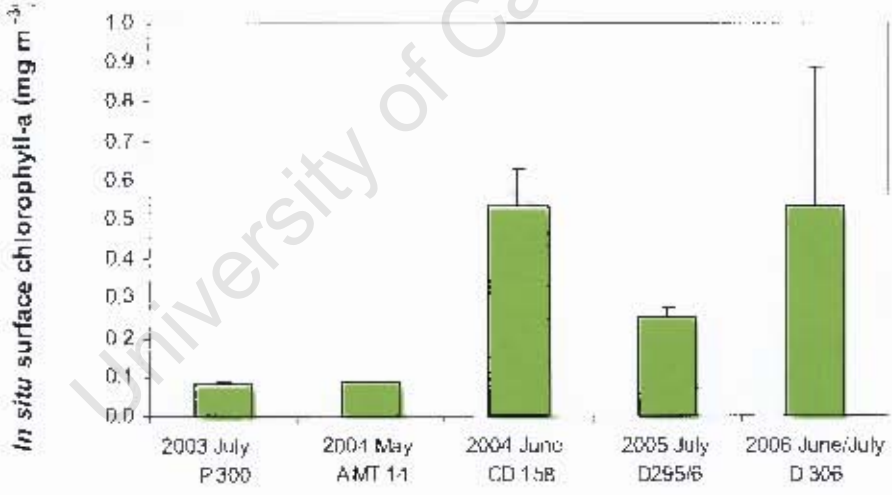

Figure 4.20. *In situ* surface chlorophyll-a (mg m^{-3}) averaged over each cruise. Error bars represent mean ± 1SD.

A striking difference is observed between satellite derived estimates of surface chlorophyll-a (Figure 4.17) and primary production (Figure 4.19) relative to *in situ* chlorophyll-a (Figure 4.20) and primary production measurements (Figure 4.7). The higher chlorophyll concentration (0.89 mg m^{-3}) observed in the satellite averages (Figure 4.17) for July 2003 (P300) is not apparent *in situ* (0.09 ± 0.01mg m^{-3}) (Figure 4.20). Conversely, the higher *in situ* chlorophyll concentrations (0.53 + 0.09 and 0.53 ± 0.35 mg m^{-3}) (Figure 4.20) observed in June 2004 and June/July 2006 (CD158 and

D306 respectively) are not evident in the satellite derived estimates (0.40 and 0.43 mg m^{-3}) (Figure 4.17). Similarly, the variability observed in *in situ* primary production rates (Figure 4.7) of a nearly three fold increase in carbon uptake from ~29 mmol C m^{-2} d^{-1} in July 2003 and May 2004 to ~75 mmol C m^{-2} d^{-1} in June 2005 and June/July 2006 is not observed in the satellite imagery (Figure 4.19) which show fairly consistent rates of integrated primary production (~80 mmol C m^{-2} d^{-1}) from 2004-2006. The higher satellite primary production (Figure 4.19) observed in 2003 (118 mmol C m^{-2} d^{-1}) is also not evident *in situ* (28.88 $\pm$ 6.95 mmol C m^{-2} d^{-1}; Figure 4.7). Such differences between *in situ* measurements and satellite derived estimates highlight the shortcomings of short term spot measurements made on cruises that are strongly influenced by small scale patchiness and can miss important temporal and mesoscale variability that is more representative of the region.

To derive time and space averaged new production estimates, *in situ* surface chlorophyll concentrations were plotted against integrated ^{15}N-derived f-ratios to ultimately calculate the fraction of new production relative to total production (see Lucas et al., in press). However, no significant relationship was evident between surface chlorophyll and integrated f-ratios (Figure 4.21a; $r = 0.06$, $n = 23$, $P > 0.05$). Instead, *in situ* surface chlorophyll-a was plotted against integrated carbon based new production (Figure 4.21b). Both linear and logarithmic regressions gave significant relationships ($r = 0.6$ and $r = 0.66$ respectively, $n = 24$, $P < 0.001$). The logarithmic fit was used to calculate time and space averaged estimates of new production (integrated over the euphotic zone) (Figure 4.22). Satellite derived new production estimates were slightly higher in June 2003 (30.75 mmol C m^{-2} d^{-1}) but similar to the remaining 4 cruises (2004-2006) which ranged from 23.04 to 25.70 mmol C m^{-2} d^{-1} (Figure 4.22). As was the case with satellite derived versus *in situ* primary production rates; the large degree of interannual variability observed in *in situ* new production (range = 3.27 to 25.65 $\pm$ 10.83 mmol C m^{-2} d^{-1}; Figure 4.8) was not evident in the satellite derived estimates (Figure 4.22).

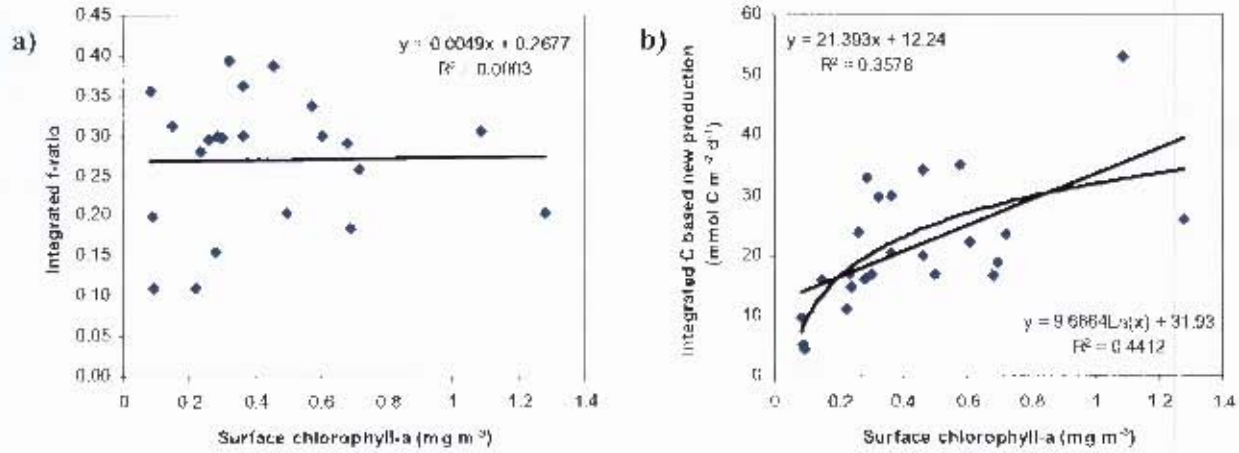

Figure 4.21. The relationship between a) *in situ* surface chlorophyll-a (mg m^{-3}) and integrated f-ratio ($r = 0.06$, $n = 23$, $P > 0.05$) and b) *in situ* surface chlorophyll-a (mg m^{-3}) and integrated carbon based new production (mmol C m^{-2} d^{-1}) ($r = 0.6$ and $r = 0.66$ for linear and logarithmic regressions respectively, $n = 24$, $P < 0.001$). Data are taken from all PAP cruises between 2003-2006.

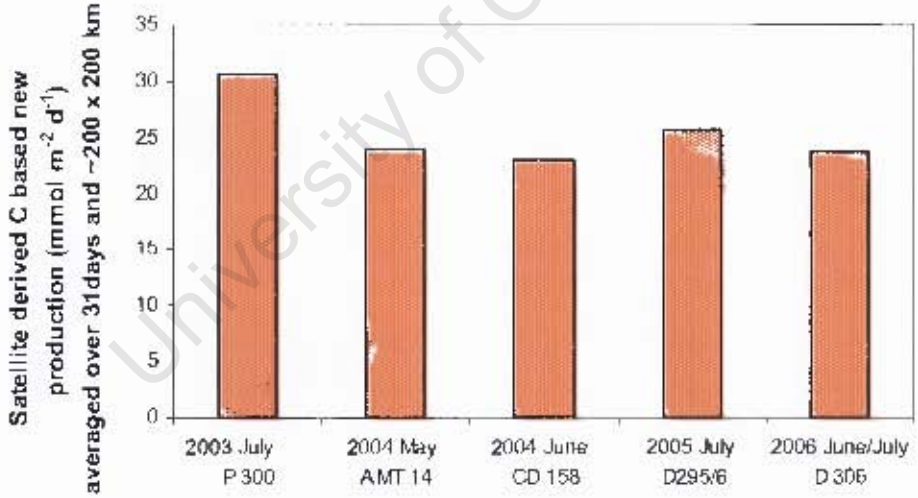

Figure 4.22. Satellite derived integrated (0.1% light depth) carbon based new production (mmol C m^{-2} d^{-1}) averaged over 47°-51°N; 14.5°-18.5°W and 31 days prior to the mid point of cruise sampling.

4.5.3 Surface POC export

Figure 4.13 shows that measured PELAGRA trap POC fluxes were generally lower than ^{234}Th based modelled fluxes using either the SAPS or PELAGRA POC/^{234}Th ratio. A positive or negative collection bias of a factor of 2-3 between upper ocean neutrally buoyant trap fluxes and those calculated from ^{234}Th water column distributions are quite common (Buesseler, 1992a). Three explanations for the observed differences in POC flux estimates are:

i) a low trap collection efficiency

ii) differing time and space scales for PELAGRA and ^{234}Th flux measurements and/or

iii) deficiencies in the ^{234}Th steady state model

The PELAGRA traps collect material that has been synthesised over previous weeks, but material collected is of near-instantaneous export flux over the time of deployment which is usually ~1-4 days, relative to thorium-based fluxes which quasi-integrate over a 31 day period. Thus, if high rates of surface export were experienced in a 31 day time period prior to thorium flux measurements, such a flux will be 'captured' by the thorium approach. However, if PELAGRA traps are deployed for a typically short period (1-2 days) at the same time, then the traps will clearly trap just a fraction of the high productivity event. Floating sediment traps collect an average particle flux which has a horizontal spatial scale related to the kinetic energy field above the trap and particle sinking speeds. Using the analysis of Siegel et al. (1990), Buesseler et al. (1992a) estimated that a fixed trap at 150 m would collect sinking particles over a horizontal scale of 5-100 km and that this scale would be slightly less for a floating trap depending on the speed of the 150 m trap relative to the water at that depth. This spatial scale is less than the ~200 x 200 km square which is thought to be representative of the ^{234}Th based modelled fluxes and could thus account for differences in modelled versus trap measured POC flux. Based on these discrepancies, the following discussion of POC flux measurements will be based only on the thorium model and not on those measured by the PELAGRA traps.

4.5.4 POC/^{234}Th ratios

The conversion of thorium fluxes into POC fluxes is very sensitive to variable POC/ ^{234}Th ratios and therefore needs careful consideration. In most data sets, POC/ ^{234}Th ratios decrease with depth (Buesseler et al., 2006) as a result of a combination of factors that include preferential mechanical breakdown and remineralisation of POC with depth but retention of ^{234}Th on sinking particles, as well as changes in surface binding ligands with depth (Buesseler et al., 2006 Speicher et al., 2006). In this study, two POC/^{234}Th ratios are available for each cruise (except May 2004); one collected at ~100 m by the SAPS pump and the other collected at 150-300 m using the PELAGRA traps (Table 4.5a-e). As the PELAGRA traps were deeper than the SAPS pumps, one would expect PELAGRA POC/^{234}Th ratios to be lower than SAPS ratios. This was however not always the case and only in June 2004 (CD 158) was the SAPS ratio (53.22 µmol dpm^{-1}) substantially higher than that of the PELAGRA trap (24.75 µmol dpm^{-1}) whereas in June/July 2006 (D306) the opposite occurred with the PELAGRA POC/^{234}Th ratio (13.03 µmol dpm^{-1}) being much higher than the SAPS POC/^{234}Th ratio (3.24 µmol dpm^{-1}).SAPS and PELAGRA POC/^{234}Th ratios were similar in July 2003 and 2005 (P300 and D295/6 respectively).

The lack of a collective trend in decreasing POC/^{234}Th ratios with depth between the shallower SAPS vs PELAGRA is likely a consequence of their different sampling strategies (see Methods). As for example in June/July 2006 (D306) where two PELAGRA traps were deployed at 150 m and 250 m, the POC/^{234}Th ratios decreased with depth from 15.84 to 10.82 µmol dpm^{-1}, illustrating the expected decline in ratio with depth. Although the higher PELAGRA POC/^{234}Th ratios relative to SAPS ratios on D306 is unusual, POC concentrations and ^{234}Th activities from all three SAPS and both PELAGRA traps fell within the range sampled on all other cruises. There is therefore no justifiable reason to favour either of the two and although the reasons for such differences remain unclear, both POC/^{234}Th ratios must be considered valid.

However this was not the case with the unusually high SAPS POC/^{234}Th ratio (53.22 µmol dpm^{-1}) in June 2004 (CD158). Although POC/^{234}Th ratios >100 µmol dpm^{-1} have been reported (Buesseler et al., 2006), the high POC/^{234}Th SAPS ratio on CD158 is considerably higher than studies in similar regions such as the equatorial Pacific

where POC/^{234}Th ratios ranged from <0.5 to 6.5 μmol dpm^{-1} (Buesseler et al., 1995, Bacon et al., 1996, Murray et al., 1996), the subtropical Atlantic where POC/^{234}Th ratios on AMT 12 and AMT 14 ranged from 1.5 to 27.4 μmol dpm^{-1} (section 2.4.4; Table 2.4a,c) and in the southern subtropical and equatorial Atlantic where POC/^{234}Th ratios averaged at 24 ± 12.2 μmol dpm^{-1} (range 0-35 μmol dpm^{-1}) (Charette and Moran, 1999). Charette and Moran (1999) suggest that different sampling techniques (i.e. bottle vs. *in situ* filtration) may yield different POC/^{234}Th ratios and attribute this to POC concentrations derived from large pumped volumes having a significantly higher POC concentration relative to the filter blank. Such differences in POC concentrations between bottle filtration and *in situ* pumps have often been documented (Gardner et al., 2003; Liu et al., 2005; Moran et al., 1999; Buesseler et al., 1996)

A high POC concentration will clearly increase the POC/^{234}Th ratio, but the unusually high POC/^{234}Th ratio on CD158 (53.22 μmol dpm^{-1}) was instead due to very low SAPS thorium activity (2 dpm m^{-3}) relative to the SAPS mean of 53 ± 25 dpm m^{-3} (range: 25-89 dpm m^{-3}, n = 7) on all other cruises. Although the POC/^{234}Th ratio in the PELAGRA trap in June 2004 (CD158) was also higher than for all other cruises (Table 4.5), its' thorium activity (346 dpm m^{-3}) fell within the overall range sampled of 234-531 dpm m^{-3} (mean = 338 ± 117 dpm m^{-3} n = 5). The high POC/^{234}Th ratio resulted from a higher POC concentration of 8.6 μmol m^{-3} compared to values in the range 1.83-8.09 μmol m^{-3} which characterised the other cruises. The reason for low ^{234}Th activity on the SAPS sample is unclear, but may be due to thorium speciation and high binding coefficients for certain organic phases, such as acidic polysaccharides (APS) produced by marine phytoplankton and bacteria on their cell surface. Polysaccharide, "sticky", surfactant-like Th(IV)-complexing ligands are likely embedded in a matrix of fibrillar exopolymeric particles (EPS) and transparent exopolymeric particles (TEP) (Santschi et al., 2006) that ^{234}Th preferentially tracks, rather than total colloidal (nm-μm) or marine snow (mm-cm) carbon (Guo et al., 2002a; Santschi et al., 2003; Passow et al., 2006). Thus if a large percentage of the particulate matter <50 μm consisted of colloidal organic carbon, rich in (acyl) polysaccharides, the POC/^{234}Th ratio of the >50 μm fraction could have low thorium activity and therefore a high POC/^{234}Th ratio. However, it is improbable that SAPS particulate material at 100 m would have such different properties to material caught

in the PELAGRA trap at 175 m. Given the similarity in POC/^{234}Th ratios between SAPS and PELAGRA samples on all other cruises, the low ^{234}Th activity of the CD158 (June 2004) SAPS sample and consequently the unusually high POC/^{234}Th ratio of 53.22 µmol dpm^{-1} (resulting in a POC flux of 50.93 mmol) is considered unlikely. Therefore just the PELAGRA POC/^{234}Th ratio from CD158 is used to calculate a POC flux. For the remaining cruises where both SAPS and PELAGRA were sampled, the mean POC/^{234}Th ratio between the SAPS and PELAGRA samples (Figure 4.23) is used to calculate POC flux. The resultant POC fluxes averaged over each cruise (Figure 4.24) for July 2003 (P300), May 2004 (AMT 14) and July 2005 (D295/6) were all low (mean = 5.34 ± 0.33 mmol C m^{-2} d^{-1}) but high on CD158 in June 2004 (23.69mmol C m^{-2} d^{-1}) and intermediate on D306 in June/July 2006 (14.70 mmol C m^{-2} d^{-1}). The average POC fluxes differed significantly between years (Kruskal-Wallis ANOVA $H_{3, 16} = 13.226$, $p<0.05$). *Post hoc* multiple comparison tests revealed that POC flux on CD158 (June 2004) was significantly higher than on P300 (July 2003) and D295/6 (July 2005). Note that AMT 14 (May 2004) could not be included in the statistical analysis as this cruise contained only a single data point.

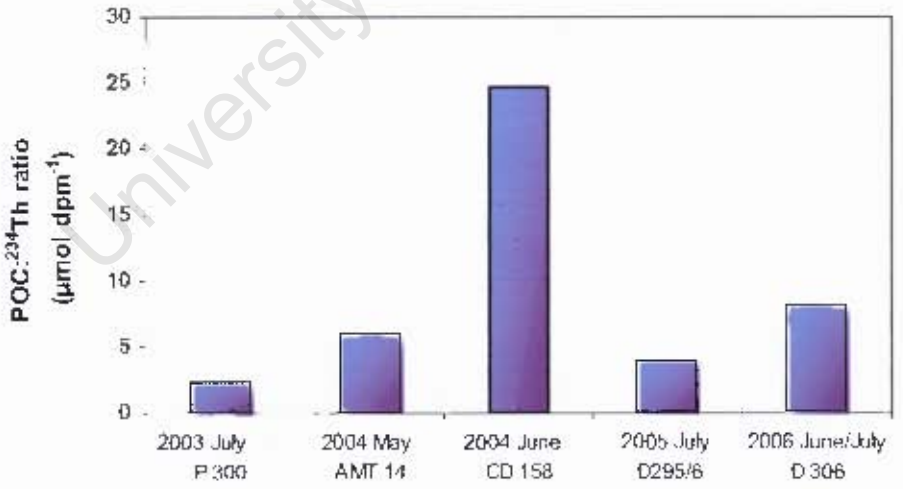

Figure 4.23. POC/^{234}Th ratios averaged between the SAPS and PELAGRA samples for P300, D295/6 and D306. On CD158 only the PELAGRA POC/^{234}Th ratio was used, see text for details. On AMT 14 only the SAPS POC/^{234}Th was used as PELAGRA was not available on this cruise.

High POC/^{234}Th ratios such as those found in June 2004 (CD158) (Figure 4.23; Table 2.5) are to be expected from large particles with low surface area to volume ratios

(Buesseler et al., 2006). Their typically faster sinking velocities also allow rapid transfer to the sea floor and less time for remineralisation/dissolution. Conversely, low POC/^{234}Th ratios, as were found on the remaining four cruises, are expected from small cells with low sinking rates (Reigstad, 2000). In such instances, slowly settling particles tend to aggregate and/or be transformed into faecal pellets by microzooplankton grazing (Landry et al., 1997). As carbon is preferentially remineralised relative to ^{234}Th during grazing and bacterial degradation of aggregates, (Arraes-Mescoff et al., 2001; Fisher et al., 1987), they become enriched in ^{234}Th and are therefore characterised by low POC/^{234}Th ratios (Copolla et al., 2002). The higher POC/^{234}Th ratios recorded in June 2004 (CD158) therefore suggest that particles settling out of the water column were either larger (i.e. rapidly settling, little re-mineralisation) and/or had less affinity for thorium (i.e. low in natural acid polysaccharide [APS]-rich TEP ligands [Santschi et al., 2006]).

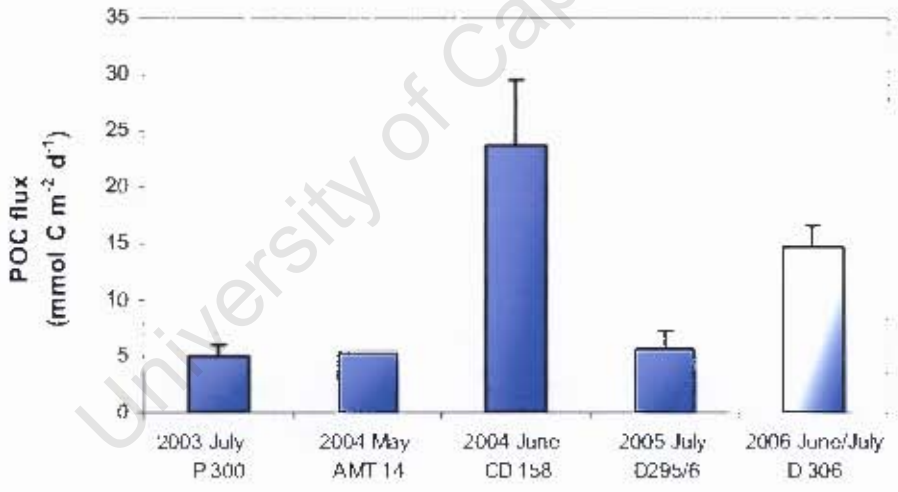

Figure 4.24. POC fluxes (mmol C m^{-2} d^{-1}) calculated from the POC/^{234}Th ratios of figure 4.21 and averaged over each cruise. Error bars represent mean ± 1SD.

What evidence do we have for these alternate types of settling particles? During two spring/summer periods at the PAP site in 1990 and 1992, marine snow flux was recorded at 3000 m by time-lapse photography and showed a strong peak in concentration during the initial downward flux of material (Lampitt et al., 2001). In both instances, peak volume flux was mainly generated by large rather than small particles, suggesting that large particles dominate at the start of the depositional pulse, while smaller aggregates dominate later in the summer (Lampitt et al., 2001).

Similarly, a study in the North Atlantic found that large diatoms dominated the spring bloom period, but was later in the season dominated by smaller nanophytoplankton (Buesseler et al., 1992; Verity et al., 1990). Higher POC/^{234}Th ratios resulting from larger particles settling at the onset of downward particulate flux could therefore account for the high POC fluxes on CD158 in June 2004.

4.5.5 PAP site sampling relative to the North Atlantic spring bloom

The start of the depositional pulse is expected to be associated with the spring bloom when nutrient depletion causes larger phytoplankton cells to become senescent and lose their buoyancy. Furthermore, with nutrient depletion, diatom communities give way to smaller nano- and pico-planktonic cells of the 'microbial loop' where vertical fluxes are greatly reduced.

Data from P300 (July 2003) and D 295/6 (July 2005) show that the surface mixed layer (Figure 4.25) was well defined and situated at ~25 and ~35 m respectively, surface NO_3 (~0.04 and ~0.23 mmol m^{-3}) (Figure 4.25) and surface chlorophyll (~0.09 and ~0.25 mg m^{-3}) (Figure 4.20) concentrations were exceptionally low and there was a DCM at ~47 and ~25 m (Figure 4.25).

The occurrence of deep chlorophyll maximum implies that phytoplankton are nutrient but not light limited in surface waters, while within the DCM where there is some access to nutrient diffusive flux across the nutricline, phytoplankton are likely to be somewhat light rather than nutrient limited. Such conditions are typical of summer rather than spring and on this basis, PAP sampling for these two cruises (P300; July 2003, D295/6; July 2005) clearly occurs after the spring bloom. This is substantiated further by the high ^{234}Th fluxes for these two cruises (mean = 1612 $\pm$ 376 dpm m^{-2} d^{-1} n = 7) (Figure 4.12) which suggests substantial removal of ^{234}Th by settling particles in the weeks prior to sampling.

Although phytoplankton can adapt to low light by increasing cellular chlorophyll concentrations, the DCM is still considered to be light limited, making it a pigment (biomass) rather than productivity maximum. Furthermore, as NO_3 uptake is considered an energy expensive process requiring a high light environment (Tett and

Edwards, 1984), this may explain low new nitrate-based production rates found in July 2003 (P300, Figure 4.8) despite high integrated NO_3 concentrations (Figure 4.4). Indeed, DCM productivity by mostly small cells best able to scavenge nutrients at low concentrations is classically based primarily on regenerated nitrogen (Timmermans et al., 2001; Veldhuis et al., 2005; Robinson et al., 2006). This supports the observation that POC/^{234}Th ratios in July 2003 and 2005 (Figure 4.23) were the lowest recorded (mean = 3.2 $\pm$ 1.07 µmol dpm^{-1} n = 4), suggesting that the phytoplankton community was dominated by smaller non-diatom cells and/or aggregates, which despite a substantial ^{234}Th flux (Figure 4.12), resulted in low carbon export (mean = 5.49 $\pm$ 1.36 mmol C m^{-2} d^{-1} n = 7) (Figure 4.24).

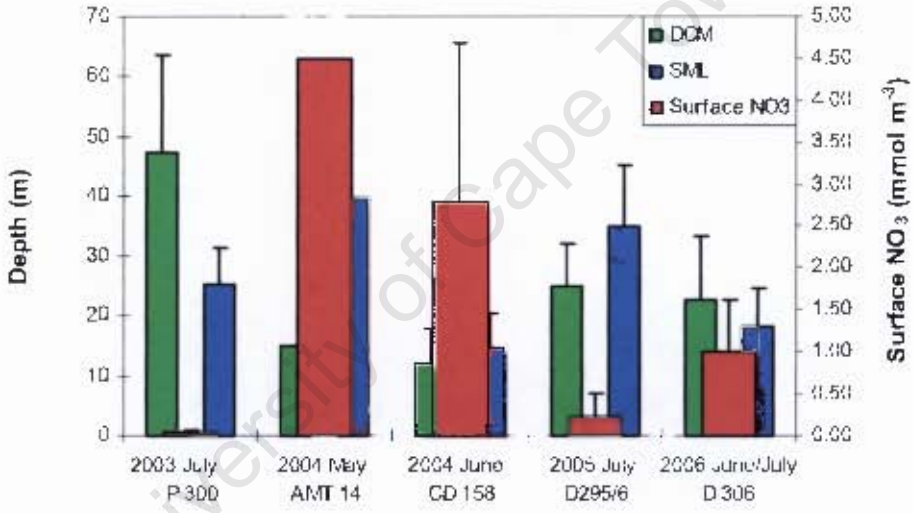

Figure 4.25. The average depth of the deep chlorophyll-a maximum (DCM) and surface mixed layer (SML) for each cruise together with surface NO_3 concentrations (mmol m^{-3}). Error bars represent mean $\pm$ 1SD.

In contrast, the AMT 14 visit to the PAP site in May 2004 sampled the region prior to the spring bloom when surface nitrate concentrations were still high (4.5 mmol m^{-3}) within a deep surface mixed layer (40-60 m), prior to summer shoaling (Figure 4.25). Low chlorophyll concentrations (~0.1 mg m^{-3}) were fairly consistent throughout the surface 60 m (Figure 4.5b), with a slight peak at 15 m (Figure 4.25). POC/^{234}Th ratios for this station were also relatively low (6 µmol dpm^{-1}) (Figure 4.23), suggesting a population dominated by small cells. Unlike the post bloom cruises P300 and D295/6 that showed a substantial ^{234}Th flux, AMT 14 exhibited the lowest ^{234}Th flux (884

dpm m^{-2} d^{-1} (Figure 4.12), indicative of low thorium removal by settling particles prior to the onset of the spring bloom.

On the other hand, CD158 and D306 (June 2004 and June/July 2006 respectively) were sampled within the peak (CD158) and early decline phase (D306) of the spring bloom. The SML on CD 158 was well defined and shallow (~15 m) (Figure 4.25), ambient concentrations of NO_3 (~544 mmol.m^{-2}), $Si(OH)_4$ (~128 mol.m^{-2}) and PO_4 (~35 mol.m^{-2}) (Figure 4.4) were still non-limiting and supported chlorophyll-a concentrations of (~0.53 mg m^{-3}) in the surface 12 m, with no indication of a DCM (Figure 4.5c). At this time, a low ^{234}Th flux (~957 dpm m^{-2} d^{-1}) may be expected as maximum particle export typically occurs only after nutrient limitation and bloom senescence (Buesseler et al., 2004). However, despite the low thorium flux, the exceptionally high POC/^{234}Th ratios (25 µmol dpm^{-1}) suggest that large cells such as diatoms were rapidly settling out of the water column, with little POC remineralisation, resulting in both the high POC/^{234}Th ratios and high POC fluxes found at this time (Figures 4.23, 4.24).

D306 sampled slightly later in the year (Table 4.1) when the SML was slightly deeper (~18 m), surface NO_3 concentrations were lower (~1.0 mmol m^{-3}) than CD158 but higher than post bloom cruises (Figure 4.25) and, although surface chlorophyll concentrations were the same (~0.53 mg m^{-3}) (Figure 4.20), there was evidence of a DCM at ~23 m (Figures 4.25, 4.5e). The high ^{234}Th flux (~1808 dpm m^{-2} d^{-1}) for this cruise (Figure 4.12) suggests substantial removal of ^{234}Th by settling particles in the previous weeks. While the POC/^{234}Th ratios (~8 µmol dpm^{-1}) were much lower than on CD158, they were higher than pre and post bloom cruises (in particular in the deeper PELAGRA traps [mean = 13 $\pm$ 3 µmol dpm^{-1} n = 2]) suggesting a transition to smaller non-diatom cells and/or aggregates, particularly as Si became depleted (Figure 4.4).

4.5.6 Comparing surface production with surface export

Temporally and spatially averaged production estimated from satellite derived chlorophyll-a can provide a useful tool for calculating mesoscale export efficiency (*ThE* = POC flux/Primary production, Buesseler 1998) at the PAP site using surface

POC flux estimates. The magnitude of export efficiencies (*ThE*) averaged over each cruise were akin to measured POC export ($r = 1$, $n = 5$, $P < 0.001$), with low *ThE* values (0.06 ± 0.02) for P300 (July 2003), AMT 14 (May 2004) and D295/6 (July 2005) compared to high *ThE* values (0.31 ± 0.07) for CD158 in June 2004 and intermediate *ThE* (0.19 ± 0.02) for D306 (June/July 2006) (Figure 4.26). *ThE* ratios differed significantly between cruises (Kruskal-Wallis ANOVA $H_{3, 16} = 13.597$, $p<0.05$). *Post hoc* multiple comparison tests revealed that *ThE* ratios on CD158 (June 2004) were significantly higher than on P300 (July 2003) and D295/6 (July 2005). Note that AMT 14 (May 2004) could not be included in this statistical analysis as this cruise had only a single data point. It thus appears that ~6% of primary production was exported during pre- and post-bloom periods, while ~31-19% was exported during the peak and early decline phase of the spring bloom, and that efficient export was independent of primary production ($r = 0.6$, $n = 5$, $P>0.05$).

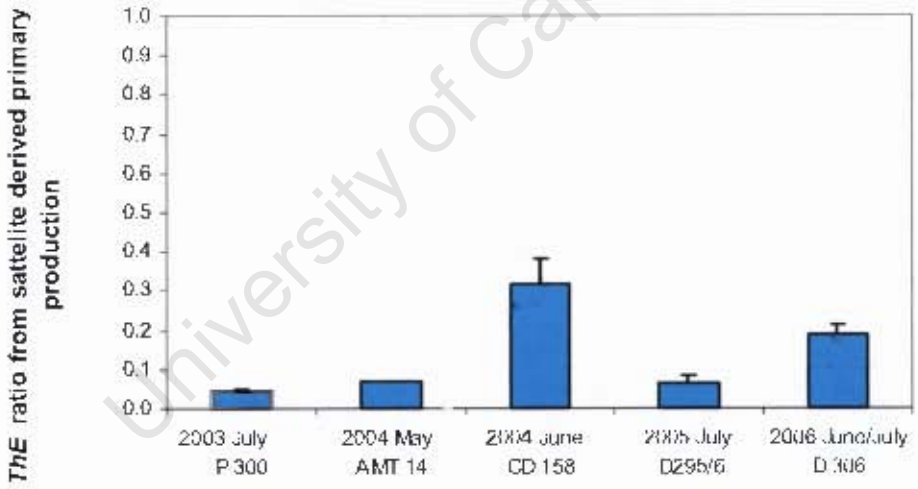

Figure 4.26. Cruise averaged *ThE* ratios (POC flux/primary production) based on satellite derived primary production averaged over 47°-51°N; 14.5°-18.5°W and 31 days. Error bars represent mean ± 1SD.

Comparing POC export to *in situ* primary production (Figure 4.27) showed a somewhat different pattern to temporally and spatially averaged production, with slightly higher *ThE* values during cruises P300 (June 2003) and AMT 14 (May 2004) (0.17, 0.18). A significant difference between cruise averaged *ThE* ratios was still observed (Kruskal-Wallis ANOVA $H_{3, 14} = 8.491$, $p<0.05$) with *ThE* on CD 158 in June 2004 (0.35 ± 0.13) being significantly higher than on D295/6 in July 2005 (0.07 ± 0.04). As only one of the two ^{234}Th based export stations on P300 coincided with an

in situ primary production station, this cruise had only one *in situ ThE* ratio and therefore both P300 and AMT 14 had to be excluded form the statistical analysis. From the *in situ* production data it thus appears that between 7 and 18% of primary production is exported during the interpreted pre- and post-bloom periods, while 32-17% is exported during the peak and early decline phase of the spring bloom. Again, as was the case with satellite derived *ThE* ratio, efficient POC flux appears independent of surface water primary production ($r = 0.15$, $n = 5$, $P > 0.05$). As *ThE* ratios calculated from satellite derived primary production integrate over temporal and spatial scales more appropriate to ^{234}Th flux calculations, they are considered the preferred approach. Export efficiencies (*ThE* ratios) hereafter will thus refer to those derived from satellite.

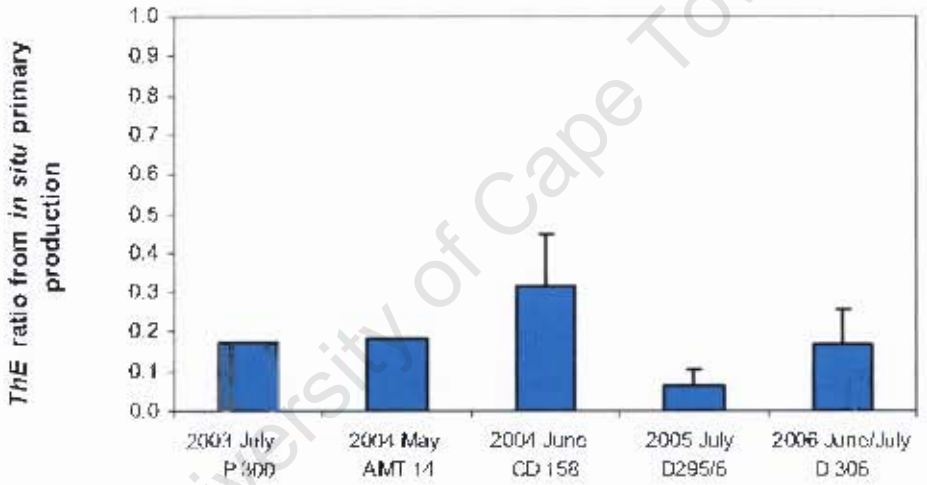

Figure 4.27. Cruise averaged *ThE* ratios (POC flux/primary production) based on *in situ* primary production measurements. Error bars represent mean ± ISD. Standard deviation for P300 was not possible as only one the two thorium CTD stations coincided with a primary production CTD station.

It is important however to remember that total primary production is not the driving force controlling downward particle flux, but rather new nitrate-based production, supported by upward nitrate flux. F-ratios (new production/primary production) provide a measure of the proportion of phytoplankton growth dependant upon NO_3 that over appropriate time and space scales theoretically and classically equates to particulate nitrogen export.

Given the absence of substantial interanual variability in satellite derived estimates of both primay and new production, it is not surprising that f-ratios based on these parameters (Figure 4.28) show very little differentiation between cruises. It is not possible to statistically determine differences between satellite derived f-ratios as only one data point is available for primary and new production for each cruise. However, as the satellite derived f-ratio in July 2003 was only slightly lower (0.26) yet similar to the following 4 cruises (0.30-0.31) in 2004-2006, it seems likely that such differences are consistent with natural variability. These f-ratio results suggest that between 26 and 31% of primary production was exported during the 5 cruises that sampled the PAP site. Such similarities in f-ratios show no distinction between pre-, post- or bloom conditions at the PAP site, as was the case with *ThE* ratios. The absence of a relationship between satellite derived f-ratios and *ThE* ratios ($r = 0.55$, $n = 5$, $P > 0.05$) is therefore not entirely surprising albeit contrary to the original hypothesis.

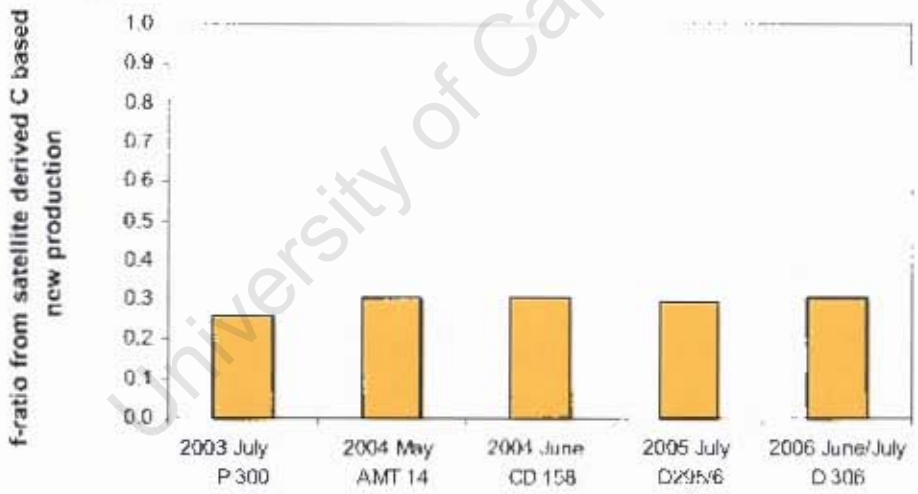

Figure 4.28. f-ratios (new production/primary production) calculated from satellite derived primary and new production averaged over 47°-51°N; 14.5°-18.5°W and 31 days

F-ratios derived from *in situ* measurements of primary and new production (see Methods for details) did however show interanual variability with respect to the seasonal timing of the spring bloom (Figure 4.29) and significantly correlated with *ThE* ratios ($r = 1$, $n = 5$, $P < 0.001$).

Unlike POC flux and *ThE* ratios however, differences between cruise averaged f-ratios were not statistically significant (Kruskal-Wallis ANOVA $H_{3,\ 23} = 4.2236$, $p>0.05$). Note however that AMT 14 (May 2003) had to be excluded from the analysis due to only one data point. F-ratios were highest for CD158 (0.34 ± 0.11) in June 2004 and in the same range as corresponding *ThE* ratios (0.31 ± 0.07). Intermediate f-ratios for D306 (0.29 ± 0.06) in June/July 2006 were slightly higher than their corresponding *ThE* ratios (0.19 ± 0.02) while f-ratios for the pre and post bloom cruises (0.23 ± 0.09) (P300, AMT 14, D295/6) were substantially higher than their corresponding *ThE* ratios (0.06 ± 0.02) (Figures 4.26, 4.29). These f-ratio results suggest that ~23% of primary production was exported from the PAP site during pre- and post bloom periods compared to ~31% and ~29% during peak and early decline bloom periods. Higher f-ratios than *ThE* ratios for AMT 14 (May 2004) and D306 (June/July 2006) could be a true reflection of increased rates of new production relative to primary production as there was more available NO_3 in surface waters (Figure 4.25) than on post bloom cruises (P300, D295/6). However, intrinsic in new production estimates is the linear relationship between NO_3 concentration and NO_3 uptake (Rees et al., 1999) such that the higher integrated NO_3 uptake rates may simply be a function of higher ambient NO_3 concentration.

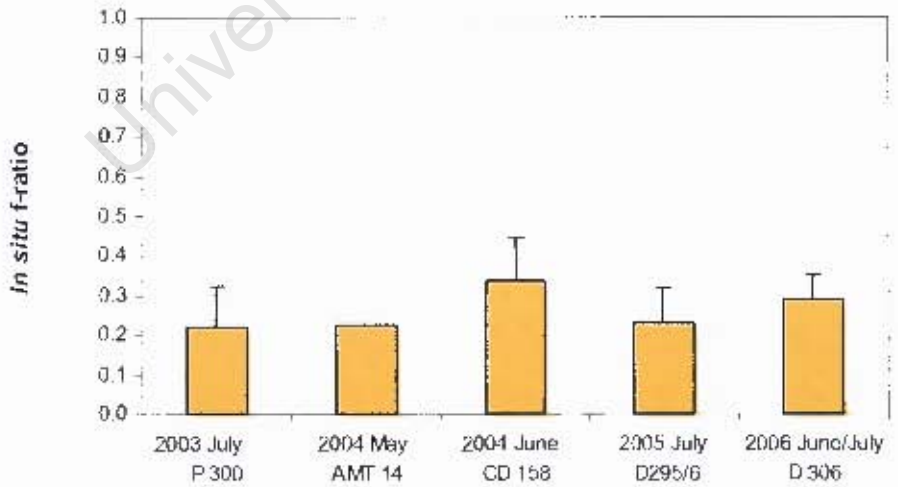

Figure 4.29. f-ratios (new production/primary production) calculated from *in situ* carbon based new production and total primary production (see text for details). Error bares represent mean ± 1SD.

Furthermore, ^{15}N-derived f-ratios need to be considered with some caution in this region at least. Apart from CD158 (June 2004), the remaining cruises exhibited higher

f-ratios than corresponding *ThE* ratios. Overestimates of f-ratios in subtropical gyres in particular may be substantial due to recently discovered nitrification in surface waters. Thus "regenerated" nitrate may account for >70% of nitrate uptake, so that the classically 'new' fraction is very much lower (Yool et el., in press). From these results, it appears that overestimating NO_3 uptake was more prevalent when POC export was low which is in agreement with Yool et al. (in press) whose model results showed that the largest overestimates of f-ratios were in unproductive oligotrophic regions where there is little available new nitrate and production is dominated by regenerated nutrient uptake.

Lampitt (1985) and Waniek et al. (2005) found a close correspondence between the timing and magnitude of surface productivity and the timing and magnitude of deep sea fluxes (2000/3000 m) that reflect the seasonal signal with pronounced maxima during the summer. Lampitt (1985) also accurately predicted fluxes at 3000 m based on satellite-derived primary production and an upper ocean biogeochemical model. Despite the established link between seasonal increases in production and export, when carried out over the high productivity summer season only, comparisons of *in situ* (Figure 4.7) and satellite derived (Figure 4.19) primary production with surface carbon export (Figure 4.24) showed no relationship ($r = 0.50$ and $r = 0.55$ respectively, $n = 5$, $P > 0.05$).

Although *in situ* f-ratios showed a significant relationship with POC flux ($r = 1$, $n = 5$, $P < 0.001$) and both *in situ* and satellite derived *ThE* ratios ($r = 0.77$ and $r = 1$ respectively, $n = 5$, $P < 0.01$), f-ratios for all cruises were overestimated with respect to *ThE* ratios and no significant differences were evident between cruises, as was the case with POC flux and efficient carbon export (*ThE*). F-ratio calculations rely on numerous assumptions such as steady state, no storage of N in surface waters, minimal N_2 fixation, negligible euphotic layer nitrification and consistent Redfield ratio stoichiometry. These assumptions are however not always the case, particularly in the subtropical gyres, where f-ratio results were not an ideal proxy for the magnitude of carbon export or efficient carbon flux as originally hypothesized.

POC flux and efficient POC export (*ThE*) instead appeared to be largely determined by the POC/^{234}Th ratios of the settling material ($r = 1$, and $r = 0.95$ respectively, $n = 5$, $P < 0.001$). This implies that (over the summer season at least), the efficient export of

carbon depends more on the characteristics of the phytoplankton community (and timing of the spring bloom) which determine the composition of the settling material (POC/^{234}Th ratio) than on primary production or the percentage new production (f-ratios). Despite comparable rates of primary and new production on CD158 (June 2004) (f-ratio = 0.34 $\pm$ 0.11) and D306 (June/July 2006) (f ratio = 0.29 $\pm$ 0.06) it was only on CD158 where Si and light were not limiting that larger cells (high POC/^{234}Th ratio) such as diatoms were able to grow. Larger cells have faster sinking rates and can better avoid degradation making them more efficient at transporting organic carbon to the deep ocean. Thus despite a low ^{234}Th flux associated with the beginning of the bloom period, CD158 (June 2004) had the highest POC flux. Although larger cells can out compete smaller ones in high NO_3 conditions, limiting factors such as Si, Fe and/or light will favour smaller cells which have higher surface area to volume ratios and longer particle residence times in surface waters that result in preferential carbon losses relative to ^{234}Th and leads to lower POC/^{234}Th ratios. The intermediate POC flux on D306 (June/July 2006) thus appeared to be governed by its timing with respect to the spring bloom (early decline phase, high ^{234}Th flux) where Si and light (DCM) limitations lead to a transition in the phytoplankton community to smaller cells (lower POC/^{234}Th ratios) and ultimatly a lower POC flux.

4.5.7 Comparing surface export to deep export

One of the 'unknowns' in biological oceanography is what happens to particles in the so-called twilight zone between surface productivity and export, and particle export at abyssal (3000 m) depths. Comparing surface export derived from the ^{234}Th/^{238}U disequilibrium approach with deep export at 3000 m (moored traps) ought to provide some information on the largely unknown "twilight zone" processes.

Due to deep sediment trap malfunctions, it is only possible to compare surface and deep export for 2003 and 2004, which includes three cruises (P300, AMT 14 and CD158). Based on particle sinking rates of 120 m day^{-1} derived from the time lag observed between surface production and the arrival of material on the seafloor (Lampitt, 1985), particles exported from the surface 100 m should settle into a 3000 m sediment trap in 24 days. A key issue in the comparisons is the normalisation of surface export data to a single depth horizon, since mass flux and its composition will

change significantly with depth due to organic matter degradation and mineral dissolution. A number of attempts have been made to quantitatively describe decreasing POC flux with depth. Bishop (1989) compared eight empirical equations that described POC mineralization with depth and concluded that the relationship derived by Martin et al., (1987) best fitted the available data. Boyd and Newton (1995) also provided evidence that extrapolating export production to depth (equivalent to new production; Eppley, 1989) using the Martin equation was satisfactory at the PAP site, but that the relationship between primary productivity and export production was more problematic.

For cruises P300, AMT 14 and CD158 (2003/4), surface POC fluxes (from ^{234}Th) were extrapolated to predicted deep (3000 m) POC fluxes using the Martin exponent (Martin et al., 1987). These predicted values were then compared with measured deep POC fluxes at 3000 m by plotting the values 24 days after the mid point of sampling, taking into account the time needed for particles settling at 120 m day^{-1} to reach 3000 m (Figure 4.30). Figure 4.30 shows that extrapolated POC fluxes for P300 (0.27 mmol m^{-2} d^{-1}) and AMT 14 (0.29 mmol m^{-2} d^{-1}) (July 2003 and May 2004 respectively) were slightly lower than measured fluxes at 3000 m at this time (0.55 and 0.74 mmol C m^{-2} d^{-1} respectively). However, CD158's (June 2004) extrapolated flux (1.28 mmol C m^{-2} d^{-1}) was much higher than the measured flux (0.10 mmol C m^{-2} d^{-1}). Possible reasons accounting for differences in the measured versus extrapolated POC fluxes include:

i) space scales corresponding to thorium based surface flux measurements differ to those of deep-sea sediment trap measurements

ii) the assumed particle settling speed of 120 m d^{-1} is either too fast or too slow

iii) the change in POC flux with depth is not adequately predicted by the Martin equation and / or

iv) in the case of CD158, the trap may have been under-sampling.

v) Inaccuracies in the ^{234}Th model and steady state assumptions

Each of these possibilities will be dealt with in turn.

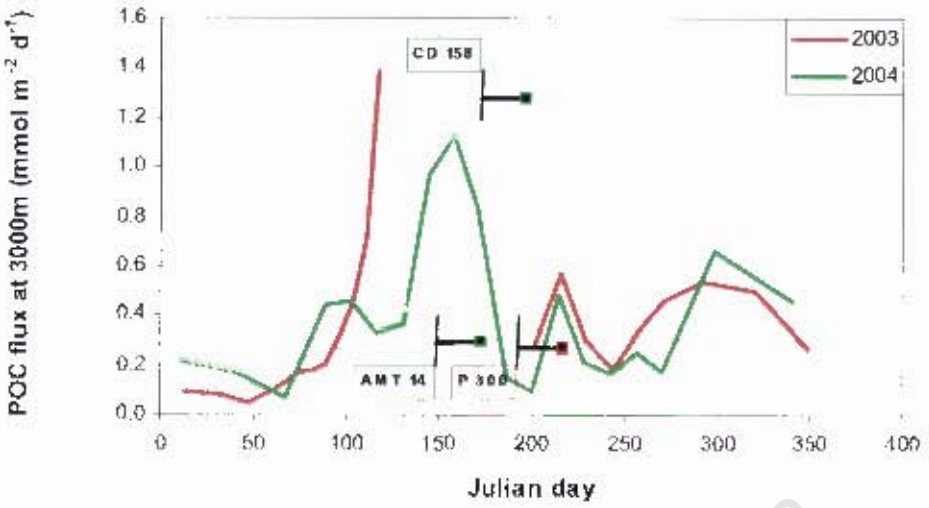

Figure 4.30. POC flux (mg m^{-2} d^{-1}) measured by the 3000m sediment trap at the PAP site for the years 2003 and 2004 (J. Salter personal communication). The vertical black line represents the mid point of the respective cruises, the horizontal black line represents the 24days required for particles exported from 100m to reach 3000m based on an assumed settling speed of 120m d^{-1}. The black squares indicate the flux expected at 3000m based on an extrapolation of the surface POC flux measurements (from the $^{234}Th/^{238}U$ disequilibrium approach) according to the Martin equation (Martin et al., 1987).

i) Space scales.

Particle fluxes to fixed sediment traps are observed as a function of time at a fixed point. Such traps notionally collect particles from a prescribed "statistical funnel", the size and location of the surface imprint depending on particle sinking rates and on regional hydrography (Siegel and Deuser, 1997). Faster sinking particles will originate from closer to the mooring position than those sinking more slowly. Without information on the spectrum of particle sinking speeds and an adequate hydrographic description of the region, only a crude estimate of the statistical funnel dimensions is possible. Based on a particle sinking rate of 120 m d^{-1} (Lampitt, 1985) and a residual current speed of 9 cm s^{-1}, the potential surface imprint of a 3000 m trap at the PAP site has a surface diameter of 400 km (Lampitt et al., 2001). However, this provides no information on the location of the source area relative to the trap (Deuser et al., 1988, 1990).

Model estimates of flux at 3000 m, based on an upper ocean biogeochemical model that used a 400 km diameter circle (125,664 km^2) centred on the trap location did however show good agreement with measured organic carbon flux, both in terms of

the timing and magnitude of the annual integrated flux (Lampitt et al., 2001). This spatial scale is however considerably larger than the spatial scale expected to represent thorium based export measurements (~200 x 200 km square; i.e. 40,000 km^2).

A comparison of surface chlorophyll concentrations averaged for 31 days prior to cruise P300 (July 2003) over a 200 x 200 km square (^{234}Th flux funnel) relative to a 400 x 400 km square (which although not a 400 km diameter circle is depicted to give a better conception of the moored trap funnel) centred on the PAP site (Figure 4.16a) show that surface chlorophyll concentrations were substantially higher north of the PAP site (covered by the 400 x 400 km square) than at the PAP site itself (covered by the 200 x 200 km square). Assuming that increased surface chlorophyll concentrations result in increased deep POC export (Lampitt, 1985), then the higher chlorophyll concentrations within the 400 x 400 km square (trap funnel) in July 2003 (P300) would alone account for the higher measured POC fluxes at 3000 m relative to extrapolated surface fluxes derived from the 200 x 200 km square (^{234}Th flux funnel). Such differences clearly illustrate the discrepancies that can arise when the relative "statistical trapping funnels" are so different in an environment where mesoscale patchiness is a characteristic feature. However, this was not always the case as time averaged satellite-derived chlorophyll concentrations at the PAP site in May 2004 (AMT 14) and June 2004 (CD158) showed very little variability regardless of whether 200 km square or 400 km square areas were considered (Figure 4.16b,c). Alternate reasons than differing space scales for these two cruises (AMT 14, CD158).must therefore account for higher measured POC flux in the 3000 m traps than that derived from extrapolated surface ^{234}Th measurements

ii) Particle settling speeds

The extrapolated POC fluxes were compared to measured POC fluxes at 3000 m based on a settling speed of 120 m day^{-1} (Lampitt, 1985) However, changes in particle composition due to changes in upper water column ecosystems will be expected to alter the settling speeds and arrival time of export flux at depth. The settling speeds were therefore adjusted along the time scale so that surface and deep fluxes are compared at the time particles are expected to have reached the deep traps (i.e. 24 days after the midpoint of cruise sampling) (Figure 4.30). Adjusting the horizontal bar

along the time line on Figure 4.30, so that extrapolated surface flux intercepts measured flux gives two alternate scenarios for P300 (July 2003). Either the surface flux would have to arrive at 3000 m just 9 days after sampling (instead of 24) at a settling speed of 322 m s^{-1}, or 40 days after sampling at a settling speed of 73 m s^{-1}. Given the nature of the PAP surface water ecosystem at this time (i.e. low f-ratios, lowest POC/^{234}Th, small cells), a settling speed faster than 120 m s^{-1} (Lampitt, 1985) appears unlikely and the slower settling speed of 73 m s^{-1} more feasible. Similarly, for the extrapolated surface flux to intercept the measured POC flux on AMT 14 (May 2004), the horizontal bar would have to adjust along the time line to arrive at 3000 m 35 days after cruise sampling giving a settling speed of 83 m.s^{-1}. As the extrapolated surface flux of CD158 (June 2004) was higher than that measured at 3000 m, at any time following the cruise, it is not possible to adjust the settling speed to intercept surface and deep fluxes.

iii) Variation of the Martin exponent.

Apart from differing settling speeds, rates of remineralisation with depth that differ from those predicted by the Martin equation could also account for disparities in predicted versus measured fluxes. Martin et al. (1987) predicts the decrease of POC flux with depth according to the following equation:

$$\text{deep flux} = \text{surface flux}/(\text{deep depth}/\text{shallow depth})^{0.858}$$

Assuming that the particle settling speed of 120 m d^{-1} is correct, the Martin equation exponent (0.858) can be adjusted so that surface fluxes will match measured fluxes at 3000 m. To achieve this on cruises P300 and AMT 14 (July 2003 and May 2004), the Martin exponent would have to decrease to 0.65 and to 0.58 respectively, implying that remineralisation rates must decrease to achieve the higher measured fluxes at 3000 m. Conversely, on CD158 (June 2004), the Martin exponent must increase to 1.60, thereby substantially increasing remineralisation rates before the lower measured fluxes are matched. Such deviations in remineralisation rates are related to the properties that characterise the surface water ecosystem. These include pelagic food web structure, the proportion of faecal pellets versus phytoplankton aggregates, the fraction of export associated with ballast minerals and their sinking rates, water temperature, and carbon demand of the mesopelagic bacteria and zooplankton

communities (Buesseler et al., 2007). Similar deviations in remineralisation rates relative to Martin et al. (1987) were measured by Buesseler et al. (2007) whos' Martin exponent was lower than predicted (0.51) in the northwest Pacific subarctic gyre and higher than predicted (1.33) at the Hawaii Ocean time series (HOT) site. When applied to global biogeochemical models (e.g. Laws et al., 2000), such variability in transfer efficiency has large implications for carbon sequestration below 500 m and equates to a difference of more than 3 Pg C $year^{-1}$ (Buesseler et al., 2007).

It is impossible to tell which (if either) of the two adjustments (settling speeds vs. Martin exponent) most likely accounts for the differences in extrapolated versus measured fluxes. However, in the case of CD158 (June 2004), a fourth possibility also exists.

iv) Trapping inefficiency

Trapping inefficiency (i.e. under or over-sampling) has been a contentious issue for some time, particularly during periods of high flux (e.g. Sherrell et al., 1998; Lampitt et al., 2001). While it has long been recognised that near-surface traps provide unreliable estimates of flux (Buesseler, 1991; Buesseler et al., 1994; Murray et al., 1996; Gustafsson et al., 2004). Takahashi et al., (2000) also suspected that under certain circumstances the deep trap funnel can become plugged with material, so preventing further collection. This was proposed to have occurred on two occasions (1990, 1992) at the PAP site where low measured flux coincided with a peak in modelled flux and a peak in marine snow concentration that was dominated by large particles (Lampitt et al., 2001). It is thus also possible that the higher extrapolated POC flux calculated for CD158, in summer 2004 may result from sediment trap under-sampling during a period of high flux dominated by large marine snow particles. Based on the characteristics of the surface water ecosystem in June 2004 (high f-ratios, *ThE* ratios, POC/^{234}Th ratios, mid spring bloom), it is unlikely that the extrapolated surface flux would require such a significant increase in remineralisation rates (relative to that predicted by Martin et al., 1987) and more likely that the lower measured fluxes at 3000m were due to trapping inefficiency.

v) ^{234}Th flux model and steady state assumptions

As time series data covering the characteristic time scale of ^{234}Th (mean half life: 34.8 d) were not available, a steady-state approach was used to calculate ^{234}Th export fluxes. Although it has been argued that a non-steady state system was unlikely (see section 4.4.5.1), the PAP site is part of a temporally highly dynamic region and there is the possibility that the sampled snapshot is part of a non-steady state system on a time scale of a few weeks (the time scale of ^{234}Th decay). Furthermore, the poorly constrained impact of lateral advection adds an unknown level of uncertainty to the ^{234}Th flux estimates. Steady-state estimates of export flux in a non-steady state system will tend to underestmate the true magnitude of flux variability and ultimately can add an unknown level of uncertainty to the POC flux estimates.

4.5.6 Comparison of export from the PAP site and the NABE

The PAP site is about 350 km northeast of the 1989 JGOFS North Atlantic Bloom Experiment (NABE) site (47°N, 20°W) (Figure 4.1) from which a considerable body of information on upper ocean processes was accumulated (Ducklow and Harris, 1993b). Given the relative proximity of the two sites, they may be considered similar (Lampitt et al., 2001) and worthy of comparison. However, from a benthic perspective the PAP site is significantly different, because the seabed is flatter and the absence of topographic undulations makes the site less spatially variable. Such variability can result in problems when interpreting data and this provided the reason for locating the PAP site long-term study in its present position (Lampitt et al., 2001).

Carbon flux measurements during the NABE were carried out earlier in the year (24 April to 30 May) than at the PAP site (typically June/July). During NABE, the onset of stratification in late April was associated with primary production rates of ~100 mmol C m^{-2} d^{-1}, a large diatom bloom, and a decrease in surface NO_3 from ~6 to ~1 mmol m^{-3} (Buesseler et al., 1992a) as well as decreased silicate (Lochte et al., 1993). It was during this diatom-dominated period in early May, that surface ^{234}Th export fluxes (at 35 m) peaked from 1280 to 2610 dpm m^{-2} d^{-1}, after which they decreased to ~1000 dpm m^{-2} d^{-1} by the second half of May (Figure 4.31). The deeper ^{234}Th flux at 75 m however continually increased from late April (1720 dpm m^{-2} d^{-1}) through May to reach a maximum at the end of May (3600 dpm m^{-2} d^{-1}), suggesting that as the bloom progressed, a two-layered system was established, with more of the export

originating from below the mixed layer in the later stages of the bloom (Buesseler et al., 1992a). As the observed change in ^{234}Th activity with time was often the largest term in the budget, a non-steady state model was used to estimate carbon flux for three time intervals; early bloom in late April (24/4-5/5), mid bloom in early May (5/5-19/5) and late bloom toward the end of May (19/5-30/5).

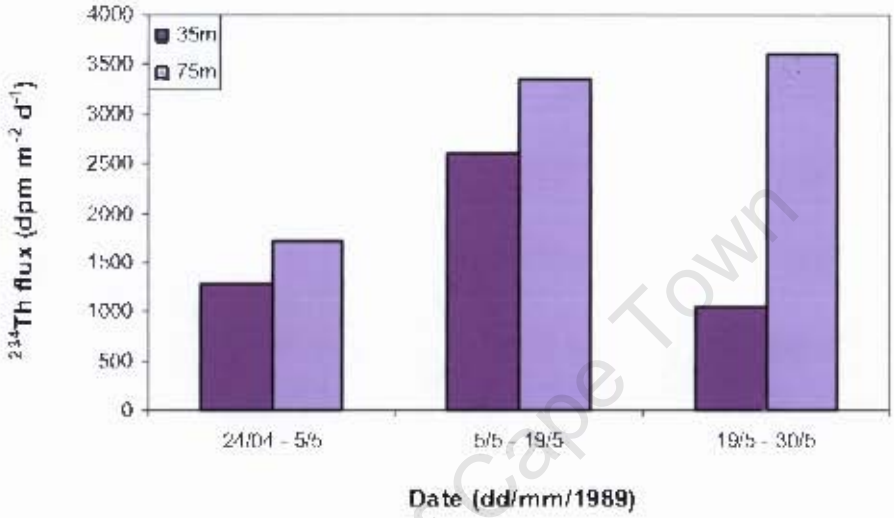

Figure 4.31. Net ^{234}Th flux (dpm m^{-2} d^{-1}) from 35m and 75m on the 1989 JGOFS North Atlantic Bloom Experiment (NABE). Buesseler et al. (1992).

As >50 µm bulk water samples were not available to derive POC/^{234}Th ratios, Buesseler et al. (1992a) proposed an upper and lower limit on POC export by using POC/^{234}Th ratios from the total particulate fraction >1 µm and from the 150 m sediment trap (see Table 4.6). As the measured or assumed POC/^{234}Th ratios of settling material plays a crucial role in determining POC export, their method of deriving POC/^{234}Th ratios is considered further. The POC/^{234}Th ratios and hence POC export from particulate material >1 µm were much higher than those from their 150 m trap (Table 4.6), possibly due to living phytoplankton >1 µm that attract only very low concentrations of thorium (Coale, 1990; Buesseler et al., 1992a; Cochran et al., 1993). Although absolute fluxes measured by surface (i.e. 150 m) sediment traps are known to under or over sample by a factor of 2 to 3 (Buesseler 1992a), it is assumed that the sample they collect is representative of the sinking material (Buesseler et al., 1992). As the NABE sediment trap at 150 m was below the base of the euphotic zone (35 m),

POC flux from this trap should however be considered a lower limit as some preferential remineralisation of carbon relative to ^{234}Th would be expected.

Table 4.6 POC/^{234}Th ratios from >1µm total particulate material and from a 150m floating sediment trap. Data collected during the JGOFS North Atlantic Bloom Experiment (NABE) in May 1989 by Buesseler et al (1992b).

Dates (dd/mm/1989)	Depth (m)	>1µm POC/^{234}Th (µmol dpm-1)	Trap POC/^{234}Th (µmol dpm-1)
24/4 - 5/5	35	14.2	(3.9)
	75	20.5	(3.9)
5/5 - 19/5	35	15.7	(5.9)
	75	23	(5.9)
19/5 - 30/5	35	22.5	(7.4)
	75	14.3	(7.4)

Values in parentheses are taken from a 150m floating trap

Given that POC flux estimates from the NABE >1 µm POC/^{234}Th ratios are probably overestimated, while at the PAP site, the POC flux estimates were based on SAPS >50 µm and PELAGRA POC/^{234}Th ratios (Figure 4.14), only POC fluxes estimated from the NABE 150 m sediment trap POC/^{234}Th ratios (Figure 4.32) are compared to PAP POC flux estimates (Figure 4.24).

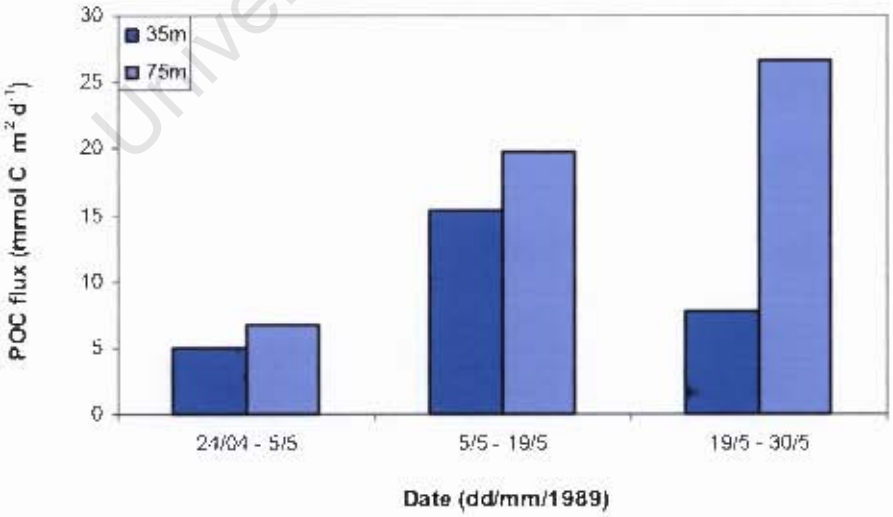

Figure 4.32. Particulate Organic Carbon (POC) flux (mmol C m^{-2} d^{-1}) at 35 m and 75 m calculated using the POC/^{234}Th ratios from the 150 m sediment trap on the 1989 JGOFS North Atlantic Bloom Experiment (NABE). Buesseler et al. (1992).

The POC flux (75 m) during the NABE was lowest at the beginning of the bloom period in late April (6.7 mmol C m^{-2} d^{-1}; Figure 4.32); higher yet comparable to pre bloom conditions measured at the PAP site on AMT 14 (5.3 mmol C m^{-2} d^{-1}) as well as post bloom fluxes measured in July 2003 (P300; 5.03 ± 1.04 mmol C m^{-2} d^{-1}) and July 2005 (D295/6; 5.68 ± 1.53 mmol C m^{-2} d^{-1}) (Figure 4.24).POC flux during the NABE increased in the middle of the bloom in mid May to 19.8 mmol C m^{-2} d^{-1} (Figure 4.32). Despite a ~50% decrease in surface (35 m) POC flux from 15.4 to 7.7 mmol C m^{-2} d^{-1}), the 75 m flux continued to increase to 26.6 mmol C m^{-2} d^{-1} during the late bloom at the end of May (Buesseler et al., 1992a) (Figure 4.32). These bloom fluxes are comparable to those measured at the PAP site on CD158 (23.69 ± 5.75 mmol C m^{-2} d^{-1}) and D306 (14.70 ± 1.79 mmol C m^{-2} d^{-1}) (Figure 4.24).

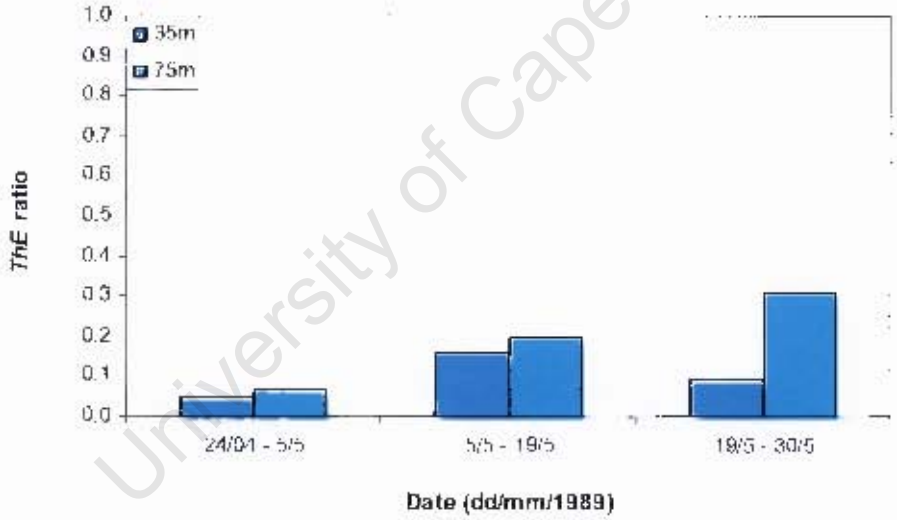

Figure 4.33. *ThE* ratios at 35 and 75m calculated from integrated primary production (mmol C m^{-2} d^{-1}) and POC export estimated from the 150m sediment trap POC/^{234}Th ratios on the 1989 JGOFS North Atlantic Bloom Experiment (NABE). Buesseler et al. (1992).

ThE ratios for the NABE (75 m) (Figure 4.33) and the PAP site (Figure 4.26) were also similar with low *ThE* ratios (0.07) of the early bloom period on NABE corresponding to similarly low *ThE* ratios in pre (0.07; AMT 14) and post (0.04 ± 0.01, P300 and 0.07 ± 0.02; D295/6) bloom conditions at the PAP site (Figure 4.26). Whereas high *ThE* ratios in the mid and late bloom on NABE (0.20 and 0.31) (Figure

4.33) are comparable to those estimated during bloom conditions at the PAP site (0.31 $\pm$ 0.07; CD 158 and 0.19 $\pm$ 0.02; D306) (Figure 4.26).

Surface *ThE* ratios (35 m) at the NABE (Figure 4.33) tracked the progression of the food web and bloom dynamics, ranging from 0.05 to 0.16, with the peak in surface *ThE* coinciding with the middle and later part of the bloom (Buesseler et al., 1998) (Figure 4.33). Peaks in surface export and surface *ThE* occurred as the mixed coccolithophore and diatom-dominated assemblage evolved into one dominated entirely by diatoms. The later transition to lower surface POC fluxes and lower surface *ThE* ratios in late May followed Si depletion and coincided with the change in the dominance of the phytoplankton community to small phytoflagellates (Verity et al., 1990). Verity et al. (1990) suggested that small protozoans had sufficiently high grazing rates to consume the bulk of the primary production, thereby limiting particle export. *ThE*` ratios at the PAP site were also shown to track bloom dynamics, with high *ThE* ratios (0.31 $\pm$ 0.07) in June 2004 (CD158) (Figure 4.26) being associated with high POC/^{234}Th ratios (Figure 4.23) indicative of large cells (e.g. diatoms) settling quickly out of the water column. Intermediate *ThE* ratios (0.19 $\pm$ 0.02) in June/July 2006 (D306) coincided with a decrease in the POC flux and the transition from diatoms to smaller cells (lower POC/^{234}Th) following Si depletion (Figure 4.4).

Low POC/^{234}Th ratios, low POC fluxes and low *ThE* ratios were found during post bloom conditions where low surface nutrient concentrations, deep chlorophyll maxima and a stable thermocline resulted in a tightly coupled microbial food web dominated by small cells and effective microzooplankon grazing. Low *ThE* ratios found in pre bloom conditions were associated with high nutrient concentrations but low chlorophyll concentrations where growth was probably constrained by an unstable surface mixed layer due to insufficient warming.

4.6 Summary and Conclusion

Fluxes of POC from surface waters in the North East Atlantic (PAP) have been estimated using the natural tracer ^{234}Th. POC fluxes were low in July 2003 (P300; 5.03 mmol C m^{-2} d^{-1}), May 2004 (AMT 14; 5.30 mmol C m^{-2} d^{-1}) and July 2005

(D295/6; 5.68 mmol C m^{-2} d^{-1}) but high in June 2004 (CD158; 23.69 mmol C m^{-2} d^{-1}) and intermediate in June/July 2006 (D306; 14.70 mmol C m^{-2} d^{-1}).

The inter-annual variability in POC flux is governed by the timing of each cruise with respect to the seasonal development of the North Atlantic spring bloom. Low POC flux was associated with pre (May 2004; AMT 14) and post (July 2003/5; P300 and D295/6) bloom conditions, whereas high POC flux was associated with peak (June 2004; CD158) and early declne (June/July 2006; D306) bloom conditions. Similarly, estimates of temporally and spatially averaged primary production compared with ^{234}Th derived POC export (*ThE*) gave low export efficiencies (~6%) in pre and post bloom conditions (May 2004, July 2003/5) compared to higher export efficiencies (31 -19%) in spring and early decline bloom conditions (June 2004, June/July 2006). Although surface production and deep carbon export (3000 m) are directly coupled over the annual seasonal cycle with pronounced maxima during the summer (Lampitt et al., 2001), comparisons of primary production and surface carbon export carried out only in the high productivity summer season showed no relationship.

Although *in situ* f-ratios showed a significant relationship with POC flux and *ThE* ratios, f-ratios for all cruises were overestimated with respect to *ThE* ratios and no significant differences were evident between cruises, as was the case with POC flux and efficient carbon export (*ThE*). However f-ratio calculations are only valid on appropriate time scales and depend on a number of assumptions (e.g. steady state, negligible nitrification and N_2 fixation). As these assumptions are not always the case, particularly in the subtropical gyres, and as our comparisons were made over the same productive season, it is not confounding that f-ratio estimates did not provide an ideal proxy for POC flux or efficient POC export.

POC flux and efficient POC export (*ThE*) instead appeared to be largely determined by the POC/^{234}Th ratios of the settling material, with high POC/^{234}Th ratios (25 µmol dpm^{-1}) associated with the spring bloom in June 2004 (CD158) compared to pre and post bloom conditions (mean = 4 µmol dpm^{-1}) in July 2003, May 2004 and July 2005 (P300, AMT 14, D295/6). These results suggest that (in the summer season at least) efficient carbon export is governed by the characteristics of the phytoplankton community which determine the composition of the settling material. The

phytoplankton community (succession between diatoms and pico-nanophytoplankton) is in turn governed by environmental controls (physical stability, light, nutrients) on the surface water ecosystem that determines the timing, magnitude and duration of the spring bloom and its associated carbon flux.

Results from the PAP site compare well with those of the 1989 JGOFS NABE which tracked the North Atlantic spring bloom over a 5 week period to give POC flux measurements for early, mid and late spring bloom. POC flux (75 m) at the beginning of the NABE (6.7 mmol C m^{-2} d^{-1}) was higher yet comparable to pre and post bloom fluxes at the PAP site (~5.34 mmol C m^{-2} d^{-1}), while POC flux in mid (19.8 mmol C m^{-2} d^{-1}) and late (26.6 mmol C m^{-2} d^{-1}) bloom on the NABE were analogous to those measured during the spring bloom (~23.69 and 14.70 mmol C m^{-2} d^{-1}) at the PAP site. *ThE* ratios for the NABE (75 m) and the PAP site were also similar with low *ThE* ratios corresponding to the early bloom period on NABE (7%) and pre and post bloom (6%) at the PAP site. Whereas high *ThE* ratios in the mid and late bloom on NABE (20% and 31%) were comparable to those estimated at the PAP site (~31% and 19%).

The combination of particle modification and decay, advection and variable sinking speeds has the potential to significantly modify the surface signal of POC flux relative to that measured at 3000 m. Surface POC fluxes (~100 m) extrapolated to 3000 m according to the Martin exponent (Martin et al., 1987) are compared to measured POC fluxes 24 days after the mid point of cruise sampling; i.e. the time it would take for particles sinking at 120 m day^{-1} (Lampitt, 1985) to reach a 3000 m trap. Lower extrapolated POC fluxes for July 2003 (0.27 mg m^{-2} d^{-1}) and May 2004 (0.29 mmol m^{-2} d^{-1}) (P300 and AMT 14 respectively) than measured fluxes at 3000 m (0.55 and 0.74 mmol m^{-2} d^{-1} respectively) suggest that particles were either settling slower than the assumed 120 m d^{-1} and or remineralised less than predicted by the Martin equation. In June 2004 (CD158) the extrapolated flux (1.28 mmol m^{-2} d^{-1}) was much higher than the measured flux (0.10 mmol m^{-2} d^{-1}) implying a remineralisation rate much higher than that predicted by the Martin exponent. However given the characteristics of the surface water ecosystem at the time (high f-ratios, *ThE* ratios, POC/^{234}Th ratios, mid spring bloom) it is more likely that the sediment trap is under sampling during a high flux period of large particles as has previously been suggested (Sherrell et al., 1998;

Takahashi et al., 2000; Lampitt et al., 2001). Alternatively, an incorrect assumption of steady state in the ^{234}Th flux model could have resulted in an overestimation of the surface POC flux estimates. If this is the case then although difficult to predict using a standardised sinking and remineralisation rate, seasonal and inter-annual variability in new production and surface export is translated into comparable variability at depth.

Thesis Summary

The central subtropical gyres of the open oceans have long been regarded as "marine deserts" with consistently low rates of primary production and export (Karl et al., 1996, Teira at al., 2005). However more recent studies have shown a large degree of variability in phytoplankton productivity which coupled with the immense size of the gyres, makes their overall contribution to global carbon export significant. Nevertheless, very little is known about the specific role of the north and south Atlantic gyres in the context of the global carbon budget. This study set out to address some of these shortcomings with the following aims in mind;

i) to measure how much photosynthetically fixed CO_2 is exported from the surface waters of the north and south Atlantic gyres and the efficiency of the biological pump in transferring this carbon to below the seasonal thermocline,
ii) to asses the degree of seasonal and temporal variability in carbon export,
iii) to test the "ballast hypothesis" by ascertaining whether a relationship exists between sizeable and efficient export of organic carbon and that of biominerals, and
iv) to determine the link between surface phytoplankton production and surface and deep carbon export and the spatial and temporal variability that regulates this flux.

To better constrain carbon and mineral export from the North and South Atlantic subtropical gyres, the above aims were addressed using the $^{234}Th/^{238}U$ disequilibrium technique to estimate fluxes of particulate organic carbon on three Atlantic Meridional Transect (AMT) cruises between ~ 50°S and ~ 50°N (AMT 12 in May/June 2003, AMT 13 in September/October 2003 and AMT 14 in April/June 2004). Simultaneous biomineral (calcite and opal) flux was estimated on AMT 14. Additional time series data was provided by 5 cruises to the PAP site (49° N 16.5° W) in the north east Atlantic in June/July 2003 to 2006. The export efficiency of the biological pump was determined by the amount of export relative to surface production and expressed as *ThE* ratio. Results from this study suggest the following;

i) Carbon export in the oligotrophic centres of the gyres was low and characterise tightly coupled regeneration based microbial food webs. The equatorial divergence and upwelling regions were characterised by a shallower surface mixed layer, increased NO_3 in subsurface waters and enhanced POC export. At the gyres' northern and southern temperate fringes, higher productivity is supported by increased nutrient supply from the deep ocean and POC export was substantial. The majority of *ThE* ratios are low and consistent with small cells and efficient regeneration of the microbial loop. However occasional high *ThE* ratios, particularly at the poleward edges of the oligotrophic gyres, suggests uncoupling of primary production and export. This points to the occurrence of pulsed high export events that may result from episodic nutrient loading processes associated with submesoscale features that significantly influence annual export.

ii) Seasonal variation between the two oligotrophic gyres showed more enhanced particle removal from surface waters in austral autumn compared to boreal spring. As export lags production, the higher flux results for autumn are attributed to the summer growth period. Despite relatively little difference between phytoplankton community structure and primary production between the cruises, ambient NO_3 concentrations, NO_3 uptake rates and POC fluxes for the entire AMT 14 transect were higher than those of AMT 12 and AMT 13. The reasons for such differences remain unclear but but provide a good focus for future research.

iii) Although the relationships observed between organic carbon and biomineral flux and the similarities in average *ThE* for the different particle types suggests a mechanistic relationship between carbon and biomineral export, this breaks down when viewed on a regional basis. Efficient carbon export from the euphotic zone appears less dependant on efficient biomineral export than on the mechanisms by which biominerals and POC become associated. These mechanisms are determined by latitudinal differences in the characteristics of the planktonic community composition (e.g. size spectra, taxa) and ecology (e.g. physiology, grazing pressure). Exceptions to the general pattern do however occur and effective ballasting by biominerals may enhance the efficient export of

carbon following pulsed high export events where the flux is likely dominated by senescent diatoms and or large aggregates that sink faster than the timescale for significant biomineral dissolution. Due to significant remineralisation of organic carbon relative to biominerals during sinking, opal and calcite are 'chemically' decoupled from organic carbon below the euphotic zone such that their potential for effective ballasting of the remaining organic carbon increases with depth.

iv) Inter-annual variability in the magnitude and efficiency of POC flux at the PAP site is governed by the timing of each cruise with respect to the seasonal development of the North Atlantic spring bloom and highlights the environmental controls on productivity and POC flux. POC flux and *ThE* over the summer season did not appear to be determined by net primary production or to the proportion of productivity based on new production (f-ratios). However the POC/^{234}Th ratio of the settling material did provide a good proxy for POC flux and *ThE* and emphasizes the important role that community structure plays in governing particle formation and the characteristics of the sinking flux, which ultimately determines the efficiency of carbon export. Higher export flux and efficiencies were associated with higher POC/^{234}Th ratios characteristic of larger cells such as diatoms that have faster settling rates allowing less time for remineralisation/dissolution, whereas lower POC/^{234}Th ratios characterise smaller cells and aggregates of the microbial loop where efficient remineralisation in surface waters leads to inefficient export. If indeed the 3000m sediment trap was under sampling during a high flux period of large cells in summer 2004 then seasonal and inter-annual variability in surface POC export appears to be translated into comparable variability at depth. However it is clear from deviations in standardised settling speeds and remineralisation rates that the composition of the settling flux will largely determine the efficiency with which it is exported to depth. Such variability is poorly constrained by existing data and not yet taken into account in ocean models however it has significant implications for carbon sequestration below 500m and therefore needs to be considered more fully in the context of global carbon export.

POC flux results compare well with other ^{234}Th based POC export studies carried out in the Atlantic Ocean. These include i) The JGOFS spring bloom study at the Antarctic Polar Front (APF) (Rutgers van der Loeff et al., 1997), ii) The subtropical and equatorial study by Charette and Moran, (1999), iii) the Bermuda Atlantic Time Series study (BATS) (Michaels et al., 1994) and iv) the JGOFS North Atlantic Bloom Experiment (NABE) (Buesseler et al., 1992). These direct measurements of POC export also fit modelled estimates from the Princeton General Circulation Model (a phosphorus-based nutrient cycling model) remarkably well throughout the transect despite the different approaches and time scales of the two methods. Time series analysis at the PAP site which sampled different stages of the North Atlantic spring bloom also compared well to a time series analysis of a spring bloom at the NABE. Pre and post bloom POC fluxes and *ThE* at the PAP site were lower yet comparable to early bloom conditions at the NABE, while mid and late bloom fluxes and *ThE* were similar at both sights.

References

Aiken, J., Bale, A.J., 2000. An introduction to the Atlantic Meridional Transect (AMT) Programme. Progress in Oceanography 45(3-4), 251-256.

Aiken, J., Rees, N., Hooker, S., Holligan, P., Bale, A., Robins, D., Moore, G., Harris, R., Pilgrim, D., 2000. The Atlantic Meridional Transect: overview and synthesis of data. Progress in Oceanography 45(3-4), 257-312.

Alldredge, A.L., Silver, M.W., 1988. Characteristics, dynamics and significance of marine snow. Progress in Oceanography 20, 41-82.

Alldredge, A.L., Gotschalk, C.C., 1989. Direct observations of the mass flocculation of diatom blooms:characteristics, settling velocities and formation of diatom aggregates. Deep-Sea Research 36, 159-171.

Alldredge, A.L., Jackson, G.A., 1995. Aggregation in marine systems. Deep-Sea Research II 42, 1-8.

Alvarado-Quiroz, N., Hung, C.C., Santschi, P.H., 2006. Binding of thorium(IV) to carboxylate, phosphate and sulfate functional groups from marine exopolymeric substances (EPS) Marine Chemistry 100(3-4), 337-353.

Amiel, D., Cochran, J.K., Hirschberg, D.J., 2002. $^{234}Th/^{238}U$ disequilibrium as an indicator of the seasonal export flux of particulate organic carbon in the North Water. Deep-Sea Research II 49, 5191-5209.

Anderson, T.R., Williams, P.J.L., 1999. A one-dimensional model of dissolved organic carbon cycling in the water column incorporating combined biological- photochemical decomposition. Global Biogeochemical Cycles 13(2), 337-349.

Antia, A.N., Koeve, W., Fischer, G., Blanz, T., Schulz-Bull, D., Scholten, J., Neuer, S., Kremling, K., Kuss, J., Peinert, R., Hebbeln, D., Bathmann, U., Conte, M., Fehner, U., Zeitzschel, B., 2001. Basin-wide particulate carbon flux in the Atlantic Ocean: regional export patterns and potential for atmospheric CO_2 sequestration. Global Biogeochemical Cycles 15, 845-862.

Antoine, D., Andre, J.M., Morel, A., 1996. Oceanic primary production 2. Estimation at global-scale from satellite (coastal zone colour scanner) chlorophyll. Global Biogeochemical Cycles 10, 57-69.

Armstrong, R.A., Lee, C., Hedges, J.I., Honjo, S., Wakeham, S.G., 2002. A new, mechanistic model for organic carbon fluxes in the ocean based on the quantitative association of POC with ballast minerals. Deep-Sea Research II 49, 219-236.

Arraes-Mescoff, R., Roy-Barman, M., Coppola, L., Tachikawa, K., Souhaut, M., Sempéré, R., Yoro, S., Jeandel, C., 2001. The behavior of Al, Mn, Ba, Sr, REE and Th isotopes during in vitro degradation of large marine particles. Marine

Chemistry 73, 1–19.

Arrigo, K.R., 2005. Marine microorganisms and global nutrient cycles. Nature 437(7057), 349-355.

Arrigo, K.R., Robinson, D.H., Worthen, D.L., Dunbar, R.B., DiTullio, G.R., VanWoert, M., Lizotte, M.P., 1999. Phytoplankton community structure and the drawdown of nutrients and CO2 in the Southern Ocean. Science 283(5400), 365-367.

Arrigo, K.R., Dunbar, R.B., Lizotte, M.P., Robinson, D.H., 2002. Taxon-specific differences in C/P and N/P drawdown for phytoplankton in the Ross Sea, Antarctica. Geophysical Research Letters 29(19), 44.1-44.4.

Azam, F., 1998. Microbial control of oceanic carbon flux: the plot thickens. Science 280, 694-696.

Azam, F., Fenchel, T., Field, J.G., Gray, J.S., Meyer-Reil, L.A., Thingstad, F., 1983. The ecological role of water-column microbes in the sea. Marine Ecology Progress Series 10, 257-263.

Bacon, M.P., Cochran, J.K., Hirschberg, D., Hammar, T.R., Fleer, A.P., 1996. Export flux of carbon at the equator during the EqPac time-series cruises estimated from 234Th measurements. Deep-Sea Research II 43(4-6), 1133-1153.

Baines, S.B., Pace, M.L., Karl, D.M., 1994. Why does the relationship between sinking flux and planktonic primary production differ between lakes and oceans? Limnology and Oceanography 39, 213-226.

Baker, E.T., Milburn, H.B., Tennant, D.A., 1988. Field assessment of sediment trap efficiency under varying flow conditions. Journal of Marine Research 46, 573–592.

Baker, A.R., Kelly, S.D., Biswas, K.F., Witt, M., Jickells, T.D., 2003. Atmospheric deposition of nutrients to the Atlantic Ocean. Geophysical Research Letters 30(24), 2296, doi:10.1029/2003GLO18518

Bakker, D.C.E., Watson, A.J., Law, C.S., 2001. Southern Ocean iron enrichment promotes inorganic carbon drawdown. Deep-Sea Research II 48, 2483-2507.

Bakker, D.C.E., Bozec, Y., Nightingale, P.D., Goldson, L.E., Messias, M.J., Baar, H.J.W., de, L., M.I., Skjelvan, I., Strass, V., Watson, A.J., 2005. Iron and mixing affect biological carbon uptake in SOIREE and EisenEx, two Southern Ocean iron fertilisation experiments. Deep-Sea Research I 51, 1001-1019.

Bakker, D.C.E., Boyd, P.W., Charette, M.A., Hall, J.A., Nodder, S.D., Safi, K., Singleton, R.J., Trull, T.W., Waite, A.M., Watson, A.J., Zeldis, J., Abraham, E.R., Law, C.S., Tanneberger, K., 2006. Matching carbon pools and fluxes for the Southern Ocean Iron Release Experiment (SOIREE). Deep-Sea Research I 52, 1941-1960.

Balch, W.M., Kilpatrick, K., 1996. Calcification rates in the equatorial Pacific along 140°W. Deep-Sea Research II 43, 971 - 993.

Balch, W.M., Drapeau, D.T., Fritz, J.J., 2000. Monsoonal forcing of calcification in the Arabian Sea. Deep-Sea Research II 47(7-8), 1301-1337.

Banse, K., 1982. algae and ciliates, and the role of marinc ciliates in the marine pelagial. Limnology and Oceanography 27, 1059-1071.

Banse, K., 1995. Zooplankton: pivotal role in the control of oceanic production. ICES. Journal of Marine Science 52, 265-277.

Barlow, R.G., Aiken, J., Holligan, P.M., Cummings, D.G., Maritorena, S., Hooker, S., 2002. Phytoplankton pigment and adsorption characteristics along meridional transects in the Atlantic Ocean. Deep-Sea Research I 47, 637-660.

Barlow, R.G., Aiken, J., Moore, G.F., Holligan, P.M., Lavender, S., 2004. Pigment adaptations in surface phytoplankton along the eastern boundary of the Atlantic Ocean. Marine Ecology Progress Series 281, 13-26.

Bates, T.S., Quinn, P.K., Coffman, D.J., Johnson, J.E., Miller, T.L., Covert, D.S., Wiedensohler, A., Leinert, S., Nowak, A., Neusuess, C., 2001. Regional physical and chemical properties of the marine boundary layer aerosol across the Atlantic during AEROSOLS99: an overview. Journal of Geophysical Research 106(20),767-782.

Bathmann, U.V., 1998. Ecology and biogeochemistry in the Atlantic sector of the Southern Ocean during austral spring: The first JGOFS expedition aboard RV Polarstern. Journal of Marine Systems 17, 77-85.

Baumann, K.H., Bockel, B., Frenz, M., 2004. Coccolith contribution to South Atlantic carbonate sedimentation. In Thierstein, H. R.Young, J. R. (Eds.), Coccolithophores; from molecular processes to global impact. Springer, New York, pp. 367-402.

Behrenfeld, M.J., Falkowski, P.G., 1997. Photosynthetic rates derived from satellite-based chlorophyll concentration. Limnology and Oceanography 42, 1-20.

Behrenfeld, M.J., Esaias, W.E., Turpie, K.R., 2002. Assesment of primary production at the global scale. In Williams, P. J. l. B., Thomas, D. N.Reynolds, C. S. (Eds.), Phytoplankton Productivity. Blackwell Science Ltd., Oxford, pp. 156-187.

Bellerby, R.G.J., Olsen, A., Furevik, T., L.G., A., 2005. Response of the surface ocean CO_2 system in the Nordic Seas and northern North Atlantic to climate change. In: Bellerby, R. G. J., Olsen, A., Furevik, T., L.G., A., Drange, H., Dokken, T., Gerdes, R.Berger, W. (Eds.), The Nordic Seas: An Integrated Perspective. Oceanography, Climatology, Biogeochemistry and Modelling.

Benitez-Nelson, C., Buesseler, K.O., Crosselin, G., 2000. Upper ocean carbon export, horizontal transport, and vertical eddy diffusivity in the southwestern Gulf of Maine. Continental Shelf Research 20, 707-736.

Benitez-Nelson, C., Buesseler, K.O., Karl, D.M., Andrews, J., 2001. A time-series study of particulate matter export in the North Pacific Subtropical Gyre based on ^{234}Th:^{238}U disequilibrium. Deep-Sea Research I 48, 2595-2611.

Bianchi, M., Feliatra, F., Tréguer, P., Vincendeau, M.-A., Morvan., J., 1997. Nitrification rates, ammonium and nitrate distribution in upper layers of the water column and in sediments of the Indian sector of the Southern Ocean. Deep-Sea Research II 44, 1017-1032.

Bidigare, R.R., Frank, T.J., Zastrow, C., Brooks, J.M., 1986. The distribution of algal chlorophylls and their degradation products in the Southern Ocean. Deep-Sea Research 33, 923-937.

Bidle, K.D., Azam, F., 1999. Accelerated dissolution of diatom silica by marine bacterial assemblages. Nature 397, 508-512.

Bidle, K.D., Manganelli, M., Azam, F., 2002. Regulation of oceanic silicon and carbon preservation by temperature control on bacterial activity. Science 298, 1980– 1984.

Billett, D.S.M., Lampitt, R.S., Rice, A.L., Mantoura, R.F.C., 1983. Seasonal sedimentation of phytoplankton to the deepsea benthos. Nature 302, 520–522.

Billett, D.S.M., Rice, A.L., 2001. The BENGAL programme: introduction and overview. Progress in Oceanography 50,13-25.

Bishop, J.K.B., 1989. Regional extremes in particulate matter composition and flux: effects on the chemistry of the ocean interior. In Berger, W. H., Smetacek, V. S.Wefer, G. (Eds.), Productivity of the ocean: Present and past. J. Wiley and Sons, Chichester, U.K., pp. 117-137.

Bishop, J.K., Edmond, J.M., Ketten, D.R., Bacon, M.B., Silker, W.B., 1977. The chemistry, biology and vertical flux of particulate matter from the upper 400m of the equatorial Atlantic Ocean. Deep-Sea Research I 24, 511-548.

Blain, S., Treguer, P., Belviso, S., Bucciarelli, E., Denis, M., Desabre, S., et al, 2001. A biogeochemical study of the island mass effect in the context of the iron hypothesis: Kerguelen Islands, Southern Ocean. Deep-Sea Research II 48(1), 163-187.

Boyd, P., Newton, P., 1995. Evidence of the potential influence of planktonic community structure on the interannual variability of particulate organic carbon flux. Deep-Sea Research I 42, 619–639.

Boyd, P.W., La Roche, J., Gall, M., Frew, R., McKay, R.M.L., 1999. The role of iron, light and silicate in controlling algal biomass in sub-Antarctic waters of SE

New Zealand. Journal of Geophysical Research 104, 13395-13408.

Boyd, P.W., Watson, A.J., Law, C.S., Abraham, E.R., Trull, T., Murdoch, R., Bakker, D.C.E., Bowle, A.R., Buesseler, K.O., Chang, H., Charette, M., Croot, P., Downing, K., Frew, R., Gall, M., Hadfield, M., Hall, J., Harvey, M., Jameson, G., LaRoche, J., Liddicoat, M., Ling, R., Maldonado, M.T., McKay, R.M., Nodder, S., Pickmere, S., Pridmore, R., Rintoul, S., Safi, K., Sutton, P., Strzepek, R., Tanneberger, K., Turner, S., Walte, A., Zeldis, J., 2000. A mesoscale phytoplankton bloom in the polar Southern Ocean stimulated by iron fertilisation. Nature 407, 695-702.

Boyd, P.W., Law, C.S., 2001. The Southern Ocean Iron Release Experiment (SOIREE)- introduction and summary. Deep-Sea Research II 48, 2425-2438.

Boyd, P.W., Jickell, T., Law, C.S., Blain, S., Boyle, E.A., Buesseler, K.O., Coale, K.H., Cullen, J.J., de Baar, H.J.W., Follows, M., Harvey, M., Lancelot, C., Levasseur, M., Owens, N.P.J., Pollard, R., Rivkin, R.B., Sarmiento, J., Schoemann, V., Smetacek, V., Takeda, S., Tsuda, A., Turner, S., Watson, A.J. 2007. Mesoscale Iron enrichment experiments 1993-2005: Synthesis and future directions. Science 315, 612-617.

Bracher, A.U., Kroon, B.M.A., Lucas, M.I., 1999. Primary production, physiological state and composition of phytoplankton in the Atlantic Sector of the Southern Ocean. Marine Ecology Progress Series 190, 1-16.

Broeker, W.S., Kaufman, A., Trier, R.M., 1973. The residence time of thorium in surface sea water and its implication regarding the rate of reactive pollutants. Earth and Planetary Science Letters 20, 35-44.

Broeker, W.S., Peng, T.H., Engh, R., 1980. Modeling the carbon system. Radiocarbon 22, 565-598.

Bronk, D.A., Glibert, P.M., Ward, B.B., 1994. Nitrogen uptake, dissolved organic nitrogen release and new production. Science 265, 1843-1846.

Brown, L., Sanders, R., Savidge, G., Lucas, C.H., 2003. The uptake of silica during the spring bloom in the Northeast Atlantic Ocean. Limnology and Oceanography 48(5), 1831-1845.

Brown, L., Sanders, R., Savidge, G., 2006. Relative mineralisation of C and Si from biogenic particulate matter in the upper water column during the North East Atlantic diatom bloom in spring 2001. Journal of Marine Systems 63, 79-90.

Bruland, K.W., Coale, K.H., 1986. Surface water $^{234}Th/^{238}U$ disequilibria: spatial and temporal variations of scavenging rates within the Pacific Ocean. In Burton, J.D. et al. (Eds.), Dynamic processes in the chemistry of the upper ocean, [NATO Conference Series IV]. Plenum Press, New York 17, pp. 159-172.

Brzezinski, M.A., 1985. The Si:C:N ratio of marine diatoms. Interspecific variability and the effect of some environmental variables. Journal of Phycology 21, 347-

357.

Brzezinski, M.A., Kosman, C.A., 1996. Silica production in the Sargasso sea during spring 1989. Marine Ecology Progress Series 142, 39-45.

Brzezinski, M.A., Phillips, D.R., 1997. Evaluation of ^{32}Si as a tracer for measuring silica production rates in marine waters. Limnology and Oceanography 42, 856-865.

Brzezinski, M.A., Alldredge, A.L., O'Bryan, L.M., 1997. Silica cycling within marine snow. Limnology and Oceanography 42, 1706– 1713.

Brzezinski, M.A., Pride, C.J., Franck, V.M., Sigman, D.M., Sarmiento, J.L., Matsumoto, K., Gruber, N., Rau, G.H., Coale, K.H., 2002. A switch from $Si(OH)_4$ to NO_3^- depletion in the glacial Southern Ocean. Geophysical Research Letters 29(12). doi:10.1029/2001GL014349.

Brzezinski, M.A., Dickson, M.L., Nelson, D.M., Sambrotto, R., 2003. Ratios of Si, C and N uptake by microplankton in the Southern Ocean. Deep-Sea Research II 50, 619-633.

Bucciarelli, E., Blain, S., Tréguer, P., 2001. Iron and manganese in the wake of the Kerguelen Islands (Southern Ocean). Marine Chemistry 73, 21-36.

Buesseler, K.O., 1991. Do upper-ocean sediment traps provide an accurate record of particle flux? Nature 353, 420-423.

Buesseler, K.O., 1998. The decoupling of production and particulate export in the surface ocean. Global Biogeochemical Cycles 12(2), 297-310.

Buesseler, K.O., Bacon, M.P., Cochran, J.K., Livingston, H.D., 1992a. Carbon and nitrogen export during the JGOFS North Atlantic Bloom Experiment estimated from ^{234}Th:^{238}U disequilibria. Deep-Sea Research I 39, 1115-1137.

Buesseler, K.O., Cochran, J.K., Bacon, M.B., Livingston, H.D., Casso, S.A., Hirschberg, D., Hartman, M.C., Fleer, A.P., 1992b Determination of thorium isotopes in seawater by non-destructive and radiochemical procedures. Deep-Sea Research I 39, 1103-1114

Buesseler, K.O., Michaels, A.F., Siegel, D.A., Knap, A.H., 1994. A three dimensional time dependent approach to calibrating sediment trap fluxes. Global Biogeochemical Cycles 8(2), 179-193.

Buesseler, K.O., Andrews, J.A., Hartman, M.C., Belastock, R., Chai, F., 1995. Regional estimates of the export flux of particulate organic carbon derived from thorium-234 during JGOFS EqPac program. Deep-Sea Research II 42(2-3), 777-804.

Buesseler, K.O., Lamborg, C.H., Boyd, P.W., Lam, P.J., Trull, T.W., Bidigare, R.R., Bishop, J.K., Casciotti, K.L., Dehairs, F., Elskens, M., Honda, M., Karl, D.M.,

Silver, M.W., Steinberg, D.K., Valdes, J., Van Mooy, B., Wilson, S., 1997. Revisiting carbon flux through the ocean's twilight zone. Science 316, 567-570.

Buesseler, K.O., Ball, L., Andrews, J., Benitez-Nelson, C., Belastock, R., Chai, F., Chao, Y., 1998. Upper ocean export of particulate organic carbon in the Arabian Sea derived from thorium-234. Deep-Sea Research II 45, 2461-2487.

Buesseler, K.O., Steinberg, D.K., Michaels, A.F., Johnson, R.J., Andrews, J.E., Valdes, J.R., Price, J.F., 2000. A comparison of the quantity and composition of material caught in a neutrally buoyant versus surface-tethered sediment trap. Deep-Sea Research I 47, 277-294.

Buesseler, K.O., Ball, L., Andrews, J., Cochran, J.K., Hirschberg, D., Bacon, M.B., Fleer, A.P., Brzezinski, M., 2001a. Upper ocean export of particulate organic carbon and biogenic silica in the Southern Ocean along 170°W. Deep-Sea Research II 48, 4275-4297.

Buesseler, K.O., Benitez-Nelson, C., van der Loeff, M.M.R., Andrews, J., Ball, L., Crossin, G., Charette, M.A., 2001b. An intercomparison of small- and large-volume techniques for thorium-234 in seawater. Marine Chemistry 74, 15-28.

Buesseler, K.O., Andrews, J.E., Pike, S.M., Charette, M.A., 2004. The Effects of Iron Fertilization on Carbon Sequestration in the Southern Ocean. Science 304, 414-417.

Buesseler, K.O., Andrews, J.E., Pike, S.M., Charette, M.A., Goldson, L.A., Brzezinski, M.A., Lance, V.P., 2005. Particle export during the Southern Ocean Iron Experiment (SOFeX). Limnology and Oceanography 50, 311-327.

Buesseler, K.O., Benitez-Nelson, C.R., Moran, S.B., Burd, A., Charette, M., Cochran, J.K., Coppola, L., Fisher, N.S., Fowler, S.W., Gardner, W.D., Guo, L.D., Gustafsson, O., Lamborg, C., Masque, P., Miquel, J.C., Passow, U., Santschi, P.H., Savoye, N., Stewart, G., Trull, T., 2006. An assessment of particulate organic carbon to thorium-234 ratios in the ocean and their impact on the application of ^{234}Th as a POC flux proxy. Marine Chemistry 100(3-4), 213-233.

Burd, A.B., Moran, S.B., Jackson, G.A., 2000. A coupled adsorption-aggregation model of the POC/^{234}Th ratio of marine particles. Deep-Sea Research I 47, 103-120.

Butman, C.A., Grant, W.D., Stolzenbach, K.D., 1986. Predictions of sediment trap biasis in turbulent flows: a theoretical analysis based on observations from the literature. Journal of Marine Research 44, 601-644.

Capone, D.G., Zehr, J.P., Paerl, H.W., Bergman, B., Carpenter, E.J., 1997. *Trichodesmium*, a globally significant marine cyanobacterium. Science 276,1221-1229.

Capone, D.G., Burns, J.A., Montoya, J.P., Subramaniam, A., Mahaffy, C., Gunderson, T., Michaels, A.F., Carpenter, E.J., 2005. Nitrogen fixation by *Trichodesmium* spp.: An important source of new nitrogen to the tropical and subtropical North Atlantic Ocean. Global Biogeochemical Cycles 19, doi:10.1029/2004GB002331.

Carpenter, E., Capone, D. (Eds.), 1983. Nitrogen in the Marine Environment, Academic Press, 900pp.

Charette, M.A., Moran, S.B., 1999. Rates of particle scavenging and particulate organic carbon export estimated using ^{234}Th as a tracer in the subtropical and equatorial Atlantic Ocean. Deep-Sea Research II 46, 885-906.

Charette, M.A., Buesseler, K.O., 2000. Does iron fertilisation lead to rapid carbon export in the Southern Ocean? Geochemical Geophysical Geosystems, 2000GC000069.

Charette, M.A., Moran, S.B., Pike, S.M., Smith, J.N., 2001. Investigating the carbon cycle in the Gulf of Maine using the natural tracer thorium 234. Journal of Geophysical Research 106, 11553-11579.

Charlson, R.J., Lovelock, J.E., Andreae, M.O., Warren, S.G., Andreae, M.D., 1987. Oceanic phytoplankton, atmospheric sulphur, cloud albedo and climate. Nature 326, 655-661.

Chase, Z., Anderson, R.F., Fleisher, M.Q., Kubik, P.W., 2002. The influence of particle composition and particle flux on scavenging of Th, Pa and Be in the ocean. Earth and Planetary Science Letters 204(1-2), 215-229.

Chen, J.H., Edwards, R.L., Wasserburg, G.J., 1986. ^{238}U, ^{234}U and ^{232}Th in seawater. Earth and Planetary Science Letters 80, 241-251.

Chrisholm, S.W., 1992. Phytoplankton size. In: Falkowski, P. G., Woodhead, A. G. (Eds.), Primary productivity and biogeochemical cycles in the sea, Plenum, pp. 213-237.

Christian, J.R., Verschell, M.A., Murtugudde, R., Busalacchi, A.J., McClain, C.R., 2002. Biogeochemical modelling of the tropical Pacific Ocean. I: Seasonal and interannual variability. Deep-Sea Research II 49, 509-543.

Claquin, P.V., Martin-Jézéquel, V., Kromkamp, J.C., Veldhuis, M.J.W., Kraay, G., 2002. Uncoupling of silicaon compared to carbon and nitrogen metabolisms, and the role of the cell cycle, in continuous cultures of *Thalassiosira pseudonana (Bacillariophyceae)* under light, nitrogen and phosphorous control. Journal of Phycology 38, 922-930.

Clegg, S.L., Witfield, M., 1990. A generalised model for the scavenging of trace metals in the open ocean, I, particle cycling. Deep-Sea Research I 37, 809-832.

Clegg, S.L., Bacon, M.P., Whitfield, M., 1991. Application of a generalized

scavenging model to thorium isotopes and particle data at equatorial and high-latitude sites in the Pacific Ocean. Journal of Geophysical Research 96, 20655-20670.

Coale, K.H., 1990. Labyrinth of doom: A device to minimize the "swimmer" component in sediment trap collections. Limnology and Oceanography 35(6), 1376-1381.

Coale, K.H., Bruland, K.W., 1985. ^{234}Th:^{238}U disequilibria within the California current. Limnology and Oceanography 30, 22-33.

Coale, K.H., Bruland, K.W., 1987. Oceanic stratified euphotic zone as elucidated by ^{234}Th:^{238}U disequilibria. Limnology and Oceanography 32, 189-200.

Coale, K.H., Johnson, K.S., Fitzwater, S.E., Gordon, R.M., Tanner, S., Chavez, F.P., Ferioli, L., Sakamoto, C., Rogers, P., Millero, F., Steinberg, P., Nightingale, P., Cooper, D., Cochlan, W.P., Kudela, R., 1996. A massive phytoplankton bloom induced by an ecosystem-scale fertilization experiment in the equatorial Pacific Ocean. Nature 383, 495-501.

Coale, K.H., Johnson, K.S., Chavez, F.P., Buesseler, K.O., Barber, R.T., Brzezinski, M.A., Cochlan, W.P., Millero, F.J., Falkowski, P.G., Bauer, J.E., Wanninkhof, R.H., Kudela, R.M., Altabet, M.A., Hales, B.E., Takahashi, T., Landry, M.R., Bidigare, R.R., Wang, X., Chase, Z., Strutton, P.G., Friederich, G.E., Gorbunov, M.Y., Lance, V.P., Hilting, A.K., Hiscock, M.R., Demarest, M., Hiscock, W.T., Sullivan, K.F., Tanner, S.J., Gordon, R.M., Hunter, C.N., Elrod, V.A., Fitzwater, S.E., Jones, J.L., Tozzi, S., Koblizek, M., Roberts, A.E., Herndon, J., et al. 2004. Southern ocean iron enrichment experiment: Carbon cycling in high- and low-Si waters. Science 304(5669), 408-414.

Cochlan, W.P., Harrison, P.J., Denman, K.L., 1991. Dial periodicity of nitrogen uptake by marine phytoplankton in nitrate-rich environments. Limnology and Oceanography 36(8), 1689-1700.

Cochran, J.K., Barnes, C., Achman, D., Hirschberg, D.J., 1995. Thorium-234/Uranium-238 disequilibrium as an indicator of scavenging rates and particulate organic carbon fluxes in the Northeast Water Polynya, Greenland. Journal of Geophysical Research 100, 4399-4410.

Cochran, J.K., Buesseler, K.O., Bacon, M.B., Livingston, H.D., 1993. Thorium isotopes as indicators of particle dynamics in the upper ocean: results from the JGOFS North Atlantic Bloom Experiment. Deep-Sea Research I 40, 1569-1595.

Cochran, J.K., Roberts, K.A., Barnes, C., Achman, D., 1997. Radionuclides as indicators of particle and carbon dynamics on the East Greenland Shelf. Germain, P. Guary, J.C., Guegueniat, P., Metivier, H. (Eds.), Radionuclides in the Oceans Conference 32, 129-136.

Cochran, J.K., Buesseler, K.O., Bacon, M.P., Wang, H.W., Hirschberg, D.J., Ball, L.,

Andrews, J., Crossin, G., Fleer, A.P., 2000. Short-lived thorium isotopes (^{234}Th, ^{228}Th) as indicators of POC export and particle cycling in the Ross Sea, Southern Ocean. Deep-Sea Research II 47, 3451-3490.

Coppola, L., Roy-Barman, M., Wassmann, P., Mulsow, S., Jeandel, C., 2002. Calibration of sediment traps and particulate organic carbon export using ^{234}Th in the Barents Sea. Marine Chemistry 80, 11–26.

Cota, G.F., Smith, W.O.J., Mitchell, B.G., 1994. Photosynthesis of *Phaeocystis* in the Greenland Sea. Limnology and Oceanography 39, 948-953.

Cote, B., Platt, T., 1984. Utility of the light-saturation curve as an operational model for quantifying the effects of environmental conditions on phytoplankton photosynthesis. Marine Ecology Progress Series 18, 57-66.

Cullen, J.J., 1991. Hypotheses to explain high-nutrient conditions in the open sea. Limnology and Oceanography 36, 1578-1599.

Dai, A., Fung, I.Y., Del Genio, A., 1997. Surface observed global land precipitation variations during 1900–88. Journal of Climatology 10 (11), 2943-2962.

Danovaro, R., Dell'Anno, A., Martorano, D., Parodi, P., Marrale, D., Fabiano, M., 1999. Seasonal variation in the biochemical composition of deep-sea nematodes: bioenergetic and methodological considerations. Marine Ecology Progress Series 179, 273–283.

Davenport, R., Neuer, S., Hernadez-Guerra, A., Rueda, M.J., Llinas, O., Fischer, G., Wefer, G., 1999. Seasonal and interannual pigment concentration in the Canary Island region from CZCS data and comparison with observations from the ESTOC. International Journal of Remote Sensing 20, 1419-1433.

Davison, I.R., 1991. Environmental effects on algal photosynthesis: temperature. Journal of Phycology 27, 2-8.

de Baar, H.J.W., Buma, A.G.J., Nolting, R.F., Cadee, G.C., Jacques, G., Treguer, P.J., 1990. On iron limitation in the Southern Ocean: Experimental observations in the Weddel and Scotia Seas. Marine Ecology Progress Series 65, 105-122.

de Baar, H.J.W., 1994. von Liebig's law of the minimum and plankton ecology (1899-1991). Progress in Oceanography 33, 347-386.

de Baar, H.J.W., De Jong, J.T.M., Bakker, D.C.E., Loscher, B.M., Veth, C., Bathmann, U., Smetacek, V., 1995. Importance of iron for plankton blooms and carbon dioxide draw-down in the Southern Ocean. Nature 373, 412-415.

de Baar, H.J.W., van Leeuwe, M.A., Scharek, R., Goeyens, L., Bakker, K.M.J., Fritsche, P., 1997. Nutrient anomalies in *Fragilariopsis kerguelensis* blooms, iron deficiency and the nitrate/phosphate ratio (A.C. Redfield) of the Antarctic Ocean. Deep-Sea Research II 44, 229-260.

de Baar, H.J.W., Boyd, P.W., 2000. The role of iron in plankton ecology and carbon dioxide transfer of the global oceans. In: Hanson, R. B., Ducklow, H. W., Field, J. G. (Eds.), The dynamic ocean carbon cycle: A midterm synthesis of the Joint Global Ocean Flux Study, International Geosphere Biosphere Programme Book Series Vol. 5, Cambridge University Press, Cambridge, pp. 61-140.

de Baar, H.J.W., Boyd, P.W., Coale, K.H., Landry, M.R., Tsuda, A., Assmy, P., Bakker, D.C.E., Bozec, Y., Barber, R.T., Brzezinski, M.A., Buesseler, K.O., Boye, M., Croot, P.L., Gervais, F., Gorbunov, M.Y., Harrison, P.J., Hiscock, W.T., Laan, P., Lancelot, C., Law, C.S., Levasseur, M., Marchetti, A., Millero, F.J., Nishioka, J., Nojiri, Y., Van Oijen, T., Riebesell, U., Rijkenberg, M.J.A., Saito, H., Takeda, S., Timmermans, K.R., Veldhuis, M.J.W., Waite, A.M., Wong, C.-S., M., Bugg, W., Efremenko, Y., Kamyshkov, Y., Kozlov, A., Nakamura, Y., Karwowski, H.J., Markoff, D.M., Nakamura, K., Rohm, R.M., Tornow, W., Wendell, R., Chen, M.-J., Wang, Y.-F., Piquemal, F., Wong, C.S.D.M., 2005. Synthesis of iron fertilization experiments: From the Iron Age in the Age of Enlightenment. Journal of Geophysical Research 110, C09S16, doi:10.1029/2004JC002601.

De La Rocha, C.L., Hutchins, D.A., Brzezinski, M.A., Zhang, Y., 2000. Effects of iron and zinc deficiency on the elemental composition and silica production by diatoms. Marine Ecology Progress Series 195, 71-79.

DeMaster, D.J., 1981. The Supply and Accumulation of Silica in the Marine Environment. Geochemica Cosmochemica Acta 45(10), 1715-1732.

DeMaster, D.J., Nelson, T.M., Harden, S.L., Nittrouer, C.A., 1991. The cycling and accumulation of biogenic silica and organic carbon in Antarctic deep-sea and continental margin environments. Marine Chemistry 35, 489-502.

Deuser, W.G., Jickells, T.D., King, P., Commeau, J.A., 1995. Decadal and annual changes in biogenic opal and carbonate fluxes to the deep Sargasso Sea. Deep-Sea Research I 42, 1923–1932.

Diaz, F., Raimbault, P., 2000. Nitrogen regeneration and dissolved organic nitrogen release during spring in a NW Mediterranean coastal zone (Gulf of Lions): implications for the estimation of new production. Marine Ecology Progress Series 197, 51- 65.

Doney, S.C., Lindsay, K., Moore, J.K., 2003. Global ocean carbon cycle modelling. In: Fasham, M. J. R. (Ed.), Ocean Biogeochemistry: The role of the ocean carbon cycle in global change. Springer-Verlag, Berlin, pp. 217-238.

Dore, J.E., Karl, D.M., 1996. Nitrification in the euphotic zone as a source for nitrite, nitrate, and nitrous oxide at station ALOHA. Limnology and Oceanography 41, 1619-1628.

Dring, M.J., 1990. Light harvesting and pigment composition in marine phytoplankton and macroalgae. In: Herring, P. J., Campbell, A. K., Whitfield,

M.Maddock, L. (Eds.), Light and life in the sea, Cambridge University Press, Cambridge, pp. 89-103.

Duce, R.A., Tindale, N.W., 1991. Atmospheric transport of iron and its deposition in the ocean. Limnology and Oceanography 36, 1715-1726.

Ducklow, H.W., Harris, R.P., 1993a. Introduction to the JGOFS North Atlantic Bloom Experiment. Deep-Sea Research II 40, 1-8.

Ducklow, H.W., Harris, R.P., 1993b. JGOFS: The North Atlantic Bloom Experiment [special issue]. Deep-Sea Research II 40, 1–641.

Ducklow, H.W., Steinberg, D.K., Buesseler, K.O., 2001. Upper Ocean Carbon Export and the Biological Pump. Oceanography 14(4), 50-58.

Dugdale, R.C., Goering, J.J., 1967. Uptake of new and regenerated forms of nitrogen in primary productivity. Limnology and Oceanography 12(2), 196-206.

Dugdale, R.C., Wilkerson, F.P., 1991. Low specific nitrate uptake rate: A common feature of high-nutrient, low-chlorophyll marine ecosystems. Limnology and Oceanography 36(8), 1678-1688.

Dugdale, R.C., Wilkerson, F.P., 1992. Nutrient limitation of new production in the sea. In: Falkowski, P.G., Woodhead, A.D. (Eds.), Primary productivity and biogeochemical cycles in the sea. Plenum, pp. 107-122.

Dugdale, R.C., Wilkerson, F.P., Barber, R.T., Chavez, F.P., 1992. Estimating new production in the equatorial Pacific Ocean at 150°W. Journal of Geophysical Research 97(C1), 681-686.

Dugdale, R.C., Wilkerson, F.P., Minas, H.J., 1995. The role of a silicate pump in driving new production. Deep-Sea Research I 42, 697–719.

Dugdale, R.C., Wilkerson, F.P., 1998. Silicate regulation of new production in the equatorial Pacific upwelling. Nature 391, 270-273.

Dunne, J.P., Murray, J.W., 1999. Sensitivity of ^{234}Th export to physical processes in the central equatorial Pacific. Deep-Sea Research I 46, 831-854.

Dunne, J.P., Murray, J.W., Rodier, M., Hansell, D.A., 2000. Export flux in the western and central equatorial Pacific: zonal and temporal variability. Deep-Sea Research I 47(5), 901-936.

Dyhram, S.T., Palenik, B., 2003. Characterisation of ectoenzyme activity and phosphate regulated proteins in the coccolithophorid *Emiliania huxleyi*. Journal of Planktonic Research 25, 1215-1225.

Eglinton, G., Elderfield, H., Whitfield, M., Williams, P.J.L.B., 1995. The role of the North Atlantic in the global carbon cycle: a discussion. Philosophical Transactions of the Royal Society of London Conference, B, 348(1324),

London: Royal Society.

Eppley, R.W., 1989. New Production: History, Methods and Problems. In: Berger, W. H., Smetacek, V. S.Wefer, G. (Eds.), Productivity of the Ocean: Present and Past. John Wiley and Sons, New York, pp. 85-97.

Eppley, R.W., Peterson, B.J., 1979. Particulat organic matter flux and planktonic new production in the deep ocean. Nature 282, 677-680.

Eppley, R.W., Renger, E.H., 1988. Nanomolar increase in surface layer nitrate concentrations following a small wind event. Deep-Sea Research 35, 1119-1125.

Esaias, W.E., Feldman, G.C., McClain, C.R., Elrod, J.A., 1986. Monthly satellite derived phytoplankton pigment distribution for the North Atlantic Ocean Basin. Eos 67, 835-837.

Falkowski, P.G., 1980. Light-shade adaptation in marine phytoplankton. In: Falkowski, P. G. (Ed.), Primary productivity in the sea. Plenum, New York, pp. 99-117.

Falkowski, P.G., 2000. Rationalising elemental ratios is unicellular algae. Journal of Phycology 16, 3-6.

Falkowski, P.G., Ziemann, D., Kolber, Z.S., Biefang, P.K., 1991. Nutrient pumping and phytoplankton response in a subtropical mesoscale eddy. Nature 352, 544-551.

Falkowski, P.G., Raven, J.A., 1997. Aquatic photosynthesis. Blackwell Science, Oxford.

Falkowski, P.G., Barber, R.T., Smetacek, V., 1998. Biogeochemical controls and feedbacks on ocean primary production. Science 281, 200-206.

Falkowski, P.G., Scholes, R.J., Boyle, E., Canadell, J., Canfield, D., Elser, J., Gruber, N., Hibbard, K., Högberg, P., Linder, S., Mackenzie, F.T., Moore III, B., Pedersen, T., Rosenthal, Y., Seitzinger, S., Smetacek, V., Steffen, W., 2000. The global carbon cycle: a test of our knowledge of earth as a system. Science 290, 291-296.

Falkowski, P.G., Laws, E.A., Barber, R.T., Murray, J.W., 2003. Phytoplankton and their role in primary, new and export production. In: Fasham, M. J. R. (Ed.), Ocean Biogeochemistry: The role of the ocean carbon cycle in global change, Springer-Verlag, Berlin, pp. 99-121.

Fanning, K.A., 1989. Influence of atmospheric pollution on nutrient limitation in the ocean. Nature 339, 460-463.

Feely, R.A., Sabine, C.L., Lee, K., Millero, F.J., Lamb, M.F., Greeley, D., Bullister, J.L., Key, R.M., Peng, T.H., Kozyr, A., Ono, T., Wong, C.S., 2002. I*n situ*

calcium carbonate dissolution in the Pacific Ocean. Global Biogeochemical Cycles 16, 1144.

Fernandez, E., Marañón, E., Moran, X.A.G., Serret, P., 2003. Potential causes for the unequal contribution of picophytoplankton to total biomass and productivity in oligotrophic waters. Marine Ecology Progress Series 254, 101-109.

Fernandez, C., Raimbault, P., in press. Nitrogen regeneration in the Northeast Atlantic Ocean and its impact on seasonal new, regenerated and export production. Marine Ecology Progress Series.

Fisher, N.M.U., Teyssie, J.L., Krishnaswami, S., Baskaran, M., 1987. Accumulation of Th, Pb, and Ra in marine phytoplankton and its geochemical significance. Limnology and Oceanography 32, 131-142.

Fowler, S.W., Knauer, G.A., 1986. Role of large particles in the transport of elements and organic compounds through the oceanic water column. Progress in Oceanography 16, 147-194.

Franck, V.M., Brzezinski, M.A., Coale, K.H., Nelson, D.M., 2000. Iron and silicic acid concentrations regulate Si uptake north and south of the Polar Frontal Zone in the Pacific Sector of the Southern Ocean. Deep-Sea Research II 47, 3315-3338.

Franck, V.M., Smith, G.J., Bruland, K.W., Brzezinski, M.A., 2005. Comparison of size-dependent carbon, nitrate, and silicic acid uptake rates in high- and low-iron waters. Limnology and Oceanography 50, 825-838.

Francois, R., Honjo, S., Krishfield, R., Manganini, S., 2002. Factors controlling the flux of organic carbon to the bathypelagic zone of the ocean. Global Biogeochemical Cycles 16, 1087-1107.

Fuji, M., Chai, F., 2005. Effects of biogenic silica dissolution on silicon cycling and export production. Geophysical Research Letters 32, L05617, doi:05610.01029/02004GL022054.

Fung, I.Y., Meyn, S.K., Tegen, I., Doney, S.C., John, J.G., Bishop, J.K.B., 2000. Iron supply and demand in the upper ocean. Global Biogeochemical Cycles 14, 281-295.

Gao, Y., kaufman, Y.J., Tanre, D., Kolber, D., Falkowski, P.G., 2001. Seasonal distribution of aeolian iron fluxes to the global ocean. Geophysical Research Letters 28, 29-32.

Garcon, V.C., Oschlies, A., Doney, S.C., McGillicuddy, D.J., Waniek, J., 2001. The role of mesoscale variability on plankton dynamics in the North Atlantic. Deep-Sea Research II 48, 2199-2226.

Gardner, W.D., 1980a. Sediment trap dynamics and calibration: a laboratory evaluation. Journal of Marine Research 38, 17-39

Gardner, W.D., 1980b. Field assessment of sediment traps. Journal of Marine Research 38, 41-52

Gardner, W.D., 1997. The flux of particles to the deep sea: methods, measurements, and mechanisms. Oceanography 10, 116-121.

Gardner, W.D., Richardson, M.J., Carlson, C.A., Hansell, D.A., Mishonov, A.V., 2003. Determining true particulate organic carbon: bottles, pumps and methodologies. Deep-Sea Research II 50, 655-692.

Garside, C., Garside, J.C., 1993. The f-ratio on 20 degrees W during the North Atlantic Bloom Experiment. Deep-Sea Research 40, 75– 90.

Geider, R.J., La Roche, J., 1994. The role of iron in phytoplankton photosynthesis, and the potential of iron limitation of primary productivity in the sea. Photosynthesis Research 39, 275-301.

Geider, R.J., La Roche, J., 2002. Redfield revisited: variability of C:N:P in marine microalgae and its biochemical basis. European Journal of Phycology 37, 1-17.

Gervais, F., Riebesell, U., Gorbunov, M.Y., 2002. Changes in primary productivity and chlorophyll a in response to iron fertilization in the Southern Polar Frontal Zone. Limnology and Oceanography 47, 1324-1335.

Gibb, S.W., Barlow, R.G., Cummings, D.G., Rees, N.W., Trees, C.C., Holligan, P., Suggett, D., 2000. Surface phytoplankton pigment distributions in the Atlantic Ocean: an assessment of basin scale variability between 50°N and 50°S. Progress in Oceanography 45, 339-368.

Glibert, P.M., Goldman, J.C., Carpenter, E.J., 1982a. Seasonal variations in the utilization of ammonium and nitrate by phytoplankton in Vineyard Sound, Massachusetts, USA. Marine Biology 70, 237-249.

Glibert, P.M., Lipschultz, F., McCarthy, J.J., Altabet, M.A., 1982b. Isotope dilution models of uptake and remineralization of ammonium by marine plankton. Limnology and Oceanography 27(4), 639-650.

Gnanadesikan, A., 1999. A global model of silicon cycling: sensitivity to eddy parameterization and dissolution. Global Biogeochemical Cycles 13, 199-220.

Goes, J.I., Saino, T., Oaku, H., Ishizaka, J., Wong, C.S., Nojiri, Y., 2000. Basin scale estimates of sea surface nitrate and new production from remotely sensed sea surface temperature and chlorophyll. Geophysical Research Letters 27, 1263–1266.

Gowing, M.M., Silver, M.W., 1985. Minipellets: a new abundant size class of marine fecal pellets. Journal of Marine Research 43, 395-418.

Graf, G., 1989. Pelagic–benthic coupling in a deep-sea benthic community. Nature 341, 437–439.

Graziano, L.M., Geider, R.J., Li, W.K.W., Olaizola, M., 1996. Nitrogen limitation of North Atlantic phytoplankton: analysis of physiological condition in nutrient enrichment experiments. Aquatic Microbial Ecology 11, 53-64.

Greene, R.M., Kolber, Z.S., Swift, D.G., Tindale, N.W., Falkowski, P.G., 1994. Physiological limitation of phytoplankton photosynthesis in the eastern equatorial Pacific determined from natural variability in the quantum yield of fluorescence. Limnology and Oceanography 39, 1061-1074.

Guo, L., Santschi, P.H., Baskaran, M., 1997. Interactions of thorium isotopes with colloidal organic matter in oceanic environments. Colloids and Surfaces. Physicochemical and Engineering Aspects 120, 255-271.

Guo, L., Hung, C.C., Santschi, P.H., Walsh, I.D., 2002a. ^{234}Th scavenging and its relationship to acid polysaccharide abundance in the Gulf of Mexico. Marine Chemistry 78(2-3), 103-119.

Guo, L., Santschi, P.H., Ray, S.M., 2002b. Metal partitioning between colloidal and dissolved phases and its relation with bioavailability to American oysters. Marine Environmental Research 54(1), 49-64.

Gust, G., Byrne, R.H., Bernstein, R.E., Betzer, P.R., Bowles, W., 1992. Particle flux and moving fluids: experience from synchronous trap collections in the Sargasso Sea. Deep-Sea Research 39, 1071-1083.

Gust, G., Michaelis, A.F., Johnson, R., Deuser, W.G., Bowles, W., 1994. Mooring line motions and sediment trap hydromechanics: *in situ* intercomparison of three common deployment designs. Deep-Sea Research I 41, 831–857.

Gustafsson, O., Gschwend, P.M., Buesseler, K.O., 1997a. Settling removal rates of PCBs into the northwestern Atlantic derived from ^{238}U-^{234}Th disequilibria. Environmental Science and Technology 31(12), 3544-3550.

Gustafsson, O., Haghseta, F., Chan, C., Macfarlane, J., Gschwend, P.M., 1997b. Quantification of the dilute sedimentary soot phase: implications for PAH speciation and bioavailability. Environmental Science and Technology 31(1), 203-209.

Gustafsson, O. Buesseler, K.O., Geyer, W.R., Moran, S.B. Gschwend, P.M. 1998. An assessment of the relative importance of horizontal and vertical transport of particle-reactive chemicals in the coastal ocean. Continental Shelf Research 18, 805-829.

Gustafsson, O., Widerlund, A., Andersson, P.S., Ingri, J., Roos, P., Ledin, A., 2000. Colloid dynamics and transport of major elements through a boreal river -- brackish bay mixing zone. Marine Chemistry 71(1-2), 1-21.

Gustafsson, O., Andersson, P., Roos, P., Kukulska, Z., Broman, D., Larsson, U., Hajdu, S., Ingri, J., 2004. Evaluation of the collection efficiency of upper ocean sub-photic-layer sediment traps: a 24-month *in situ* calibration in the open Baltic Sea using ^{234}Th. Limnology and Oceanography Methods 2, 62-74.

Haider, A.T., Thierstein, H.R., 2001. Coccolithophore dynamics off Bermuda (N. Atlantic). Deep-Sea Research II 48, 1925-1956.

Hall, I.R., Schmidt, S., McCave, I.N., Reyss, J.L., 2000. Particulate matter distribution and ^{234}Th/^{238}U disequilibrium along the Northern Iberian Margin: implications for particulate organic carbon export. Deep-Sea Research I 47, 557-582.

Hamm, C.E., Merkel, R., Springer, O., Jurkojc, P., Maier, C., Prechtel, K., Smetacek, V., 2003. Architecture and material properties of diatom shells provide effective mechanical protection. Nature 421, 841–843.

Hamner, W.M., Hamner, P.P., Strand, S.W., Gilmer, R.W., 1983. Behaviour of Antarctic krill, *Euphausia superba*; chemoreception, feeding, schooling and molting. Science 220, 433-435.

Hamner, W.M., Hamner, P.P., 2000. Behavior of Antarctic krill (*Euphausia superba*): schooling, foraging, and antipredatory behavior. Canadian Journal of Fisheries and Aquatic Sciences 57(3), 192-202.

Hansen, B., Bjornsen, P.K., Hansen, P.J., 1994. The size ratio between planktonic predators and their prey. Limnology and Oceanography 39, 395-403.

Hansen, F.C., Witte, H.J., Passarge, J., 1996. Grazing in the heterotrophic dinoflagellate *Oxyrrhis marina*: size selectivity and preference for calcified *Emiliania huxley*i cells. Aquatic Microbial Ecology 10, 307-313.

Harris, R.P., 1994. Zooplankton grazing on the coccolithophore *Emiliania huxleyi* cells. Aquatic Microbial Ecology 10, 307-313.

Harrison, W.G., Harris, L.R., Irwin, B.D., 1996. The kinetics of nitrogen utilization in the oceanic mixed layer: Nitrate and ammonium interactions at nanomolar concentrations. Limnology and Oceanography 41(1), 16-32.

Hart, T.J., 1934. On the phytoplankton of the southwest Atlantic and the Bellingshausen Sea. Discovery Reports 8, 1-268.

Herbland, A., Voituriez, B., 1979. Hydrological structure analysis for estimating the primary production in the tropical Atlantic Ocean. Journal of Marine Research 37, 87-101.

Herbland, A., Le Bouteiller, A., Raimbault, P., 1987. Does the nutrient enrichment of the equatorial upwelling influence the size structure of phytoplankton in the Atlantic Ocean? Oceanologica Acta, 6, 115-120.

Heywood, J.L., Zubkov, M.V., Tarran, G.A., Fuchs, B.M., Holligan, P.M., 2006.

Prokaryoplankton standing stocks in oligotrophic gyre and equatorial provinces of the Atlantic Ocean: Evaluation of inter-annual variability. Deep-Sea Research II 53, 1530-1547.

Higginbottom, I.R., Hosie, G.W., 1989. Biomass and population structure of a large aggregation of krill near Prydz Bay, Antarctica. Marine Ecology Progress Series 58(1-2), 197-203.

Hill, P.S., 1992. Reconciling aggregation theory with observed vertical fluxes following phytopklankton blooms. Journal of Geophysical Research 97, 2295-2308.

Hilton, J., Lishman, J.P., Mackness, S., Heaney, S.I., 1986. An automated method for the analysis of particulate carbon and nitrogen in natural waters. Hydrobilogica 141, 269-271.

Hoffert, M.I., Caldeira, K., Jain, A.K., Haites, E.F., Harvey, L.D.D., Potter, S.D., Schlesinger, M.E., Schneider, S.H., Watts, R.G., Wigley, T.M.L., Wuebbles, D.J., 1998. Energy implications of future stabilization of atmospheric CO_2 content. Nature 395, 881-884.

Hoffmann, L.J., Peeken, I., Lochte, K., Assmy, P., Veldhuis, M., 2006. Different reactions of Southern Ocean phytoplankton size classes to iron fertilization. Limnology and Oceanography 51(3), 1217-1229.

Holeton, C.L., Nedelec, F., Sanders, R., Brown, L., Moore, C.M., Stevens, D.P., Heywood, K.J., Statham, P.J., Lucas, C.H., 2005. Physiological state of phytoplankton communities in the Southwest Atlantic sector of the Southern Ocean, as measured by fast repetition rate fluorometry. Polar Biology 29(1), 44-52.

Holligan, P.M., Fernández, E., Aiken, J., Balch, W.M., Boyd, P., Burkill, P.H., Finch, M., Groom, S.B., Malin, G., Muller, K., Purdie, D.A., Robinson, C., Trees, C.C., Turner, S.M., van der Wal, P., 1993. A biogeochemical study of the coccolithophore, *Emiliania huxleyi*, in the North Atlantic. Global Biogeochemical Cycles 7, 879-900.

Holm-Hansen, O., 1985. Nutrient cycles in Antarctic marine ecosystems. In: Siegfried, W. R., Condy, P. R.Laws, R. M. (Eds.), Antarctic nutrient cycles and food webs. Springer-Verlag, Heidelberg, pp. 6-10.

Holm-Hansen, O., El-Sayed, S.Z., Franceschini, G.A., Cuhel, R.L., 1977. Primary production and the factors controlling phytoplankton growth in the Southern Ocean. In: Liano, G. A. (Ed.), Adaptations within Antarctic ecosystems, Smithsonian Institute, Washington, D.C., pp. 11-50.

Honjo, S., 1976. Coccoliths: Production, transportation and sedimentation. Marine Micropaleontology 39, 87-112.

Honjo, S., Manganini, S., Cole, J.J., 1982a. Sedimentation of biogenic matter in the

deep ocean. Deep-Sea Research I 29, 609-625.

Honjo, S., Manganini, S., Poppe, L.J., 1982b. Sedimentation of lithogenic particles in the deep ocean. Marine Geology 50, 199-220.

Honjo, S., Manganini, S.J., 1993. Annual biogenic particle fluxes to the interior of the North Atlantic Ocean; studied at 34EN 21EW and 48EN 21EW. Deep-Sea Research II 30, 587–607.

Hooker, S.B., Rees, N.W., Aiken, J., 2000. An objective methodology for identifying oceanic provinces. Progress in Oceanography 45, 313-338.

Houghton, J.T., Jenkins, G.J., Ephraums, J.J. (Eds.), 1996a. Climate Change: The IPCC Scientific Assessment. Cambridge University Press,Cambridge.

Houghton, J.T., Filho, L.G.M., Harris, C.N., Kattenberg, A., Maskell, K., 1996b. Climate change 1995: the science of climate change. Contribution of WGI to the Second Assessment Report of the Intergovernmental Panel on Climate Change. Press Syndicate of the University of Cambridge,USA.

Howarth, R., Ed, 1996. Nitrogen cycling in the North Atlantic ocean and its watersheds. Kluwer Academic,Boston, pp. Pages

Hudson, R.J.M., Morel, F.M.M., 1990. Iron transport in marine phytoplankton: kinetics of medium and cellular coordination reactions. Limnology and Oceanography 35, 1002-1020.

Hulburt, E.M., 1990. Description of phytoplankton and nutrients in spring in the western North Atlantic Ocean. Journal of Plankton Research 12, 1-28.

Hung, C.-C., Guo, L.D., Roberts, K.A., Santschi, P.H., 2004. Upper Ocean carbon flux determined by size-fractionated ^{234}Th data and sediment traps in the Gulf of Mexico. Geochemical Journals 38(6), 601-611.

Hurd, D.C., Theyer, F., 1977. Changes in physical and chemical properties of biogenic silica from Central Equatorial Pacific .2. Refractive-index, density, and water-content of acid-cleaned samples. American Journal of Science 277(9), 1168-1202.

Hurd, D.C., Birdwhistell, S., 1983. On producing a general model for biogenic silica dissolution. American Journal of Science 283, 1-28.

Huskin, I., Anadon, R., Wood-Walker, R.S., Harris, R.P., 2001. Basin-scale latitudinal patterns of copepod grazing in the Atlantic Ocean. Journal of Plankton Research 23, 1361-1371.

Hutchins, D.A., Bruland, K.W., 1998. Iron-limited diatom growth and Si : N uptake ratios in a coastal upwelling regime. Nature 393(6685), 561-564.

Hutchins, D.A., DiTullio, G.R., Bruland, K.W., 1993. Iron and regenerated

production: Evidence for biological iron recycling in two marine environments. Limnology and Oceanography 38, 495-508.

Ishikawa, Y., Kagaya, H., Saga, K., 2004. Biomagnification of ^{7}Be, ^{234}Th, and ^{228}Ra in marine organisms near the northern Pacific coast of Japan. Journal of Environmental Radioactivity 76, 103-112.

Isla, J.A., Llope, M., Anadon, R., 2004. Size-fractionated mesozooplankton biomass, metabolism and grazing along a 50°N-30°S transect of the Atlantic Ocean. Journal of Plankton Research 26, 1301-1313.

Ittekkot, V., 1993. The abiotically driven biological pump in the ocean and short-term fluctuations in atmospheric CO_2 contents. Global and Planetary Change 8, 17-25.

Jackson, G.A., 1990. A model of the formation of marine algal flocs by physical coagulation processes. Deep-Sea Research 37, 1197-1211.

Jacobson, D.M., Anderson, D.M., 1986. Thecate heterotrophic dinoflagellates: Feeding behaviour and mechanisms. Journal of Phycology 22, 249-258.

Jansen, H., Wolf Gladrow, D.A., 2001. Carbonate dissolution in copepod guts: A numerical model. Marine Ecology Progress Series 221, 199-207.

Jansen, H., Zeebe, R.E., Wolf Gladrow, D.A., 2002. Modelling dissolution of settling $CaCO_3$ in the ocean. Global Biogeochemical Cycles 16, doi: 10.1029/2000GB001279.

Jaques, G., 1983. Some ecophysiological aspects of the Antarctic phytoplankton. Polar Biology 2, 27-33.

Jaques, G., 1989. Primary production in the Antarctic Ocean during the austral summer. A review. Vie Milieu 39, 1-17.

Jeandel, C., Ruiz-Pino, D., Gjata, E., Poisson, A., Brunet, C., Charriaud, E., Dehairs, F., Delille, D., Fiala, M., Fravalo, C., Miquel, J.C., Par, Y.-H., Pondaven, P., Queguiner, B., Razouls, S., Shauer, B., Treguer, P., 1998. KERFIX, a time-series station in the Southern Ocean: a presentation. Journal of Marine Systems 17, 555-569.

Jickells, T.D., Newton, P.P., King, P., Lampitt, R.S., Boutle, C., 1996. A comparison of sediment trap records of particle fluxes from 19 to 48°N in the northeast Atlantic and their relation to surface water productivity. Deep-Sea Research I 43, 971–986.

Jickells, T.D., Spokes, L.J., 2001. Atmospheric iron inputs to the oceans. In: Turner, D. R.Hunter, K. (Eds.), The biogeochemistry of Iron in seawater, Wiley, Chichester, pp. 85-121.

Joos, F., Plattner, G.-K., Stocker, T.F., Marchal, O., Schmittner, A., 1999. Global

warming and marine carbon cycle feedbacks on future atmospheric CO_2. Science 284, 464-467.

Kamatani, A., 1982. Dissolution rates of silica from diatoms decomposing at various temperatures. Marine Biology 68, 91–98.

Karl, D.M., 1999. A Sea of Change: Biogeochemical Variability in the North pacific Subtropical Gyre. Ecosystems 2, 181-214.

Karl, D.M., Winn, C.D., 1991. A sea of change: Monitoring the ocean's carbon cycle. Environmental Science and Technology 25, 1976-1981.

Karl, D.M., Letelier, R.M., Hebel, D.V., Tupas, L.M., Dore, J., Christian, J., Winn, C.D., 1995. Ecosystem changes in the North Pacific subtropical gyre attributed to the 1991-92 El Nino. Nature 373, 230-234.

Karl, D.M., Lukas, R., 1996. The Hawaii Ocean Time-series (HOT) program: Background, rationale and field implementation. Deep-Sea Research II 43, 129-156.

Karl, D.M., Christian, J.R., Dore, J.E., Hebel, D.V., Letelier, R.M., Tupas, L.M., Winn, C.D., 1996. Seasonal and interannual variability in primary production and particle flux at Station ALOHA. Deep-Sea Research II 43(2-3), 539-568.

Karl, D., Letelier, R., Tupas, L., Dore, J., Christian, J., Hebel., D., 1997. The role of nitrogen fixation in biogeochemical cycling in the subtropical North Pacific Ocean. Nature 388(6642), 533-538.

Karl, D.M., Bidigare, R.R., Letelier, R.M., 2001. Long-term changes in plankton community structure and productivity in the subtropical North Pacific Ocean. Nature 388, 533-538.

Karl, D.M., Laws, E.A., Morris, P., Williams, P., Emerson, S., 2003. Metabolic balance of the open sea. Nature; 426(6962), 32-32.

Keeling, C.D., Bacastow, R.B., Carter, A.F., Piper, S.C., Whorf, T.P., Heinmann, M., Mook, W.G., Roeloffzen, H., 1989. A three-dimensional model of atmospheric CO_2 transport based on observed winds, 1, Analysis of observational data. In: Peterson, D. H. (Ed.), Aspects of climate variability in the Pacific and the western Americas, Geophys.Monogr. Ser.Vol. 55. AGU, Washington, D.C, pp. 165-236.

Keller, M.D., Bellows, W.K., Guillard, R.R.L., 1989. Dimethyl sulfide production in marine phytoplankton [American Chemical Society Symposium Series, 393]. In Saltzman, E.Cooper, J. (Eds.), Biogenic sulfur in the environment . American Chemical Society, Washington, DC, pp.167-182.

Kheshgi, H.S., Flannery, B.P., Hoffert, M.I., 1991. Marine biota effects on the compositional structure of the world oceans. Journal of Geophysical Research 96, 4957-4969.

Kiriakoulakis, K., Stutt, E., Rowland, S.J., Vangriesheim, A., Lampitt, R.S., Wolff, G.A., 2001. Controls on the organic chemical composition of settling particles in the Northeast Atlantic Ocean. Progress in Oceanography 50, 65–87.

Kirk, J.T.O., 1994. Light and photosynthesis in aquatic ecosystems (2nd Edition). Cambridge University Press,Cambridge.

Kirkwood, D.S., 1989. Simultaneous determination of selected nutrients in seawater. Paper presented at the International Council for the Exploration of the Sea. Contribution to Hydrography Committee, C.M.1989/C:29, Ref. E, 12pp. The Haugue.

Klaas, C., Archer, D.E., 2002. Association of sinking organic matter with various types of mineral ballast in the deep sea: Implications for the rain ratio. Global Biogeochemical Cycles 16, 1116, 2002.

Klausmeier, C.A., Litchman, E., Levin, S.A., 2004. Phytoplankton growth and stoichiometry under multiple nutrient limitation. Limnology and Oceanography 49, 1463-1470.

Kleypas, J.A., Buddemeier, R.W., Archer, D., Gattuso, J.-P., Langdon, C., Opdyke, B.N., 1999. Geochemical consequences of increased atmospheric carbon dioxide on coral reefs. Science 284, 118-120.

Knauer, G.A., Karl, D.M., Martin, J.H., Hunter, C.N., 1984. *In situ* effects of selected preservatives on total carbon, nitrogen and metals collected in sediment traps. Journal of Marine Research 42(2), 445-462.

Knox, G.A., 1994. Phytoplankton and primary production. In: Studies in Polar Research; the biology of the Ocean. Cambridge University Press, London, pp. 13-39.

Koeve, W., 2001. Wintertime nutrients in the North Atlantic - new approaches and implications for new production estimates. Marine Chemistry 74(4), 245-260.

Koike, I., Ronner, U., Holm-Hansen, O., 1981. Microbial nitrogen metabolism in the Scotia Sea. Antarctic Journal 16, 165-166.

Koike, I., Holm-Hanson, O., Biggs, D.C., 1986. Inorganic nitrogen metabolism by Antarctic phytoplankton with special reference to ammonium cycling. Marine Ecology Progress Series 30, 105-116.

Korb, R., Whitehouse, M., 2004. Contrasting primary production regimes around South Georgia, Southern Ocean: large blooms versus high nutrient, low chlorophyll waters. Deep-Sea Research I 51, 721-738.

Kortzinger, A., Schulz-Bull, D.E., Petrick, G., Duinker, J.D., 1994. Evidence for dissolution of fatty acids in sediment traps: impacts on flux estimates. Journal of Geophysical Research 99, 3407-3415.

Krishnaswami, S., Baskaran, M., Fowler, S.W., Heyraud, M., 1985. Comparative role of salps and other zooplankton in the cycling and transport of selected elements and natural radionuclides in Mediterranean waters. Biogeochemistry 1, 335-360.

Kudo, I., Noiri, Y., Imai, K., Nojiri, Y., Nishioka, J., Tsuda, A., 2005. Primary productivity and nitrogenous nutrient assimilation dynamics during the Subarctic Pacific Iron Experiment for Ecosystem Dynamics Study. Progress in Oceanography 64, 207-221.

Kuypers, M.M.M., Sliekers, A.O., Lavik, G., Schmid, M., Jørgensen, B.B., Kuenen, J.G., Sinninghe Damsté, J.S., Strous, M., Jetten, M.S.M., 2003. Anaerobic ammonium oxidation by Anammox bacteria in the Black Sea. Nature 422, 608–611.

La Roche, J., Breitbarth, E., 2005. Importance of diazotrophs as a source of new nitrogen in the ocean. Journal of Sea Research 53, 67-91.

Lam, P.J., Bishop, J.K., in press. High biomass low export regimes in the Southern Ocean. Deep-Sea Research II.

Lampitt, R.S., 1985. Evidence for the seasonal deposition of detritus to the deep-sea floor and its subsequent resuspension. Deep-Sea Research 32, 885–897.

Lampitt, R.S., Antia, A., 1997. Particle flux in deep seas: regional characteristics and temporal variability. Deep-Sea Research I 44, 1377-1403.

Lampitt, R.S., Bett, B.J., Kiriakoulakis, K., Popova, E.E., Ragueneau, O., Vangriesheim, A., Wolff, G.A., 2001. Material supply to the abyssal seafloor in the Northeast Atlantic. Progress in Oceanography 50, 27–63.

Landry, M.R. Barber, R.T., Bidigare, R.R., Chai, Fei., Coale, K.H., Dam, H.G., Lewis, M.R., Lindley, S.T., McCarthy, J.J., Roman, M.R., Stoecker, D.K., Verity, P.G., White, J.R., 1997. Iron and grazing constraints on primary production in the central equatorial Pacific: An EqPac synthesis. Limnology and Oceanography 42(3), 405-418.

Laws, E.A., Falkowski, P.G., Smith, W.O., Ducklow, H., McCarthy, J.J., 2000. Temperature effects on export production in the open ocean. Global Biogeochemical Cycles 14(4), 1231-1246.

Lecourt, M., Muggli, D.L., Harrison, P.J., 1996. Comparison of growth and sinking rates of non-coccolith- and coccolith-forming strains of *Emiliania huxleyi* (*Prymnesiophyceae*) grown under different irradiance and nitrogen sources. Journal of Phycology 32, 17-21.

Lee, C., Wakeham, S.G., Hedges, J.I., 1988. The measurement of oceanic particle fluxes - are swimmers a problem. Oceanography 1, 234-236.

Lee, T., Barg, E., Lal, D., Azam, F., 1993. Bacterial scavenging of ^{234}Th in surface ocean waters. Marine Ecology Progress Series 96, 109-116.

Lewin, J.C., 1961. The dissolution of silica from diatom walls. Geochemica Cosmochemica Acta 21, 182–198.

Li, X.S., Berger, A., Loutre, M.F., 1998. CO_2 and northern hemisphere ice volume variations over the middle and late quaternary. Climate Dynamics 14, 537-544.

Lipschultz, F., 2001. A time-series assessment of the nitrogen cycle at BATS. Deep-Sea Research II 48, 1897-1924.

Liu, Z., Stewart, G., Cochran, J.K., Lee, C., Armstrong, R.A., Hirschberg, D., Gasser, B., Miquel, J.C., 2005. Why do POC concentrations measured using Niskin bottle collections differ from those using *in situ* pumps? Deep-Sea Research I 52, 1324-1344.

Lochte, K., Duclow, H.W., Fasham, M.J.R., Steinen, C., 1993. Plankton succession and carbon cycling at 47°N 20°W during the JGOFS North Atlantic Bloom Experiment. Deep-Sea Research II 40, 91-114.

Lochte, K., Anderson, R., Francois, R., Jahnke, R.A., Shimmield, G., Vetrov, A., 2003. Benthic processes and the burial of carbon. In: Fasham, M. J. R. (Ed.), Ocean biogeochemistry: The role of the ocean carbon cycle in global change, Springer-Verlag, Berlin, pp. 195-216.

Longhurst, A., 1993. Seasonal cooling and blooming in tropical oceans. Deep-Sea Research II 40, 2145-2165.

Longhurst, A. (Ed.). 1998. Ecological geography of the sea. CA, Academic Press, San Diego.

Longhurst, A.R., Sathyendranath, S., Platt, T., Caverhill, C., 1995. An estimate of global primary production in the ocean from satellite radiometer data. Journal of Planktonic Research 17, 1245-1271.

Losno, R., Bergametti, G., Carlier, P., 1992. Origins of atmospheric particulate matter over the North Sea and the Atlantic Ocean. Journal of Atmospheric Chemistry 15, 333-352.

Louanchi, F., Najjar, R.W., 2000. A global monthly mean climatology of phosphate, nitrate, and silicate in the upper ocean: spring-summer production and summer remineralisation. Global Biogeochemical Cycles 14, 959-977.

Lucas, M., Seeyave, S., Sanders, R., Moore, M., Williamson, R., in press. New and regenerated production during the Crozex study. Deep-Sea Research II.

Madin, L.P., 1982. Production, composition and sedimentation of salp fecal pellets in oceanic waters. Marine Biology 67, 39-45.

Malin, G., 1997. Sulphur, climate and the microbial maze. Nature 387, 857-859.

Malone, T.C., Neale, P.J., 1981. Parameters of light dependent photosynthesis for phytoplankton size fractions in temperate estuarine and coastal environments. Marine Biology 61, 289-297.

Manabe, S., Stouffer, R.J., 1993. Century-scale effects of increased atmospheric CO_2 on the ocean-atmosphere system. Nature 364(6434), 215-218.

Marañón, E., Holligan, P.M., Varela, M., Mourino, B., Bale, A.J., 2000. Basin-scale variability of phytoplankton biomass, production and growth in the Atlantic Ocean. Deep-Sea Research I 47(5), 825-857.

Marañón, E., Holligan, P.M., Barciela, R., González, N., Mouriño, B., Pazó, M.J., Varela, M., 2001. Patterns of phytoplankton size structure and productivity in contrasting open-ocean environments. Marine Ecology Progress Series 216, 43-56.

Margalef, R., 1978. Life-forms of phytoplankton as survival alternatives in an unstable environment. Oceanologica Acta, 1, 493-509.

Martin, J.H., Knauer, G.A., Karl, D.M., Broenkow, W.W., 1987. VERTEX: carbon cycling in the northeast Pacific. Deep-Sea Research I 34, 267-285.

Martin, J.H., Gordan, R., Fitzwater, S., Brokenkow, W., 1989. VERTEX: phytoplankton/iron studies in the Gulf of Alaska. Deep-Sea Research 36, 649-680.

Martin, J.H., Fitzwater, S., Gordan, R.M., 1990. Iron deficiency limits phytoplankton growth in Antarctic waters. Global Biogeochemical Cycles 4, 5-13.

Martin, J.H., Fitzwater, S.W., Gordon, R.M., 1991. The case for Iron. Limnology and Oceanography 36(8), 1793-1802.

Martin, J.H., Fitzwater, S.E., Gordan, R.M., Hunter, C.N., Tanner, S.J., 1993. Iron, primary production and carbon nitrogen flux studies during the JGOFS North Atlantic bloom experiment. Deep-Sea Research II 40, 115-134.

Martin-Jézéquel, V., Hildebrand, M., Brzezinski, M.A., 2000. Silicon metabolism in diatoms: Implications for growth. Journal of Phycology 36, 821-840.

Marty, J.C., Chiaverini, M.D., Pizay, M.D., Avril, B., 2001. Seasonal and interannual dynamics of nutrients and phytoplankton pigments in the Western Mediterranean Sea at the DYFAMED time-series station (1991-1999). Deep-Sea Research II 49, 1965-1985.

Matsumoto, E., 1975. ^{234}Th-^{238}U radioactive disequilibrium in the surface layer of the ocean. Geochemica Cosmochemica Acta 39, 205-212.

McCarthy, J.J., Taylor, W.R., Taft, J.L., 1977. Nitrogenous nutrition of the phytoplankton in the Cheasapeake Bay. 1. Nutrient availability and phytoplankton preferences. Limnology and Oceanography 22(6), 996-1011.

McClain, C.R., Signorini, S.R., Christian, J.R., 2004. Subtropical gyre variability observed by ocean-colour satellites. Deep-Sea Research II 51, 281-301.

McGillicuddy, D.J., Jr., Robinson, A.R., 1997. Eddy-induced nutrient supply and new production in the Sargasso Sea. Deep-Sea Research I 44(8), 1427-1450.

Michaels, A.F., Silver, M.W., Gowing, M.M., Knauer, G.A., 1990. Cryptic zooplankton "swimmers" in upper ocean sediment traps. Deep-Sea Research 37(1285-1296).

Michaels, A.F., Bates, N.R., Buesseler, K.O., Carlson, C.A., Knap, A.H., 1994. Carbon-cycle imbalances in the Sargasso Sea. Nature 372, 537-540.

Michaels, A.F., Knap, A.H., 1996. Overview of the U.S. JGOFS Bermuda Atlantic Time-series Study and the Hydrostation S program. Deep-Sea Research II 43(2-3), 157-198.

Mikaloff-Fletcher, S.E., Gruber, N., Jacobson, A.R., Doney, S.C., Dutkiewicz, S., Gerber, M., Follows, M., Joos, F., Lindsay, K., Menemenlis, D., Mouchet, A., Mueller, S.A., Sarmiento, J.L., 2006. Inverse estimates of anthropogenic CO_2 uptake, transport, and storage by the ocean. Global Biogeochemical Cycles 20, GB2002, doi:2010.1029/2005GB002530.

Miller, L.A., Sværen, I., 2003. ^{234}Th distributions in coastal and open ocean waters by non-destructive ß-counting. Journal of Radioanalytical and Nuclear Chemistry 256, 431-444.

Mills, M.M., Ridame, C., Davey, M., La Roche, J., Geider, R.J., 1994. Iron and phosphorus co-limit nitrogen fixation in the eastern tropical North Atlantic. Nature 429, 292-294.

Milliman, J.D., Troy, P.J., Balch, W.M., Adams, A.K., Li, Y.-H., Mackenzie, F.T., 1999. Biologically mediated dissolution of calcium carbonate above the chemical lysocline? Deep-Sea Research I 46, 1653-1669.

Mills, M.M., Ridame, C., Davey, M., Roche, J.L., Geider, R.J., 2004. Iron and phosphorous co-limit nitrogen fixation in the eastern tropical North Atlantic. Nature 429, 292-294.

Minas, H.J., Minas, M., Packard, T., 1986. Productivity in upwelling areas deduced from hydrographic and chemical fields. Limnology and Oceanography 31, 1182-1206.

Mitchell, J.F.B., Johns, T.C., Gregory, J.M., Tett, S.F.B., 1995. Climate response to increasing levels of greenhouse gases and sulphate aerosols. Science 376, 501-504.

Moore, J.K., Abbott, M.R., 2002. Surface chlorophyll concentrations in relation to the Antarctic Polar Front: seasonal and spatial patterns from satellite observations. Journal of Marine Systems 37, 69-86.

Moore, C.M., Mills, M.M., Milne, A., Langlois, R., Achterberg, E.P., Lochte, K., Geider, R.J., La Roche, J., 2006. Iron limits primary productivity during spring bloom development in the central North Atlantic. Global Change Biology 12, 626-634.

Moore, M.C., Seeyave, S., Hickman, A.E., Allen, J.T., Lucas, M.I., Planquette, H., Pollard, R., Poulton, A.J., in press. Iron-light interactions during the CROZet natural iron bloom and EXport experiment (CROZEX) I: phytoplankton growth and photophysiology. Deep-Sea Research II.

Moore, M.C., Hickman, A.E., Poulton, A.J., Seeyave, S., Lucas, M.I., in press. Iron-light interactions during the CROZet natural iron bloom and Export experiment (CROZEX) II: taxonomic responses and elemental stoichiometry. Deep-Sea Research II.

Moran, S.B., Buesseler, K.O., 1993. Size-fractionated ^{234}Th in continental shelf waters off New England: implications for the role of colloids in oceanic trace metal scavenging. Journal of Marine Research 51, 893-922.

Moran, S.B., Charette, M., Pike, S.M., Wicklund, C.A., 1999. Differences in seawater particulate organic carbon concentration in samples collected using small-volume and large-volume methods: the importance of DOC adsorption to the filter blank. Marine Chemistry 67, 33-42.

Moran, S.B., Weinstein, S.E., Edmonds, H.N., Smith, J.N., Kelly, R.P., Pilson, M.E., Harrison, W.G., 2003. Does ^{234}Th/^{238}U disequilibrium provide an accurate record of the export flux of particulate organic carbon from the upper ocean? Limnology and Oceanography 48(3), 1018-1029.

Moriceau, B., Ragueneau, O., Garvey, M., Passow, U., 2007. Evidence for reduced biogenic silica dissolution rates in diatom aggregates Marine Ecology Progress Series 333, 129-142.

Mortlock, R.A., Charles, C.D., Froelich, P.N., Zibello, M.A., Saltzmann, J., Hayes, J.D., Burckle, L.H., 2001. Evidence for lower productivity in the Antarctic Ocean during the last glaciation. Nature 351, 220-223.

Mouriño, B., Fernández, E., Etienne, H., Hernández, F., Giraud, S., 2003. Significance of cyclonic STORM (Sub-Tropical Oceanic Rings of Magnitude) eddies for the carbon budget of the euphotic layer in the subtropical NE Atlantic. Journal of Geophysical Research 108(C12), 3383.

Mouriño, B., Fernández, E., Alves, M., 2004. Thermohaline structure, ageostrophic vertical velocity fields and phytoplankton distribution and production in the North East Atlantic subtropical front. Journal of Geophysical Research 109,

C04020.

Murray, J., Renard, A.F., 1981. Report of deep-sea deposits. In: Reports on the Scientific Results of the Voyage of the HMS Challenger, London.

Murray, J.W., Downs, J.N., Strom, S., Wei, C., Jannasch, H.W., 1989. Nutrient assimilation, export production and ^{234}Th scavenging in the eastern equatorial Pacific. Deep-Sea Research I 36(10), 1471-1489.

Murray, J.W., Young, J., Newton, J., Dunne, J., Chapin, T., Paul, B., 1996. Export flux of particulate organic carbon from the central equatorial pacific determined using a combined drifting trap-^{234}Th approach. Deep-Sea Research II 43, 1095-1132.

Najjar, R.W., Sarmiento, J.L., Toggweiler, J.R., 1992. Downward transport and fate of organic matter in the ocean: simultaneous with a general circulation model. Global Biogeochemical Cycles 6, 45-76.

Nejstgaard, J.C., Witte, H.J., van der Wal, P., Jacobsen, A., 1994. Copepod grazing during a mesocosm study of an *Emiliania huxleyi* (*Prymnesiophyceae*) bloom. Sarsia 79, 369-377.

Nelson, D.M., Goering, J.J., 1978. Assimilation of silicic acid by phytoplankton in the Baja California and northwest Africa upwelling systems. Limnology and Oceanography 23, 508-517.

Nelson, D.M., Smith, W.O., 1991. Sverdrup re-visited: critical depths, maximum chlorophyll levels, and the control of Southern Ocean productivity by the irradiance-mixing regime. Limnology and Oceanography 36, 1650-1661.

Nelson, D.M., Treguer, P., 1992. Role of silicon as a limiting nutrient to Antarctic diatoms: Evidence from kinetic studies in the Ross Sea ice-edge zone. Marine Ecology Progress Series 80, 255-264.

Nelson, D.M., Treguer, P., Brzezinski, M.A., Leynaert, A., Queguiner, B., 1995. Production and dissolution of biogenic silica in the ocean: Revised global estimates, comparison with regional data and relationship to biogenic sedimentation. Global Biogeochemical Cycles 9, 359-372.

Nelson, D.M., Brzezinski, M.A., 1997. Diatom growth and productivity in an oligotrophic mid-ocean gyre: A 3-yr record from the Sargasso Sea near Bermuda. Limnology and Oceanography 42, 473-486.

Nelson, D.M., Brzezinski, M.A., Sigmon, D.E., Franck, V.M., 2001. A seasonal progression of Si limitation in the Pacific sector of the Southern Ocean. Deep-Sea Research II 48, 3973-3995.

Newton, P.P., Lampitt, R.S., Jickells, T.D., King, P., Boutle, C., 1994. Temporal and spatial variability of biogenic particle fluxes during the JGOFS northeast Atlantic process studies at 47°N, 20°W. Deep-Sea Research I 41, 1617-1642.

Niven, S.E.H., Kepkay, P.E., Boraie, A., 1995. Colloidal organic carbon and colloidal ^{234}Th dynamics during a coastal phytoplankton bloom. Deep-Sea Research II 42, 257–273.

Noji, T.T., Bathmann, U.V., von Bodungen, B., Voss, M., Antia, A., Krumbholz, M., Klein, B., Peeken, I., CI-M, N., Rey, F., 1997. Clearance of picoplankton-sized particles and formation of rapidly sinking aggregates by the pteropod *Limacina retroversa*. Journal of Plankton Research 19, 863-875.

Officer, C.B., Ryther, J.H., 1980. The possible importance of silicon in marine eutrophication. Marine Ecology Progress Series 3, 83–91.

Olson, R.J., 1981. Differential photoinhibition of marine nitrifying bacteria: a possible mechanism for the formation of the primary nitrite maximum. Journal of Marine Research 39, 227-238.

Osthols, E., 1995. Thorium sorption on amorphous silica. Geochemica Cosmochemica Acta 59, 1235-1249.

Owens, N.J.P., Priddle, J., Whitehouse, M.J., 1991. Variations in the phytoplanktonic nitrogen assimilation around South Georgia and in the Bransfield Strait (Southern Ocean). Marine Chemistry 35, 287-304.

Painter, S.C., Sanders, R., Waldron, H., Lucas, M., Woodward, E.M.S., Chamberlain, K., in press. Nitrate uptake along repeat meridional transects of the Atlantic Ocean. Journal of Marine Systems.

Palter, J.B., Lozier, M.S., Barber, R.T., 2005. The effect of advection on the nutrient reservoir in the North Atlantic subtropical gyre. Nature 437, 687-692.

Parsons, T., Takahashi, T., Hargrave, B., 1984. Biological oceanographic processes. Pergamon, New York.

Passow, U., 2002. Transparent exopolymer particles (TEP) in aquatic environments. Progress in Oceanography 55(3-4), 287-333.

Passow, U., 2004. Switching perspectives: Do mineral fluxes determine particulate organic carbon fluxes or visa versa? Geochemical Geophysical Geosystems 5, Q04002 doi: 04010.01029/02003GC000670.

Passow, U., Alldredge, A.L., Logan, B.E., 1994. The role of particulate carbohydrate exudates in the flocculation of diatom blooms. Deep-Sea Research I 41(2), 335-357.

Passow, U., Engel, A., Ploug, H., 2003. The role of aggregation for the dissolution of diatom frustules. FEMS Microbiology Ecology 46, 247-255.

Passow, U., De La Rocha, C.L., 2006. Accumulation of mineral ballast on organic aggregates. Global Biogeochemical Cycles 20, GB1013, doi:1010.1029/2005

GB002579.

Perez, V., Fernandez, E., Maranon, E., Serret, P., Garcia-Soto, C., 2005a. Seasonal and interannual variability of chlorophyll *a* and primary production in the Equatorial Atlantic: *in situ* and remote sensing observations. Journal of Plankton Research 27(2), 189-197.

Perez, V., Fernandez, E., Maranon, E., Serret, P., Varela, R., Bode, A., Varela, M., Varela, M.M., Anxelu, X., Moran, G., Woodward, E.M.S., Kitidis, V., Garcia-Soto, C., 2005b. Latitudinal distribution of mircobial plankton abundance, production, and respiration in the Equatorial Atlantic in autumn 2000. Deep-Sea Research I 52, 861-880.

Peterson, M.L., Thoreson, D.S., Hedges, J.I., Lee, C., Wakeham, S.G. 1993. Field evaluation of a valved sediment trap. Limnology and Oceanographyy 38, 1741-1761.

Peterson, M.L., Wakeham, S.G., Lee, C., Meaghan, A.A., Miquel, J.C. 2005. Novel techniques for collection of sinking particles in the ocean and determining their settling rates. Limnology and Oceanography Methods 3, 520-532.

Pike, S.M., Buesseler, K.O., Andrews, J., Savoye, N., 2005. Quantification of ^{234}Th recovery in small volume sea water samples by inductively coupled plasma mass spectrometry. Journal of Radioanalytical and Nuclear Chemistry 263, 355-360.

Planquette, H. Statham, P.J., Fones, G.R., Charette, M.A., Moore, M., Salter, I., Nédélec, H., Taylor, S.L., French, M., Baker, A.R., Mahowald, N., Jickells, T.D., in press. Dissolved iron in the vicinity of the Crozet Islands, Southern Ocean. Deep-Sea Research II.

Platt, T., Harrison, W.G., 1985. Biogenic fluxes of carbon and oxygen in the ocean. Nature 318, 55-58.

Pollard, R.T., Venables, H.J., Read, J.F., Allen, J.T., in press. Large scale circulation around the Crozet Plateau controls an annual phytoplankton bloom in the Crozet Basin. Deep-Sea Research II.

Pond, D.W., R.P., H., Brownlee, C.A., 1995. Microinjection technique using pH-sensitive dye to determine the gut pH of *Calanus helgolandicus*. Marine Biology 123, 75-79.

Pondaven, P., Ruiz-Pino, D., Druon, J.N., Fravalo, C., Treguer, P., 1999. Factors controlling silicon and nitrogen biochemical cycles in the high nutrient, low chlorophyll systems (the Southern Ocean and North Pacific): comparison with a mesotrophic system (the North Atlantic). Deep-Sea Research I 46, 1923-1968.

Pondaven, P., Ragueneau, O., Treguer, P., Hauvespre, A., Dezileau, L., Reyss, J.L., 2000. Resolving the `opal paradox' in the Southern Ocean. Nature 405, 168-172.

Poulton, A.J., 2002. Spatial and temporal variability of phytoplankton community composition in the Tropical and Subtropical Atlantic Ocean (40°N - 40°S). Unpublished PhD, University of Southampton, Southampton.

Poulton, A.J., Sanders, R., Holligan, P.M., Sinchcombe, M.C., Adey, T.R., Brown, L., Chamberlain, K., 2006a. Phytoplankton mineralisation in the tropical and subtropical Atlantic Ocean. Global Biogeochemical Cycles 20, GB4002, doi:4010.1029/2006GB002712.

Poulton, A.J., Holligan, P.M., Hickmann, A., Kim, Y., Adey, T.R., Stinchcombe, M.C., Holeton, C., Root, S., Woodward, E.M., 2006b. Phytoplankton carbon fixation, cholorophyll-biomass and diagnostic pigments in the Atlantic Ocean. Deep-Sea Research II 53, 1593-1610.

Prezelin, B., Matlick, H.A., 1980. Time course of photoadaptation in the photosynthesis irradiance relationship of a dinoflagellate exhibiting photosynthetic periodicity. Marine Biology 58, 85-96.

Price, N.M., 2005. The elemental stoichiometry and composition of an iron-limited diatom. Limnology and Oceanography 50(4), 1159-1171.

Price, N.M., Ahner, B.A., Morel, F.M.M., 1994. The equatorial Pacific Ocean: grazer-controlled phytoplankton populations in an iron-limited ecosystem. Limnology and Oceanography 39, 520-534.

Priddle, J., Boyd, I.L., Whitehouse, M.J., Murphy, E.J., Croxall, J.P., 1998. Estimates of southern ocean primary production—constraints from predator carbon demand and nutrient drawdown. Journal of Marine Systems 17, 275–288.

Probyn, T.A., 1988. Nitrogen utilization by phytoplankton in the Namibian upwelling region during an austral spring. Deep-Sea Research 35(8), 1387-1404.

Probyn, T.A., 1992. The inorganic nitrogen nutrition of phyto-plankton in the southern Benguela: new production, phyto-plankton size and implications for pelagic food webs. South African Journal of Marine Science 12, 411-420.

Probyn, T., Painting, S.J., 1985. Nitrogen uptake by size fractionated phytoplankton populations in Antarctic surface waters. Limnology and Oceanography 30(6), 1327-1332.

Probyn, T.A., Waldron, H.N., Searson, S., Owens, N.J.P., 1996. Dial variability in nitrogenous nutrient uptake at photic and subphotic depths. Journal of Plankton Research 18, 2063-2079.

Purdie, D.A., Finch, M.S., 1994. Impact of a coccolithophorid bloom on dissolved carbon dioxide in sea water enclosures in a Norwegian ford. Sarsia 79, 379-387.

Queguiner, B., Treguer, P., Peekin, I., Scharek, R., 1997. Biogeochemical dynamics

and the silicon cycle in the Atlantic sector of the Southern Ocean during austral spring. Deep-Sea Research II 44, 69-89.

Queguiner, B., Brzezinski, M.A., 2002. Biogenic silica production rates and particulate organic matter distribution in the Atlantic sector of the Southern Ocean during austral spring 1992. Deep-Sea Research II 49, 1765-1786.

Quigg, A., Finkel, Z.V., Irwin, A.J., Rosenthal, Y., Ho, T.Y., Reinfelder, J.R., Schofield, O., Morel, F.M.M., Falkowski, P.G., 2003. The evolutionary inheritance of elemental stoichiometry in marine phytoplankton. Nature 425(6955), 291-294.

Quigley, M.S., Santschi, P.H., Hung, C.C., Guo, L., Honeyman, B.D., 2002. Importance of acid polysaccharides for ^{234}Th complexation to marine organic matter. Limnology and Oceanography 47, 367–377.

Radlein, N., Heumann, K., 1992. Trace analysis of heavy metals in aerosols over the Atlantic Ocean from Antarctica to Europe. International Journal of Environmental Analytical Chemistry(48/2), 127-150.

Ragueneau, O., Tréguer, P., Leynaert, A., Anderson, R.F., Brzezinski, M.A., DeMaster, D.J., Dugdale, R.C., Dymond, J., Fisher, G., François, R., Heinze, C., Maier-Reimer, E., Martin-Jézéquel, V., Nelson, D.M., Quéguiner, B., 2000. A review of the Si cycle in the modern ocean: recent progress and missing gaps in the application of biogenic opal as a paleoproductivity proxy. Global and Planetary Change 26, 317-365.

Ragueneau, O., Gallinari, M., Corrin, L., Grandel, S., Hall, P., Hauvespre, A., Lampitt, R.S., Rickert, D., Stahl, H., Tengberg, A., Witbaard, R., 2001. The benthic silica cycle in the Northeast Atlantic: annual mass balance, seasonality, and importance of nonsteady-state processes for the early diagenesis of biogenic opal in deep-sea sediments. Progress in Oceanography 50, 171–200.

Ragueneau, O., Dittert, N., Corrin, L., Treguer, P., Pondaven, P., 2002. Si:C decoupling in the world ocean: Is the Southern Ocean different? Deep-Sea Research II 49, 3127– 3154.

Ragueneau, O., Schultes, S., Bidle, K., Claquin, P., Moriceau, B., 2006. Si and C interactions in the world ocean: Importance of ecological processes and implications for the role of diatoms in the biological pump. Global Biogeochemical Cycles 20, GB4S02, doi:10.1029/2006GB002688.

Raimbault, P., Slawyk, G., Boudjellal, B., Coatanoan, C., Conan, P., Coste, B., Garcia, N., Moutin, T., Pujo-Pay, M., 1999. Carbon and nitrogen uptake and export in the equatorial pacific at 150°W: Evidence of an efficient regenerated production cycle. Journal of Geophysical Research(104), 3341-3356.

Ramus, J.A., 1990. A form-function analysis of photon capture for seaweeds. Hydrobiologica 204/205, 65-71.

Raven, J.A., 1983. The transport and function of silicon in plants. Biology Review 58, 178–207.

Raven, J.A., 1988. The iron and molybdenum use efficiencies of plant growth with different energy, carbon and nitrogen sources. New Phytology 109, 279-287.

Raven, J.A., 1990. Predictions of Mn and Fe use efficiencies of phototrophic growth as a function of light availability for growth and of C assimilation pathway. New Phytology 116, 1-18.

Read, J.F., Lucas, M.I., Holley, S.E., Pollard, R.T., 2000. Phytoplankton, nutrients and hydrography in the frontal zone between the Southwest Indian Subtropical gyre and the Southern Ocean. Deep-Sea Research Part I 47, 2341-2368.

Redfield, A.C., Ketchum, B.H., Richards, F.A., 1963. The influence of organisms on the composition of sea-water. In Hill, M. N. (Ed.), The Sea: Vol 2: Composition of Seawater Comparative and Descriptive Oceanography. Interscience, London, pp. 26-77.

Rees, A.P., Woodward, M., Joint, I., 1999. Measurement of nitrate and ammonium uptake at ambient concentrations in oligotrophic waters of the North-East Atlantic Ocean. Marine Ecology Progress Series 187, 295-300.

Rees, A.P., Malcolm, E., Woodward, S., Robinson, C., Cummings, D.G., Tarran, G.A., Joint, I., 2002. Size-fractionated nitrogen uptake and carbon fixation during a developing coccolithophore bloom in the North Sea during June 1999. Deep-Sea Research Part II 49(15), 2905-2927.

Reigstad, M., 2000. Thesis: Plankton community and vertical flux of biogenic matter in the north Norwegian fjords: regulating factors, temporal and spatial variations. University of Tromsø, Tromsø, Norway, 88pp.

Richardson, K., Beardall, J., Raven, J.A., 1983. Adaptation of unicellular algae to irradiance: an analysis of strategies. New Phytology 93, 157-171.

Richardson, T.L., Jackson, G.A., 2007. Small phytoplankton and carbon export from the surface ocean. Science 315, 838-840.

Riebessel, U.I.F., Zondervan, I., Rost, B., Tortell, P.D., Zeebe, R.E., Morel, F.M.M., 2000. Reduced calcification of marine plankton in response to increased atmospheric CO_2. Nature 407, 364-367.

Riebessel, U.I.F., Wolf Gladrow, D.A., 2002. Supply and uptake of inorganic nutrients. In Williams, P. J. L., Thomas, D. N., Reynolds, C. S. (Eds.), Phytoplankton productivity: carbon assimilation in marine and freshwater ecosystems. Blackwell Science, Oxford, pp. 109-141.

Robinson, C., Poultan, A.J., Holligan, P.M., Baker, A.R., Forster, G., Gist, N., Jickells, T.D., Malin, G., Upsill-Goddard, R., Williams, R.G., Woodward,

E.M., Zubkov, M.V., 2006. The Atlantic Meridional Transect (AMT) Programme: A contextual overview 1995-2005. Deep-Sea Research II 53, 1485-1515.

Rocap, G., Larimer, F.W., Lamerdin, J., Malfatti, S., Chain, P., Ahlgren, N.A., Arellano, A., Coleman, M., Hauser, L., Hess, W.R., Johnson, Z.I., Land, M., Lindell, D., Post, A.F., Regala, W., Shah, M., Shaw, S.L., Steglich, C., Sullivan, M.B., 2003. Genome divergence in two Prochlorococcus ecotypes reflects oceanic niche differentiation. Nature 424(6952), 1042-1047.

Rodriguez, Y., Baena, A.M., Metian, M., Teyssie, J.L., De Broyer, C., Warnau, M., 2006. Experimental evidence for ^{234}Th bioaccumulation in three Antarctic crustaceans: potential implications for particle flux studies. Marine Chemistry 100(3-4), 354-365.

Roman, M.R., Rublee, P.A., 1980. Containment effects in copepod grazing experiments: A plea to end the black box approach. Limnology and Oceanography 25, 982– 990.

Rueter, J.G., 1998. Iron stimulation of photosynthesis and nitrogen fixation in *Anabaena* 7120 and *Trichodesmium* (Cyanophyceae). Journal of Phycology 24, 249-254.

Rutgers van der Loeff, M.M., Friedrich, J., Bathmann, U.V., 1997. Carbon export during the Spring Bloom at the Antarctic Polar Front, determined with the natural tracer ^{234}Th. Deep-Sea Research II 44(1-2), 457-478.

Rutgers van der Loeff, M.M., Moore, W.S., 1999. Determination of natural radioactive tracers. In: Grasshoff, K., Kremling, K.Ehrhardt, M. (Eds.), Methods of Seawater Analysis, Wiley-VCH, pp. 365-397.

Rutgers van der Loeff, M.M., Buesseler, K.O., Bathmann, U., Hense, I., Andrews, J., 2002. Comparison of carbon and opal export rates between summer and spring bloom periods in the region of the Antarctic Polar Front, SE Atlantic. Deep-Sea Research II 49, 3849-3869.

Rutgers van der Loeff, M.M., Sarin, M.M., Baskaran, M., Benitez-Nelson, C., Buesseler, K.O., Charette, M., Dai, M., Gustafsson, Ö., Masque, P., Morris, P.J., Orlandini, K., Rodriguez y Baena, A., Savoye, N., Schmidt, S., Turnewitsch, R., Vöge, I., Waples, J.T., 2006. A review of present techniques and methodological advances in analyzing ^{234}Th in aquatic systems. Marine Chemistry 100, 190-212.

Sakshaug, E., A. Bricaud, Y. Dandonneau, P.G. Falkowski, K.A. Kiefer, L. Legendre, A. Morel, J. Parslow and M. Takahashi, 1997. Parameters of photosynthesis: definitions, theory and interpretation of results. Journal of Plankton Research 19(11), 1637-1670.

Salter, I., Lampitt, R.S., Sanders, R., Poulton, A.J., Boorman, B., Saw, K., in press. Estimating Export Production From CROZEX using PELAGRA: a Novel Drifting sediment trap. Deep-Sea Research II.

San Martin, E., Harris, R.P., Irigoien, X., 2006. Latitudinal variation in plankton size spectra in the Atlantic Ocean. Deep-Sea Research II 53, 1560-1572.

Sanders, R., Brown, L., Henson, S., Lucal, M., 2005. New production in the Irminger Basin during 2002. Journal of Marine Systems 55, 291-310.

Santschi, P.H., Hung, C.C., Schultz, G., Alvarado-Quiroz, N., Guo, L., Pinckney, J., Walsh, I., 2003. Control of acid polysaccharide production and ^{234}Th and POC export fluxes by marine organisms. Geophysical Research Letters 30(2), 1044-1047.

Santschi, P.H., Murray, J.W., Baskaran, M., Benitez-Nelson, C.R., Guo, L.D., Hung, C.C., Lamborg, C., Moran, S.B., Passow, U., Roy-Barman, M., Hung, C., 2006. Thorium speciation in seawater. Marine Chemistry 100(3-4), 250-268.

Sanudo-Wilhelmy, S.A., Kusta, A.B., Gobler, C.J., Hutchins, D.A., Yang, M., Lwiza, K., Burns, J.A., Capone, D.G., Raven, J.A., Carpenter, E.J., 2001. Phosphorus limitation of nitrogen fixation by Trichodesmium in the central Atlantic Ocean. Nature 411(6833), 66-69.

Sarmiento, J.L., 2006. Silicate cycle. In: Sarmiento, J. L.Gruber, N. (Eds.), Ocean Biogeochemical Dynamics. Princeton University Press, Princeton, N.J., pp. 270-317.

Sarmiento, J.L., Orr, J.C., Siegenthaler, U., 1992. A perturbation simulation of CO_2 uptake in the ocean general circulation model. Journal of Geophysical Research 94, 3621-3645.

Sarmiento, J.L., Bender, M., 1994. Carbon biogeochemistry and climate-change. Photosynthesis Research 39, 209-234.

Sarmiento, J.L., Hughes, T.M.C., Stouffer, R.J., Manabe, S., 1998. Simulated response of the ocean carbon cycle to anthroprogenic climate warming. Nature 393, 245-249.

Sarmiento, J.L., Gruber, N., Brzezinski, M.A., Dunne, J.P., 2004a. High-latitude controls of thermocline nutrients and low latitude biological productivity. Nature 427(6969), 56-60.

Sarmiento, J.L., Dunne, J., Armstrong, R.A., 2004b. Do we now understand the ocean's biological pump? U.S. JGOFS News 12, 1-5.

Savoye, N., Buesseler, K.O., Cardinal, D., Dehairs, F., 2004. ^{234}Th deficit and excess in the Southern Ocean during spring 2001: particle export and remineralisation. Geophysical Research Letters 31, L12301. doi:10.1029/2004GL019744.

Savoye, N., Benitez-Nelson, C., Burd, A.B., Cochran, J.K., Charette, M., Buesseler, K.O., Jackson, G.A., Roy-Barman, M., Schmidt, S., Elskens, M., 2006. ^{234}Th sorption and export models in the water column: a review. Marine Chemistry 100(3-4), 234-249.

Scharek, R., van Leeuwe, M.A., de Baar, H.J.W., 1997. Responses of Southern Ocean phytoplankton to the addition of trace metals. Deep-Sea Research II 44, 209-227.

Schmidt, S., Andersen, V., Belviso, S., Marty, J.C., 2002. Strong seasonality in particle dynamics of north-western Mediterranean surface waters as revealed by ^{234}Th/^{238}U. Deep-Sea Research I 49, 1507-1518.

Scholten, J.C., Fietzke, J., Vogler, S., Rutgers van der Loeff, M.M., Mangini, A., Koeve, W., Waniek, J., Stoffers, P., Antia, A., Kuss, J., Neuer, S., 2001. Trapping efficiencies of sediment traps from the deep eastern North Atlantic: the ^{230}Th calibration. Deep-Sea Research II 48, 2383–2408.

Seeyave, S., Lucas, M.I., Moore, C.M., Poulton, A.J., in press. Phytoplankton productivity and community structure across the Crozet Plateau. Deep-Sea Research II.

Shackleton, N.J., 2000. The 100 000-year ice-age cycle identified and found to lag temperature, carbon dioxide, and orbital eccentricity. Science 289, 1897-1902.

Sharples, J., Moore, M., Rippeth, T.P., Holligan, P.M., Hydes, D.J., Fisher, N., 2001. Phytoplankton distribution and survival in the thermocline. Limnology and Oceanography 46, 486-496.

Sherrell, R.M., Field, M.P., Gao, Y., 1998. Temporal variability of suspended mass and composition in the Northeast Pacific water column: relationships to sinking flux and lateral advection. Deep-Sea Research II 45, 733–761.

Sieburth, J.M., 1979. Sea Microbes. Oxford University Press, New York.

Siefermann-Harms, D., 1985. Location in photosynthetic membranes and light-harvesting function. Biochimica et Biophysica Acta 811, 325-355.

Siegel, D.A., Granata, A.F., Michaels, A.F., Dickey, T.D., 1990. Mesoscale eddy diffusion, particle sinking, and the interpretation of sediment trap data. Journal of Geophysical Research 95, 5305-5311.

Siegel, D.A., Deuser, W.G., 1997. Trajectories of sinking particles in the Sargasso Sea: modelling of statistical funnels above deep-ocean sediment traps. Deep-Sea Research I 44, 1519–1541.

Siegel, D.A., Karl, D.M., Michaels, A.F., 2001. Interpretations of biogeochemical processes from the US JGOFS Bermuda and Hawaii time-series sites. Deep-Sea Research II 48, 1403-1404.

Siegenthaler, U., Sarmiento, J.L., 1993. Atmospheric carbon dioxide and the ocean. Nature 365, 119-125.

Smetacek, V.S., 1985. Role of sinking in diatom life-history cycles: ecological, evolutionary and geological significance. Marine Biology 84, 239-251.

Smetacek, V.S., Von Bockel, K., Zeitschel, B., Zenk, W., 1978. Sedimentation of particulate matter during a phytoplankton spring bloom in relation to the hydrographical regime. Marine Biology 47, 211-226.

Smetacek, V., Assmy, P., Henjes, J., 2004. The role of grazing in structuring Southern Ocean pelagic ecosystems and biogeochemical cycles. Antarctic Science 16(4), 541-558.

Smith, D.C., Simon, M., Alldredge, A.L., Azam, F., 1992. Intense hydrolytic enzyme activity on marine aggregates and implications for rapid particle dissolution. Nature 359, 139-142.

Smith, H., Fischer, H., Wahlen, M., Mastroianni, D., Deck, B., 1999. Dual modes of the carbon cycle since the Last Glacial Maximum. Nature 400, 248-250.

Smith, W.O., Anderson, R.F., Moore, J.K., Codispoti, L.A., Morrison, J.M., 2000. The US Southern Ocean Joint Global Ocean Flux Study: an introduction to AESOPS. Deep-Sea Research II 47, 3073-3094.

Smith, W.O., Asper, V.L., 2001. The influence of phytoplankton assemblage composition on biogeochemical characteristics and cycles in the southern Ross Sea, Antarctica. Deep-Sea Research I 48(1), 137-161.

Smith, K.J., Vintro, L.L., Mitchell, P.I., Bois, P.B., de Boust, D., 2004. Uranium-thorium disequilibrium in north-east Atlantic waters. Journal of Environmental Radioactivity 74, 199-210.

Soltwedel, T., Pfannkuche, O., Thiel, H., 1996. The size structure of deep-sea meiobenthos in the north-eastern Atlantic: nematode size spectra in relation to environmental variables. Journal of Marine Biological Association UK 76, 327–344.

Speicher, E.A., Moran, S.B., Burd, A.B., Delfanti, R., Kaberi, H., Kelly, R.P., Papucci, C., Smith, J.N., Stavrakakis, S., Torricelli, L., Zervakis, V., 2006. Particulate organic carbon export fluxes and size-fractionated POC/^{234}Th ratios in the Ligurian, Tyrrhenian and Aegean Seas. Deep-Sea Research I 53, 1810–1830.

Steinberg, D.K., Pilskaln, C.H., Silver, M.W., 1998. Contribution of zooplankton associated with detritus to sediment trap "swimmer" carbon in Montrerey Bay, CA. Marine Ecology Progress Series 164, 157-166.

Steinberg, D.K., Carlson, C.A., Bates, N.R., Johnson, R.J., A.F., M., Knap, A.H.,

2001. Overview of the US JGOFS Bermuda Atlantic Time-series Study (BATS): a decade-scale look at ocean biology and biochemistry. Deep-Sea Research II 48, 1405-1448.

Stewart, J., Evans, J. (Eds.), 1978. Oceanography, Units 9 and 10 Biological Environments The Open University Press. Milton Keynes.

Subramaniam, A., Carpenter, E.J., 1994. An empirically derived protocol for the detection of blooms of the marine cyanobacterium *Trichodesmium* using CZCS imagery. International Journal of Remote Sensing 15, 1559-1569.

Suess, E., 1980. Particulate organic carbon flux in the oceans - surface productivity and oxygen utilization. Nature 288, 260-263.

Sunda, W.G., Huntsman, S.A., 1995. Iron uptake and growth limitation in oceanic and coastal phytoplankton. Marine Chemistry 50, 389-392.

Sunda, W.G., Huntsman, S.A., 1997. Interrelated influence of iron, light and cell size on marine phytoplankton growth. Nature 390, 389-392.

Sverdrup, H.U., 1953. On conditions for the vernal blooming of phytoplankton. Journal du Conseil Permanent International Pour L'Exploration de la Mer 18, 287-295.

Sverdrup, H.U., Johnson, N.W., Fleming, R.H., 1941. The Oceans. Prentice-Hall, Englewood Cliffs, NJ.

Takahashi, K., Fujitani, N., Yanada, M., Maita, Y., 2000. Long-term biogenic particle fluxes in the Bering Sea and the central subarctic Pacific Ocean. Deep-Sea Research I 47, 1723–1759.

Takahashi, T., Olaffson, J., Goddard, J.G., Chipman, D.W., Sutherland, S.C., 1993. Seasonal variation of CO_2 and nutrients in the high-latitude surface oceans: a comparative study. Global Biogeochemical Cycles 7(4), 843-878.

Takahashi, T., Feely, R.A., Weiss, R.F., Wanninkhof, R.H., Chipman, D.W., Sutherland, S.C., Takahashi, T.T., 1997. Global air-sea flux of CO_2: an estimate based on measurements of sea-air pCO_2 difference. Proceedings of the National Academy of Science 94, 8292-8299.

Takeda, S., 1998. Influence of iron availability on nutrient consumption ratio of diatoms in oceanic waters. Nature 393, 774-777.

Tanaka, N., Takeda, Y., Tsunogai, S., 1983. Biological effect on removal of Th-234, Po-210 and Pb-210 from surface water in Funka Bay, Japan. Geochemica Cosmochemica Acta 47, 1783-1790.

Tarran, G.A., Zubkov, M.V., Fuchs, B., Hewood, J., 2006. Latitudinal changes in the standing stocks of nano- and picoplankton in the Atlantic Ocean. Deep-Sea Research II 53, 1516-1529.

Taylor, N.J., 1985. Silica incorporation in the diatom *Coscinodiscus granii* as affected by light intensity. British Phycology Journal 20, 365– 374.

Teira, E., Mouriño, B., Marañón, E., Pérez, V., Pazó, M.J., Serret, P., de Armas, D., Escánez, J., Woodward, E.M., Fernández, E., 2005. Variability of chlorophyll and primary production in the Eastern North Atlantic Subtropical Gyre: potential factors affecting phytoplankton activity. Deep-Sea Research I 52, 569-588.

Tett, P., Edwards, A., 1984. Mixing and plankton: an interdisciplinary theme in oceanography. Oceanography Marine Biology Annual Review 22, 99-123.

Thingstad, T.F., Ovreas, L., Egge, J.K., Lovdal, T., Heldal, M., 2005. Use of non-limiting substrates to increase size; a generic strategy to simultaneously optimize uptake and minimize predation in pelagic osmotrophs? Ecology Letters 8(7), 675-682.

Tilzer, M.M., von Bodungen, B., Smetacek, V., 1985. Light-dependence of phytoplankton photosynthesis in the Antarctic Ocean: Implications for regulating productivity. *In* Antarctic nutrient cycles and food webs, Siegfried, W. R., Condy, P. R.Laws, R. M. (Eds.), (pp. 60-69). Heidelberg, Springer-Verlag.

Tilzer, M.M., Elbrachter, M., Gieskes, W.W., Beese, B., 1986. Light-temperature interactions in the control of photosynthesis in Antarctic phytoplankton. Polar Biology 5, 105-111.

Tilzer, M.M., Dubinsky, Z., 1987. Effects of temperature and day length on the mass balance of Antarctic phytoplankton. Polar Biology 7, 35-42.

Timmermans, K.R., al., e., 2001. Co-Limitation by iron and light of *Chaetoceros brevis, C. dichaeta* and *C. calcitrans* (Bacillariophyceae). Marine Ecology Progress Series 217, 287-297.

Timmermans, K.R., van der Wagt, B., de Baar, H.J.W., 2004. Growth rates, half-saturation constants, and silicate, nitrate, and phosphate depletion in relation to iron availability of four large, open-ocean diatoms from the Southern Ocean. Limnology and Oceanography 49(6), 2141-2151.

Tomczak, M., Godfrey, J.S., 1994. Regional oceanography: an introduction. Pergamon Press.

Tranter, D.J., 1982. Interlinking of physical and biological processes in the Antarctic Ocean. Oceanography Marine Biology Annual Review 20, 11-35.

Treguer, P., Legendre, L., Rivkin, R.T., Ragueneau, O., Dittert, N., 2003. Water column biogeochemistry below the euphotic zone. In: Fasham, M. J. R. (Ed.), Ocean Biogeochemistry: The role of the ocean carbon cycle in global change. Springer-Verlag, Berlin, pp. 145-156.

Tremblay, J.E., Legendre, L., 1994. A model for the size-fractionated biomass and production of marine phytoplankton. Limnology and Oceanography 39, 2004-2014.

Tremblay, J.E., Klein, B., Legendre, L., 1997. Estimation of f-ratios in oceans based on phytoplankton size structure. Limnology and Oceanography 42, 595-601.

Tremblay, J.E., Legendre, L., Klein, B., Therriault, J.C., 2000. Size-differential uptake of nitrogen and carbon in a marginal sea (Gulf of St. Lawrence, Canada): Significance of deil periodicity and urea uptake. Deep-Sea Research I 47(3-4), 489-518.

Tsurushima, N., Nojiri, Y., Imai, K., Watanabe, S., 2002. Seasonal variations of carbon dioxide system and nutrients in the surface mixed layer at station KNOT (44°N, 155°E) in the subarctic western North Pacific. Deep-Sea Research II 49, 5377-5394.

Turnewitsch, R., Springer, B.M., 2001. Do bottom mixed layers influence ^{234}Th dynamics in the abyssal near-bottom water column? Deep-Sea Research I 48(5), 1279-1307.

Tyrrell, T., Marañón, E., Poultan, A.J., Bowie, A.R., Harbour, D.S., Woodward, E.M.S., 2003. Large-scale latitudinal distribution of *Trichodesmium* spp. in the Atlantic Ocean. Journal of Plankton Research 25, 405-416.

Valdes, J.R., Buesseler, K.O., Price, J.F., 1997. A new way to catch rain. Oceanus 40(2), 33-35.

Valdes, J.R., Price, J.F., 1999. Development and testing of a neutrally buoyant sediment trap for studies of biogeochemical cycling in the Upper Ocean. Journal of Atmospheric and Oceanographic Technology 17(1), 62-68.

Valdes, J.R., Price, J.F., 2000. A neutrally buoyant upper ocean sediment trap. American Meteorological Society 17(1), 62-68.

Van Cappellen, P., Dixit, S., Van Beusekom, J., 2002. Biogenic silica dissolution in the oceans: Reconciling experimental and field-based dissolution rates. Global Biogeochemical Cycles 16, 1075, doi:1010.1029/2001GB001431.

Vangriesheim, A., Springer, B., Crassous, P., 2001. Temporal variability of near-bottom particle resuspension and dynamics at the Porcupine Abyssal Plain, Northeast Atlantic. Progress in Oceanography 50, 123–145.

Vanucci, S., Dell'Anno, A., Pusceddu, A., Fabiano, M., Lampitt, R.S., Danovaro, R., 2001. Microbial assemblages associated with sinking particles in the Porcupine Abyssal Plain (NE Atlantic Ocean). Progress in Oceanography 50, 105-121.

Veldhuis, M.J.W., Timmermans, K.R., Croot, P., Van der Wagt, B., 2005.

Picophytoplankton a comparative study of their biochemical composition and photosynthetic properties. Journal of Sea Research 53(1-2), 7-24.

Venables, H.J., Pollard, R.T., Popova, E.E., in press. Physical conditions controlling the early development of a regular phytoplankton bloom north of the Crozet Plateau, Southern Ocean, described using remotely sensed data. Deep-Sea Research II.

Verity, P.G., Stoecker, D.K., Sieracki, M.E., 1990. The impact of grazing by microzooplankton on the North Atlantic spring bloom: initial results. Eos 71, 102.

Verstraete, D., Storch, R., Dunham, V.L., 1980. A comparison of the influence of iron and nitrate metabolism of Anabaena and Scenedesmus. Physiology of Plant 50, 47-51.

Vidussi, F.C., H., Manca, B.B., Luchetta, A., Marty, J.C., 2001. Phytoplankton pigment distribution in relation to upper thermocline circulation in the eastern Mediterranean Sea during winter. Journal of Geophysical Research 106, 19939-19956.

Villareal, T.A., Pilskaln, C.H., Brzezinski, M.A., Lipschultz, F., Dennet, M., Gardener, G.B., 1999. Upward transport of oceanic nitrate by migrating diatom mats. Nature 397, 423-425.

Volkening, J., Heumann, K.G., 1990. Heavy metals in the near-surface aerosol over the Atlantic Ocean from 60 degrees South to 54 degrees North. Journal of Geophysical Research 95, 20623-20632.

von Bodungen, B., Smetacek, V.S., Tilzer, M.M., Zeitschel, B., 1986. Primary production and sedimentation during spring in the Antarctic Peninsula region. Deep-Sea Research 33, 177-194.

Wakeham, S.G., Hedges, J.I., Lee, C., Pease, T.K., 1993. Effects of poisons and preservatives on the composition of organic matter in a sediment trap experiment. Journal of Marine Research 51, 661-696.

Walsh, J.J., Whitledge, T.E., Barvenick, F.W., Wirick, C.D., Howe, S.O., 1978. Wind events and food chain dynamics within the New York Bight. Limnology and Oceanography 23, 659-683.

Waniek, J.J., Schulz-Bull, D.E., Blanz, T., Prien, R.D., Oschlies, A., Muller, T.J., 2005. Interannual variability of deep water particle flux in relation to production and lateral sources in the northeast Atlantic. Deep-Sea Research I 52, 33–50.

Watkins, J.L., 2000. Aggregation and vertical migration. In Everson, I. (Ed.), Krill: Biology, Ecology and Fisheries. Fish and Aquatic Resources Series, vol. 6. Blackwell Science, Oxford, UK, pp. 80-102.

Watson, A.J., Orr, J.C., 2003. Carbon dioxide fluxes in the global ocean. In: Fasham, M. J. R. (Ed.), Ocean Biogeochemistry: The role of the ocean carbon cycle in global change. Springer-Verlag, Berlin, pp. 123-143

Wei, C.-L., Murray, J.W., 1991. $^{234}Th/^{238}U$ disequilibria in the Black Sea. Deep-Sea Research I 38(2), 855-873.

Weinstein, S.E., Moran, S.B., 2005. Vertical flux of particulate Al, Fe, Pb, and Ba from the upper ocean estimated from 234Th/238U disequilibria. Deep-Sea Research I 52(8), 1477-1488.

Welschmeyer, N.A., 1994. Fluorometric analysis of chlorophyll a in the presence of chlorophyll b and phaeopigments. Limnology and Oceanography 39(8), 1985-1992.

Wheeler, P.A., Kokkinakis, S.A., 1990. Ammonium recycling limits nitrate use in the oceanic subarctic Pacific. Limnology and Oceanography 35(6), 1267-1278.

Williams, R.G., Follows, M.J., 2003. Physical transport of nutrients and the maintenance of biological production. In: Fasham, M. J. R. (Ed.), Ocean Biogeochemistry: The role of the ocean carbon cycle in global change. Springer-Verlag, Berlin, pp. 18-51.

Willson, H.R., Rees, N.W., 2000. Classification of mesoscale features in the Brazil-Falkland Current confluence zone. Progress in Oceanography 45, 415-426.

Witek, Z., Pastuszak, M., Grelowski, A., 1982. Net-phytoplankton abundance in western Antarctica and its relation to environmental conditions. Meeresforshung 29, 166-181.

Wolf-Gladrow, D.A., Riebessel, U.I.F., Burkhardt, S., Bijma, J., 1999. Direct effects of CO_2 concentration on growth and isotopic composition of marine phytoplankton. Tellus B 51, 461-476.

Woodward, E.M.S., 2002. Nanomolar detection for Phosphate and Nitrate using Liquid Waveguide technology (2002 Ocean Sciences Meeting, published as supplement to Eos, Transactions, American Geophysical Union 83(4), 92.

Woodward, E.M.S., Rees, A.P., 2001. Nutrient distributions in an anticyclonic eddy in the northeast Atlantic Ocean, with reference to nanomolar ammonium concentrations. Deep-Sea Research Part II: Topical Studies in Oceanography 48, 775-793.

Wooster, W.S., Bakun, A., McLain, D.R., 1976. The seasonal upwelling cycle along the eastern boundary of the North Atlantic. Journal of Marine Research 34, 131-141.

Wu, J., Boyle, E., 2002. Iron in the Sargasso Sea: implications for the process controlling dissolved Fe distribution in the ocean. Global Biogeochemical Cycles 16, 1086, doi: 1010.1029/2001GB001453,002002.

Wu, J.F., Sunda, W., Boyle, E.A., Karl, D.M., 2000. Phosphate depletion in the western North Atlantic Ocean. Science 289, 759-762.

Yentsch, C.S., 1974. Some aspects of the environmental physiology of marine phytoplankton: a second look. Oceanography Marine Biology Annual Review 12, 41-75.

Yoder, J.A., Bishop, S.S., 1985. Effects of mixing-induced irradiance fluctuations on photosynthesis of natural assemblages of coastal phytoplankton. Marine Biology 90(1), 87-93.

Yool, A., Martin., A.P., Fernandez, C., Clark, R.J., in press. Not so new: the significance of nitrification for oceanic "new" production. Nature.

Zubkov, M.V., Sleigh, M.A., Tarran, G.A., Burkill, P.H., Leakey, R.J.G., 1998. Picoplanktonic community structure on an Atlantic transect from 50°N to 50°S. Deep-Sea Research 45, 1339-1355.

Zubkov, M.V., Sleigh, M.A., Burkill, P.H., Leakey, R.J.G., 2000. Picoplankton community structure on the Atlantic Meridional Transect: a comparison between seasons. Progress in Oceanography 45, 369-386.